

NGU Rapport 2011.055

Mapping of unstable and potentially unstable
rock slopes in Sogn og Fjordane
(work report 2008-2010)

Rapport nr.: 2011.055		ISSN 0800-3416	Gradering: Åpen
Tittel: Mapping of unstable and potentially unstable rock slopes in Sogn og Fjordane (work report 2008-2010)			
Forfatter: Hermanns, R.L., Fischer, L., Oppikofer, T., Böhme, M., Dehls, J.F., Henriksen, H., Booth, A. Eilertsen, R., Longva, O., Eiken, T.		Oppdragsgiver: Norges vassdrags- og energidirektorat	
Fylke: Sogn og Fjordane		Municipality:	
Kartblad (M=1:250.000)		Kartbladnr. og -navn (M=1:50.000)	
Forekomstens navn og koordinater:		Sidetall: 195 Pris: 750 Nkr Kartbilag:	
Feltarbeid utført: April 2008 – Sept. 2010	Rapportdato: August 2011	Prosjektnr.: 310100	Ansvarlig: <i>Dyestein Nordgulen</i>
Sammendrag: For the past three years NGU has worked on 25 unstable and potentially unstable rock slopes in Sogn og Fjordane. In addition Fjørlandsfjord, Hyenfjord and Årdalsvatnet were systematically mapped for deposits of prehistoric and historic rock slope failures onshore and with help of a bathymetry. Mapping on land included structural mapping of ten sites by on-site field mapping and nine sites by remote structural mapping using terrestrial laser scanning technology (TLS). Field work also included periodic monitoring of 14 sites using differential Global Positioning Systems (dGPS) and TLS at 4 sites. Synthetic Aperture Radar was applied for the entire county but slide velocities could only be mapped out at one locality at Osmundneset (Gloppen municipality). A large amount of work was carried out on the slope east of Flåm in the Aurland valley, and results have been reported separately (NGU 2011.025). Three large instabilities have been discovered or taken into the monitoring program. These are Osmundneset in Gloppen municipality, Skrednipa in Sogndal municipality, and the Ovrís valley in Vik municipality. The largest movements with 1.5 cm horizontal and 1.5 cm vertical displacement were measured on the instability with a volume of approx. 1 Mm ³ in Ovrís valley. Opening of cracks has been measured at that site also in the 1960's, 1970's and 1980's. Our data suggest a slight acceleration of this instability. Acceleration was also documented for a 100.000 m ³ large instability called Lifjellet, although velocity of that site is less than half of the velocity of the block in Ovrís valley. However at that site a collapse of a rockslope with a volume of 25.000 to 30.000 m ³ occurred only 19 years ago. Installation of continuous monitoring and early-warning systems should be considered at both of those sites as well as at similar sites where relatively small instabilities that might fail without a long acceleration phase are positioned above settlements (Gråberget in Høyanger municipality). Similarly all other monitored instabilities in Sogn og Fjordane are in the order of mm/yr and not considered to be critical on a short term. However, periodic monitoring has to be continued. Cosmogenic nuclide dating (CN) has been applied to determine ages of rockslide deposits in Fjørlandfjord (Sogne municipality) and at the slope E of Flåm (Aurland community), resulting in Late Pleistocene and Holocene ages. CN dating has also applied to the sliding planes at Skjeringahaugane (Luste municipality). The results indicate that the movement initiated at the beginning of the Holocene and is progressive. Long term slip rates are in the same order of slip rates measured by dGPS.			
Emneord:	Rock slope stability	Structural mapping	
Periodic monitoring	Differential GPS	Terrestrial Lidar Scanning	
Synthetic Aperture Radar	Cosmogenic nuclide dating	Rock avalanches	

CONTENTS

1. Samandrag	7
2. Introduction	9
2.1 Background and earlier works	9
2.2 Methods	10
2.2.1 Mapping of unstable and potential unstable areas and structures	10
2.2.2 Mapping of deposits on land	10
2.2.3 Structural analyses of discontinuities and kinematic analyses of rock	11
2.2.4 Dating of deposits.....	12
2.2.5 Mapping of deposits on the Fjord bottom	13
2.2.6 Differential Global Positioning System (dGPS)	13
2.2.7 Terrestrial laser scanning (TLS).....	14
2.2.8 InSAR.....	15
3. Results	16
3.1 Municipalities where no unstable or potentially unstable slopes have been found... 16	
3.2 Municipalities where unstable or potentially unstable slopes have been found but no work was carried out in 2008 – 2010 and results have been reported earlier	16
3.3 Municipalities where unstable or potentially unstable slopes have been investigated in 2008 – 2010.....	16
3.3.1 Gloppen municipality	16
3.3.2 Stryn municipality	29
3.3.3 Flora municipality	29
3.3.4 Gaular municipality.....	32
3.3.5 Hyllestad municipality	33
3.3.6 Høyanger municipality	36
3.3.7 Sogndal municipality.....	39
3.3.8 Vik municipality.....	50
3.3.9 Leikanger municapility	61
3.3.10 Aurland municipality.....	65
3.3.11 Lærdal municipality	77
3.3.12 Luster municipality	79
3.3.13 Årdal municipality.....	91
4. Suggestion for future work.....	106
4.1 Further work on known sites	106
4.2 Systematic mapping for unknown sites and rock avalanche deposits	107
4.3 Continuation of dGPS periodic monitoring.....	107
4.4 Future TLS work	107
4.5 Future InSAR work	107
5. Conclusions	108
6. References	109

TABLES

Table 1: Measurements on metal bolts along one crack at Lifjellet east indicating an acceleration of movement in the past years	34
Table 2: Ages of obtained by ¹⁰ Be cosmogenic nuclide dating on samples in Fjærland fjord and sigma 1 uncertainty levels	38

Table 3: Ages of obtained by ^{10}Be cosmogenic nuclide dating on samples in Flåm valley and sigma 1 uncertainty levels.	61
Table 4: Overview of sample location along sliding plane for CN dating and results of dating	77
Table 5: Slip rates and start of sliding calculated based on CN exposure ages.	78
Table 6: Location and volume of rockfalls at Ramneberget (Øvre Årdal) between July 2009 and June 2010.	100

APPENDICES

Appendix 1: Rapport om Deformasjonsmålingar i potensielle fjellskred Sogn og Fjordane 2005-10

Appendix 2: Analysis of groundbased LiDAR data from Sogn og Fjordane County (Norway)

1. Samandrag

Dei tre siste tre åra har NGU arbeidd med 25 ustabile og potensielt ustabile fjellsider i Sogn og Fjordane. Langs dei fleste fjellsidene er det observert ulik grad av deformasjon i ustabil område. I storparten av dei undersøkte områda finst det strukturar (foliasjon, sprekker og forkastingar) som kan føre til at dei ustabile blokkene vil brytast opp i mindre delar slik at ein unngår eitt stort fjellskred. Dette tyder på at det i framtida er meir sannsynleg med kollaps av avgrensa fjellparti som vil ha mindre rørsle og rekkevidde ein eit fjellskred. I busette område, eller der det kan skje utrasing i vatn eller fjordar, kan et stort steinsprang også ha alvorlege konsekvensar. Dette er i tråd med ei historisk analyse, som viser at det i dette fylket har skjedd mange flere steinsprang enn fjellskred (Henderson et al., 2008).

Fjærlandsfjorden, Hyenfjorden og Årdalsvatnet har vore systematisk kartlagt for å avdekke kor det har vore førhistoriske og historiske steinskred og fjellskred. Kartlegging på land har saman med batymetriske kart vist at det har vore fleire førhistoriske skredhendingar i Fjærlandsfjorden og Årdalsvatnet. Fylket sett under eitt er det sannsynleg at det på land og på botn av fjordar finst spor etter fleire hundre steinskred og fjellskred. Det blir sterkt tilrådd å kartlegge dette systematisk for å få betre grunnleggande kunnskap om faren for utrasing i eit fjellparti.

På bakken er det i ti område utført feltkartlegging med vekt på strukturar i berggrunnen. Målingar med bakkebasert laserskanning-teknologi (TLS) er utført i ni område som ikkje er lett tilgjengelege. Kombinasjonen av begge metodane gjer det mogleg å få svært god kunnskap om både den romlege fordelinga av strukturar i bergmassen og rørslemønsteret (kinematikken) i ei fjellskråning der bergmassen blir deformert. Desse analysene er ein viktig del av all kartlegging av ustabile fjellparti og må derfor ha høg prioritet. Kinematiske analyser (vurdering av mogleg rørsle) vart utført for alle desse områda og er presentert i denne rapporten. Analysene vil i neste omgang bli brukt i farevurdering for kvart område.

Feltarbeidet har også omfatta regelmessig kontroll av 14 område der det er montert utstyr for rørslemåling med differensiell Global Positioning Systems (dGPS) og bruk av TLS på 4 stader. Dei fleste områda som er overvaka med dGPS er besøkt årleg. Desse målingane gjev dei mest robuste deformasjonsdata vi har i dag. Resultata viser at i dei fleste undersøkte områda er rørsle på grunn av deformasjon i fjellet avgrensa til nokre få mm per år eller mindre. Dette krev innsamling av data i ein lang periode (fleire år) før ein kan stadfeste om og kor rask rørsle det er i eit stabilt fjellparti.

Satellittbaserte radarmålingar (Syntetic Aperture Radar – SAR) er analysert for heile fylket. Med denne metoden vart det kartlagt rørsle i eit fjellparti på Osmundneset (Gloppen kommune). I åra framover vil ein kunne ta i bruk nye satellittradarar med betre oppløysing i tid og rom. Med slike data vil ein ha betre grunnlag for å kartlegge deformasjon og rørsle. I tillegg vart det installert bakkebasert RADAR-instrument ved Flåm i april 2011. Innan eitt til to år ventar vi å få robuste data for å betre kartlegge deformasjon og utgliding i dette området.

Det er utført mykje på fjellpartia aust for Flåm i Aurlandsdalen og resultata er lagt fram i ein eigen rapport (NGU 2011.025). I dei siste tre åra er det påvist tre store ustabile fjellparti: Osmundneset i Gloppen kommune, Skrednipa i Sogndalkommune, og Ovrisdalen i Vik

kommune. Alle desse fjellssidene har eit stort volum og eit potensielt fjellskred kan dermed føre til stor skade. Derfor skal områda følgast opp i åra framover. På den ustabile fjellmassen i Ovrisdalen er det er målt størst rørsle i Sogn og Fjordane. I fjellskråninga på Osmundneset kan det målast rørsle, men i dette området er deformasjonen truleg ujamt fordelt i det ustabile fjellpartiet. Sjølv om resultatata av målingane så langt ikkje er urovekkande, vil det vere naudsynt å halde fram med vidare undersøkingar og periodisk måling. Undersøkingane i Skrednipa-området er i ein tidleg fase, og her må det arbeidast vidare med for å få betre kunnskap om rørsle (kinematikk) og deformasjon. Vi kan ikkje stadfeste kor stor rørsle det er i dag og meir innsats vil bli brukt på dette området sommaren 2011.

Den største målte rørsla (1,5 cm vassrett og 1,5 cm vertikalt) vart målt på eit ustabil fjellparti med eit volum på omtrent 1 million m³ i Ovrisdalen. Åpning langs sprekker vart påvist i dette området også på 60-, 70- og 80-talet. Nye data kan tyde på ein liten akselerasjon i rørsle. Ein liknande akselerasjon vart også dokumentert for eit ustabil fjellparti med eit førebels utrekna volum på 100.000 m³ ved Lifjellet (Hyllestad). Rørsla i det ustabile området er mindre enn halvparten samanlikna med blokka i Ovrisdalen, men det er verdt å merke seg at på Lifjellet gjekk det eit steinskred med eit volum på 40.000 m³ for berre 19 år siden. Her kan det bli aktuelt å installere utstyr for kontinuerlig overvaking og varslings. Ei liknande løysing kan bli vurdert for relativt små ustabile fjellparti som kan rase ut utan ein lang akselerasjonsfase, og som er lokalisert over tett busette område (Gråberget i Høyanger kommune). Merk at rørsla er her mindre enn på Lifjellet.

For andre ustabile fjellparti i Sogn og Fjordane viser målingar rørsle er i storleik mm/år. Dei blir ikkje sett på som kritiske på kort sikt, men bør likevel takast med i vidare periodisk måling.

Datering med "Cosmogenic Nuclide Dating (CN-datering)" av eitt fjellskred i Fjærlandsfjorden og eitt i fjellskåninga aust for Flåm viser sein pleistocen og holocen alder. CN-datering vart også brukt på glideplanet på Skjeringahaugane (Luster kommune). Resultatene tyder på at det ustabile fjellpartiet byrja å bevege seg i starten av holocene, og at rørsla held fram i dag. Sett over tid viser resultatet frå datering ei gliderørsle som er i godt samsvar med gliderørsle utrekna på grunnlag av målingar med dGPS. Bruk av denne teknikken blir tilrådd også i framtida for å datere skred og for å få kunnskap om gliderørsle over lang tid. Dette er særleg viktig for å kunne påvise akselererande rørsle i ustabile område.

2. Introduction

This report contains an overview of activities and their results carried out by NGU with project partners since spring 2008 on unstable and potential unstable rock slopes in Sogn og Fjordane county. This project was a common project between NGU, Sogn og Fjordane county, Oslo University, Sogn og Fjordane University College in 2008, and became a common project between NGU, NVE, Oslo University, Sogn og Fjordane University College on January 1st, 2009 when NVE took over responsibility for landslide mapping in Norway. Results of this work have been also reported to Sogn og Fjordane county and its municipalities during meetings on November 26th, 2008 in Vik and on November 17th, 2010 in Skei.

This project is part of the national plan for mapping unstable rock slopes in Norway with the potential to cause rock avalanches or rock avalanche/rock fall triggered tsunamis and has been financed since 2009 by NVE. Systematic studies have also been carried out during these years in Troms and Møre og Romsdal counties.

In Sogn og Fjordane, 39 unstable rock slopes have been discovered by reports from municipalities, reports from the county geologist, by aerial photo interpretation of selected areas of aerial photos of generally low resolution (available freely on the web prior to 2009), and systematic helicopter reconnaissance of selected fjords, prior to 2008 (Henderson et al., 2008). In 2008, a complete cover of interferometric synthetic aperture radar (InSAR) data became available for the county and a further large instability was discovered (Osmundneset). A further site was discovered by aerial photo interpretation when high resolution images became available on the web in 2009 (Skrednipa), and additional sites were reported by the county geologist and municipalities in 2008 (Vik, Årdal municipalities). One site was found during fieldwork while flying by helicopter through the area (Gaular municipality). In total 45 unstable or potentially unstable sites are known today in Sogn og Fjordane county.

As the instabilities at Osmundneset and Skrednipa had not been discovered during earlier systematic mapping from helicopter, we did not proceed with this method. The success of actually finding unstable rock slopes depends too much on the selected flight height of the helicopter and the scale of instabilities searched for (when searching for sites of a few 100.000 to a few million cubic kilometres, sites of a size of a few hundred million cubic kilometres can easily be overseen due to low flight height). A systematic mapping of the county based on high-resolution aerial photos has not been carried out yet. In addition, slopes in Sogn og Fjordane are mostly covered by dense forest up to an altitude of approx. 800 m. Opening of cracks on those densely forested slopes are unlikely to be detectable, by aerial photo interpretation, InSAR, or helicopter reconnaissance, and unstable slopes can only be found on the densely forested slopes by timeconsuming systematic mapping by foot.

2.1 Background and earlier works

With 179 casualties due to large rock slope failures and related displacement waves in three individual historical events during the past three centuries, Sogn og Fjordane county is the Norwegian county with the highest number of casualties (Høst, 2006). An additional 47 large rock slope failures have caused casualties in this county in historical time (NVE rapport 14/2011) and further rock avalanches occurred in the 20th century that did not cause any casualties (Hermanns et al., 2006). Therefore, this county is in the highest priority group for mapping of unstable rock slopes (NVE rapport 14/2011).

Mapping of unstable slopes in this county go back to the 1960's, when a rock slope with open cracks was mapped in high detail in Ovriss valley, Vik municipality (NGI, 1966). An interdisciplinary research project between NGI, NGU, and others focussed on various sites in the unstable phyllite areas in the Flåm valley, Aurland municipality, and suggested follow up mapping activities (Domaas et al., 2002).

In 2007 NGU started a county-wide mapping project on unstable rock slopes, which resulted in a list of 39 unstable rock slopes in an extensive NGU report (Henderson et al., 2008). The basis of the work of the past 3 years was that report and recommendations given in the report. In the following we will report only on the work and results carried out in the past 3 years. Hence, sites that were not revisited in the past 3 years will not be reported again and we refer to the earlier publication. An overview of sites is given in Figure 1. In addition, the unstable rockslopes at Joasete, Furekampen, Ramnanosi above the Flåm valley had an outstanding body of work in the past three years, therefore results have been published in a separate report (Hermanns et al, 2011). In this report we only summarize and interpret the latest results that became available since the publication of that report. The numbering used in this report follows the numbering used in the earlier report (Figure 2) (Henderson et al., 2008). However, we are aware that a new standardized numbering of unstable rock slopes in Norway will be proposed soon as it will become necessary due to the development of a national database on unstable rock slopes. This will be introduced with the database and in subsequent county reports. Sites not described earlier will be only listed by municipality and name of the site.

2.2 Methods

2.2.1 Mapping of unstable and potential unstable areas and structures

In this report all unstable slopes are mapped either on aerial photos, photos taken in the field, digital elevation models or on maps. The purpose of the mapping was to document slope deformation that can be associated with gravitational movements. As these gravitational movements are strongly controlled by the structural properties of the rock, a strong emphasis was given to understanding the distribution of all structural discontinuities to assess the kinematics of slope deformation.

2.2.2 Mapping of deposits on land

Mapping of the deposits of historic and prehistoric rock slope failures has not been the focus of mapping activities in this project. However, during mapping activities it became evident that it is necessary to better understand historic and also prehistoric rock slope failures. Here we also briefly summarize results of the mapping activities focussed on deposits carried out between 2008 and 2010. In addition, mapping and dating of deposits of rock avalanches was also carried out both on and offshore in Fjærlandsfjord and Bøyadalen, Sogndal municipality, in order to get an understanding of the temporal distribution of rock slope failures in this area and are reported here.

A workshop was held in Molde in June 2010 focussing on creating a national classification system for hazard and risk assessment for unstable rock slopes. During that workshop it was agreed between the national and international experts that one essential step to estimate the likelihood of failure of an unstable rock slope is to understand the spatial and temporal distribution of historic and prehistoric events. Therefore, systematic mapping of rock avalanche deposits is defined as a goal in the national mapping plan (Nasjonal plan for

skredfarekartlegging) and became part of the Sogn og Fjordane unstable rock slope mapping project in 2011.

2.2.3 Structural analyses of discontinuities and kinematic analyses of rock

The structural analyses of naturally occurring breaks in the rock mass such as schistosity bedding planes, joints, faults are called discontinuities. These were measured in the field using structural compasses or remotely using high resolution digital elevation models (DEM) and software tools. Here these data are represented in stereographic projections and the influence of their geometry on the stability of the rock slopes is interpreted (kinematic analyses). This work is a standard procedure in slope stability estimations and can be read up in relevant text books. See for example Wyllie and Mah, 2004, chapter 2 and 3.

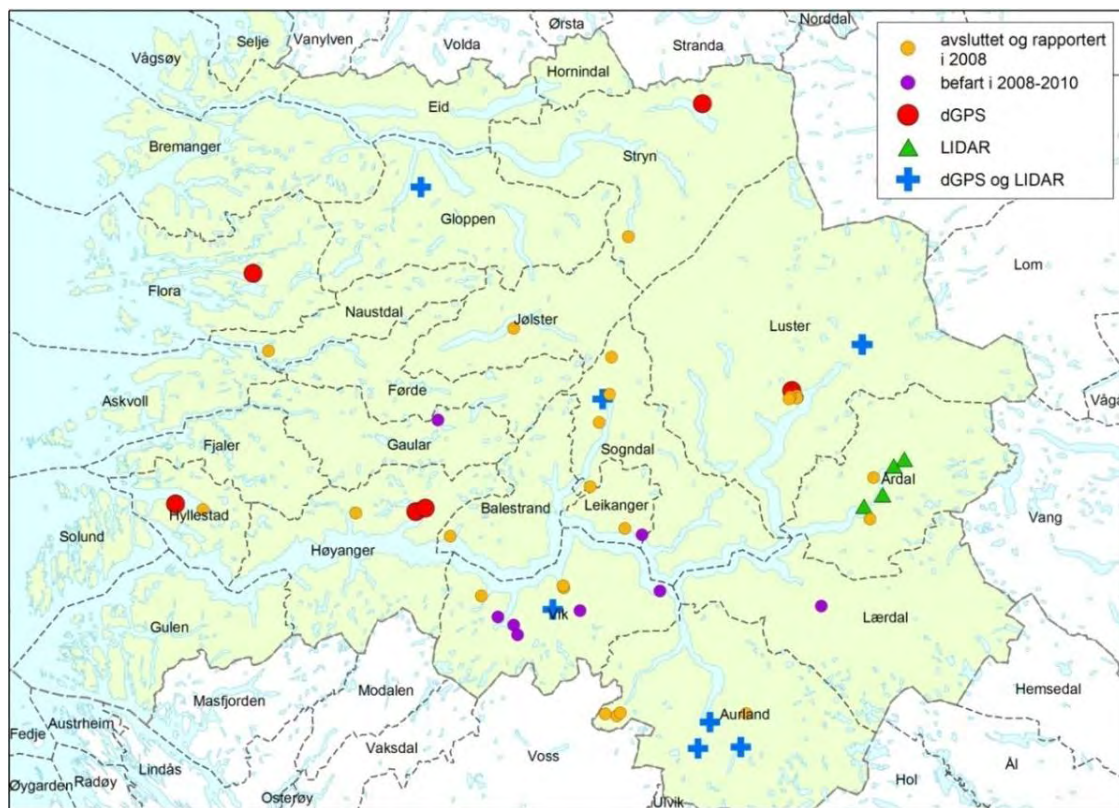


Figure 1. Overview of unstable and potentially unstable rock slopes in Sogn og Fjordane.

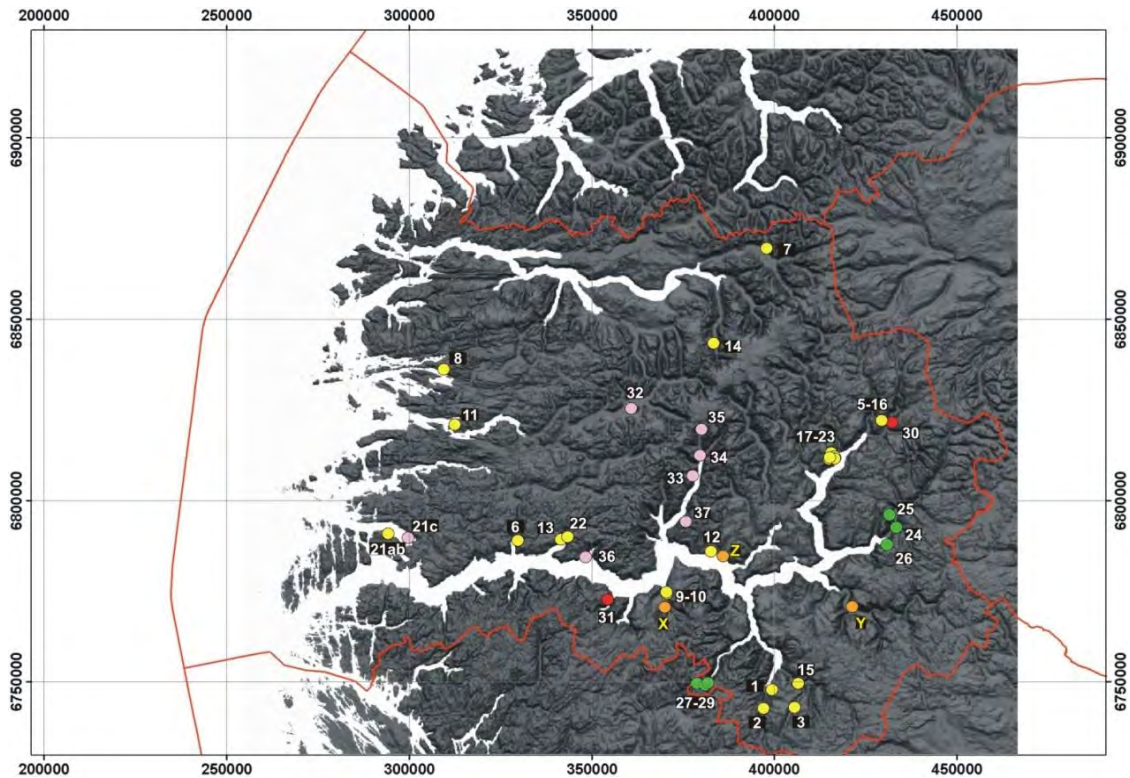


Figure 2. Numbering of sites given in NGU 2008.2026.

2.2.4 Dating of deposits

Dating the deposits of rock slope failures has long been a difficult task as vegetation cover in many areas of Norway is scarce or was scarce at the end of the last glaciations. To find dateable organic material related to the impact of a rock slide, natural or artificial cuts have to exist or must be dug into the deposit. In some cases rock avalanches that dropped into the ocean and were subsequently lifted from the sea by isostatic rebound, could be dated based on shell findings or dust layers associated with rock avalanches were dated and linked to a certain event (Blikra et al., 2006 and references therein). In any case finding appropriate material was a tedious undertaking often related to large geologic uncertainties. Hence only 10 deposits have been successfully dated by absolute dating techniques and a even smaller number of deposits by relative dating techniques in Norway (Blikra et al., 2006 and references therein).

Surface exposure dating using cosmogenic nuclides became an additional tool to date Quaternary deposits in the late 1990's, and was also successfully approved to date rock fall deposits in 1998 in Scotland (Ballantyne, 1998). Since the beginning of this decade, surface exposure dating has been established as a reliable method to date rock avalanche deposits (Hermanns et al., 2001; 2004) and has been frequently used in the past years (e.g. Hormes et al., 2008; Ivy Ochs et al., 2009; Welkner et al., 2010). It has also been used to date slope deformation (Bigot-Cormier, et al., 2005; Sanchez et al., 2010). Although dating with this method is expensive and the entire process takes a long time, this method has the advantage that the dateable material is produced by the rockslide event itself by exposing fresh material to the cosmic radiation. Although great care has to be taken in the sampling procedure to avoid inherited exposure or any kind of uncontrolled post rockslide shielding or block rotation, in general every deposit older than about 1000 years can be dated. Our sampling

procedure here focussed on taking at least two samples for each deposit to have a control on pre-exposure, uncontrolled shielding or block rotation for deposits. Rock deformations were sampled along direction of movement and at least two samples were dated from each sliding plane to have a control on post-sliding erosion. All ages reported here were calibrated for geographical latitude, altitude, surface angle of the sample location on the surface, shielding, and snow cover as outlined in Gosse and Phillips (2001). Ages were calculated with the CRONUS calculator (http://hess.ess.washington.edu/math/al_be_v22/al_be_multiple_v22.php). Ages given within this report are mean values of all possible age calculations assuming the various discussed production rates for cosmogenic nuclides. We did not calibrate for uplift related to isostatic rebound at this varies significantly over the region, is relatively poorly mapped and its effect on the final age is small in comparison to the statistical errors (Fenton et al., 2011).

2.2.5 Mapping of deposits on the Fjord bottom

In order to obtain high-resolution bathymetric data from the fjord bottom, a 125 kHz GeoSwath interferometric sidescan sonar (GeoAcoustics™) was used during a cruise in 2008. The sonar gives high-resolution depth information with an accuracy of sub-metre scale. Sound velocity profiles (SVP) were measured using a Valeport 650 SVP. Differential GPS was used for positioning, giving an accuracy of ± 1 m. A gyroscope was also used for navigation. Processing was conducted using the GeoSwath software, and included sound velocity correction, calibration to reduce signal-to-noise ratios, and adjustment of the position between profiles. The sonar has a range of approx. 200m in saltwater (depending among other things on salinity), so in some parts the data coverage was not 100% (shown as white gaps in the dataset).

In addition, high-resolution seismic data, giving information on the sub-surface sediments, were obtained using a high resolution parametric sonar (TOPAS). This equipment has a chirp function with frequencies between 2 and 6 kHz and low penetration. Data was collected during cruises in 2000 and 2008. Some of the data from the 2000 cruise have been reported by Bøe et al. (2002).

Debris from large avalanches can be recognized as morphologic elevations on the sea floor, occasionally even if they are buried by younger sediments. Recent avalanches have a rougher surface compared to older ones, and the first approach to identify slide events and their relative ages is based on the morphology (Longva et al., 2009). This was followed by interpretation of the seismic data, where avalanche debris will have a chaotic seismic signature in contrast to the transparent or acoustically laminated hemipelagic deposits above or below it.

2.2.6 Differential Global Positioning System (dGPS)

Most of the measuring points were installed during field activity in 2007 and 2008. At all sites measuring points were installed in presumably stable rock (fixed points) and on blocks in movement (rover points). A network of vectors is measured with relative GNSS method between points and coordinates of points are calculated using a least squares adjustment. A change in coordinates of the rover points are interpreted as slope deformation. A confidence level based on the estimated coordinate standard deviations from first and second measurements is used to test if the points are moving or not. All these sites have been measured at least twice in the interval 2008 - 2010. At one of the earlier installed localities (Tussen, Lustrafjord) an additional fixed point was installed because a further crack was

found behind the presumably fixed point to rule out that the earlier fixed point is not in movement. On the sites Osmundneset (Gloppen), Vik (Vik), and Skjeringahaugane (Luster) new networks of measurement points were installed in 2008 and on Skrednipa (Sogndal) in 2009.

In this report we will give results measured of rover points in reference to the fixed points and calculated mean velocities between first and last measurement. We will also report if the movement is significant or not. Significant in this case means that the movement is higher than the uncertainty of the method, based on the standard deviations of estimated coordinates. A level of 3 standard deviations or 99% probability has been used for significance tests. Vertical deformations have an additional uncertainty from atmospheric variations and the significance level is often estimated to be too low. Furthermore, we will indicate with the terms "certain gravitational movement" and "uncertain gravitational movement displacements" the quality of those data to be interpreted in relation with gravitational slope deformation. "Certain gravitational movement" can be expected if slope deformation follows a trend over several years. The movement becomes uncertain if deformation spreads rather chaotically over the years or reverses in the following year. This can be the effect of meteorological conditions during the time of measurement that might affect the travel path of the satellite signals leading to apparent deformation. Alternatively, reversible slope deformation may be caused by thermal expansion and opening and closing of cracks due to the change of pore water pressure. "Uncertain gravitational movement displacements" cannot be interpreted unequivocally in the first year they are detected, but if deformation reverses in the following year or continues spreading chaotically in following years this "uncertain movement" can be interpreted as the effect of meteorological conditions during the time of measurement.

In addition, we will give a recommendation for each site on future measurement intervals. All GPS measurements are summarized in appendix 1 and 2 (dGPS report 2009 and 2010, respectively).

2.2.7 Terrestrial laser scanning (TLS)

Terrestrial laser scanning (TLS) is based on the reflectorless and contactless acquisition of a point cloud of the topography using the time-of-flight distance measurement of an infrared laser pulse. The Optech ILRIS-3D used for this study has a wavelength of 1500 nm and a range in practice of about 800 to 1200 m on rock slopes, depending on the reflectivity of the object. See Oppikofer et al. (2009) for a detailed description of the instrument.

The high-resolution point clouds of the topography provided by TLS can be used for the structural analysis of rock slopes and for displacement measurements using sequential (multi-temporal) TLS data. The detailed methodology is described by Oppikofer et al. (2009) and includes several steps:

- Co-registration (alignment) of individual scans of the same epoch
- Co-registration of sequential TLS scans using only the (supposed) stable area, i.e. the surroundings of the rock slope instability
- Georeferencing of the entire dataset using ground-control points or a DEM
- Structural analysis using Coltop3D software (Jaboyedoff et al., 2007)

- Shortest distance comparison between sequential scans for the visualisation and a preliminary quantification of displacements

2.2.8 InSAR

Synthetic Aperture Radar (SAR) is a microwave imaging system. It uses microwaves, which can penetrate clouds. By comparing multiple SAR images, we are able to measure changes in travel time as a function of the satellite position and time of acquisition. This allows us to generate Digital Elevation Models (DEM). Changes not related to topography include those due to changes atmosphere and topography between acquisitions.

If the topography for an area is known, two images can be used to measure deformation ranging from centimetres to metres. Smaller deformations, however, are not easy to distinguish from atmospheric effects using just two images. If we use many images (15 or more), however, we can take advantage of the differences in spatial and temporal correlation to distinguish between deformation and atmospheric effects. We can do this if we assume that atmospheric effects have a high degree of spatial correlation but are almost random in time, whereas the deformation we are looking for will have much higher temporal correlation (Ferretti et al., 2001). Over the last years, several algorithms have been developed to do this type of analysis. In this study we have used an improved version of the small baselines (SBAS) algorithm (Berardino et al., 2002; Lauknes et al., 2011).

The data used in this study were acquired by the ERS-1 and ERS-2 satellites between 1992 and 2000. The ERS satellites have an operating wavelength of 5.66 cm, and the radar looks to the right (west) with an angle of approx. 23.5° from the vertical. All snow-free scenes were used. These scenes were used to generate all possible with a maximum perpendicular baseline of 300 m and a maximum temporal separation of four years.

From the calculated interferograms, a common set of pixels is chosen that is above a preset coherence threshold in a selected fraction of the interferograms. Since interferometric phase measurements are observed modulo 2π , the interferograms must be spatially ‘unwrapped’ to determine absolute phase values. This is done using the SNAPHU program (Chen and Zebker, 2001). After phase unwrapping, all pixels are referenced to a selected (assumed stable) reference pixel with high coherence. For each interferogram, an orbital phase ramp as well as phase delay due to tropospheric stratification are estimated and removed. DEM error, atmospheric phase screen and deformation are then estimated using the technique outlined in Lauknes et al., (2011).

3. Results

3.1 Municipalities where no unstable or potentially unstable slopes have been found

In several municipalities in Sogn og Fjordane, no unstable slopes have been reported or detected yet, either by systematic satellite based InSAR analysis or reconnaissance helicopter surveys. However, this does not rule out the possibility that such unstable slopes exist. Especially on slopes with dense vegetation, potential unstable slopes might exist that have not been detected yet. All these municipalities will be also finally mapped more systematically based on air photo analyses. Municipalities where no unstable rock slopes prone to cause a failure large enough to produce a rock avalanche or a rockslide triggered fjord tsunami have been detected are: Askvoll, Bremanger, Eid, Fjaler, Førde, Gulen, Hornindal, Selje, Solund, and Vågsøy.

3.2 Municipalities where unstable or potentially unstable slopes have been found but no work was carried out in 2008 – 2010 and results have been reported earlier

Several municipalities in Sogn og Fjordane, where results have previously been reported (NGU report 2008.026), had no further work carried out in 2008 – 2010 as no recommendations for further work were given. These municipalities are: Balestrand Jølster, and Nausdal. Also in the municipalities Aurland, Hyllestad, Høyanger, Leikanger, Luster, Sogndal, Stryn, Vik, and Årdal lie several sites where no further mapping activities have been carried out, however activities at other sites have been carried out in the past 3 years. Sites are marked in Figure 1.

3.3 Municipalities where unstable or potentially unstable slopes have been investigated in 2008 – 2010

3.3.1 Gloppen municipality

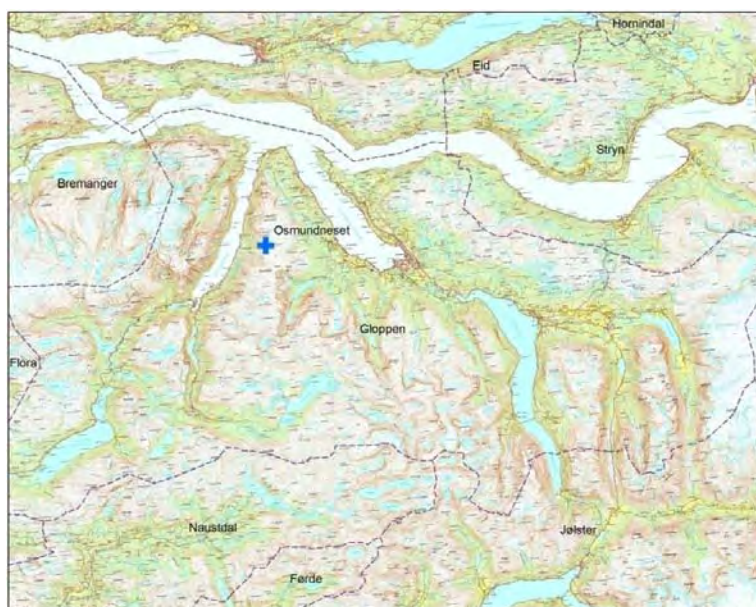


Figure 3. Position of Osmundneset locality in Gloppen municipality.

3.3.1.1 Locality Osmundneset, Hyenfjord

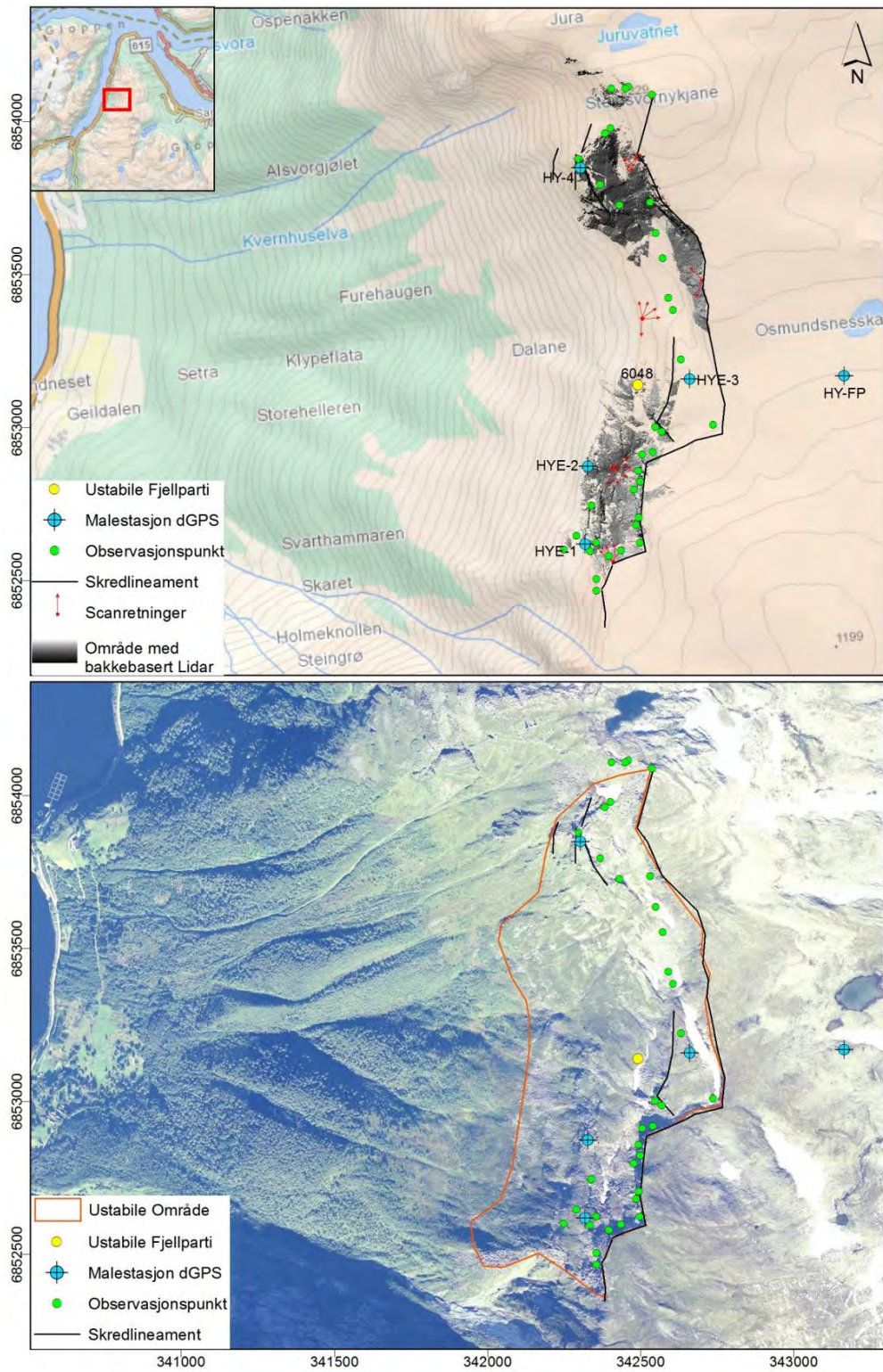


Figure 4. Overview over the unstable site Osmundneset, showing the dGPS points, areas with TLS data and the locations of manual structural measurements. The Hyenfjord is visible in the left part of the image.

The Osmundneset landslide was detected from InSAR analyses and is located on the east side of Hyenfjord, a southern branch of Nordfjord (Figure 3). Several large, displaced blocks sit along the ridgeline above the fjord at an elevation of ~1000 m above sea level, and the ground just below the ridgeline is pervasively cracked and disturbed over a fjord-parallel distance of ~1 km (Figure 4 and 5). A prominent cliff band along the ridge delineates the upper extent of the landslide area.

The main work performed in this Osmundneset landslide area consists of mapping, structure geological analyses, dGPS measurements, and TLS data acquisition.



Figure 5. Photo from the top above the unstable site Osmundneset in Hyenfjord, showing the top scar and the different detached and displaced blocks.

InSAR results

Due to the large overlap between adjacent satellite images obtained on parallel orbits, Hyenfjord is covered by three ERS datasets (Figure 6). Track 237 has 32 images, track 008 has 41 images, and track 280 has 33 images. Each of these datasets was processed independently.

The InSAR technique is only sensitive to displacement changes with a component in the radar line-of-sight (LOS) direction. For each of these datasets, the images were acquired while the satellite was travelling towards the equator (descending orbit). The satellite looks to the right with an average incidence angle of 23° from the vertical. However, since the image swaths are approx. 100 km wide, the incidence angle varies from 19° on the eastern edge to 27° on the western edge. This is illustrated in Figure 7. The LOS component of any ground motion measured will vary between the three datasets depending on the relative angle between the true direction of movement and the LOS.

In Figures 8, 9, and 10, the LOS velocities for the three datasets are all shown with the same colour scale for comparison. Movement away from the satellite is indicated with negative velocities, with all movement away from the satellite of more than 3 mm/year shown in red.

The dataset from track 237 has the shallowest LOS; approx. 19° from vertical. Within the apparent unstable area, the maximum velocity away from the satellite is 3 mm/year (Figure 8). The dataset from track 008 has a LOS of approx. 23° . Within the apparent unstable area, the maximum velocity away from the satellite is 5 mm/year (Figure 9). The dataset from track 280 has the steepest LOS; approx. 27° from vertical. Within the apparent unstable area, the maximum velocity away from the satellite is 8 mm/year (Figure 10).

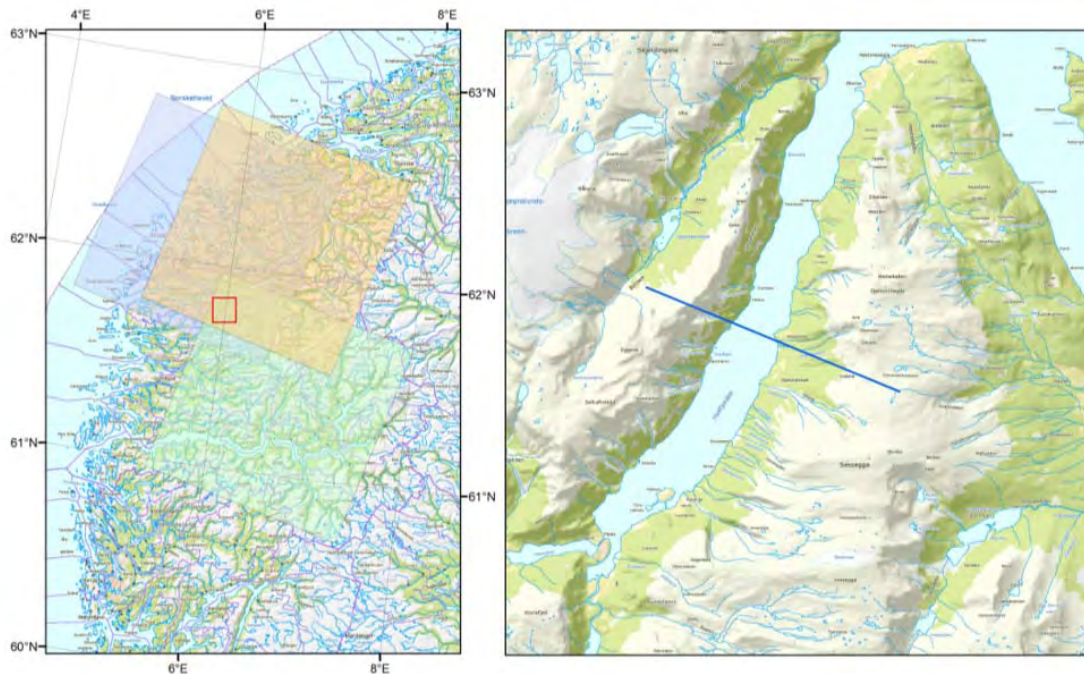


Figure 6. Left: Location map showing the three available dataset; track 237 in green, track 008 in orange and track 280 in blue. The red square shows the area of the figure to the right. Right: Hyenfjord, with the location of the elevation profile shown in Figure 7.

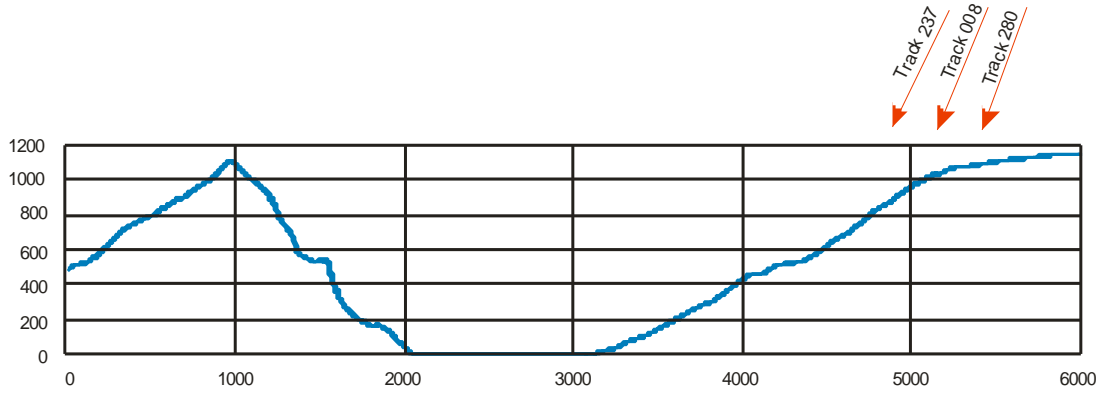


Figure 7. Elevation profile extracted along a profile perpendicular to the satellite orbit. The red arrows show the lines-of-sight (LOS) of the three datasets. Since the satellite is travelling towards the equator and looking to the right, the LOS becomes shallower towards the west. All velocities shown in the following figures are the component along the respective LOS.

Within the unstable area, different blocks with varying velocities can be distinguished. The frontal blocks show highest velocities (Figure 11), whereas the rear blocks show relatively lower displacement rates.

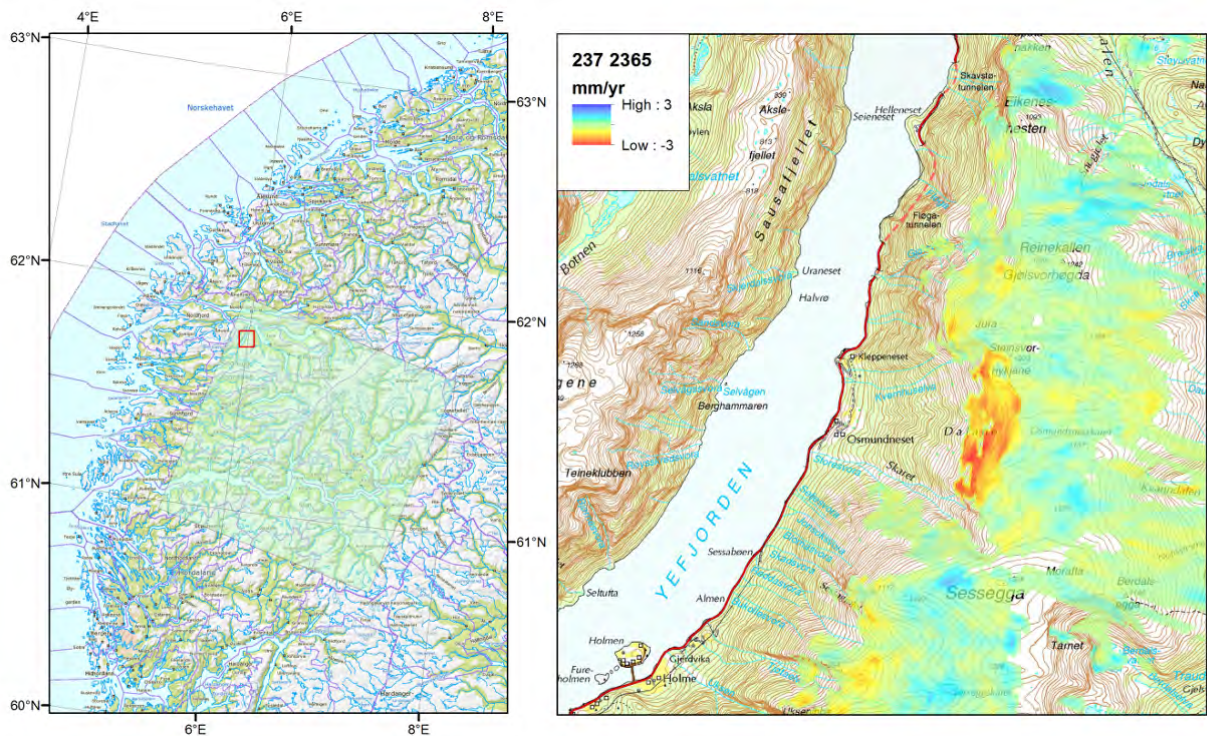


Figure 8. Average LOS velocity for track 237. The incidence angle is 19° from vertical.

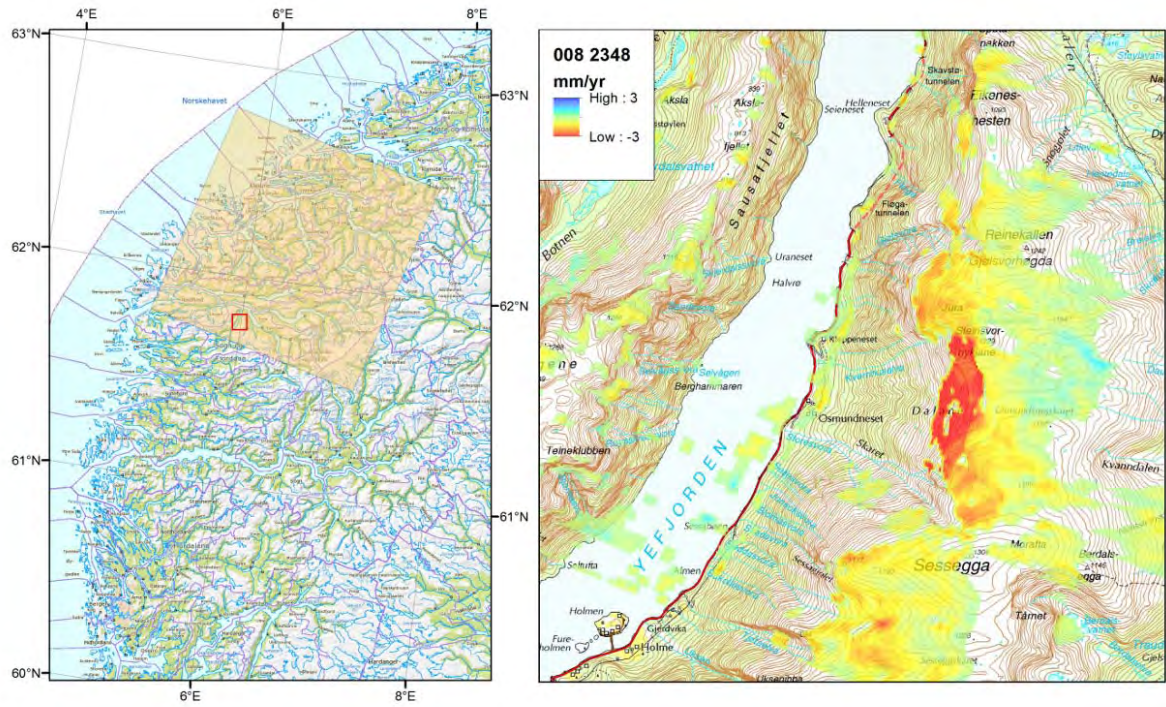


Figure 9. Average LOS velocity for track 008. The incidence angle is 23° from vertical.

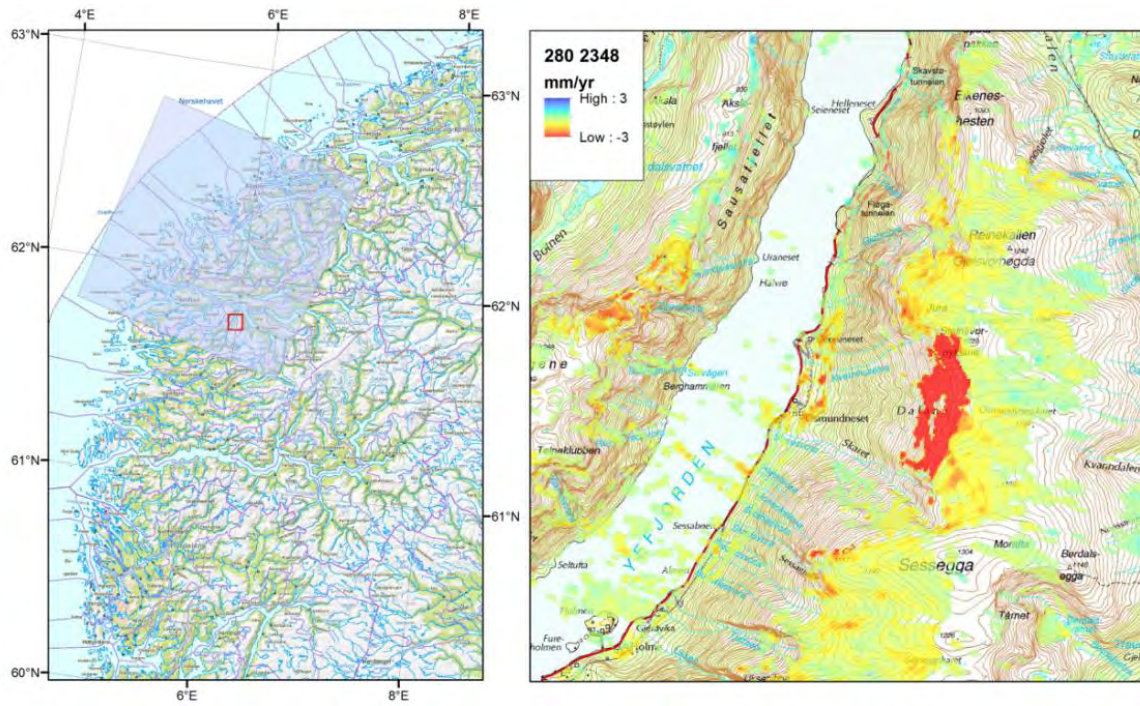


Figure 10. Average LOS velocity for track 280. The incidence angle is 27° from vertical.

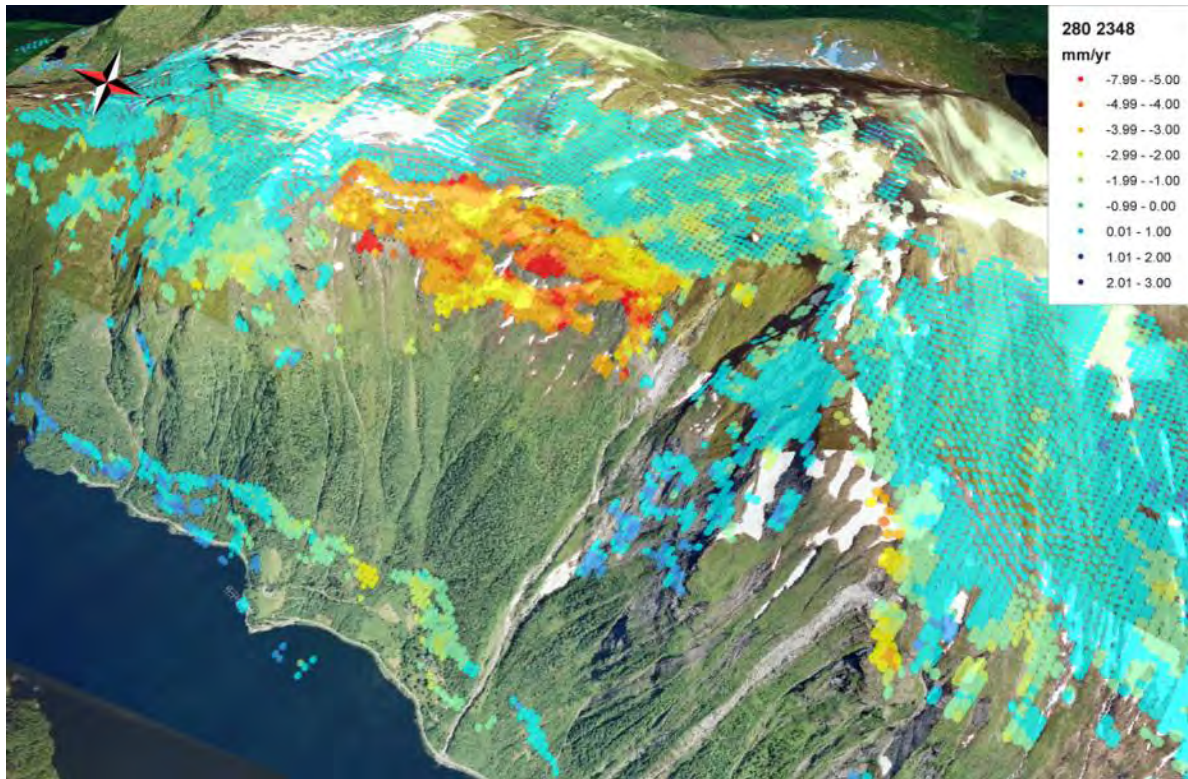


Figure 11. Average LOS velocity for track 280 draped upon a digital terrain model (DEM). The colour scale is different from that in Figures 8, 9, and 10 in order to highlight variations in velocity within the unstable area.

dGPS results

Differential GPS measurements were started in 2008 with the installation of 5 observation points (Figure 4). Four measurement points were installed on different detached and probably unstable blocks (rover points), one fixed point as reference point was installed on the stable plateau above. Repetition measurements were taken in summer 2009 and 2010. This two-year series of measurement indicates mm-scale movement of several points on the landslide complex (Figure 12). The results show small, barely significant movements in one of the points (HY-4) over the two-year measurement period. The measurements for all other points are below the significance level within the uncertainty range of the method. In elevation, there are no significant changes for 2009-10. The results after two years of measurement indicate that there may be movement at point HY-4, but to get more robust conclusions, more repetition measurements have to be performed the next years. We suggest continuing the dGPS measurements in the coming years on an annual basis.

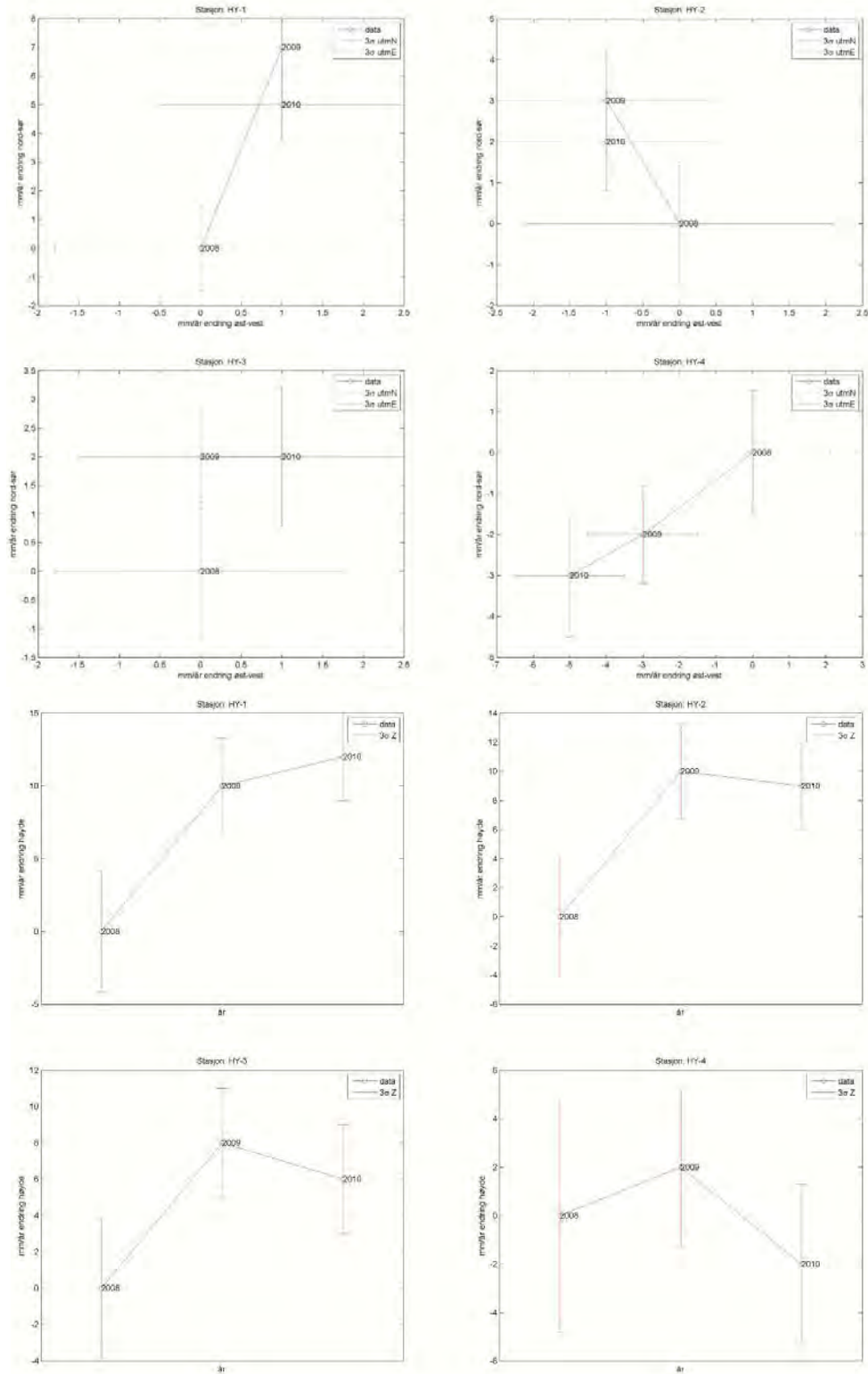


Figure 12. dGPS measurements: The two upper rows show the horizontal displacements at each point, the lower rows show vertical displacements. All vertical displacement measurements are within the uncertainty range of the method, from the horizontal displacement measurements only the HY-4 station might show significant displacements over the two-year period.

TLS results

TLS data acquisition of parts the unstable rock slope at Hyenfjord was performed in September 2010. Twenty scans were made from five scan positions above the back-scarp and on the unstable slope (Figure 13). The total 2010 TLS point cloud is formed by 53.2 million points (average resolution: 4.2 cm at a mean distance of 220 m) and was used to create a high-resolution DEM with a cell size of 25 cm (Figure13) and for the extraction of structural data.

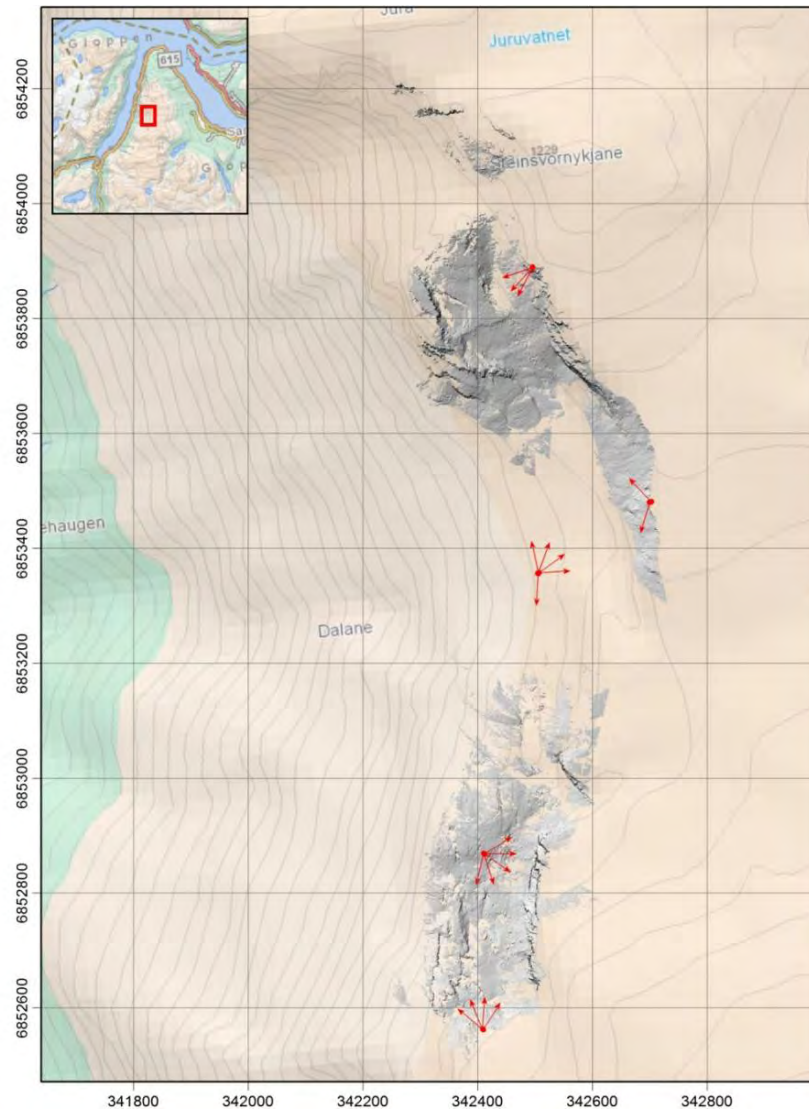


Figure 13. View-shaded representation of the high-resolution DEM created from the 2010 TLS point cloud at Hyenfjord. The scan positions and directions are indicated (red arrows).

The distribution of the scan locations allowed us to capture most of the surface of a large, displaced block in the northern section of the landslide complex, as well as large parts of the cliff face marking the back crack of the landslide complex. As we have up to now only one set of TLS measurements, no displacement or topographic change analyses can be performed. The 2010 TLS data were used for the extraction of structural data, to enhance the number of structural data for kinematic analyses. These structural analyses will be described in the next chapter.

Mapping on land

The bedrock on this side of the fjord consists mainly of gneiss, with well developed foliation and pervasive sub-vertical fractures. To document the structural trends of the unstable slope, we took 410 structural measurements in the field in 2008 and 2010, and made an additional 484 measurements using the georeferenced TLS point clouds (Figure 14).

We first selected different locations in the TLS data where many structures were clearly visible. After fitting about 20 planes at a given location, we recorded the dip and dip direction of each plane. To test the equivalency of the field and TLS-based measurement techniques, we took several measurements at the same locations as the field measurements. In all cases, there were no systematic differences between measurement types, and the mean orientation of any structural set always fell within one standard deviation of the mean of the same set determined with the other measurement type.

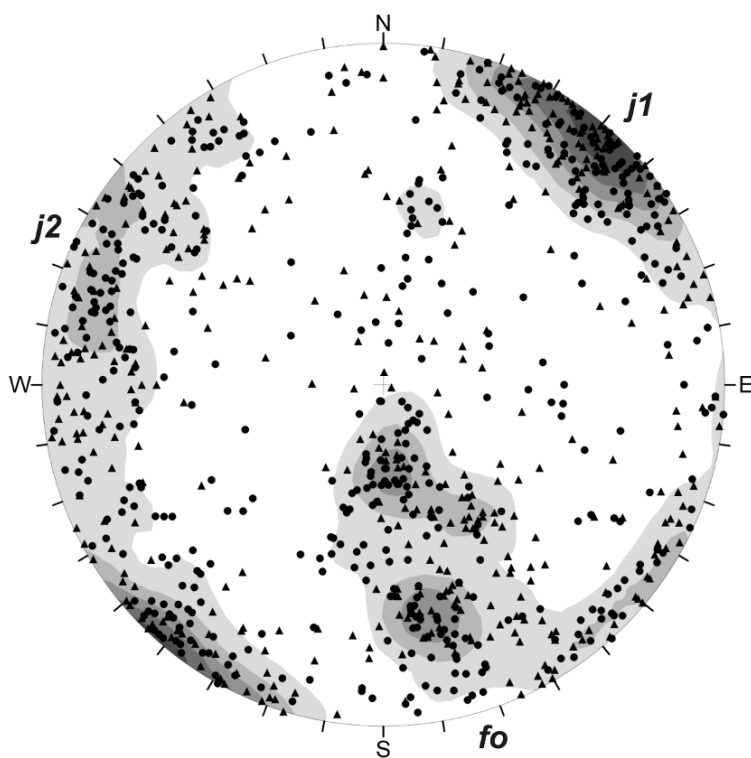


Figure 14. Lower hemisphere stereonet showing the poles of all structures measured in the field (triangles) and the structures extracted from the TLS point cloud (circles). Shaded areas indicate Fisher concentrations of 1-2%, 2-3%, 3-4%, 4-5%, and 5-6% from lightest to darkest. Three major structures are present throughout the site: foliation (Fo), and two sub-vertical joints (J1 and J2).

The south-dipping foliation measurements tend to be from the northern part of the landslide complex, the west-dipping points from the center, and the north-dipping from the southern part, which plays an important role in controlling the landslide failure style. The spatial variation in foliation orientation described above defines a broad fold over a ~1 km distance that may control the location of this large rockslide feature over the long term. The first major joint set, *J1*, is present at nearly all measurement locations and is near vertical with a southwest or northeast dip direction. The orientation of this joint also varies spatially, with northeast-dipping measurements more common in the northern part of the landslide, and

southwest-dipping measurement more common in the south (Figure 16). Lastly, a second major joint set, J_2 , is present at most measurement sites, with a tendency to dip steeply to the east-southeast, but its orientation is highly variable and does not change systematically from one part of the landslide to another.

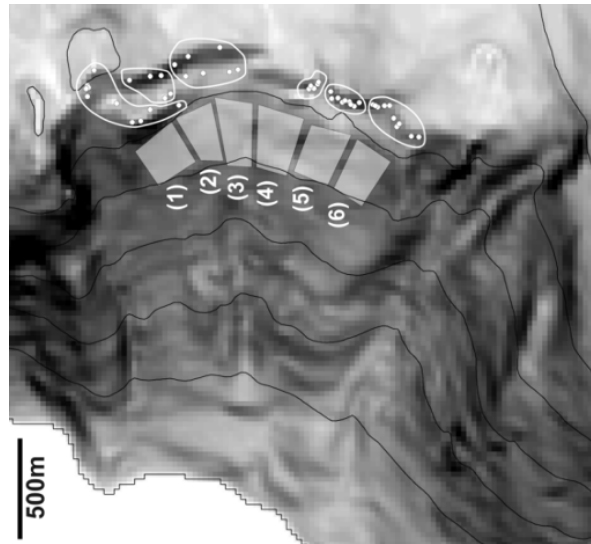


Figure 15. Locations 1 through 6 refer to parts of the landslide used for separate kinematic analyses illustrated in Figure 16. The white dots show the locations of structural measurements with white outlines enclosing the points used in each separate analysis. The white polygons show areas used to determine the average slope and aspect of the hillside for each analysis.

Kinematic tests (Figure 16) were performed for planar and wedge sliding at six sites spread across the landslide complex. The results show that both failure types are kinematically feasible at different locations within the landslide complex, and the three major structures contribute to possible movement, however in different sections. Planar sliding along the foliation is possible in the central part of the unstable slope (Figure 16, No. 3), however at the northern as well as at the southern end, planar sliding is not possible due to changes in the foliation orientation.

Wedge sliding is only possible in the northern part of the site (location 1) with an intersection of the foliation and J_2 as well as in some areas of the central part with an intersection of the foliation and J_1 .

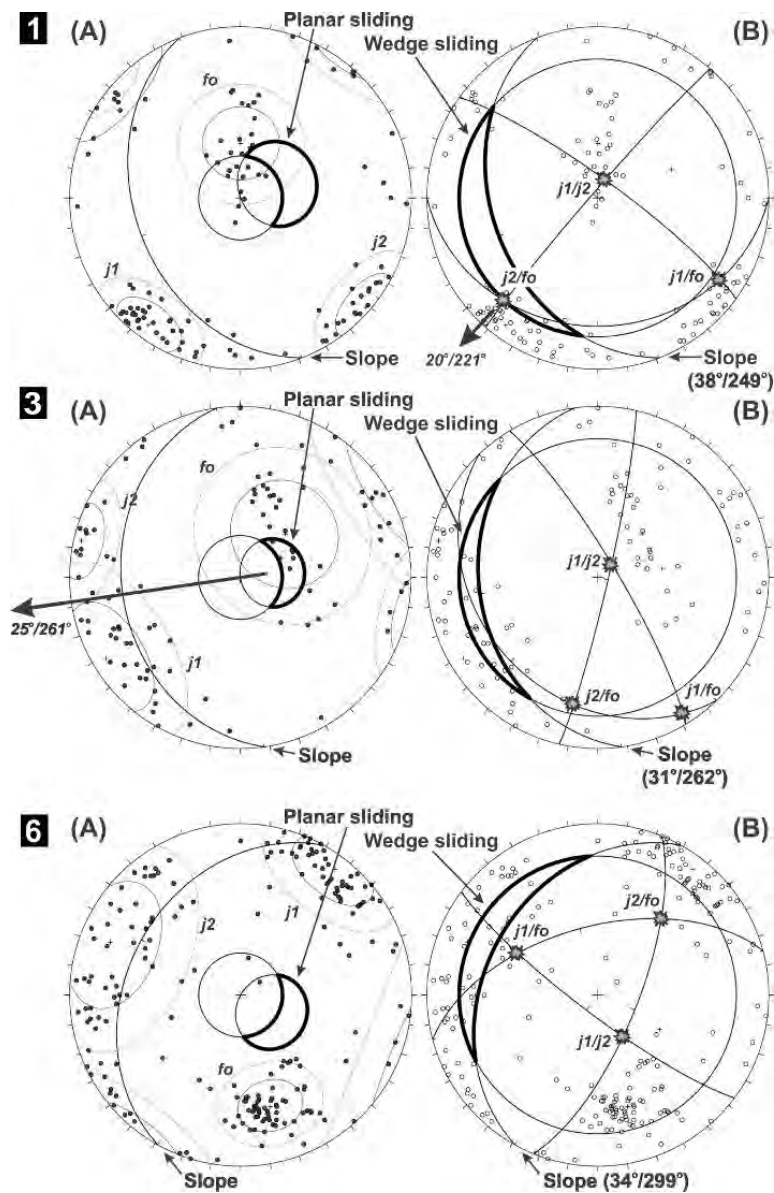


Figure 16. Results from the kinematic feasibility tests for planar and wedge sliding and toppling at different locations within the unstable area. Upper row shows the analyses based on structural measurements from the northern end of the unstable slope at location 1 (Figure 15), the middle row from the middle part (location 3), and the lower row the ones from the southern end (location 6). These analyses show that planar sliding is possible over larger areas in the central part of the flank, whereas wedge sliding is possible in along most of the instability.

Mapping on the fjord bottom

The detailed bathymetry of Hyenfjord was produced in 2008 in order to map any Holocene rockslide deposits which are visible in the morphology of the fjord bottom. The bathymetry is of high quality in the inner fjord and of poorer quality in the outer fjord with missing data due to the capacity of the equipment used (Figure 17). No large rockslide deposit could be mapped on the bathymetry of the fjord; however deposits of early postglacial collapses might have been covered by Holocene deposits.

Recommendations

We recommend continuing dGPS measurements on an annual basis for the next years until the deformation velocities are well established. Based upon airborne laser scanning (ALS) data with a resolution of 1 m, which will become available in 2011, a detailed volume and morphometry estimation should be carried out, including the estimation of the lower boundary of the unstable slope



Figure 17. The bathymetry of Hyenfjord does not indicate any sub-recent rockslide deposits.

3.3.2 Stryn municipality

3.3.2.1 Locality Oppigardshyrna (7)

This locality was mapped and reported in detail in NGU report 2008.026. Between 2008 and 2010 no further mapping activities have been carried out and the only activity carried out was a dGPS measurement in summer 2008.

dGPS results

Results of deformation measurement by dGPS of three rover points in 2006-2007 had an abnormal low significance level, which made it possible to detect significant displacements both in horizontal and vertical direction although this was only a few millimetres (NGU report 2008.026). This data cannot be interpreted as certain gravitational movement. In 2008 significance level was back to normal level and only one measurement point indicated significant movement. All deformation was in the vertical and in the horizontal in the exact opposite direction as in the measurement period 2006-2007. Therefore no certain gravitational movement can be detected. This is in line with no detectable movement by repeated measurements of steel bolts along small open cracks between 1951 and 1981 (NGU report 2008.026).

Recommendations

As no certain gravitational movement could be detected in this area for the period 1951-1981 and the period 2006-2008, we suggest a 4-6 years period for repeated measurements in the future. Therefore this site should be measured again in 2011.

3.3.3 Flora municipality

3.3.3.1 Locality Strandanipa (8)

This unstable rock-slope area is located on top of a 70 m high cliff, 620 m above the fjord on a WNW-ESE trending slope that has an average gradient of 35°. The bedrock consists of mica-rich schist and phyllite. The foliation is in general dipping northeast towards the mountains, but folds are observed locally. Widespread blocky rockfall deposits are present at the base of the cliff, some reaching the fjord.

The unstable part of Strandanipa is characterized by an irregular pattern of steep fractures that separate the unstable volume into many small blocks (Figure 18A). Several fractures are open with widths of up to 0.5 m and visible depths of 5 m (Figure 18B), while others are only expressed by topographic depressions on the surface (Figure 18A). Fractures that are visible on the top surface are not clearly noticeable on the cliff. A certain boundary at the bottom of the unstable block could not be observed in the field. Instead the bedrock shows irregular layering and fracturing increasing with depth (Figure 18C). Below an upper approx. 10 m thick, massive layer the bedrock is highly fractured. Hence the strength of the highly fractured bedrock is lower and therefore probably quite unstable. This suggests that this unstable area might only be affected by successive smaller rockfall events, and not by large slope failures that could reach the fjord and cause a tsunami.



Figure 18) Strandanipa unstable area. A) Overview. The solid line marks the border of the unstable area and the dashed lines indicate open fractures and depressions that separate the block into several parts. View to the south. B) Fracture that limits the block to the east. View from the north. C) Exposed cliff on which the unstable part is located. The bedrock is highly fractured and therefore probably quite unstable below the uppermost approx. 10 m thick massive layer. View to the northeast.

dGPS results

A dGPS measurement was carried out in summer 2008. Here we represent the location of dGPS rover points on a map showing the main cracks in Figure 19.



Figure 19. showing the main cracks and position of rover points at Strandanipa.

The results of the deformation by dGPS measurements of the two rover points indicate no significant horizontal movement and only rover point ST-2 has a significant component of block movement towards the north (Figure 20). This would indicate a closing of cracks and cannot be interpreted as certain gravitational movement.

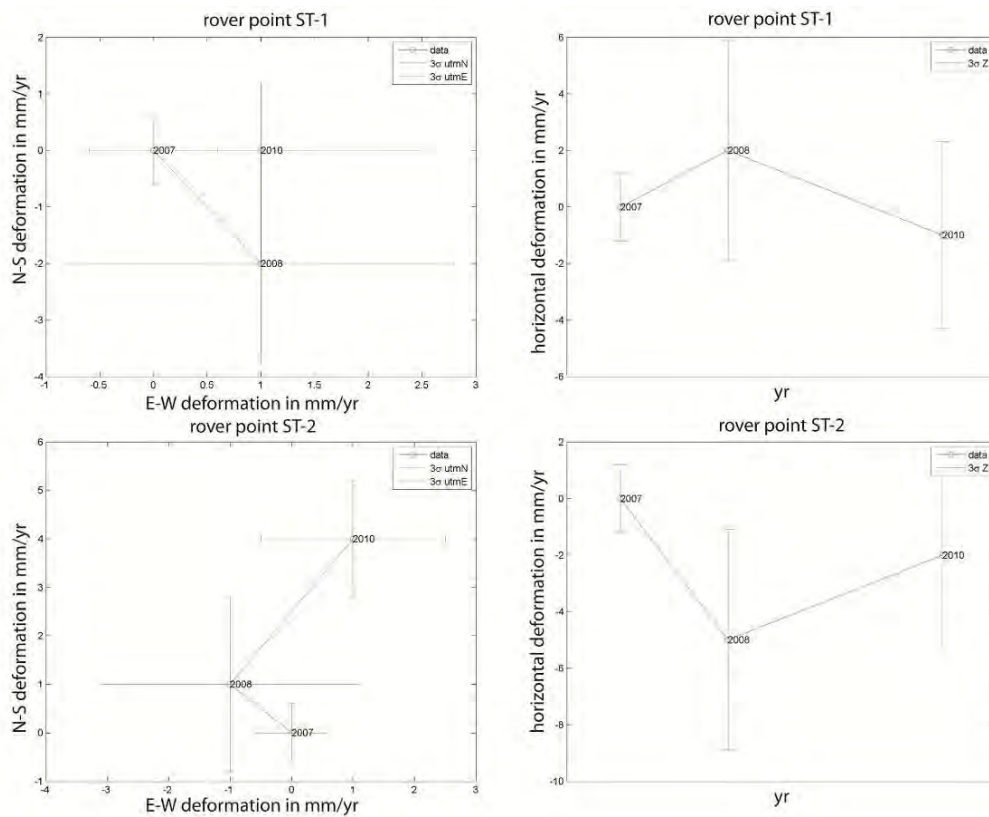


Figure 20. Diagram showing the movement detected on rover stations between 2007 and 2010 at Strandanipa.

Recommendations

As no certain gravitational movement could be detected in this area for the period 2007-2010, we suggest a 4-6 years period for repeated measurements in future. Therefore this site should be measured again in 2013.

3.3.4 Gaular municipality

Areal photo reconnaissance

A detachment zone and deposits of large rockfalls were detected during a helicopter transit (Figure 21 and 22). A preliminary evaluation based on photograph and aerial image analyses reveals open cracks in the bedrock adjacent to the old detachment zone. The surface of the larger left block is around 5000 m²; the one to the right is at most 1000 m². An estimation of the volume is difficult due to the lack of more detailed topographic data. However, based on the rough area measurements and the observation that the blocks are highly fractured internally, we conclude that possible rockfall events would not have larger volumes than past events. Due to the limited volume and shallow slope angle, no large runout distances are assumed.

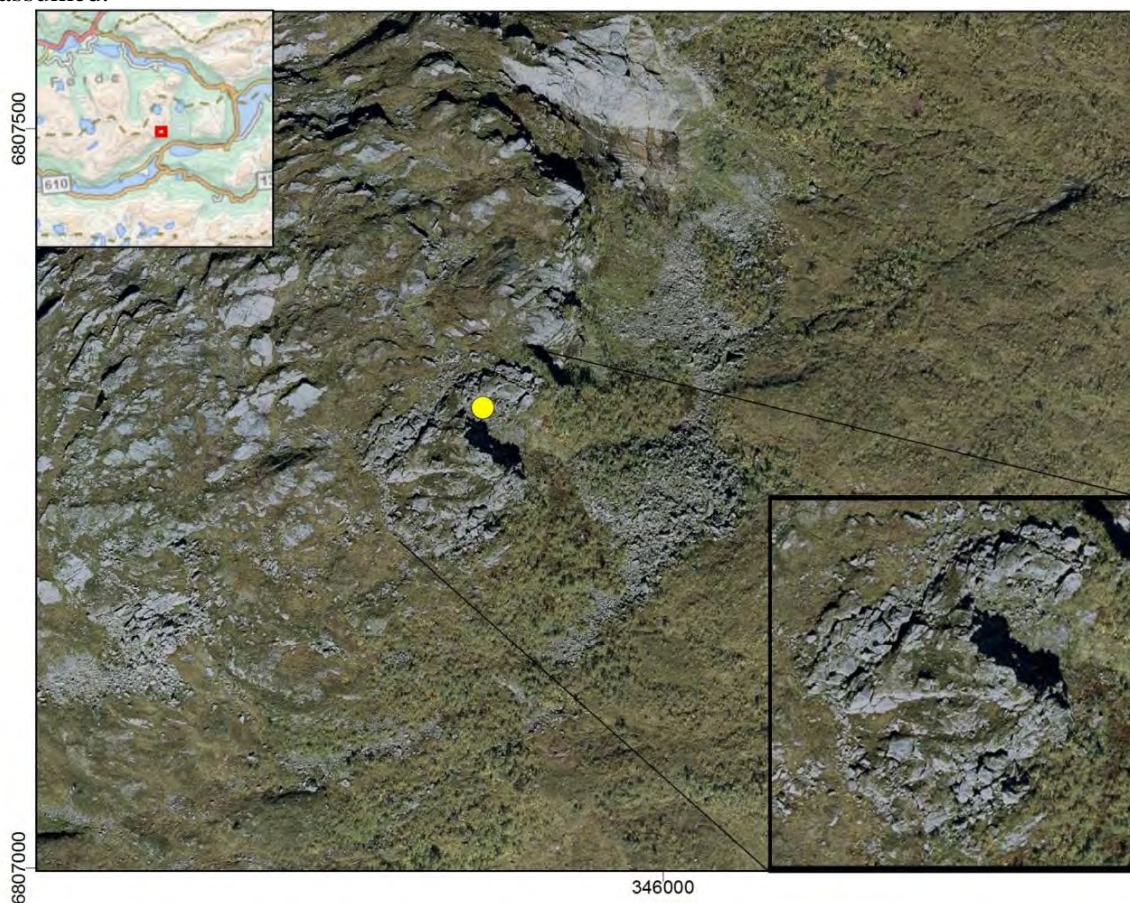


Figure 21. Possible unstable rock slope in the Skredfjell area, investigated from helicopter and aerial images. The blocks around the yellow mark show open cracks. Below the flank, deposits of old rockfalls are visible.

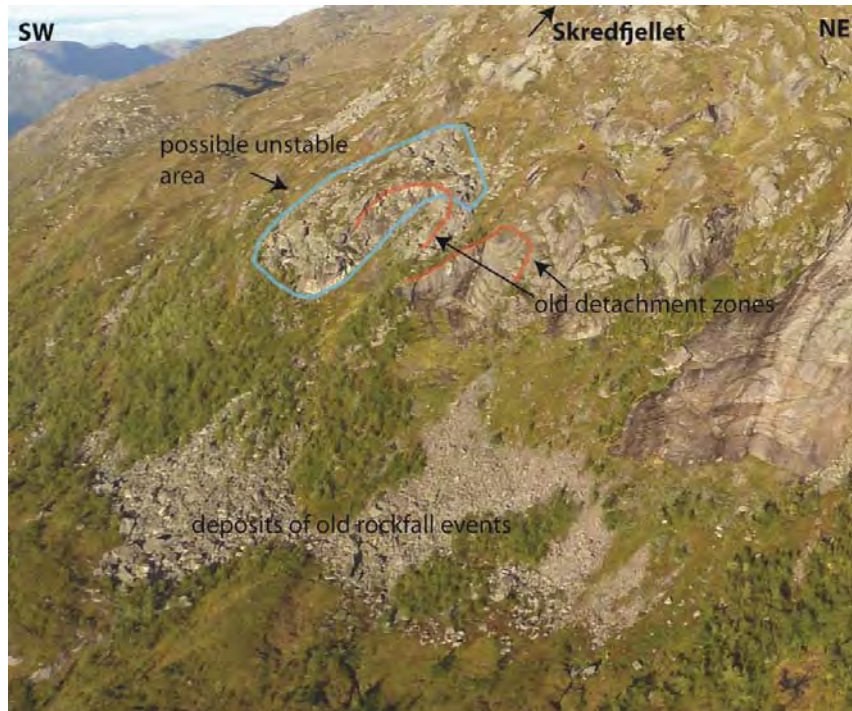


Figure 22. Photograph of the possible unstable rock slope in the Skredfjellet area in the upper middle part of the image (marked in blue). Detachment zones of old rockfalls are marked in red and their deposits are visible below the flank.

Recommendations

- Volume and run-out analyses based on a 10 m DTM during the systematic remote sensing based mapping project in summer 2011.
- If possible to combine with overfly with helicopter to other fieldwork, more detailed photograph acquisition would be advantageous.

3.3.5 Hyllestad municipality

3.3.5.1 Locality Lifjellet (21)

In February 1992 a larger rock fall with a volume of approx. 25-30.000 m³ (Harbitz et al. 2001) occurred in this locality. A displacement wave was register related to that event at the opposite fjord site 6 m high (Harbitz et al. 2001). This locality was mapped and reported in detail in NGU report 2008.026. Two unstable sections, Lifjellet west and Lifjellet east, were characterized that are controlled by a single or few mayor cracks, respectively (Figure 23 and 24). The unstable section at Lifjellet west has an approx. volume of 170.000 m³ and the section at Lifjellet east an approx. maximum volume of 90.000 m³ (Böhme et al., 2011). This is therefore 5 or 2.5 times larger than the collapse from 1992 and a rockfall-induced displacement wave might be considerably larger in the fjord. Between 2008 and 2010 no further mapping activities were carried out and the only activity were dGPS measurements in 2008, 2009, and 2010 and measurements of metal bolts installed in 1999. In addition, we tested the depth of the cracks by dropping stones and recording the time of fall in the crack. In the case of Lifjellet west this test suggests that the crack is open along most of the length for approx. 100 m, while at Lifjellet east the rock only indicates a depth of approx. 20-30 m.

However, it is important to realize that these are minimum estimates as the cracks can continue with a slight offset.

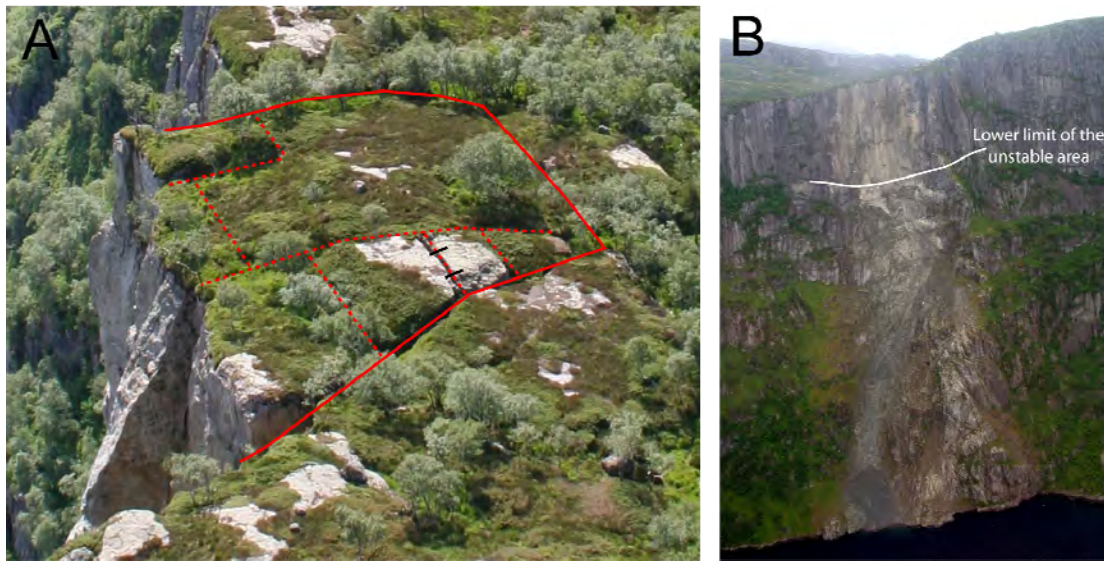


Figure 23. Airphoto view of Lifjellet east. The slope below the unstable plateau section misses vegetation indicating recent rockfall activity (after Böhme et al., 2011)



Figure 24. Airphoto-view of Lifjellet west showing the overhanging character of the cliff in front of the crack (after Böhme et al., 2011)

dGPS results

Results of the deformation by dGPS measurements of the two rover points (HY-11, HY-12) at Lifjellet east indicate significant horizontal movement towards the north in the order of 4-5 mm/yr (Figure 25). This is in good agreement with the crack opening as measured along the bolts and indicates an acceleration of deformation in comparison to the period 1999-2003 (Table 1).

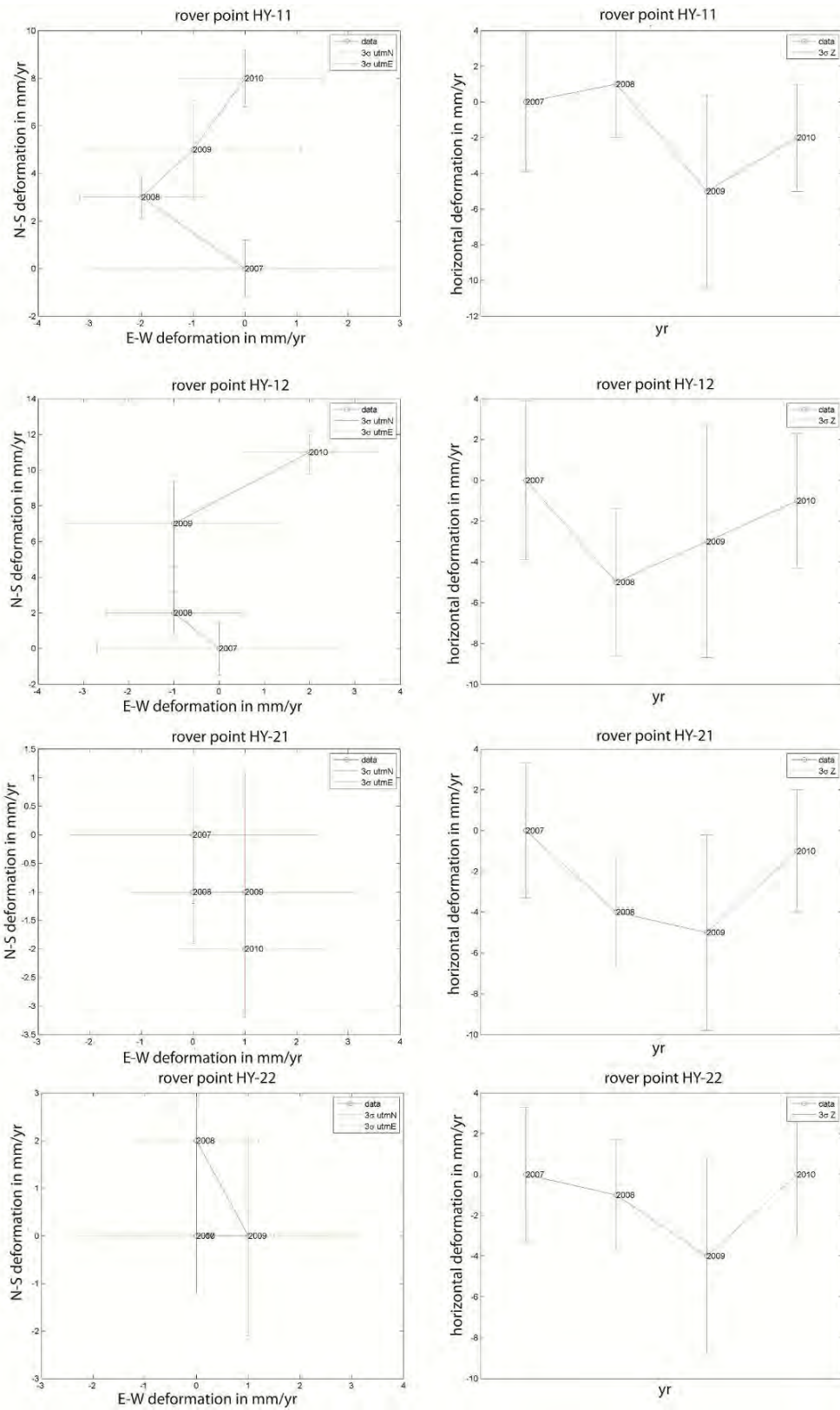


Figure 25. Results of dGPS measurements indicate significant movement towards the north at Liffjellet 1 and no displacement at Liffjellet 2.

Table 1. Measurements on metal bolts along one crack at Lifjellet east indicating an acceleration of movement in the past years.

Date	Bolts west	Bolts east	Opening [mm/yr] during last measurement interval (west)	Opening [mm/yr] during last measurement interval (east)
11. May 1999	615 mm	548 mm		
03. June 2003	616 mm	549 mm	< 1 mm/yr	< 1 mm/yr
08. June 2007	635 mm	570 mm	4-5 mm/yr	5 mm/yr
17. August 2009	639 mm	573 mm	2 mm/yr	1-2 mm/yr
16. August 2010	645 mm	577 mm	6 mm/yr	4 mm/yr

The results of the deformation by dGPS measurements of the two rover points at Lifjellet west indicate no significant horizontal or vertical movement.

Recommendations

The cliff at Lifjellet is nearly vertical, partly overhanging and approx. 500 m above sea level. Cracks at both sections in Lifjellet west and Lifjellet east are vertical, several tens of metres deep, several tens of centimetre wide, and those at Lifjellet east have significant movement and accelerated in velocity since 2003. In addition, at that site an important historical rock fall of larger magnitude has occurred. Due to this structural configuration we cannot be certain that yearly measurements will catch an acceleration of slope deformation prior to collapse to give a warning to local population, fish farms and boat traffic in the fjord. We therefore recommend alternative deformation measurements connected to an early warning system. As deformation strongly concentrates along few cracks, extensometers with data logger and transmission devices might be an alternative with relatively low cost which should be discussed.

3.3.6 Høyanger municipality

3.3.6.1 Locality Ståppelen (13)

dGPS results

This locality was mapped and reported in NGU report 2008.026. Between 2008 and 2010 no further mapping activities were carried out, and the only activity was a dGPS measurement in summer 2008. GPS measurements are not significant in the horizontal but significant in the vertical. However, similar to the period 2006-2007 the vertical variations indicate uplift. This cannot be explained as certain gravitational movement.

Recommendations

As no certain gravitational movement could be detected in this area for the period 2006-2008 we suggest a 3 years period for repeated measurements in the future. Therefore this site should be measured again in 2011.

3.3.6.2 Locality Gråberget (22)

This locality was mapped and reported in detail in NGU report 2008.026. Between 2008 and 2010 no further mapping activities were carried out and the only activity was a dGPS measurement of the 3 rover points in 2008, 2009 and 2010.

dGPS results

Results of the deformation by dGPS measurements of the rover points GB-1 and GB-2 indicated small significant vertical movement in between 2009 and 2010 (Figure 26). However as they are not consistent with previous years they cannot be interpreted as certain gravitational movement. Rover point GB-3 had a constant horizontal significant movement since 2008 of a few millimetres.

Recommendations

The back crack at Gråberget is 150 m long and various individual blocks can fail along this crack independently. A failure would rarely be of the size of a rock avalanche but rather of a rock fall. We recommend also consulting the susceptibility map rock fall published on: [http://www.ngu.no/kart/skrednett/?map=Steinsprang – aktsomhetskart](http://www.ngu.no/kart/skrednett/?map=Steinsprang%20-%20aktsomhetskart). It is evident that developed areas of Høyanger lie within the run-out area of rock fall. As the open cracks are nearly vertical and volumes are small, we consider that a failure might develop faster than over a 1 year measurement period and recommend considering other monitoring strategies and even early warning. As deformation strongly concentrates along few cracks, extensometers with datalogger and transmission devices might be an alternative with relatively low cost which should be discussed.

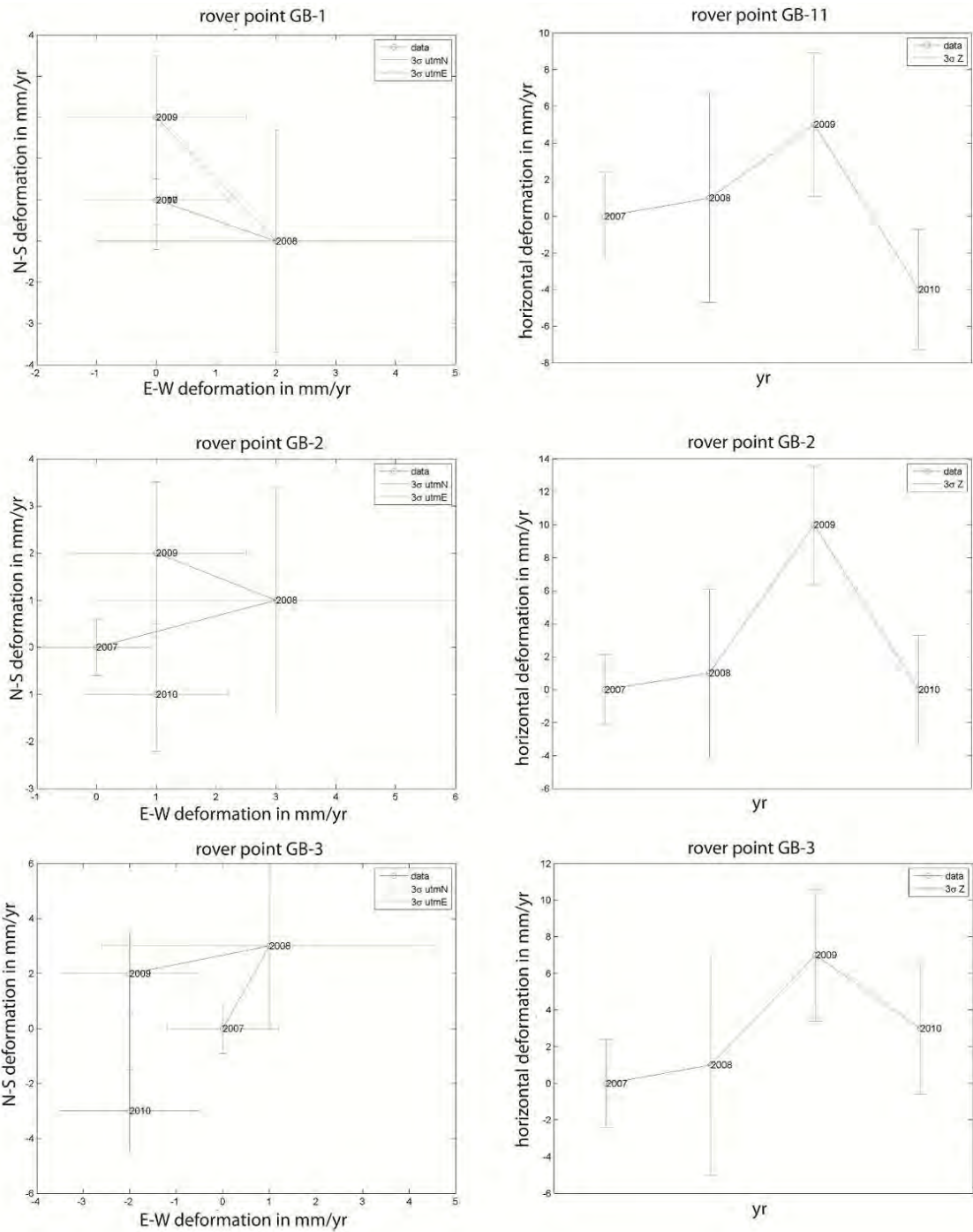


Figure 26. Results of dGPS measurements indicate no significant horizontal movement over the period 2007-2010 that can be interpreted as certain gravitational movement but there has been significant vertical movement between 2009 and 2010 at GB-1 and GB-2.

3.3.7 Sogndal municipality

3.3.7.1 Mapping and dating of deposits in Fjærlandsfjorden

Three rock avalanche deposits could have been recognized and their extension estimated by aerial photo analyses in the Bøyadalen and inner Fjærlandsfjord that were named after local names as Bøyadalen rock avalanche (B), Øyrahagestolen (C), and Uraneset (D) (Figure 27).

The Bøyadalen rock-avalanche deposit has a surface area of approx. 80,000 m² and is a relatively fresh deposit with sharp limits and block sizes of up to a few metres in diameter. A relatively small scar on the west side of the valley suggests that the rock avalanche originated on that site.

The Øyrahagestolen rock avalanche deposit is less well defined in its limitations, and within the deposit there are areas that do not have large rock avalanche boulders on the surface. Clast size is in general in the order of a few metres in diameter but several clasts pass the size of 10 m in diameter. The deposits lie on the west slope of the valley within a scar-like depression on Skrednipa mountain. This scar is much larger than the deposit itself. Opposite from this deposit, on the east slope of the valley, there are suspicious hummocky boulder deposits. The boulder size of these hummocks is often in excess of 10 m in diameter and no scarp area is visible on the east slope. On top of the hummocks, boulders stick out of a terrace-like deposit of silty to clayey composition, suggesting that the deposit was deposited under or at the marine limit.

The Uraneset deposit lies on the steep western slope above Fjærlandsfjorden and is composed of a continuous boulder deposit with a clast size of a few metres in diameter. The deposit clearly reaches down into the fjord so that the extent of the deposit cannot be defined.

Each deposit was sampled for cosmogenic nuclide dating at elevations higher than 80 m a.s.l. to be sure to be above the marine limit. Of each deposit, two samples were dated. Results of both samples on each of these deposits coincide within uncertainty limits suggesting that the ages represent the true age of the rock avalanche (Table 2). Both the Uraneset and the Øyrahagestolen rock avalanche deposits have ages slightly younger than the last readvanced of the last ice age (Younger Dryas) suggesting that those events occurred shortly after deglaciation. This fits well with marine deposits on the rock avalanche deposits on the opposite slope of Skrednipa, suggesting that these deposits also belong to the Øyrahagestolen rock avalanche deposit and that this rock avalanche crossed the entire valley floor and that today's delta deposit cover the top of the Øyrahagestolen rock avalanche deposits in its central part. Hence, the event could have been as large as the rockslide scar on Skrednipa and much larger than outcropping deposits today.

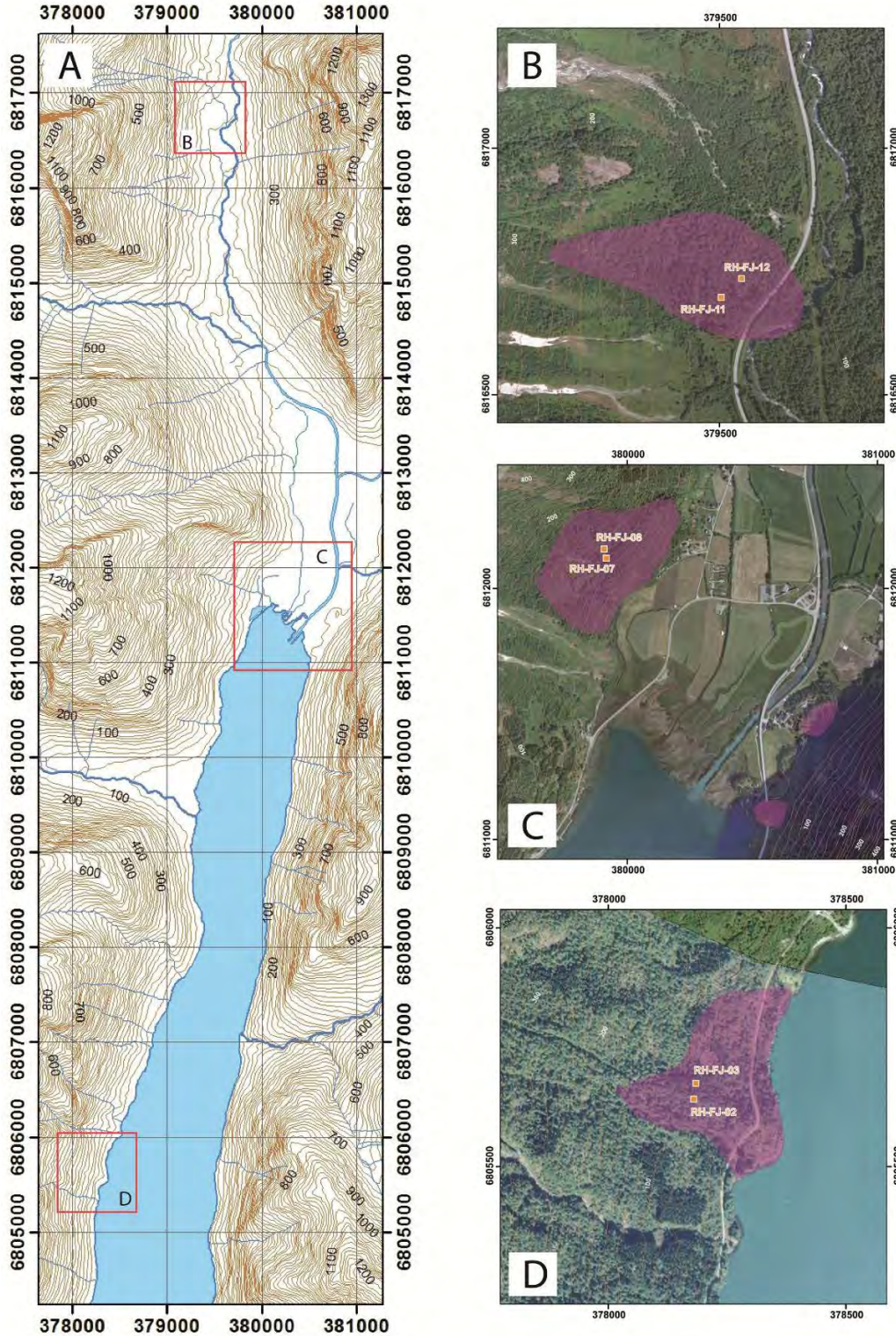


Figure 27. A) overview map of areas with rock avalanche deposits in the inner Fjærlandsfjord and Bøyadalen. B) Rock avalanche deposit in Bøyadalen. C) Øyrahagstolen rock avalanche deposit below a rockslide scar at the east slope of Skrednipa significantly larger than the volume of the mapped rock avalanche deposit, D) Uraneset rock avalanche deposit along the western shore of Fjærlandsfjord.

Table 2. Ages of obtained by ^{10}Be cosmogenic nuclide dating on samples in Fjærlandsfjorden and sigma 1 uncertainty levels. Sample height is measured by altimeter with 1 m resolution, sample locations are shown in Figure 27.

	RH-FJ-02	RH-FJ-03	RH-FJ-07	RH-FJ-08	RH-FJ-11	RH-FJ-12
Sample height [m]	82	81	124	140	113	109
Age [ka]	10.8	9.4	10.6	9.4	3.4	3.6
Uncertainty [ka] (1 sigma)	1.7	1.1	1.3	1.5	0.6	0.6

Mapping and dating of submarine deposits in Fjærlandsfjorden

Several rock avalanche deposits have been identified in Fjærlandsfjorden. The largest is clearly visible on the bathymetric data at Bærrfjøtene (Figure 28), and correlates with the slide scar observed on the mountain side. In seismic lines the deposits can be traced approx. 4 km to the southwest (Bøe et al., 2002). Bøe et al. (2002) examined cores further to the southwest, and estimated an age of <1500 years BP for the avalanche event.

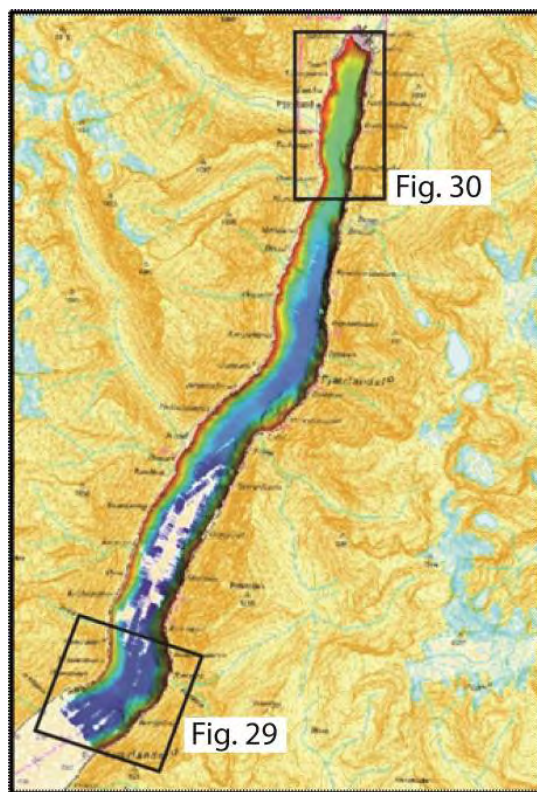


Figure 28. Location map showing the bathymetry data from Fjærlandsfjorden. The white areas with no data are caused by the limited reach of the sonar.

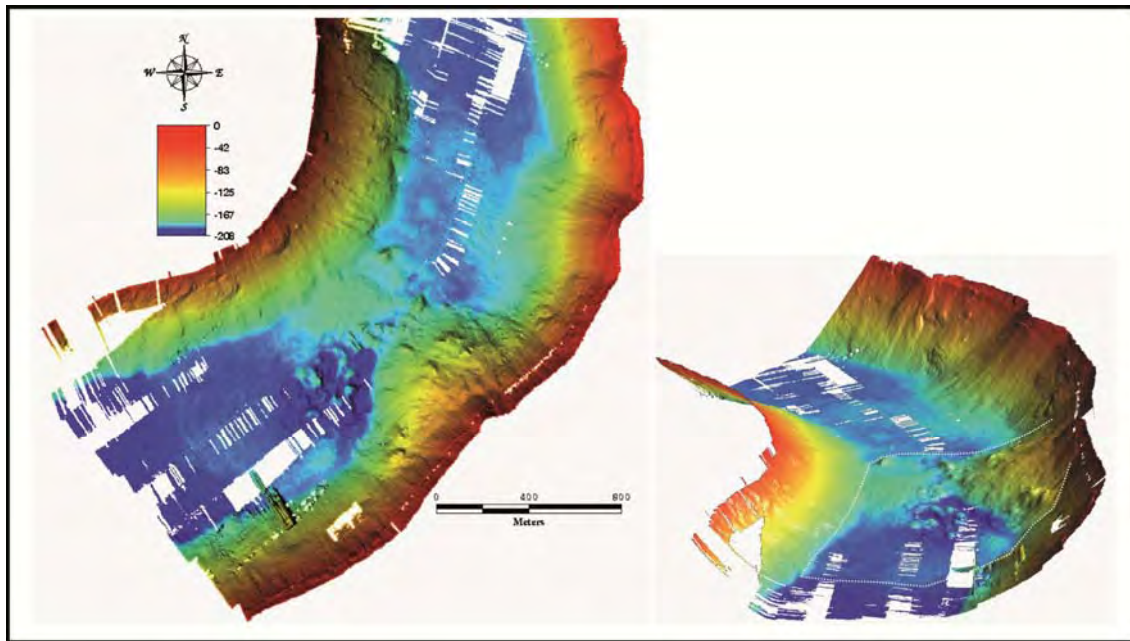


Figure 29. Bathymetry data from the outer part of Fjærlandsfjorden showing the extent of the Berrfjøttene rock avalanche deposits at the fjord bottom. See Figure 28 for location.

The bathymetry data from the inner part of Fjærlandsfjorden shows no distinct signs of rock avalanche deposits (Figure 28). However, channels (chutes) and transverse ridges on the delta slope at the head of the fjord suggest mass flows generated from the outlet of the river Storelvi at the delta rim (Figure 30).

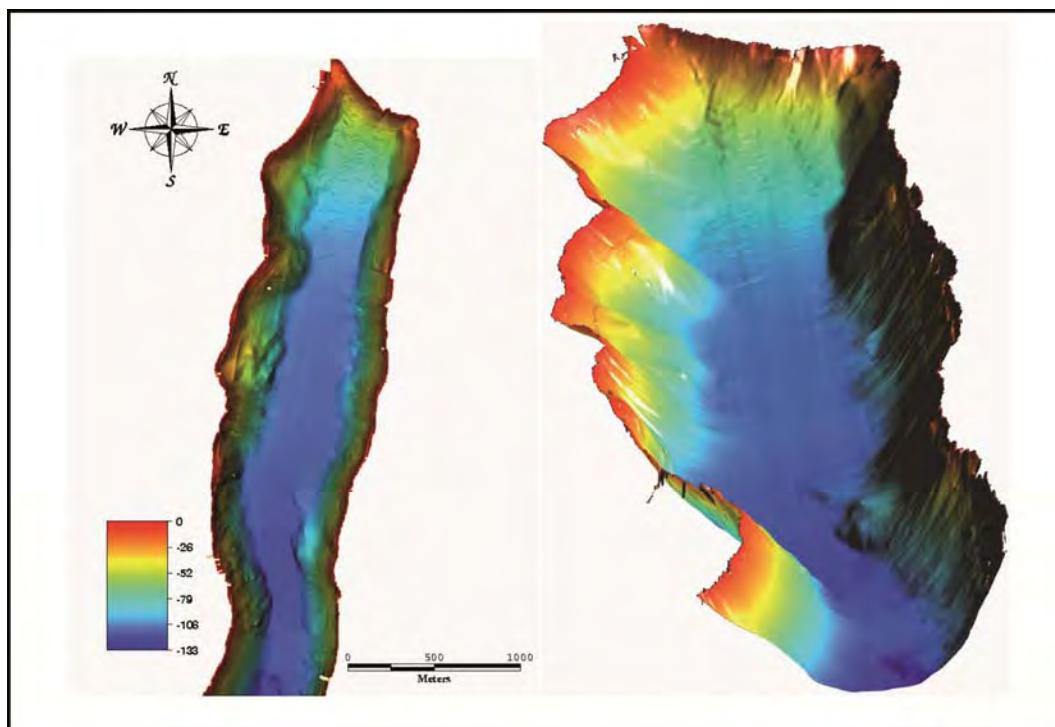


Figure 30. Overview (left) and 3D-view (right) of the inner part of Fjærlandsfjorden showing no visible traces of larger rock avalanches. See figure 28 for location.

Although of rather poor quality, five units have been identified on the seismic data from the inner Fjærlandsfjord, each with a characteristic seismic signature (Figure 31). Unit A is between 5 and 10 m thick, acoustically transparent and with a lobe shape terminating towards SSW. Its lower and upper boundary is flat and slightly undulating, respectively. Unit B is also acoustically transparent, with an upper boundary that is undulating and erratic. The lower boundary is not visible on the seismic data. Unit C is a few metres thick, and consists of a laminated seismic signature. The unit appears to be truncated by unit B. Unit D has a transparent to slightly laminated seismic signature. It is up to 10 m thick, and wedges out towards SSW. It cannot be followed towards NNE towards the fjord head delta. Unit E is the uppermost unit and is from a few to 6-7 metres thick. It thins towards SSW, and consists of a laminated seismic signature.

Judging from their characteristic shape and internal signature, units A, B and D probably consist of slide deposits. The erratic boundary of unit B and the truncation of adjacent units suggests that this unit may be the result of a rock avalanche (Bøe et al., 2002). The transparent signatures and lobe/wedge shape of units A and C, respectively, may suggest that these are debris flow deposits originating from NNW. Units C and E appears to be dominated by hemipelagic deposition within the fjord as suggested by their laminated seismic signature.

Establishing an age estimate of the inferred slide events is difficult based on the seismic data alone. However, the uppermost unit (unit E) probably represents a Holocene succession. It is possible that unit C also belongs to the Holocene (early). However, based on other regional studies (Bøe et al. 2002; Longva et al. 2009), it is also possible that this unit is of pre-Holocene age. Units A and B is interpreted as of pre-Holocene age, thus, it follows that the slide events causing the deposition of these units must be of pre-Holocene age (see above). This interpretation fits well with the dating of Øyrahagstolen rock avalanche deposit above, and that this deposit is underlying the entire delta at the northern tip of the fjord.

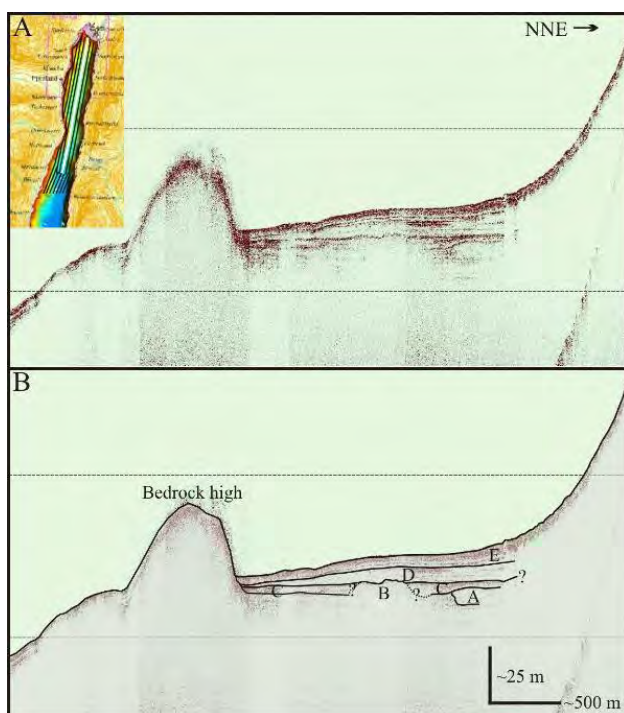


Figure 31. Seismic line (08050670) from the inner part of Fjærlandsfjorden. A) Raw-data, B) Interpretation.

3.3.7.2 Locality Skrednipa - Fjærland

The Skrednipa instability was detected from aerial image analyses and is located on the west side of Fjærlandsfjorden, a northern branch of the Sognefjorden.

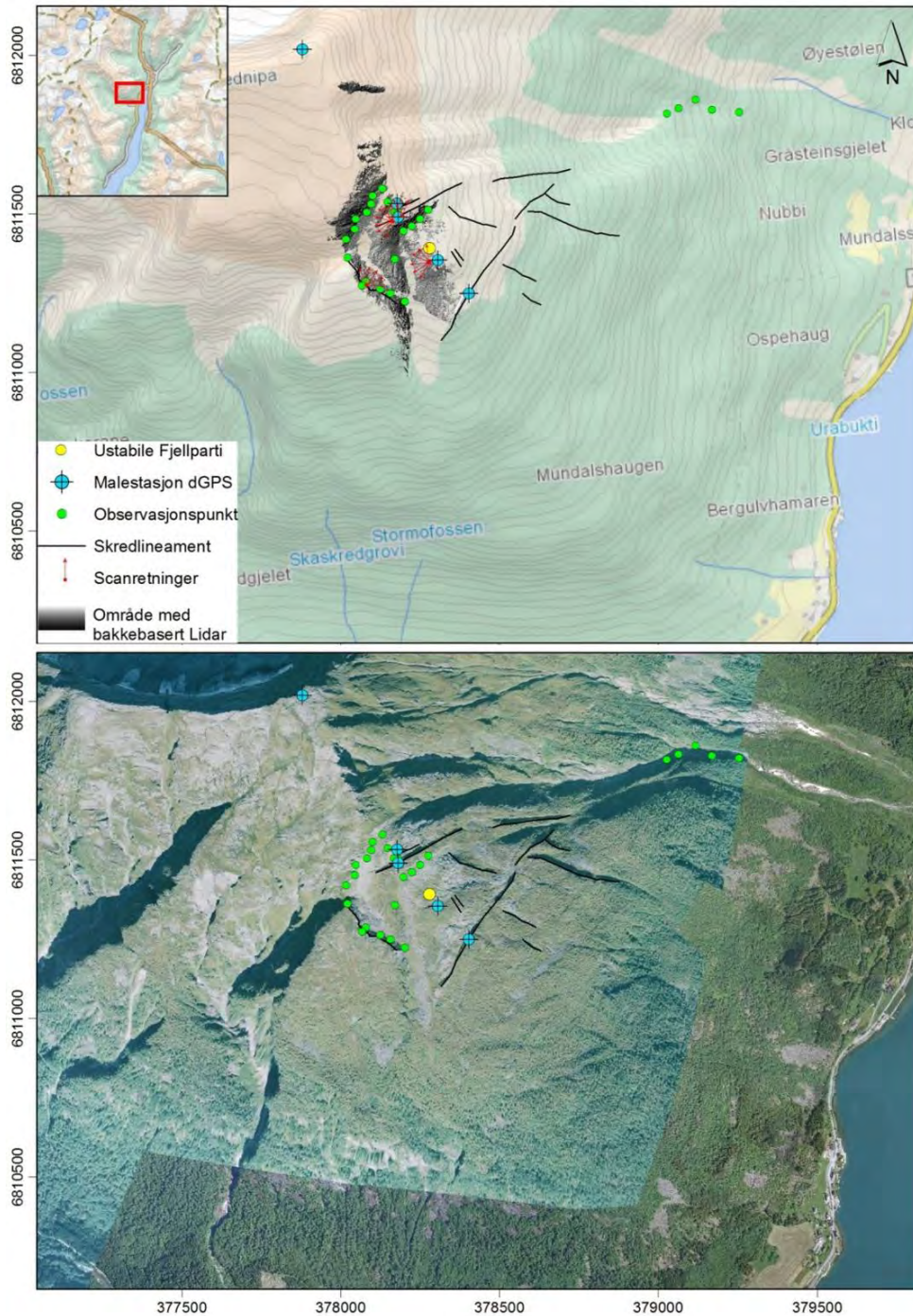


Figure 32. Overview of the unstable site Skrednipa in Fjærlandsfjorden, showing the dGPS points, areas with TLS data and the locations of manual structural measurements. Fjærlandsfjorden is visible in the lower right part of the image, with roads near the shore to give a sense of scale.

Mapping

Overview mapping of the different blocks was performed based on 2D and 3D-views of orthophotos (Figure 32). The unstable slope consists of different blocks with large vertical offsets (Figure 33 and 34), which are separated by distinct sliding planes, developing laterally distinct gorges. The lower boundary of this possible unstable slope is not yet detected. The main lithology in this area is dioritic to granitic gneiss.

The main work performed at this location consists of mapping, structural geological analyses, dGPS measurements, and TLS data acquisition.



Figure 33. Frontal view of the unstable part of the Skrednipa mountain, showing several large, vertically displaced blocks.



Figure 34. Lateral view of the topmost part of the unstable area of Skrednipa. Several large, displaced blocks as well as a distinct sliding plane at the back scar are visible.

dGPS results

Four dGPS points were installed in summer 2009 and repetition measurements have been performed for the first time in summer 2010. One fixed point (SK-FP) is located in presumably stable bedrock; the other three points (rover points, SK-1/SK-2/SK-3) are located on potentially unstable blocks (Figure 32). One additional rover point has been installed in 2010.

The results show small, barely significant movements in N-S direction for two of the points (Sk-2 and SK-3) (Figure 35). SK-2 shows 4 mm horizontal and 3 mm vertical displacements. The vertical displacement is within uncertainty margin. Similarly, SK-3 has a horizontal displacement of 4 mm. As the measurement interval is only one year, the results are uncertain and further repeated measurements have to be performed to allow confident interpretations on possible displacements.

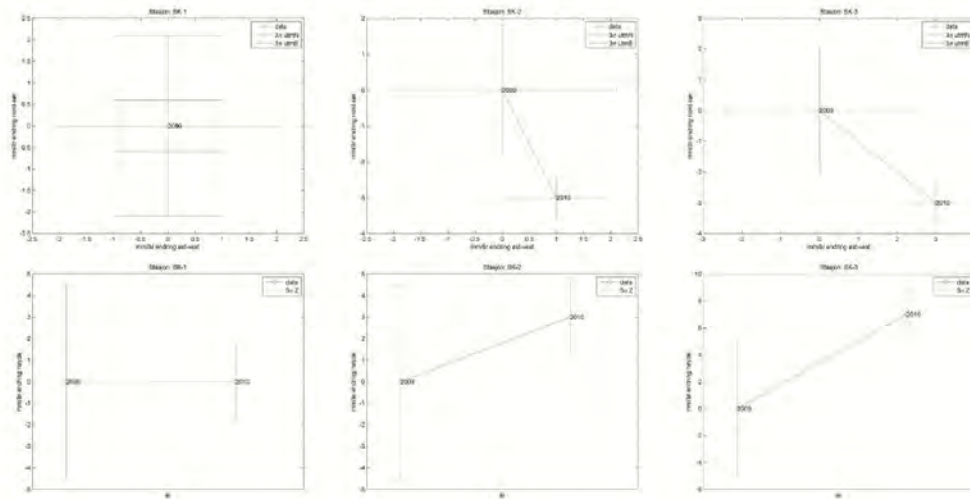


Figure 35. dGPS measurements: the upper row shows the horizontal displacements at each point, the lower row shows vertical displacements.

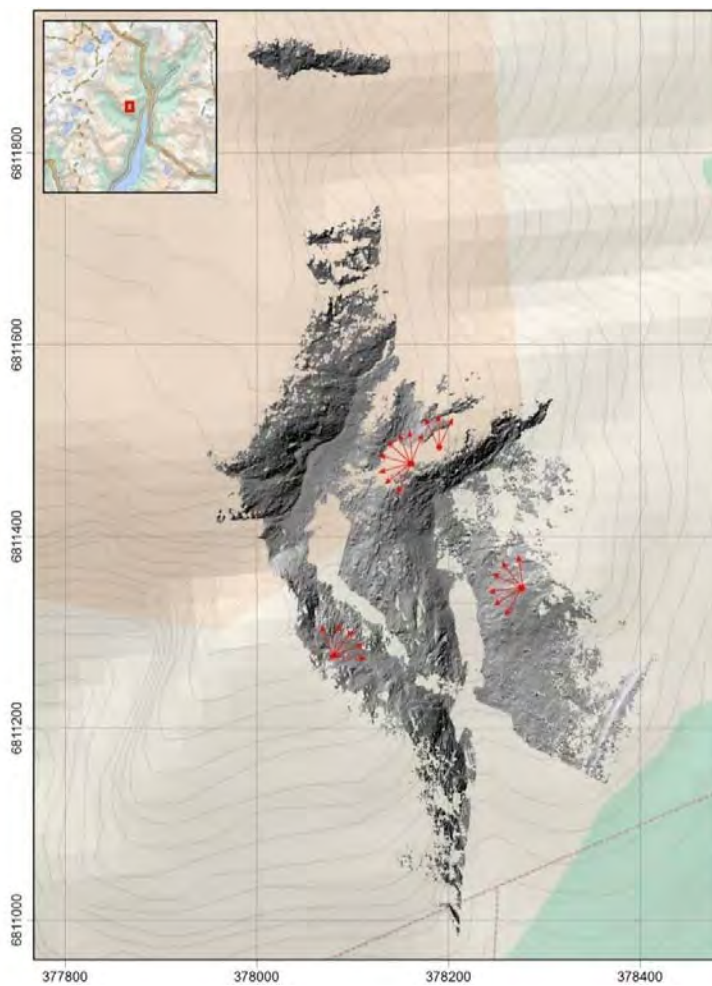


Figure 36. Hillshade of the 2010 TLS-DEM of Skrednipa. The scan positions and directions are indicated (red arrows).

TLS results

The unstable rock slope Skrednipa on the NW-flank of Fjærlandsfjorden was scanned by TLS on 6 and 7 September 2010. A total of 22 scans from four viewpoints on the unstable slope were acquired (Figure 36). The cleaned and unified point cloud is composed of 21.7 million points (average point spacing: 5.8 cm at a mean distance of 163 m). A high-resolution DEM with a cell size of 25 cm was created from the 2010 TLS point cloud (Figure 32, 36).

This point cloud was used for the extraction of planes for structural analyses and presents a first data set for multi-temporal topographic analyses.

Mapping on land

Geological structures have been measured manually at different locations on the unstable site (Figure 32) and extracted from the TLS point cloud. Two different joint systems and a foliation were observed. Figure 37 shows the orientation of these geological structure systems at different locations in the upper part of the slope, and Figure 38 the orientation in the lower north-eastern part of the slope. The foliation as well as the joint sets show slightly different pattern in the different blocks. But generally, the foliation as well as the joint sets are with approx. 45-90 degrees relatively steep. This is consistent with the observed steep offsets between the main blocks (cf. Figure 34).

Additional structural geological measurements have to be performed in the lower southern part of the slope to get information about possible sliding planes. A detailed kinematic analyses of the structural data will be completed as soon as all basis data are available and will be reported in the next report.

Recommendations

- Continuation of the dGPS measurements on an annual basis for the next years
- Additional structural measurements in the lower southern part of the slope and more detailed analyses of the lower boundary of the unstable slope
- Detailed volume and morphometry estimation based on aerial laser scanning data when it will become available
- Age dating on the sliding planes for displacement rate assessment

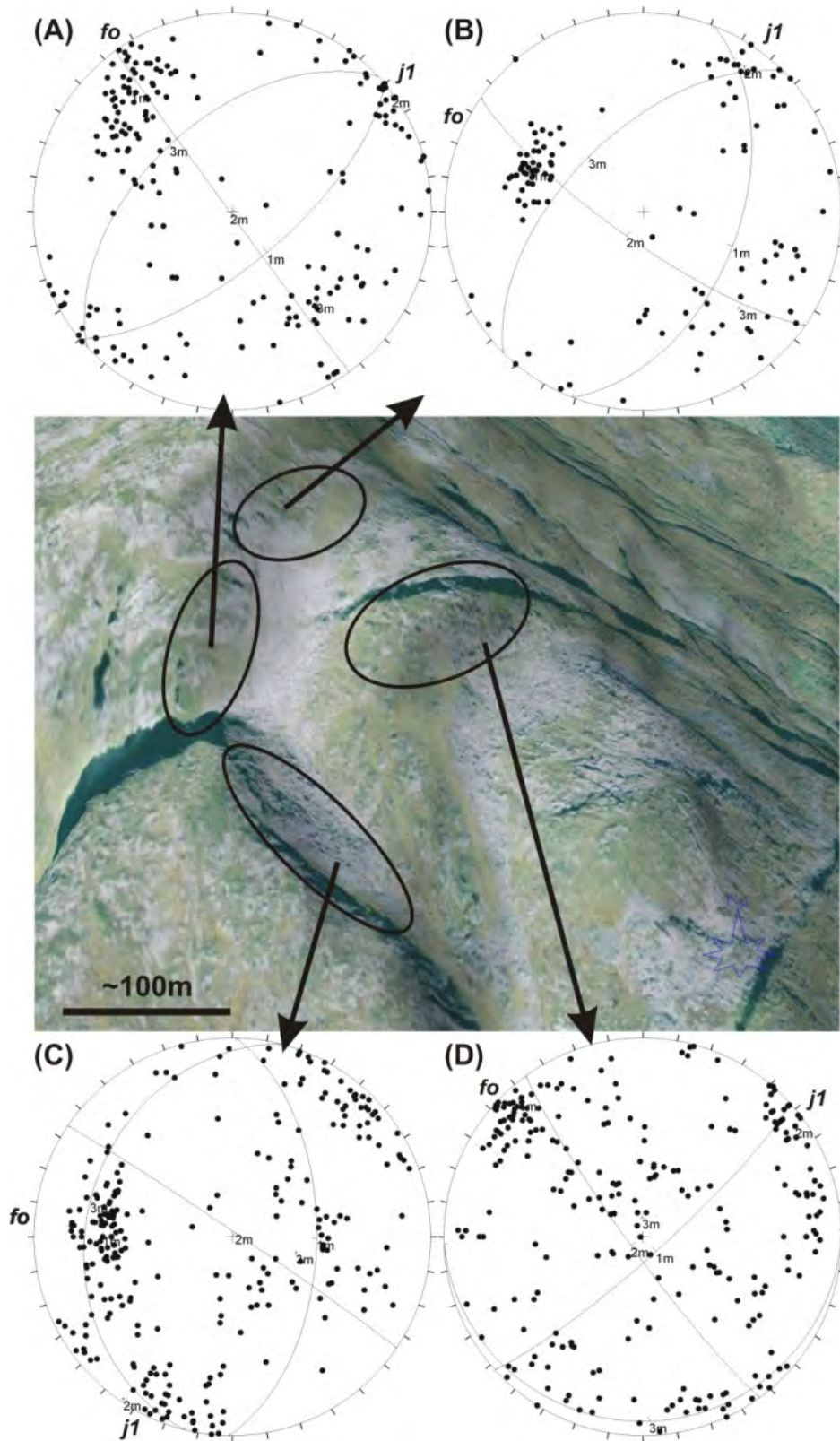


Figure 37. Lower hemisphere stereonet showing the poles of all structures measured at different sites in the field and extracted from the TLS point cloud a detailed analyses including kinematic analyses will be carried out after field season 2011 when all data are available.

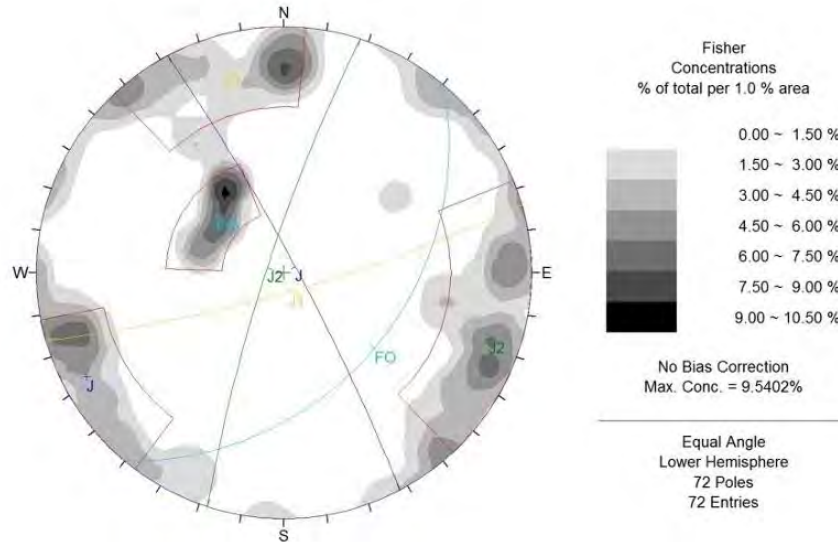


Figure 38. Lower hemisphere stereonet showing the poles of all structures measured in the channel at the lower N-E-part of the slope.

3.3.8 Vik municipality

3.3.8.1 Locality Ovrís valley

Mapping

A rockslide in phyllitic basement rock was discovered and mapped in detail in the upper Ovrís valley in the 1960's (NGI F. 299, 1966). This rockslide is clearly delimited by a back crack to the NW several metres deep and 0.5 to a few metres wide, a lateral crack more than 20 m deep towards the north, and several other cracks 0.5 to several metres wide. Towards the SE the block ends into a nearly vertical cliff approx. 50 m high. The block has a surface of 16.000 m² and is approx. 60 m thick resulting in a volume of approx. 10⁶ m³ (Figure 39). The smooth surface of the block suggests a massive, poorly fractured block as no cracks can be seen within the intact vegetation. Extending from the lateral crack, a depression and crack a few decimetres wide and a maximum of a few metres deep run parallel to the slope for several tens of metres towards the northeast. The foliation dips slope parallel moderately to steeply (NGI F. 299, 1966).

In addition, hummocky deposits below a approx. 50 m high back scar (NW limitation) and lateral scar (NE limitation) were interpreted as the deposits of a postglacial rock avalanche deposit with a volume of approx. 6 x 10⁶ m³ (NGI F. 299, 1966). Our mapping activities could not confirm this interpretation. This is mainly suggested by the lithology of boulders covering the hummocky deposits. Instead of phyllite, most of these boulders are of gneissic composition and therefore of a rock type that does not crop out on the entire slope (Figure 40). In addition, in contrast with boulders on rock avalanches these boulders are well rounded and only cover the hummocks sparsely.

Furthermore, several forest roads have been constructed on the slope since 1966; some of them exposing bedrock along the road cuts. At all these cuts the surficial cover of the basement has been in the order of a few decimetres and no angular rock avalanche material

could be found (Figure 41). Therefore, we rule out a postglacial rock avalanche for that site and suggest that the obvious scar is due to a rockslide that deposited onto the glacier and has subsequently been removed. The slide event may even have occurred prior to glaciations.

Using the relation of run-out distance over height (difference rock avalanche source-rock avalanche deposit) versus the rock-avalanche volume, as suggested by Scheidegger (1973), we estimated the run-out distance for a potential catastrophic failure of the unstable block for a scenario where the entire block would fail in a single event. This is a rough estimate and does not represent a real run-out analysis, as factors as terrain roughness related to the hummocky deposits are not taken into account. However, this rough estimate suggests that avalanche from the collapse of the block in a single event would reach the farm and would nearly reach down to the valley bottom (Figure 39).

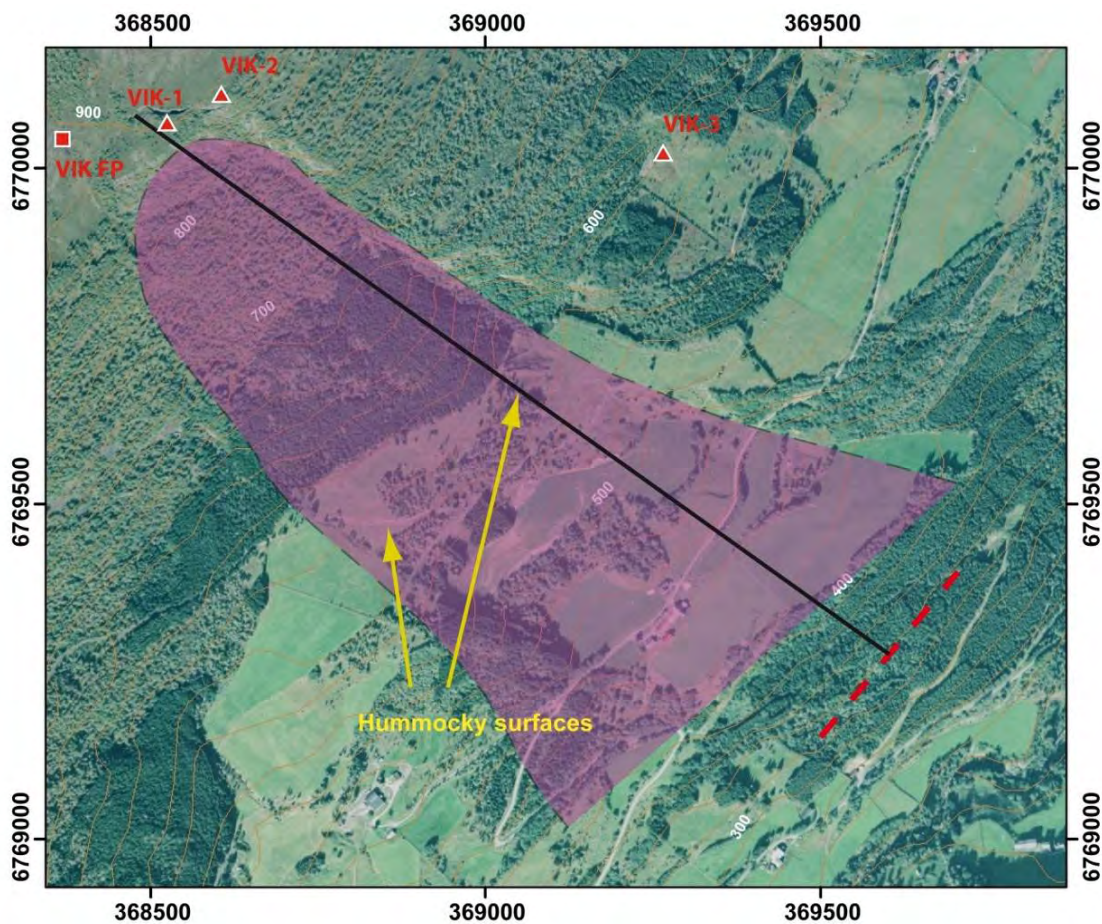


Figure 39. Overview map showing unstable area (block delimited by cracks in top right corner) and potential run-out area calculated after Scheidegger, 1973 (limit is given by dashed red line). The map also shows the area proposed for post-glacial rock-avalanche deposit (purple area) following NGI rapport 76459-1 (1966) and the location of fixed and rover points used for deformation measurement. The nature of this deposit as rock-avalanche deposit has not been confirmed by our recent mapping activities. Instead we describe this area as a late glacial deposit not related to any rockslide activity.



Figure 40. Well-rounded boulders sparsely covering hummocks on the middle and lower slope are composed of a lithology allochthonous to the slope, suggesting that these deposits represent glacial deposits and not deposits related to a post-glacial rock avalanche as suggested in NGI rapport 76459-1 (1966).



Figure 41. Phyllitic bedrock with a constantly dipping foliation over the distance of several tens of metres covered by a thin cover of soil. This supports that no post-glacial rock avalanche has occurred.

dGPS results

Deformation measurements using fixed installed metal bolts have been carried out to document the opening in the late 1960's and early 1970's resulting in opening velocities of the crack of maximum approx. 5 – 14 mm/yr (NGI 76459-1, 1976). In 1985 and 1988,

measurements of the bolts have been repeated and resulted in opening velocities of 11 mm/a (Statens Kartverk 611.2, 1988). In 2008 we could only locate one of the metal bolts. Others might have fallen into the opening cracks or are overgrown with vegetation. In 2008 we therefore installed one fixed point on the plateau behind the back crack, and 2 rover points (VIK-1) on the block and (VIK-2) between the NE-trending cracks. An additional rover point (VIK-3) was installed along the lower slope section in 2009. The point is located on a large boulder that seems to be stable as it lies on a flat part of the slope. Data from this point will allow us to verify if deformation spreads along the slope.

Results of the measurement indicate that the unstable block in the Ovrís valley is moving with a velocity of 15 mm/a towards the southeast, and also 15 mm/a in the vertical in the past two years (Figure 42). This is the upper limit of movement velocities measured in the 60's and 70s' and above the yearly average from the 80's. Rover point VIK-2 has no significant displacement and rover point VIK-3 has a significant displacement in the period 2009-2010, however, the displacement suggest upslope movement that cannot be interpreted as displacement in relation to gravitational forces. The dGPS data rather suggests that a slight acceleration of movement is occurring and that the block is not stabilizing. Displacement beyond the limits of the blocks cannot be detected.

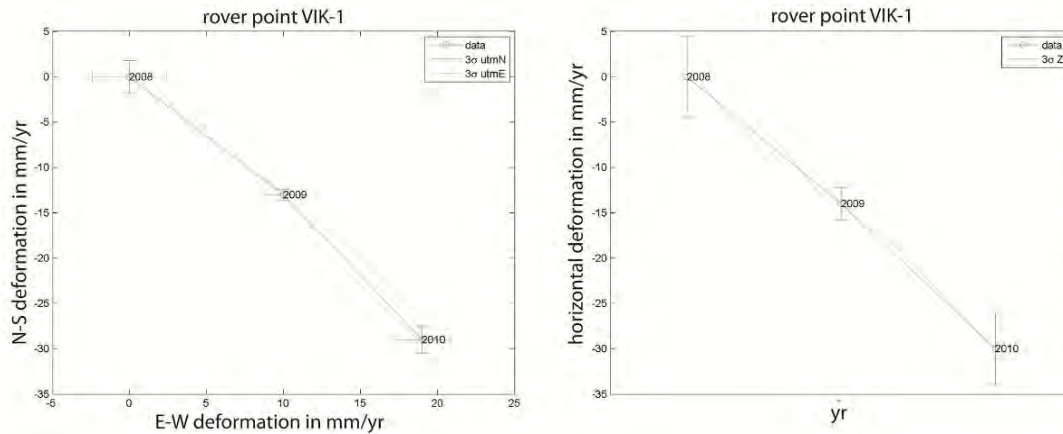


Figure 42. Rover point VIK-1 documents a horizontal movement of 15 mm/yr towards SE and 15 mm/a vertical movement downslope of the unstable block in Ovrís valley.

Terrestrial laser scanning

The Ovrís valley instability was scanned on 10 July 2009 from four viewpoints in the SW of the instability (Figure 43). After vegetation removal, the TLS point cloud is composed of 1.9 million points with an average spacing of 4.1 cm at a mean distance of 309 m. The TLS dataset was treated and analysed by the University of Lausanne, Switzerland (Carrea et al., 2010; see Appendix 2, p. 33-35) with the goal to perform a structural analysis of the exposed SW-facing cliffs.

Because of high vegetation density and long distance between the TLS scan position and the cliff, the TLS point cloud covers only the front of the Ovrís valley instability and the lateral release surface of the potential glacial-preglacial rockslide.

The structural analysis in Coltop3D revealed four main discontinuity sets (Figure 44). The kinematic feasibility tests for the front of the Ovrís valley instability (slope orientation: 160°/63°) show that planar sliding on J4 (130°/60°) is the most likely failure mechanism.

Toppling failures can occur along the subvertical J3 ($015^{\circ}/88^{\circ}$), and wedge sliding formed by the intersection of J2 ($288^{\circ}/70^{\circ}$) and J4 is partly possible (Figure 44).

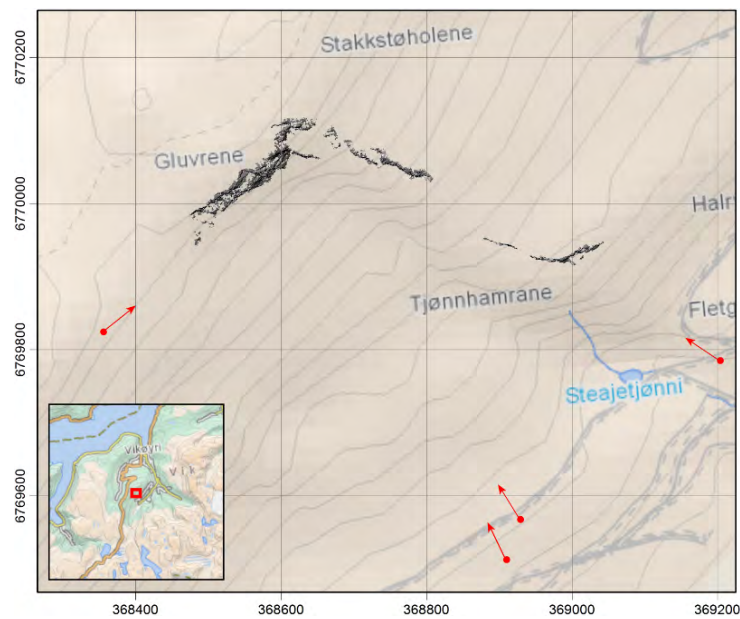


Figure 43. Hillshade map of the TLS-DEM showing the front of the Ovrís valley rock slope instability, the SW-facing lateral release surface of a former rockslide, as well as the TLS scan positions in 2009 (red arrows). Coordinates are in UTM32N.

The TLS point cloud was georeferenced using the GPS coordinates of the scanner positions and a 25 m DEM. The dataset should be re-georeferenced as soon as a high-resolution DEM is available, which will likely modify the orientation of discontinuity sets. Nonetheless, the interpretation of the kinematic feasibility tests (Figure 44) remains valid, because they are based on the geometric relationship between the discontinuity sets and the slope orientation.

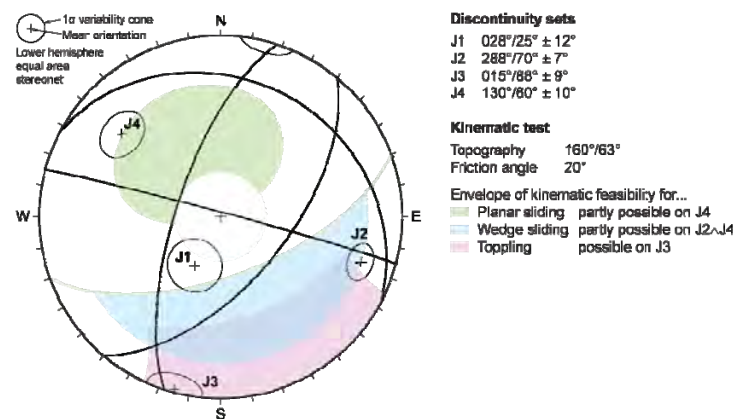


Figure 44. Stereonet of the main discontinuity sets at Ovrís valley based on the Coltop3D analysis of the 2009 TLS point cloud (modified from Carrea et al., 2010). The kinematic feasibility tests for planar and wedge sliding, as well as toppling failure are shown.

Recommendations

Due to the continuous movement of this block, which was the fastest deformation recorded since 2008 in Sogn og Fjordane, we recommend to follow up with more detailed studies in order to find out 1) if the block is moving as a single continuous block, 2) what is the property of the deformation zone along the base of the block, and 3) to analyze run-out scenarios based upon high-resolution airborne laser scanning (ALS) data. These ALS data became available in 2011 and will help to better map in detail the block and are the ideal data source for a detailed run-out analysis. Furthermore, dGPS measurements should be continued on a yearly basis and a further rover point should be set out on the southwestern end of the block in order to better understand slide kinematics. Based upon those additional data and a hazard and risk classification to be carried out in 2011, the need for further follow up such as continuous monitoring and early warning has to be assessed.

The 2009 TLS dataset should be re-georeferenced using a new high-resolution DEM in order to be able to compare the Coltop3D measurements with field investigations. New TLS acquisitions at the Ovrís valley instability are planned in 2011 or 2012 for detecting possible displacements and rockfall activity.

3.3.8.2 Localities Framfjord, Arnafjord, Øvstedalshaugen, Hamnaskredene

Mapping from helicopter

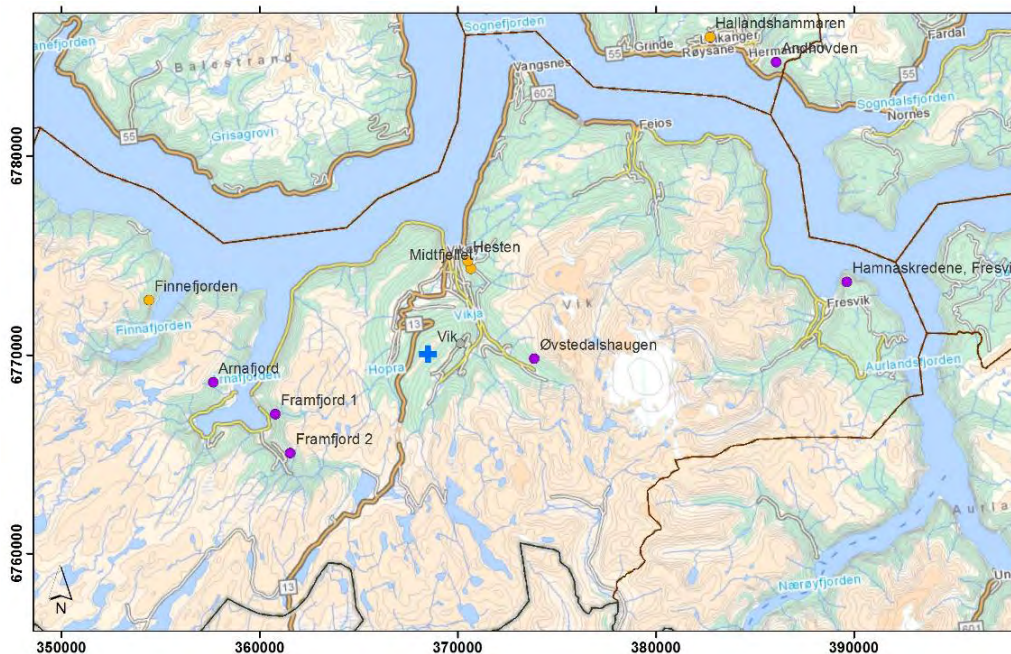


Figure 45. Overview: The sites in the Vik community that were investigated on a reconnaissance flight by helicopter in 2010 are marked in purple.

Reconnaissance work from a helicopter has been performed in September 2010 to make a first investigation on possible unstable or critical sites that were indicated from the county geologist B.F. Russenes and mentioned in the 2008 report. The five sites will be briefly described in the following based on photo documentation.

Hamnaskredene, Fresvik

In the Hamnaskredene area (Figure 46, 47, 48), only rock falls but no large slope instabilities could be observed. The south-facing side, in particular, shows pronounced joint sets and is strongly fractured. It shows some small, freshly detached areas and quite pronounced scree talus at the foot of the rockwall. However, we consider them to be mainly accumulated by continuous small-volume rock fall and not to be caused by a large-volume slope instability. One rockfall event was reported in 1950 and documented on skrednett.no, which destroyed some buildings and reached the fjord. This site is not a large unstable slope that could evolve in a major rockslide. No further investigations will be performed within this NGU project. In any case, would we recommend consulting the online susceptibility map for rock fall ([http://www.ngu.no/kart/skrednett/?map=Steinsprang – aktsomhetskart](http://www.ngu.no/kart/skrednett/?map=Steinsprang%20-%20aktsomhetskart)) and to consider producing a rockfall hazard map for that slope.



Figure 46. Approx. location of the remotely investigated Hamnaskredene site close to Fresvik.

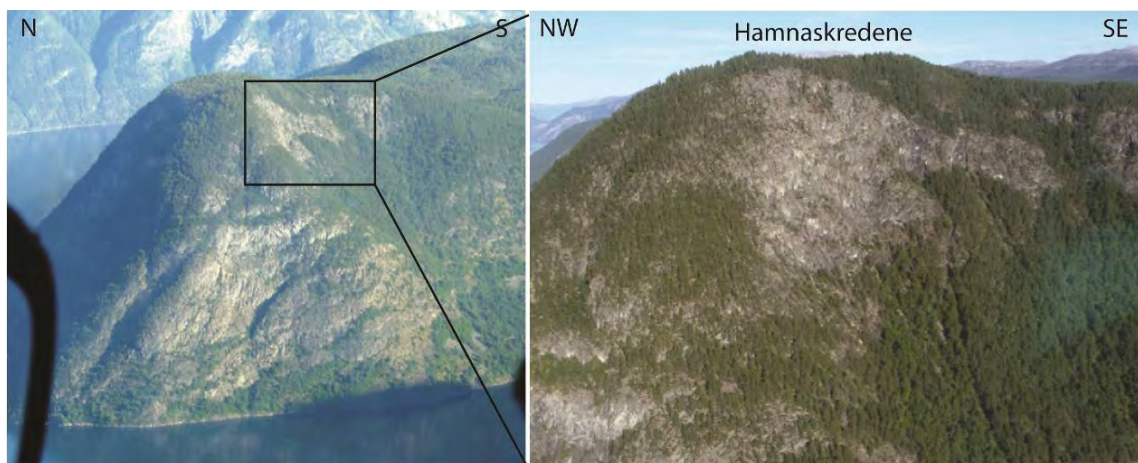


Figure 47. West-facing (left) and south-facing (right) side of the Hamnaskredene site.



Figure 48. South-facing (right) side of the Hamnaskredene site with some rock fall signs (some major tracks are marked with arrows). The detachment zone of the 1950 rock fall is probably located in the red marked area.

Øvstedalshaugen, Vik

The location of the remotely investigated Øvstedalshaugen site is situated in the Seljedalen (Figure 49). No signs of an existing large unstable bedrock area were found from the helicopter survey. In some steep riverbeds, where bare bedrock occurs, minor rockfall activity can be observed (Figure 50, lower right photograph). No historical rockfall or rock avalanche is documented on skrednett.no. This site does not need any further investigation within this project.

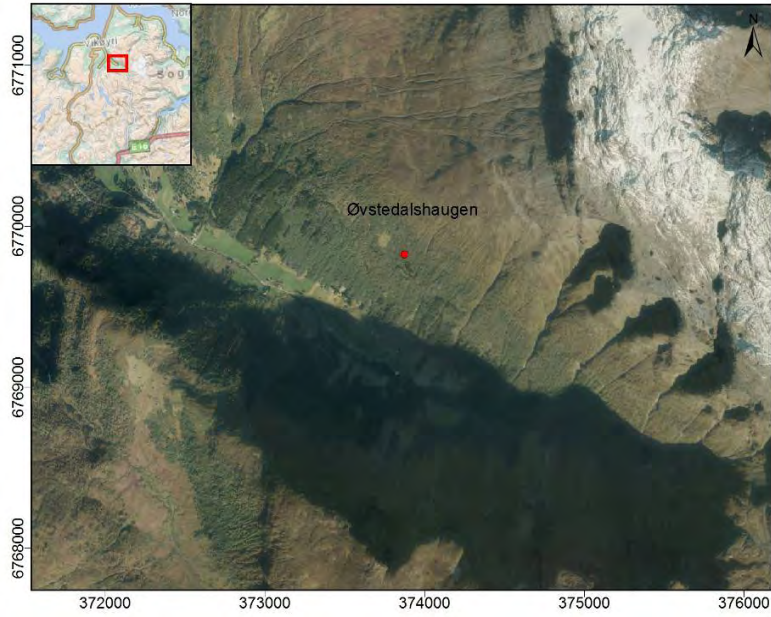


Figure 49. Location of the remotely investigated Øvstedalshaugen site. The whole area was inspected with a helicopter survey.

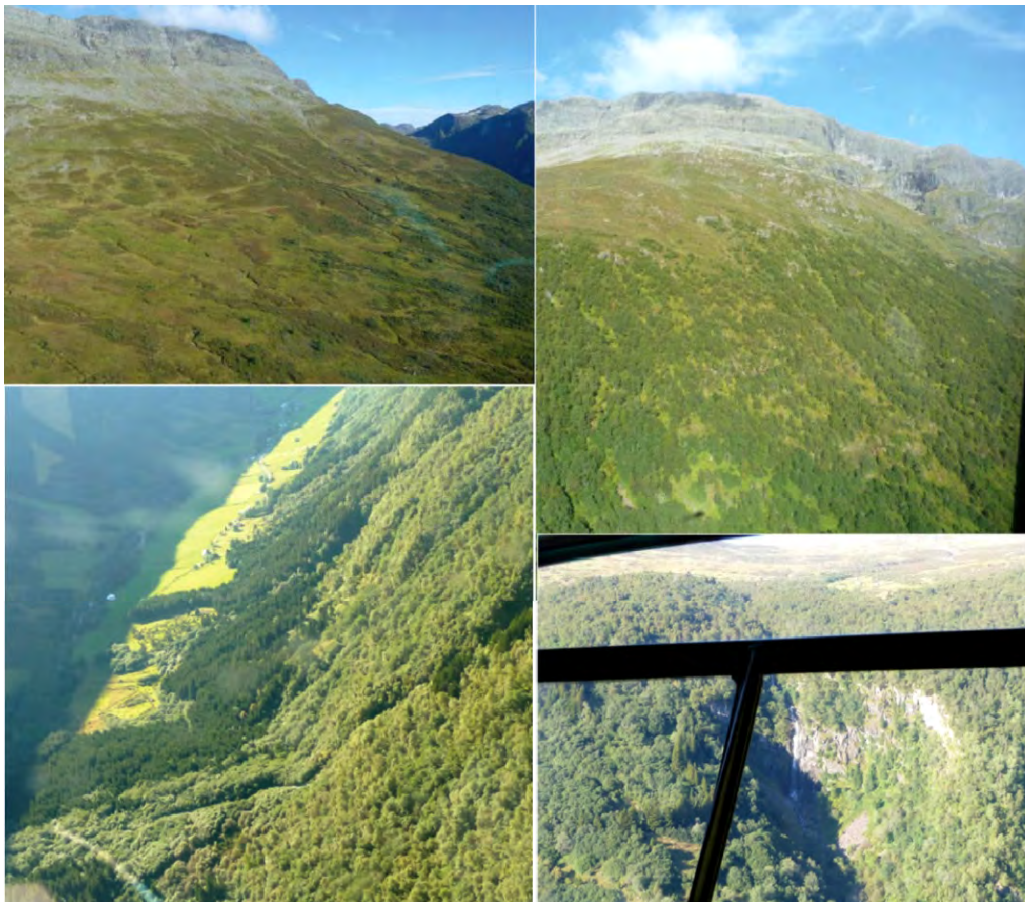


Figure 50. Overview over the Øvstedalshaugen in Vik municipality. Only a few locations show moderate rock fall activity (eg. Gray rock area in lower right photograph).

Framfjord

Two slopes were indicated by the county geologist, B.F. Russenes, that should be investigated (Figure 51). No obvious signs of an existing large unstable bedrock area were found from the helicopter survey. However, there were some tracks and deposits of old bedrock instabilities and a probable old rock avalanche scar is visible. Old rock fall events have been reported on skrednett.no, probably coming from the very steep rockwalls above the farms Le and Hola. The Framfjord area has to be investigated in more detail during the next years (Figure 51).



Figure 51. Location of the remotely investigated Framfjord site. The positions of the two red dots are representative of the whole slope, as the whole area was inspected.

Arnafjord

A rock slope collapse occurred in Arnafjord in 1811, killing 45 persons and destroying large parts of the village Arnafjord. The rock avalanche detached at an elevation of about 700 m a.s.l in the area Vardeheii below the Skarshella i Skarshellebakken.

From the helicopter reconnaissance and also from aerial image analyses, no clear signs of large instabilities can be observed (Figure 52). However, there are tracks visible from recent rockfall, debris flow and snow avalanches (Figure 53). Therefore, this site will be investigated in more detail the next years.

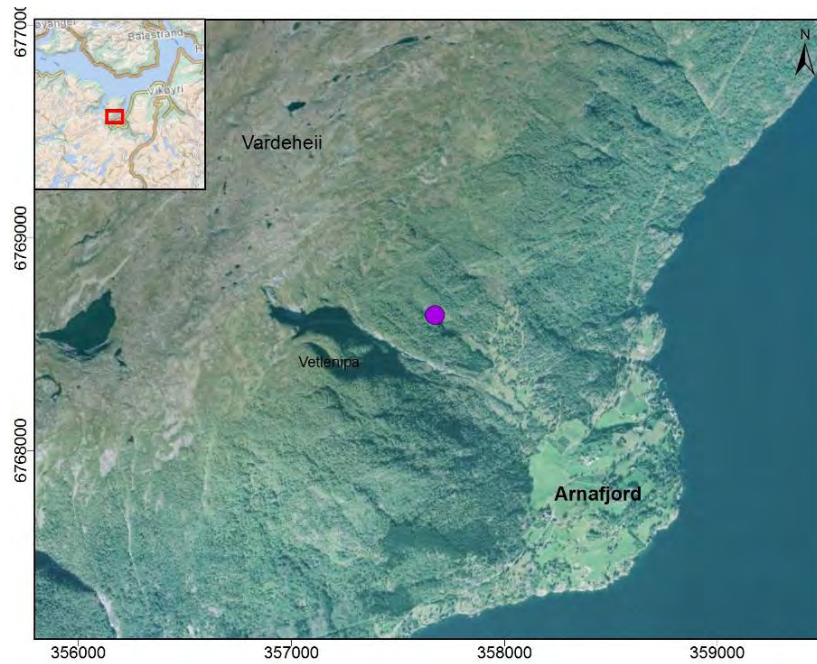


Figure 52. Location of the remotely investigated slope at Arnafjord.

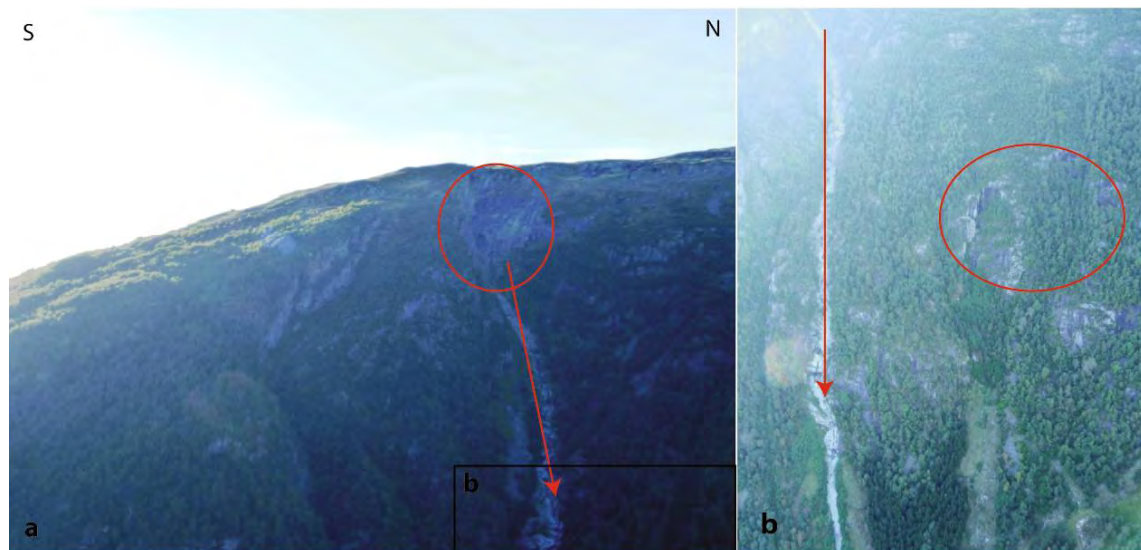


Figure 53. Detachment zones of old rock slope failures (red circles) as well as an active snow avalanche and probably also debris flow channel (red arrows) can be observed.

Recommendations

- The sites at Framfjord and Arnafjord will be investigated in more detail by NGU
- The slope around Øvstedalshaugen does not need any further investigation
- The Hamnaskredene area in Fresvik will not be further investigated by NGU as it is not a large slope instability. The rockfall activity, however, should be observed by the authorities.

3.3.9 Leikanger municipality

3.3.9.1 Locality Anhovden

Mapping

The site is located along the RV55 road between Hermansverk and Sogndal. It is close to the Caledonian thrust front and the rocks are strongly foliated mylonites, blastomylonites and mylonitic gneisses (Figure 54).

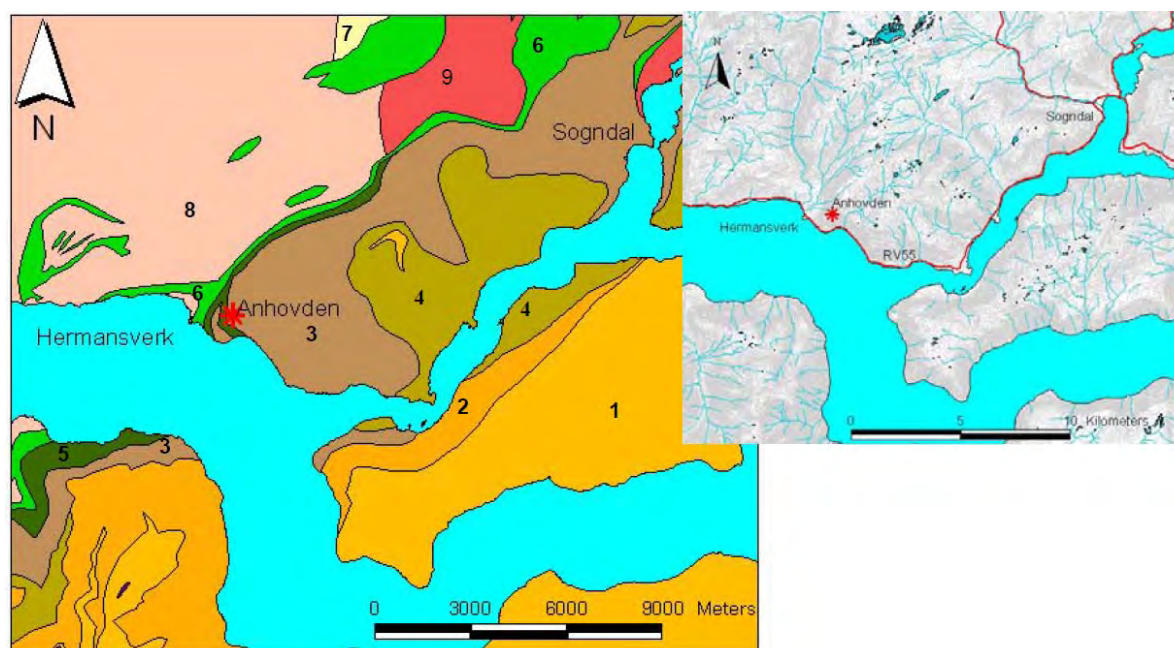


Figure 54. Bedrock geological map of the Leikanger-Sogndal area, extracted from the digital bedrock map 1: 250 000 Årdal (Lutro & Tveten 1996). Units 1- 4 are allochthonous rocks of the Jotun Nappe, units 6- 7 are Cambro-Silurian allochthonous rocks, units 8-9 are autochthonous Precambrian basement. 1: Anorthosite, leucogabbro and anorthositic gneiss, 2: Pyroxene granulite, gabbro, 3: Pyroxene granulite, gneiss of gabbroic to quartzmangeritic composition, 4: Tonalitic to mangeritic gneiss, in some places mylonitic augen gneiss and amphibolitic gneiss, 5: Mylonites and blastomylonites in Caledonian thrust-zone, 6: Micaschists, 7: Quartz-schists, 8: Autochthonous basement gneiss, 9: Quartz-monzonite

The orthophoto (Figure 54) shows the location of Anhovden and the area covered by the reconnaissance mapping that was carried out at the site in 2008. The site lies close to the Caledonian thrust front, and the rocks are mylonites and mylonitic gneisses with a well developed foliation that dips at a shallow angle (15 -30 °) towards the fjord. An earlier, small rockslide deposit is found in Fatlaviki.

The slope beneath Anhovden is dominated by rockfall-talus (Figure 55). There are possible rockslide deposits on land (Figure 55, 56) and at the fjord bottom (Figure 56). A likely source for a possible former rock slide is shown in Figure 55.

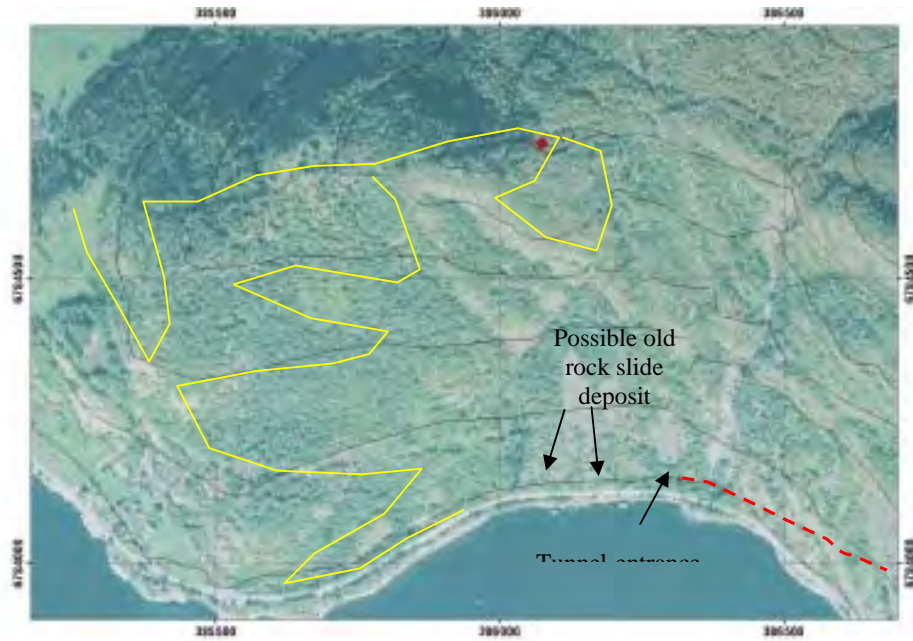


Figure 55. Orthophoto of the Anhovden area. Anhovden is marked by red dot.

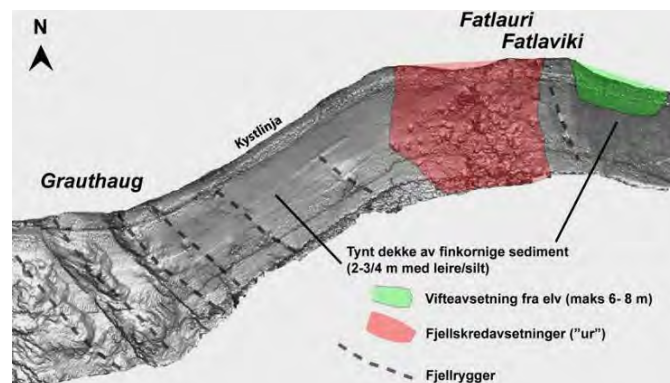


Figure 55. (left): Possible rock-slide deposit along the main road in Fatlaviki. Figure above: shaded relief image from bathymetric data indicating rockslide deposit in Fatlauri (contributed by Lars Blikra, NGU).

There is a high frequency of rock-falls in the area, particularly in the eastern parts where a new tunnel was recently built as a protection for rockfalls. The local rocks are strongly foliated mylonitic rocks with a high fracture frequency. In connection with the construction of the tunnel, a large block of approx. 10 000 m³ above the tunnel entrance was removed by blasting. Some blocks still remain, i.e. at UTM 6784456, 386327 (Figure 59).

The most prominent structure in the rocks is a mylonitic foliation that dips at 15-30° towards the fjord; i.e. south or southeast (Figure 57). In addition there is a network of “old” tectonic fractures with steep dipping NW-SE and NE-SW striking orientation. The NW-SE fractures are the most frequent.

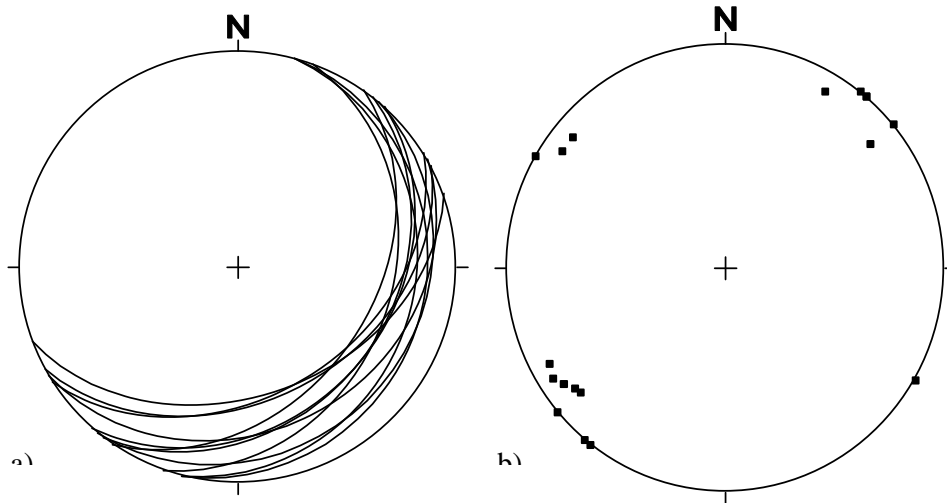


Figure 57. Stereographic plot of foliation planes (a) and poles to tectonic fractures (b)

Smaller blocks may detach from the tectonic fracture surfaces and slide some distance down slope on SE-dipping foliation planes (Figure 58). However, the dip of the foliation is too gentle (Figure 57a) to cause any significant sliding along the foliation planes.



Figure 58. Minor sliding of detached block on foliation plane

The orthophoto (Figure 55) and the reconnaissance mapping reveal no larger obvious structures or combination of structures that may develop into future rockslides.

An open structure/depression is observed at UTM 386146, 6784709. It has a width of 3-4 metres and a depth of approx. 2 metres and is filled with blocks. There is no evidence of active movements along this potential back-fracture. The fracture continues southwards and can also be followed for some distance northwards (Figure 60). Open fractures are also claimed to exist further east, in the area above the tunnel.



Figure 59. View of Anhovden from the south. Arrows indicate the weak open structure discussed above. The western entrance of the new tunnel, which was built because of the high rockfall- activity, is also shown. The red dot could represent the centre of the source area for the small rockslide in Figure 53.



Figure 60. Orthophoto of the tunnel- entrance showing rockfall- talus beneath Anhovden and a larger, partly detached block at 6784456, 386327 indicated by arrow (www.norgebilder.no)

Recommendations

No single structure or combination of structures that might develop into a future rockslide was identified at this site. Smaller blocks may detach from tectonic fracture surfaces and slide some distance downslope on the SE-dipping foliation planes. The potential for some larger rockfalls and possibly small rock-slides further to the east should be examined.

3.3.10 Aurland municipality

3.3.10.1 Locality Flåm (1)

On the unstable area at Joasete, Furekamben, and Ramnanosi significant effort has been spent in the years 2008 to 2010. Therefore, this site was reported separately (Hermanns et al., 2011, NGU report 2011.025), and results and recommendations will not be repeated here. However, since the publication of the report, new cosmogenic nuclide ages became available on lobate deposits not reported in NGU report 2011.025. Therefore, we will report here on those results only and give recommendations based on those additional results.

Dating

Two lobate boulder deposits, determined to have originated at the cliff of the slope, were sampled for surface exposure dating (each three samples) and were dated using the cosmogenic nuclide ^{10}Be (Figure 61, Table 3) in order to test if the boulder deposits are the results of single event or rather the result of long-term rock fall activity from the cliff.

The northern of these lobes reaches down into Aurlandsfjorden, and bathymetric data suggest that the deposit continues on the fjord bottom. This deposit was previously dated by ^{14}C dating of organic material extracted from overlying detritic deposits. The ^{14}C AMS date resulted in a calibrated age of 2,840-2,720 B.P. (Blikra et al., 2006). This age represents a minimum age as the boulder deposit is overlain by the sample. The other southern lobe lies below Furenkamben. This lobe is 500 m long and deposited on the eastern slope of the Flåm valley but does not reach the valley bottom suggesting a reduced mobility of the rockslide. Hence the deposit seems to be the result of several collapses or is even a deposit built up of individual rock fall events spanning a longer time period. Of both lobes three samples were taken from 3 large boulders 4 to 12 m in diameter.

Table 3. Ages of obtained by ^{10}Be cosmogenic nuclide dating on samples in Flåm valley and sigma 1 uncertainty levels. Sample height is measured by altimeter with 1 m resolution, sample locations are shown in Figure 61.

	R-FL-01	R-FL-02	R-FL-03	R-FL-05	R-FL-06
Sample height [m]	92	115	126	135	166
Age [ka]	4.3	3.8	3.5	2.3	11.5
Uncertainty [ka] (1 sigma)	0.6	0.5	0.5	0.3	1.5

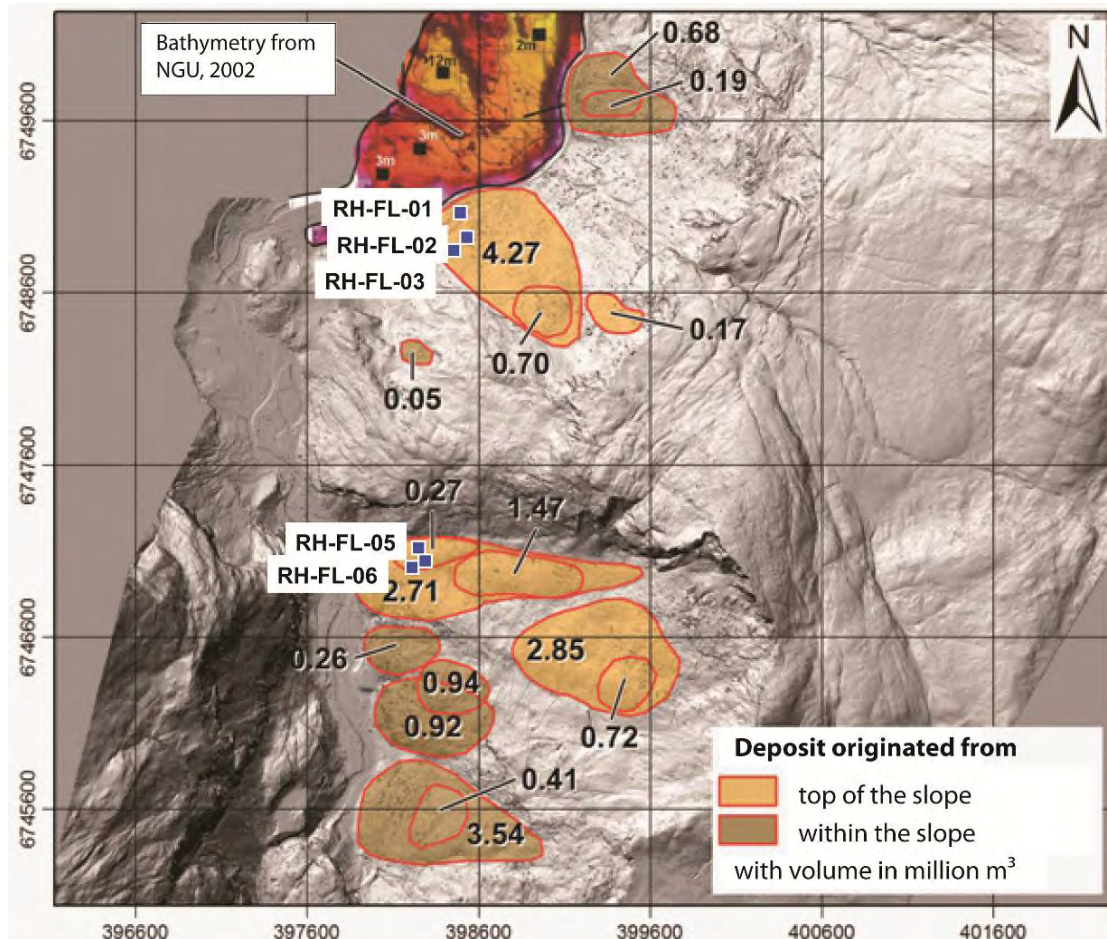


Figure 61. Map of rockslide deposits in Flåm valley and Aurlandsfjorden showing location of sample sites (after Hermanns et al. 2011)

Of those six samples, only five (three of the northern and two of the southern) samples provided enough quartz so that the sample could be dated successfully. Ages of individual boulders of the northern lobe agree well within uncertainty limits and also agree with the ^{14}C age of sediments of overlying the deposit (Tab. 3). These results suggest that this deposit indeed is the result of a single catastrophic failure that reached down into the fjord. Both ages of boulders on the southern lobe do not coincide within error margins but have very different ages. The spread of ages suggest that these boulders were not deposited at the same time. However, as pre-exposure of boulders of rockslide deposits is feasible, which would result in an overestimate of the age, (Ivy Ochs et al., 2009) the difference in age can only be taken as a preliminary result.

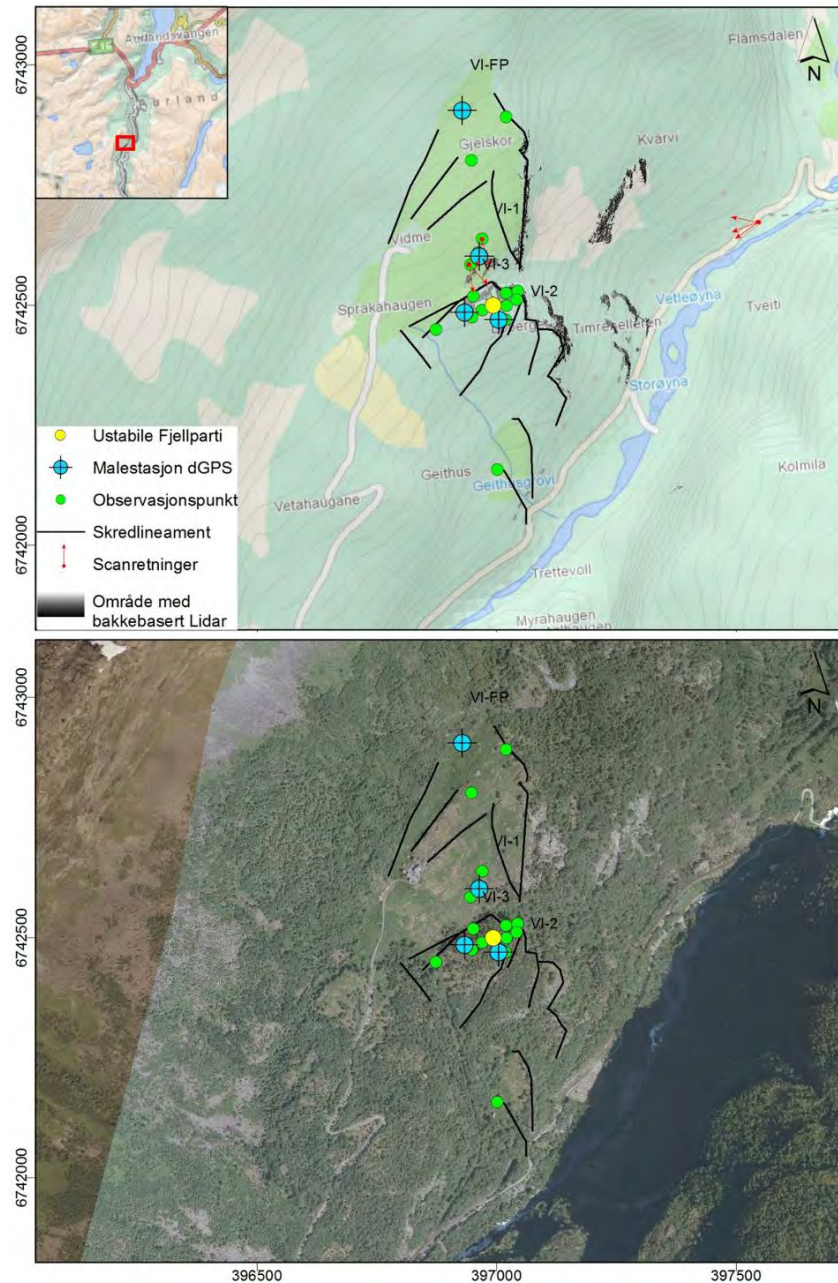
Recommendations

For recommendations we refer to the previously published report (Hermanns et al., 2011). In addition, we recommend taking at least one, or perhaps two, further samples on boulders from the southern lobe in order to test the preliminary interpretation that this deposit is built up by rock falls spanning several thousand years.

3.3.10.2 Locality Vidme (2)

This location is situated in the Flåmsdalen, the valley leading south from the Aurlandsfjorden (Figure 62). This unstable slope has been detected from aerial images and the first field investigation and reporting has already been carried out (NGU rapport 2008.026).

A first reconnaissance flight by helicopter took place in 2007, and more detailed field investigations were completed in the summers 2008 and 2010. This field work comprised geological mapping, structural geological measurements, sample collection for surface age dating, TLS data acquisition, and dGPS point installation and measurement.



Figur 62. Overview over the Vidme site and the opening cracks as well as measurement points.

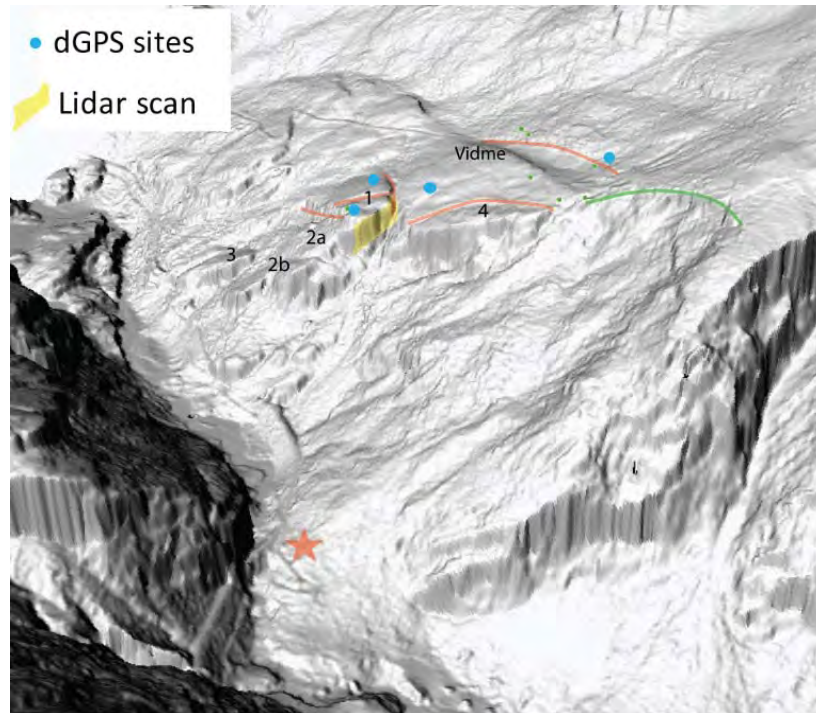


Figure 63. Perspective view of the site on a shaded relief and the main fractures marked in red. An old rock avalanche detachment scar is marked in green to the right. Samples for surface age dating from the deposits below were taken in 2010 (red star).

Mapping

The bedrocks at this location are mica-rich schists and phyllites with a pronounced foliation that dips moderately south-westwards out of the slope. Deposits of at least one old rock avalanche are visible and mapped north-east of the currently assumed unstable area (NGU rapport 2002.005). The current unstable area is divided into several blocks by a number of pronounced and deep fractures (Figure 63 and 64). A back-bounding crevasse limits the investigated area to the north-west behind the settlement Vidme. However, no recent movement signs are visible in this inhabited and cultivated area. In the frontal blocks (1-4), however, clear signs of movements and open fractures are visible. The frontal cliff of block 4 shows ongoing rockfall activity. The back-crack of block 1 shows an offset of several metres and some filling with soil. An opening of this depression/crack was observed during the recent years and reported by the residents.

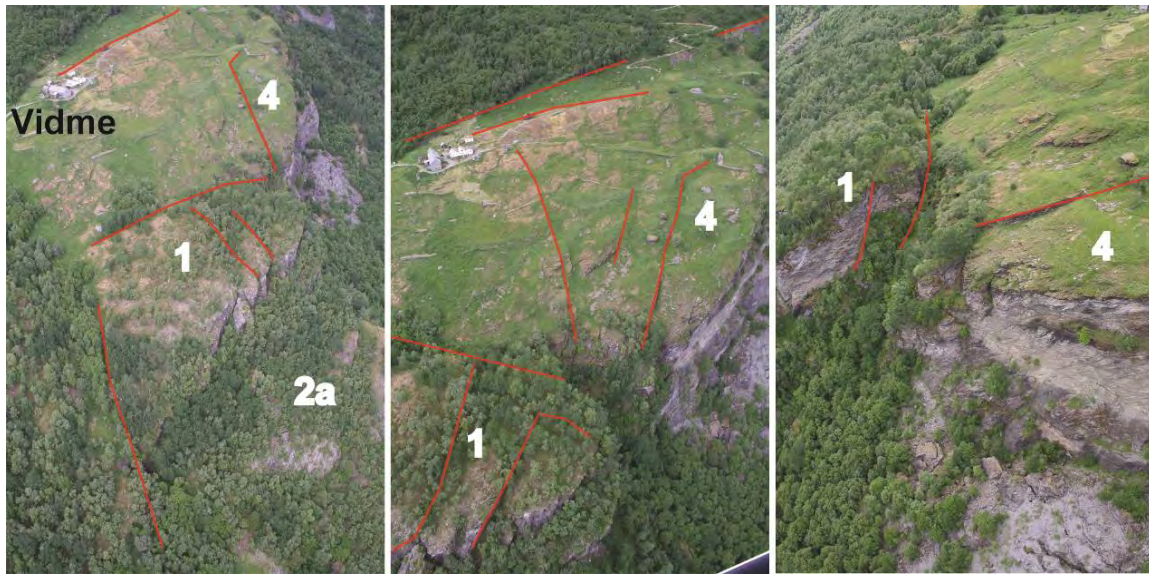


Figure 64. Photographs of the unstable area in Vidme from different perspectives. The main fractures are marked with red lines, dividing the different blocks (numbered).

dGPS results

Four new dGPS points were installed and measured for the first time in summer 2010. One fixed point (VI-FP) is located in presumably stable bedrock; the other three points (rover points, VI-1/VI-2/VI-3) are located on potentially unstable blocks (Figure 63). To get results about possible movements, repetition measurements have to be performed.

TLS data

We scanned the block 1 in summer 2010. Scanning was performed from different locations around the dGPS point VI-1 down to the lateral and back side of the block 1. The scan locations allowed us to capture a large part of the exposed bedrock surface of this large, displaced block in the southern section of the Vidme complex. The TLS data will be used for the extraction of structural data to enable enhanced structural and stability analyses, as well as for repetitive scans, in the case that the dGPS measurements show high displacement rates of this block. The processing and analysis of the TLS data will be performed in 2011.

An initial TLS acquisition was made on the Vidme unstable rock slope on 24 June 2010. The frontal part of the instability and the surrounding cliffs were scanned from three viewpoints with a total of seven scans (Figure 62, 65). The unified and cleaned point cloud has 4.3 million points with mean point spacing of 6.6 cm (at an average distance of 272 m).

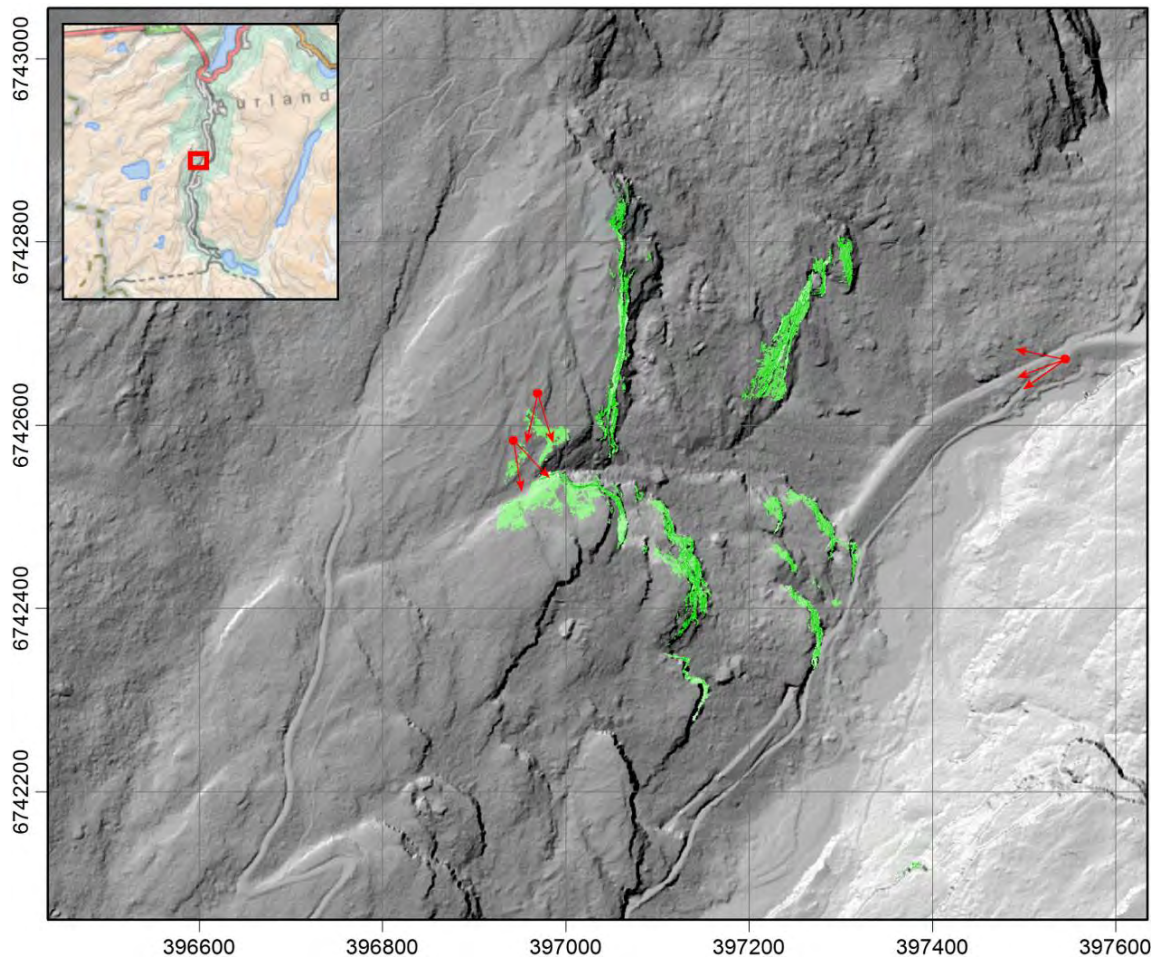


Figure 65. Hillshade map of the Vidme unstable rock slope with the airborne laser scanning hillshade in grey and the 2010 TLS hillshade in green. The location and directions of the TLS scans are shown (red arrows).

Geological Structures

Geological structures have been measured manually at several locations on the unstable slope. Three different joint systems and a pronounced foliation were observed. Figure 66 shows the orientation of these four structural features and introduces a kinematic assessment of slope deformation. This kinematic analysis, as well as observations in the field, shows that both planar failure and toppling are possible with the occurring joint systems and foliation (Figure 66). Detailed investigations in the field have revealed a probable sliding plane at block 1, delimiting a sub-block of approx. 10,000-20,000 m³ (Figure 67). However, this sliding plane confines only a superficial small part of block 1. To explain the opening/displacements at the main back-crack of block 1, more deep-seated movements are expected. However, at the current state of investigations, no such large-area sliding-plane was observed. All the main blocks depicted show internal fragmentation; mainly along the joint systems J1 and J2, building smaller sub-blocks. No distinct sliding planes were visible for other blocks, but due to impeded access, no in-situ investigations of blocks 2-4 were carried out.

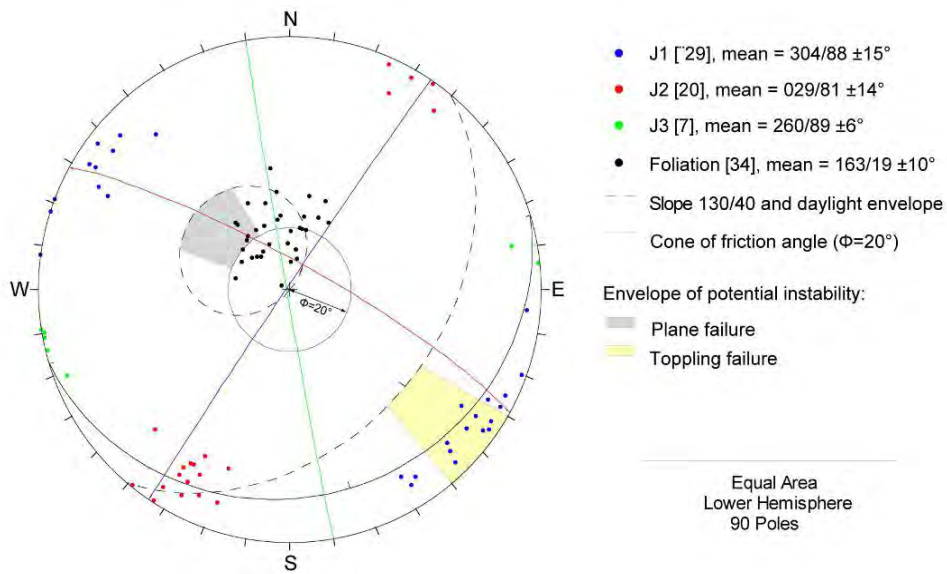


Figure 66. Stereoplot of the in-situ measured geological structures.



Figure 67. Probable sliding plane at block 1 and an open fracture at the surface.

Recommendations

- Processing and analysis of TLS data.
- Detailed structural geological and kinematic analyses based on available field measurements and TLS data in 2011 and 2012.
- Repetition of dGPS measurements.
- Analyses of the samples for surface age dating.
- The TLS point cloud will be used for a detailed structural analysis of the main discontinuity sets shaping the cliffs at Vidme. The site is also appropriate to create a 3D model of the basal failure surface based on the morphology given by the ALS-DEM and the measured structures. This work will be undertaken in 2011.

3.3.10.3 Locality Viddalen (3)

Mapping

The unstable rock slope of Viddalen is located in the Aurland region, at the SE end of the inner fjord system of Sognefjorden (Figure 1). It is situated 260 m above a water reservoir on a north–south trending slope with an average gradient of 40° (Figure 68a). The bedrock consists of mica-rich schist and phyllite with a foliation that dips moderately SE towards the mountains (mean orientation: 105/38, Figure 68b). A flat-lying thrust plane, which forms the contact with subjacent Precambrian gneiss, is cropping out approx. 200 m below the unstable area (Figure 68a). This site is especially important for detailed investigation because of the possible formation of a post-failure displacement wave in the reservoir and subsequent overtopping of the dam, similarly to the occurrence at Vaiont slide in 1963 (Hendron & Patton 1987). The consequences for the local community down river from the dam in the Aurland valley in such a scenario could be catastrophic because the wave could be several metres high and the distance to the settlement is only a few kilometres.

A 150 m-long NNE–SSW-striking back-bounding crevasse and a large NNW–SSE-striking transfer fracture limit the unstable block to the east and to the north, respectively; whereas only a ground depression indicates the southern border (Figure 68c, d). In the field, the back-bounding crevasse shows a maximum down-throw of 13 m and an opening of up to 15 m in the northern part of the instability. The volume of the unstable block is uncertain because the depth of the unstable part is not known. On the surface it covers an area of 13 600 m², but it is separated into several smaller blocks by three main fracture sets (Figure 68b). One set, which includes the back-bounding crevasse, strikes NNE–SSW (mean orientation: 120/90) and is thus slightly oblique to the general slope trend. The second set strikes NW–SE (mean orientation: 220/85), while the last set strikes west–east (mean orientation: 358/82) (Figure 68b). Several fractures are open with a width of up to 1 m and a visible depth of maximum 10 m, but there are also some fractures that are only expressed as ground depressions on the surface. The unstable area is highly fractured at its front, as highlighted by the occurrence of many smaller detached blocks (Figure 68 d). Present-day rockfall activity is observed at the front and the toe of the unstable area.

A spring is situated along the outcropping thrust plane and, consequently, indicates a layer with high permeability that drains the surface (Figure 68a, d). This sole detachment may form the lower limit of the unstable area and may also have contributed to destabilize the slope. However, it probably cannot act as a basal sliding plane because it is horizontal.

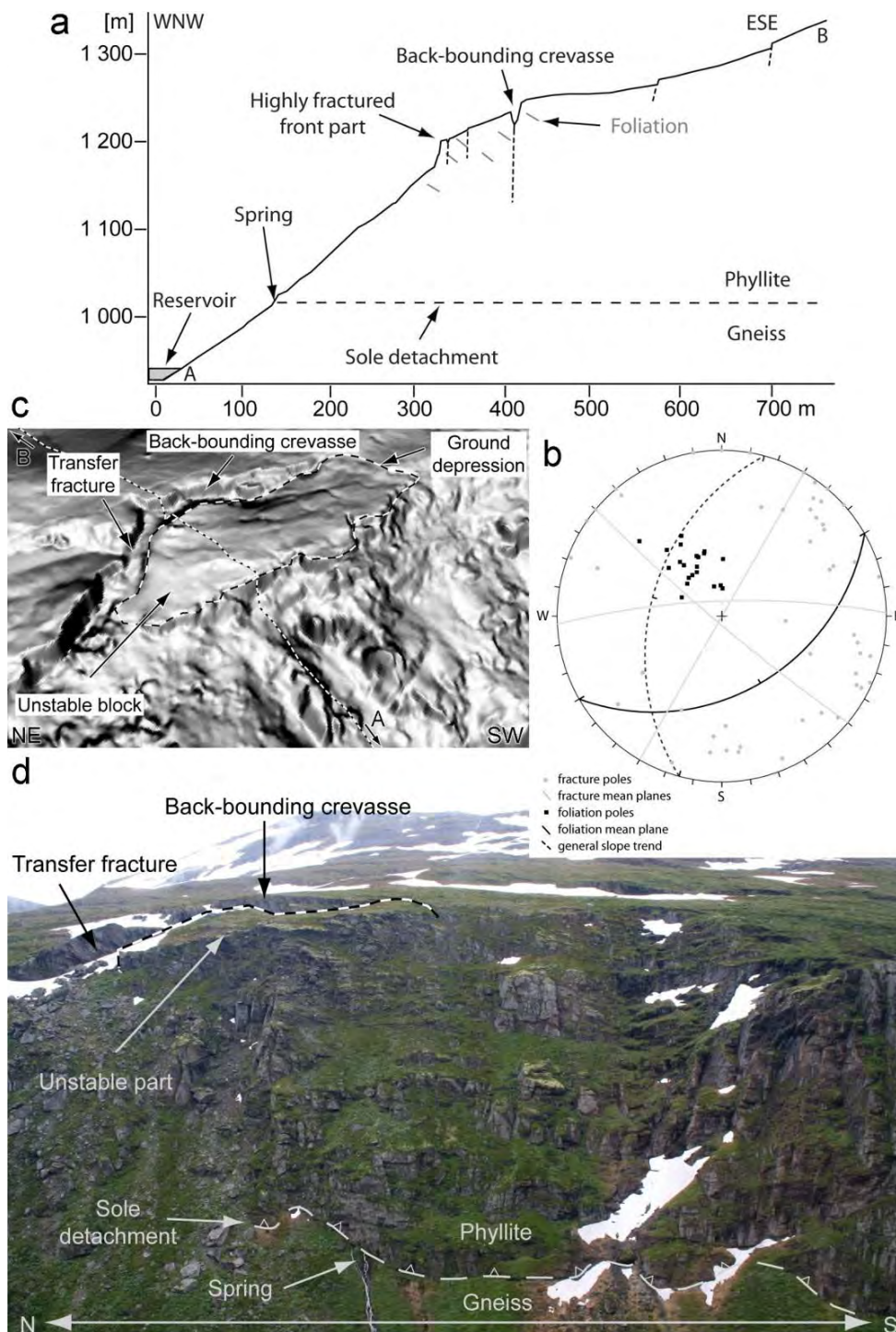


Figure 68. Viddalen unstable area. (a) Sketch cross-section of the unstable area. (b) Structural field data (equal-area projection, lower hemisphere; in black: foliation poles and mean plane; in grey: fracture poles and mean planes, black, dashed: general slope trend). (c) Three-dimensional view of a shaded digital elevation model (DEM) of the unstable area with a resolution of 1 m, based on airborne Laser scanning data. View to the SE. The dashed line indicates the extent of the unstable block on the surface and the dotted line A–B marks the location of the cross-section. (d) Overview of the area displaying a spring level that coincides with the sole detachment between the phyllite and the gneissic unit. The dashed line marks the limits of the unstable block. View to the east (after Böhme et al., 2011)

Two possibilities are discussed about how the instability might have developed (Böhme et al., 2011). The first is based on the toppling of large rock columns that are separated by steep discontinuities. Flat lying discontinuities, which might be fractures parallel to the main thrust plane, constrain the column height. Another possible failure mode is a planar failure along a complex basal sliding plane that develops by connecting various pre-existing planes with unfavourable orientations by failure of rock bridges.

Field observations suggest that the gravitational deformation is propagating towards the south. The back-bounding crevasse shows the largest opening, as well as the largest down-throw, in the northern part of the instability, whereas only a depression is visible as a continuation of it at the southern end of the unstable block (Figure 68c). Furthermore, a higher rockfall activity at the front of the northern part indicates that the deformation rate seems to be higher in this area (Figure 68d). However, this needs to be confirmed by monitoring data.

Terrestrial laser scanning

Three TLS scans were acquired from one viewpoint to the north of the unstable slope on 7 September 2008 (Figure 69). The assembled point cloud is formed by 8.4 million points and has an average point spacing of 3.6 cm (at a mean distance of 121 m). The TLS point cloud was georeferenced using the point cloud acquired by airborne laser scanning (high-resolution DEM) (Figure 69). The data treatment and analysis were carried out by the University of Lausanne, Switzerland (Carrea et al., 2010; see Appendix 2, p. 29-32)

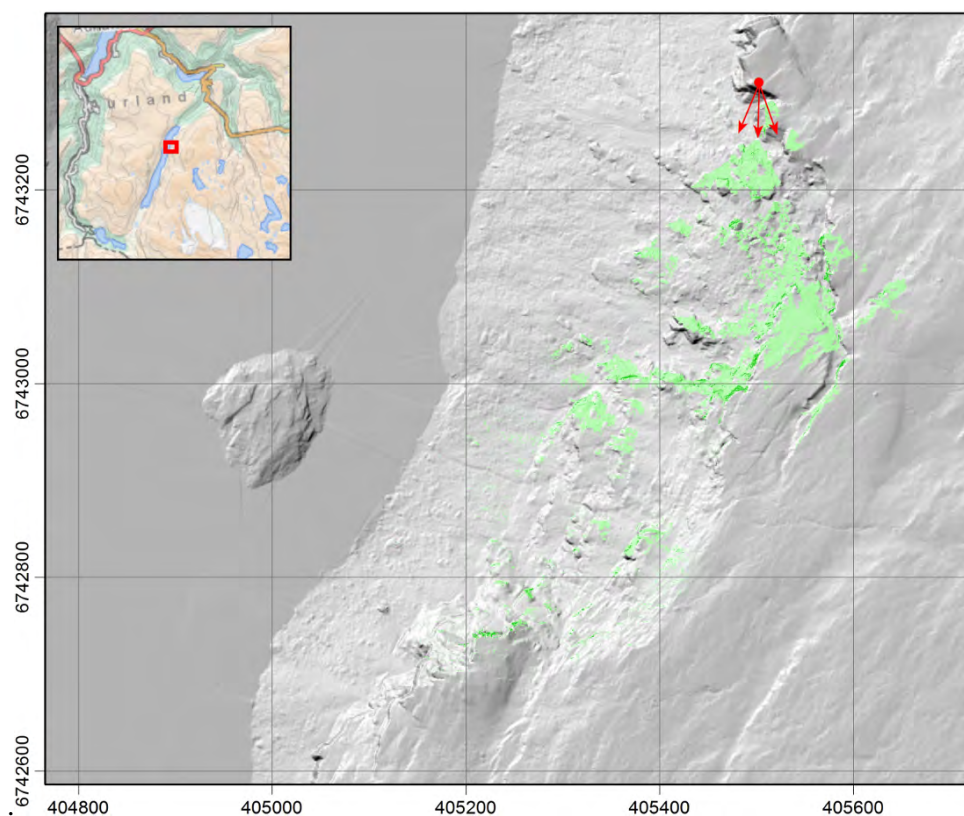


Figure 69. Hillshade map of the ALS-DEM (in grey) and the 2008 TLS-DEM (in green) of the Viddalen unstable rock slope. The scan position and directions are shown (red arrows). Coordinates are in UTM32N.

The structural analysis of the main discontinuity sets at Viddalen was made in Coltop3D on the 2008 TLS point cloud (Figure 69). The discontinuities were measured in the stable back-scarp and not on the moving slope. The foliation S1 dips moderately towards the NW ($310^{\circ}/43^{\circ}$) and the back-scarp is formed by a combination of discontinuities J2 ($274^{\circ}/55^{\circ}$), J3 ($108^{\circ}/40^{\circ}$) and J4 ($015^{\circ}/65^{\circ}$). The south-bounding lateral release surface is created by the discontinuity sets J1 ($167^{\circ}/72^{\circ}$), J5 ($226^{\circ}/82^{\circ}$) and J4. This does not entirely fit with the measurements taken in the field (see above). However, most of the mismatch can easily be related to a misinterpretation of the type of structure. What is interpreted as joint J3 is apparently the schistosity. J2, J4 and J5 fit well within both data sets. Surfaces interpreted as S1 were not mapped in the field. However, these are likely surfaces that build by connecting anisotropies as discussed as one failure scenario (see above). This suggests that a re-examination of the TLS data should be performed. In addition, as the TLS data were not taken frontally but nearly slope parallel (Figure 69), it would be recommendable to take additional data from, for example, the island opposite to the deforming slope (Figure 69).

The foliation detected in the TLS data does not coincide with the foliation measured in the field. This is based upon a misinterpretation of that discontinuity. Therefore also the kinematic feasibility test based upon the TLS results differently to results from the field. Most of this difference bases on the existence of the anisotropy S1. The kinematic feasibility tests show the possibility for planar sliding along S1, which daylight the topography (slope orientation at front of instability: $295^{\circ}/60^{\circ}$) (Figure 70). Wedge sliding is also possible, along the intersection of discontinuities S1 and J5 or S1 and J2. Toppling failure is not a likely failure mechanism for the Viddalen instability, but can occur locally (Figure 70).

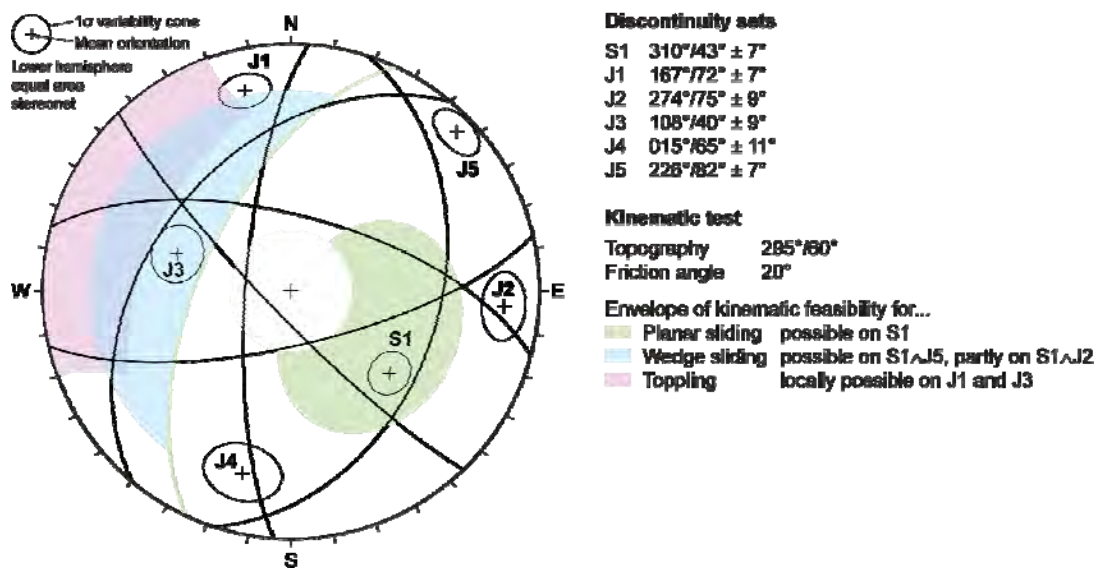


Figure 70. Stereonet of the discontinuities measured on the TLS point cloud at Viddalen (modified from Carrea et al., 2010). Kinematic feasibility test for planar and wedge sliding and toppling failure are shown.

dGPS results

Two rover points (VID-1, VID-2) and 1 fixed (VID-FP) point were installed by NGU in 2007 (Figure 71). In 2008 "E-CO Vannkraft AS" established five additional rover (VID-S1- VID-S5) and one fixed points (VID-BS) on 1.5 m high concrete pillars, which were also measured

by NGU in the last 3 years. Larger movements of some of these pillars suggest that some of them are not well established (Appendix 1).

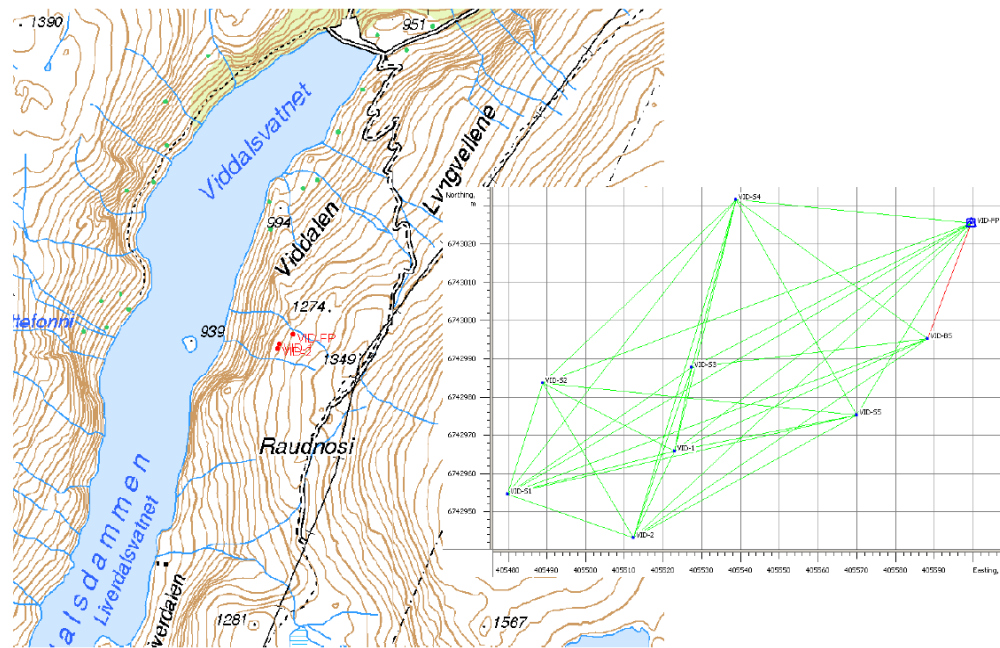


Figure 71. Map showing position of measurement points for dGPS monitoring.

Results of the deformation by dGPS measurements of the rover points VID-1 and VID-2 indicate on average no significant horizontal and vertical movement in a single year's measurement interval except between 2007 and 2008. The measured displacement 2007-2008 cannot be interpreted as certain gravitational movement as it was not consistent with movement in following years. In addition, the point would have gone up in elevation during that interval (Figure 72). Both rover points indicate small significant movement towards WNW and downward over the 4 years measurement period. No difference in velocity between the northern and southern rover point can be observed. Stable rover points established by "E-CO Vannkraft" support these observations (Appendix 1).

Recommendations

Due to the potential large consequences and significant movement over a several years interval we recommend continuing to monitor the site at least with a 1-year interval within the national monitoring program. Potentially catastrophic consequences are linked to a displacement wave within the Viddalen water reservoir that could overtop the dam and result in catastrophic flooding downriver.

We further recommend carrying out additional TLS acquisition, preferably from the island within the Viddalen reservoir.

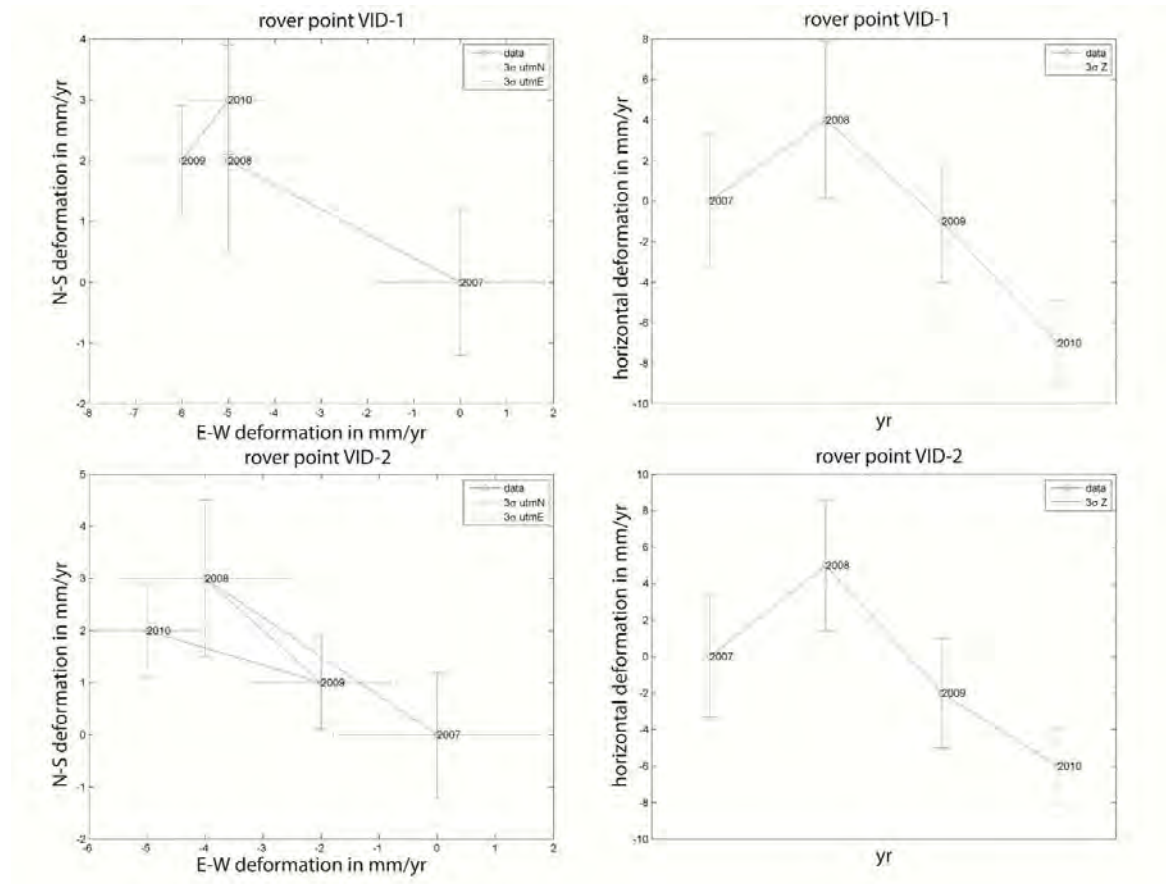


Figure 72) Diagram showing the movement detected on rover stations between 2007 and 2010 at Viddalen.

3.3.11 Lærdal municipality

2.3.11.1 Locality Kvitaberget

Mapping

Kvitaberget is located on the northern part of the Lærdalen valley, about 4 km south of the village of Lærdal (Figure 73). The local rocks are massive or weakly foliated quartz-monzonites and granites of the Precambrian autochthonous basement.

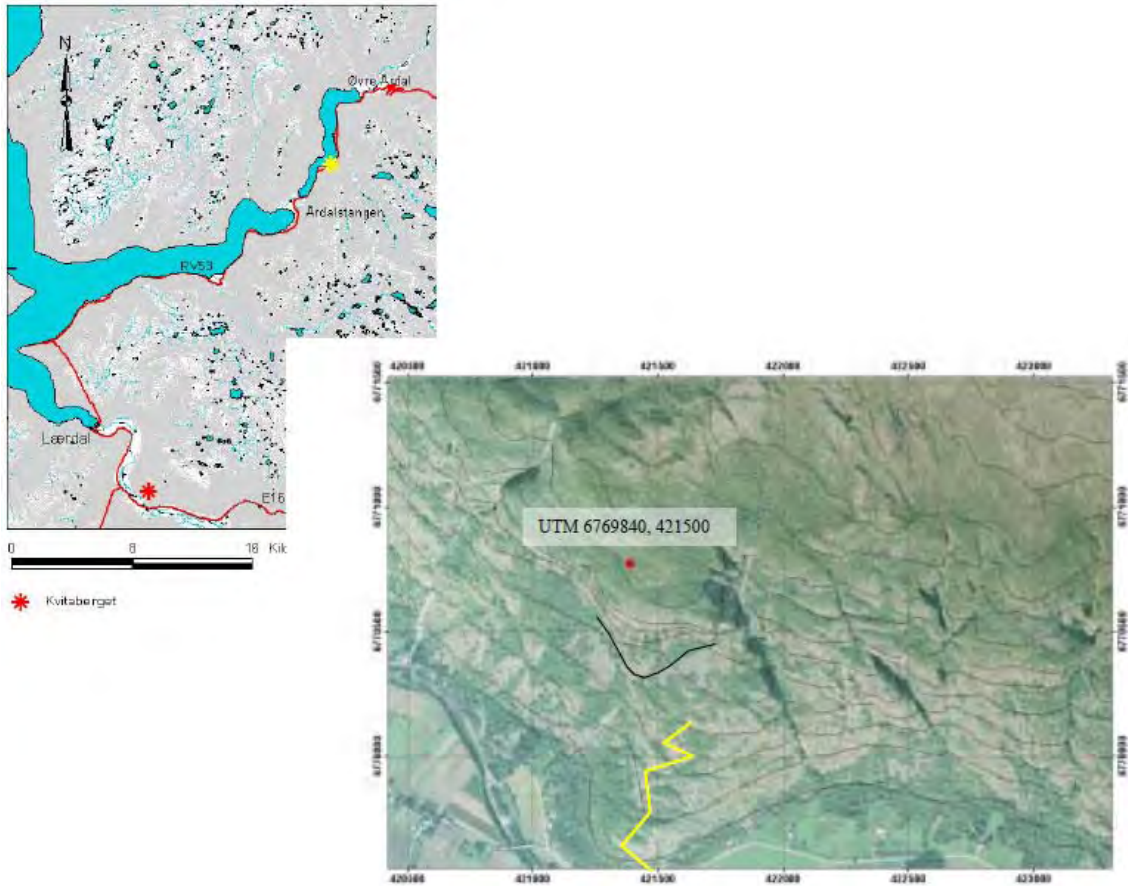


Figure 73. Location of Kvitaberget (left) and orthophoto (right).

Reconnaissance mapping was carried out at the site in 2008 along the lower SW-trending ridge. From the orthophoto, two NW-SE lineaments are clearly visible east of Kvitaberget, but no structures transverse to these lineaments are recognized.

The rock slope was inspected by binoculars from the road, and minor reconnaissance mapping was carried out in the area between the E16 road and the main escarpment (Figure 74).



Figure 74. Kvitaberget seen from the south, with thrust fault indicated in horizontal dashed line.

On the west and east-facing vertical rock faces, the binocular inspection indicates a low-angle dipping shear zone or reverse fault (Figure 73, 74). This structure is connected with minor fractures dipping more steeply towards the NE. There are also other fractures, but none of them appear to be connected.

Recommendations

A rockslide from this mountain side would be disastrous for the Lærdal community. NW-SE tectonic fractures that may act as transfer structures are present, but neither open structures at right angles nor possible sliding planes have been observed. We do not consider this area as a site for a potential future rockslide and do not recommend any further follow-up work.

3.3.12 Luster municipality

3.3.12.1 Locality Skjeringahaugane (called Luster, Røssasete in attached dGPS report Appendix 1)

This site was mapped before 2008 as a larger area of various instabilities summarized under the name "Hjellane (17-23)" and all mapping results have been reported in NGU report 2008.026. The most active area is at the locality Skjeringahaugane. This site is located 750 m above and 1.8 km away along the west shore of Lusterfjord (Figure 75) and 250 m above a building complex that has served as a hospital and a home for political refugees in the past and is unused today. At that site a block A with a surface area of approx. 10.000 m² has detached along an irregular back crack a few metres deep and a few metres wide (Figure 76). The back crack is covered with soil that is neither tilted nor split at any location indicating no active movement for a long time. In front of this block is an area (B in Figure 76) with a surface of approx. 46.000 m² that is strongly broken up in large blocks several 10 to more than 500 m² in surface area, separated by cracks several metres to more than 10 m wide and several metres to more than 20 m deep. These cracks are not filled with soil, suggesting recent activity. In front of this block field lies an approx. 130.000 m² area that is characterized by

few large cracks several metres to 10 m wide. NNE of the building complex are two springs, which suggests a deep sliding surface.

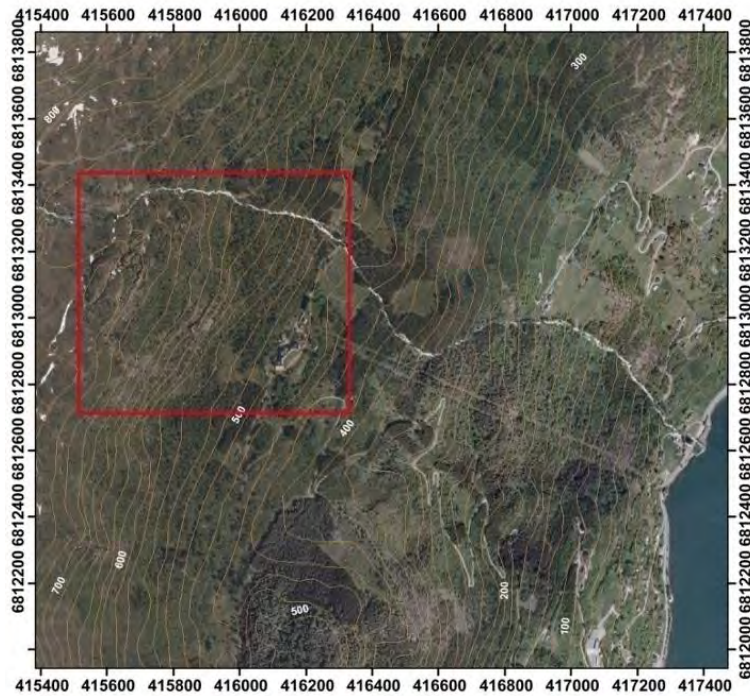


Figure 75. Overview of the unstable area at Skjeringahaugane. Red box depicts area of Fig.75.

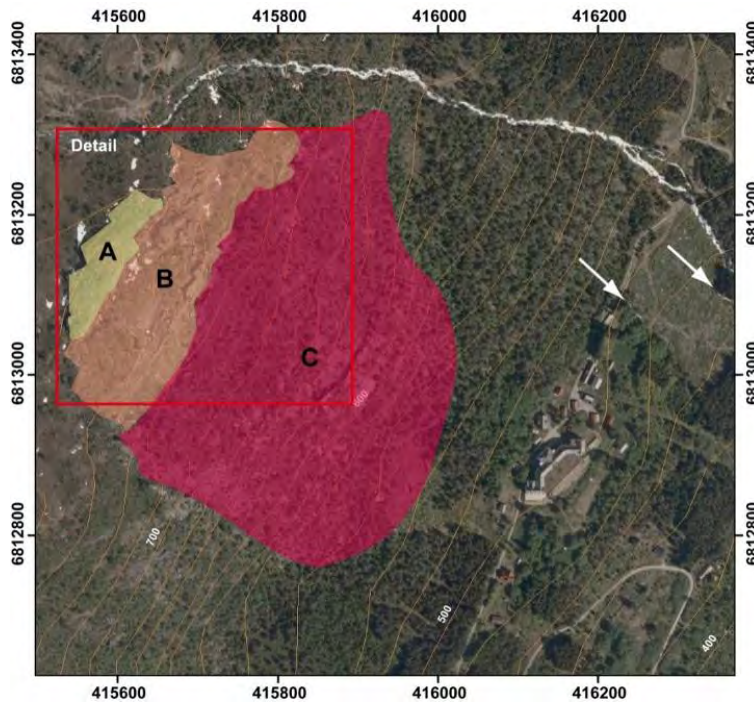


Figure 76. Three segments of the slope with different signs of deformation above an uninhabited building complex at 500 m altitude (see text). White arrows indicate springs along the slope. (Box highlights position of detail view shown in Figure 77).

Based upon the above observations indicating ongoing slope deformation, we sampled three sliding planes inclined approx. $60^{\circ} - 70^{\circ}$ (Figure 77, 78) for cosmogenic nuclide dating in 2008. This was to determine when the rock slope started to break apart and to determine long term slip rates. In a first step only a selected number of samples were sent for processing to test if sliding occurred within the time range dateable by CN dating. We took the uppermost sample at approx. 3 m depth. This is about the limit where cosmogenic irradiation gets attenuated by terrestrial matter assuming that the landscape eroded during last glaciation. Our lowermost sample was always taken well above ground (approx. 2m). This was done as snow cover at the foot of the sliding plane increases with the length of the sliding plane due to snow drift. Therefore, samples at the foot of the sliding plane are covered by increasing amounts of snow the longer the sliding plane gets. We have no possibility of calibrating for this effect as we cannot reach the sample site in winter times and therefore omitted the lower parts of the sliding plane for sampling.

In addition, bolts for a dGPS base station and 3 rover points (LU-1, LU-2, and LU-3) were installed on individual blocks and measured in 2008, 2009, and 2010 (Figure 76) to test if long term sliding rates coincide with today's sliding velocity. The bolt at position LU-3 was found loose on returning to the site in 2009 and had to be re-installed in 2009. Hence results on that point are given in two separate graphs (Figure 79).

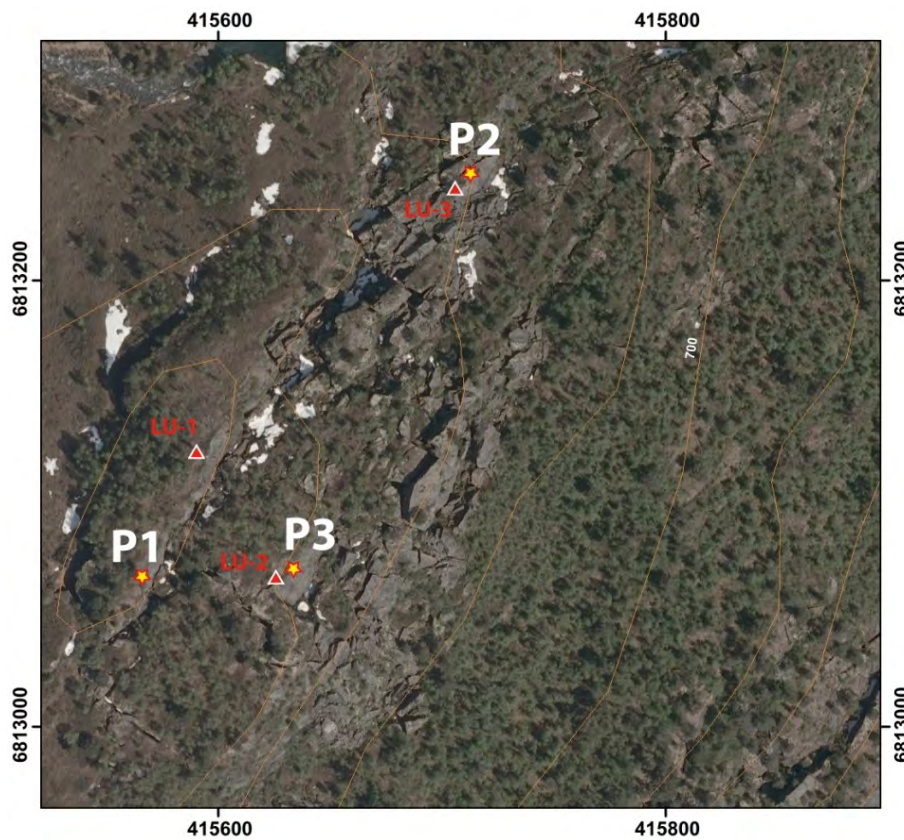


Figure 77. Detail showing position (star) of three profiles (P1 – P3) sampled for cosmogenic nuclide dating and position of dGPS rover stations (LU-1, LU-2, LU-3).

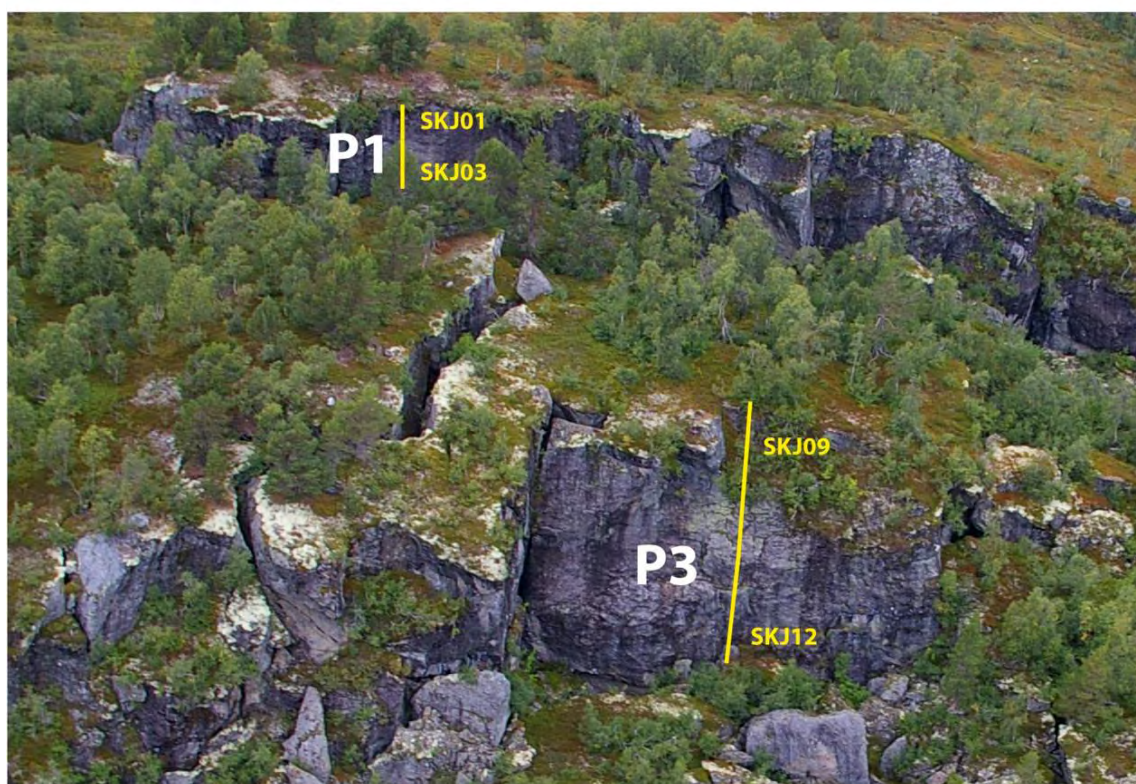


Figure 78. Oblique view from Norge i 3D (above) and from helicopter (below) indicating the position of profiles (P1 and P3) for cosmogenic nuclide dating.

Results of dating

The results of the CN dating are summarized in Tab. 4. The ages are consistent with sample position as the upper samples on each sliding plane are older than the lower one. We also calculated the inherited age (pre-sliding-exposure) of the samples, which results from the penetration of the cosmogenic radiation into the rock mass. This is restricted due to the exponential attenuation of the radiation by rock matter to the uppermost metres. The assumption taken here is that the surfaces were eroded by glacial erosion during the last glacial maximum and covered by ice until deglaciation. The assumption is most likely correct at the sample site at 750 m altitude in this part of western Norway. The inherited age is anyhow insignificant in comparison with the real age and statistical error margins of this method (Tab. 4).

The upper samples at sliding planes P1 and P2 became exposed to cosmogenic irradiation about 7 kyrs ago and the lower samples on these sliding planes became exposed to irradiation approx. 2-2.5 kyrs ago. The lower sample positions lie approx. 2 m above ground, hence sliding continued. At the profile P3 has an age 3 kyr younger at 4 kyrs ago and the lower sample resulted in an CN age 1.2 kyr ago; again 2 m of displacement below the lowest sample position indicates ongoing deformation.

Table 4. Overview of sample location along sliding plane for CN dating and results of dating (samples without any results were not processed yet, no pre-sliding exposure indicates a depth within the rock mass not reached by cosmogenic irradiation prior to sliding).

Profile	Sample Number	Length along sliding plane [mm]	Age [kyr]	1 sigma uncertainty [kyr]	Pre-sliding exposure [yr]
P1	SKJ 01	2900	7.0	0.8	210
	SKJ 02	5530	-	-	-
	SKJ 03	8250	2.1	0.2	-
	base	10050	-	-	-
P2	SKJ 04	3700	6.8	0.7	230
	SKJ 05	5900	-	-	-
	SKJ 06	13900	-	-	-
	SKJ 07	15700	-	-	-
	SKJ 08	17010	2.5	0.3	-
	base	19010	-	-	-
P3	SKJ 09	4650	4	0.6	150
	SKJ 10	7600	-	-	-
	SKJ 11	11200	-	-	-
	SKJ 12	15700	1.2	0.1	-
	base	17700	-	-	-

Based upon the CN ages obtained, we calculated the slip rate between the upper and the lower sample on each sliding surface as well as the upper sample and today's base of the sliding plane. In addition, we calculated an uncertainty interval that is based upon the uncertainty of the ages. The results indicate that sliding at the sliding plane P1 has a velocity of 1 +/- 0.2 mm/yr while those at P2 and P3 have slip rates of 3.1 +/- 0.5 mm/yr and 4.0 +/- 0.7 mm/yr, respectively (Tab. 5). The slip rates calculated based upon the uppermost sample age and the base of the sliding plane (taken as a 0 age) are lower. However, the age difference is within the uncertainty margins of the slip rate calculation (Tab. 5). The systematic younger age suggests that indeed the effect of snow accumulation along the base of the sliding plane has to be taken into account and that there is no deceleration of sliding along all sliding planes. The comparison of the age and the slip rate of profile P1 and P3, which are lying nearly in front of each other (see Figure 77), suggests that the slide is progressive and accelerating while stepping forward. This is also suggested by the calculated time when the sliding started at the different profiles. This calculation is based upon the upper exposure age and the position of the respective sample location below the top of the sliding plane and the slip rate between both sample locations. The start of sliding is calculated to the profiles P1, P2, and P3 as 9.6 kyr, 8 kyr, and 5.2 kyr, respectively.

Table 5. Slip rates and start of sliding calculated based on CN exposure ages.

Profile	Sample numbers	Slip rate [mm/yr]	Uncertainty [mm/yr]	Start of sliding [yr](using slip rate between upper and lower sample)
P1	SKJ 01 - SKJ 03	1.1	0.2	9650
	SKJ 01 - base	1.0		
P2	SKJ 04 - SKJ 08	3.1	0.5	8000
	SKJ 04 - base	2.3		
P3	SKJ 09 - SKJ 12	4.0	0.7	5200
	SKJ 09 - base	3.3		

dGPS

Results of the displacement by dGPS measurements of the rover point LU-1 indicated no significant horizontal or vertical movement. Rover point LU-2 indicates significant downward movement over a period of 2 years (Figure 79). Rover point LU-3 indicated significant downward movement between 2008 and 2009. However, the newly set bolt indicated no significant movement in the period 2009 – 2010, and therefore the movement cannot be interpreted as certain gravitational movement. When comparing slip rates calculated from CN ages and slip rates determined by dGPS at P1 (LU-1) and P3 (LU-2), the trend of progressive movement (see above) is underlined.

Recommendations

We recommend to set at least two new rover points for dGPS monitoring at Skjeringahaugane because both CN dating and dGPS measurements indicate propagation of deformation towards the fjord. These points should be set in the lower part of area B and a large block below the largest crack in area C (see Figure 76). We also recommend dating one more sample along profile P2 and P3. This is to test if the apparent slow-down of movement, as suggested by the comparison of both the slip rates on each sliding plane, is real or the effect of snow accumulation as discussed above.

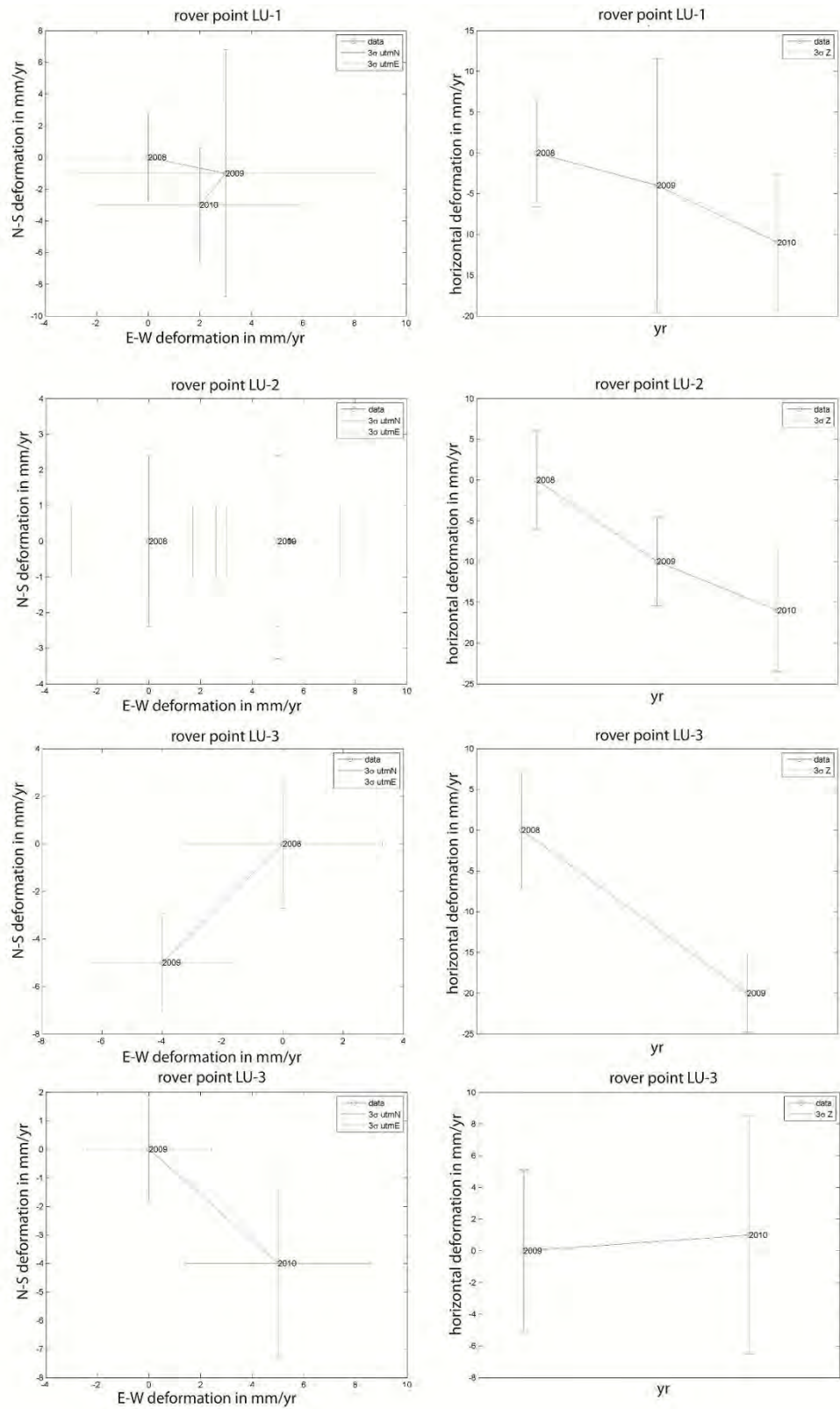


Figure 79. Results of dGPS measurements indicate significant downward movement at point LU-2. Note that the last two rows of diagrams represent the same location of rover point LU-3. This measurement bolt had to be re-set in 2009.

3.3.12.2 Locality Tussen

Mapping

This potential rockslide area is located at the NE end of the inner fjord system of Sognefjorden (Figure 1). It is situated 1100 m above the valley floor on a NNE–SSW-trending slope that has an average gradient of 35°, but exceeds 60° in the uppermost part where the instability is located at the edge of the plateau (Figure 80a). In this region a Caledonian thrust boundary forms the contact between the phyllitic nappe, in which the instability is located, and the underlying Precambrian gneiss. However, a direct relationship between the presence of this thrust fault? and the development of the rock slope instability is unlikely because the thrust is located relatively deep (>500 m) below the unstable area, as well as gently dipping (c. 10°) and trending oblique to the valley. The bedrock of the unstable area consists of mica schists and phyllites, as well as in some areas of mylonitic quartz-rich gneisses and quartzites. The foliation dips approx. 30° to SSW (mean orientation: 203/31) and is, therefore, oblique to the valley (Figure 80b)(this corresponds to S1 in the terrestrial laser data below – but there exists a difference of 100° in orientation!).

The whole area is characterized by two sets of regional structures. NNE–SSW-striking lineaments (mean orientation: 117/90) with a persistence of several hundreds of metres contribute to the major structural influence of the unstable area (J4 and J5 in the terrestrial laser data below). They are most probably reactivated structures that have now developed large graben-like structures behind the unstable area (Figure 80 b, c) link missing. A set of less-developed SE–NW-striking joints (mean orientation: 055/90) act as transfer structures (Figure 80b) (J2 in the terrestrial laser data below).

The currently most active block comprises only a part of the structurally weakened zone at the front, and the volume of this block is estimated to be approx. 7 Mm³ (Figure 80a, c). It is bounded by a 300 m-long graben-like structure to the NW, while the other three sides are free (Figure 80c, d). Northeastwards and southwestwards are scarps of older slope failures with widespread talus at their base. The instability is thus a remaining part of the former slope. Several smaller fractures behind the main unstable block occur until approx. 250 m inside the plateau (Figure 80a). Those fractures are up to 1.5 m wide and up to several tens of metres deep, but disappear laterally. Using these fractures to delimit a maximum volume and to estimate a worst-case scenario gives a volume of 10 Mm³. Measured opening vectors, determined by matching definite pairs of edges on the opposite walls of a fracture, indicate movement directions perpendicular to the NNE–SSW-striking graben-like structures (Figure 80b). A major basal sliding plane could not be observed in the field, but it may be covered by the thick scree deposits on the slope. However, a limited number of field data indicate a third set of joints, dipping approx. 30° to the ESE (mean orientation: 105/34) and hence towards the valley (Figure 80b). These structures are clearly visible on both side-cliffs and may contribute to the formation of a basal sliding plane. A sliding plane at the base of the unstable block with a dip of 30° coincides with the furthest open fractures going inwards the plateau (Figure 80a).

Recent rockfall activity is detected along the cliff at both ends of the back-bounding graben-like structure, as well as at the front of the block where the proposed sliding plane may daylight. Both ends of the graben-like structure exhibit several smaller blocks or columns with average volumes of 90 m³ that are almost completely detached from the cliff.

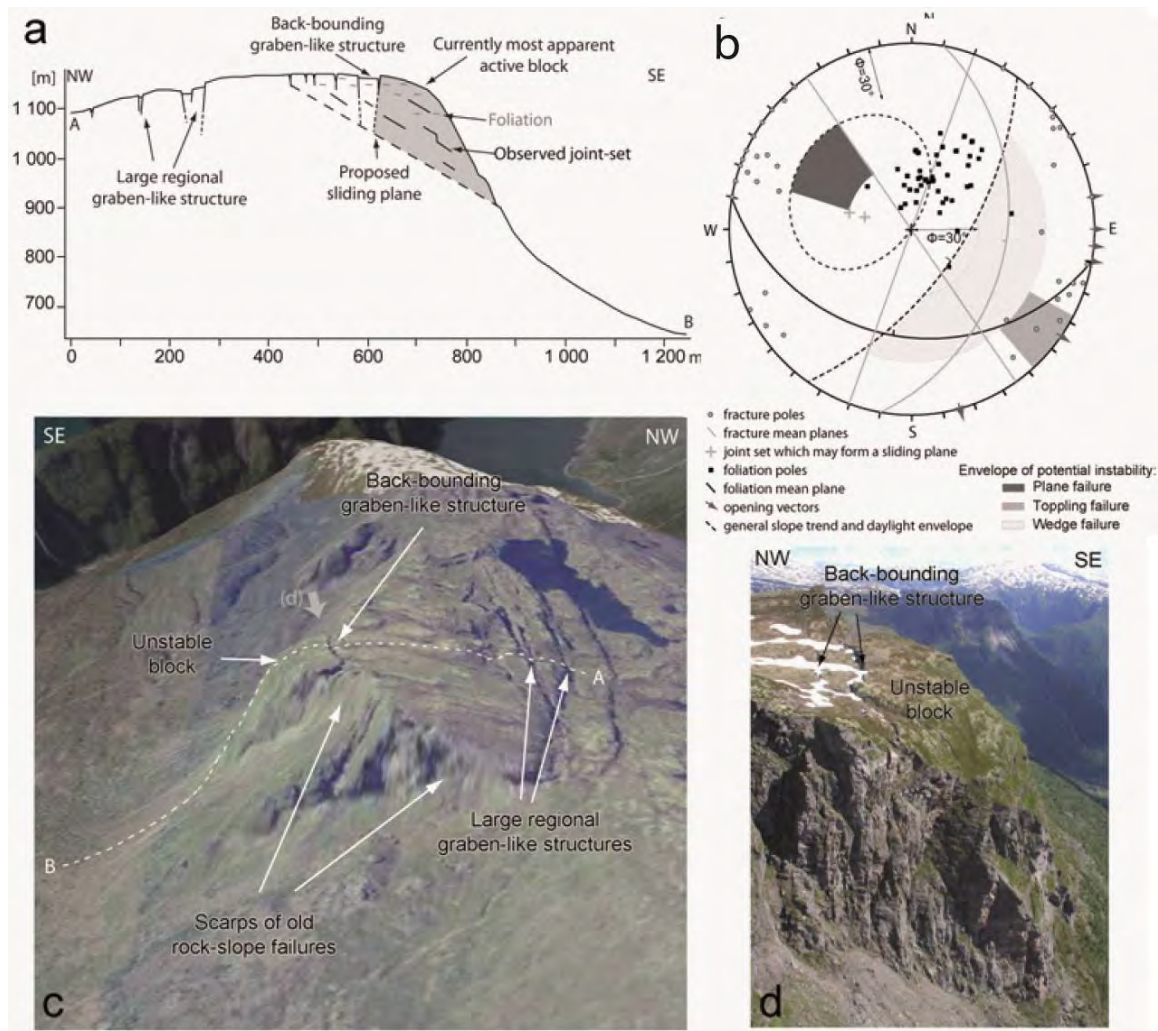


Figure 80. Tussen rockslide area. (a) Sketch cross-section of the unstable area. Structures that dip 30° towards the valley display weakened planes that could develop into a basal sliding plane. (b) Structural field data (equal-area projection, lower hemisphere; in black: foliation poles and mean plane; in grey: fracture poles and mean planes, grey arrows: opening vectors, black, dashed: general slope trend). Grey crosses represent the joint set that may form a basal sliding plane. (c) Three-dimensional view with aerial photograph overlay (www.norgei3d.no) of the study area showing the spatial arrangement of structures. View to the SW. The NW border of the unstable block is a back-bounding graben-like structure and the other three sides are free. Dashed line A–B marks the location of the cross-section. (d) Unstable block, view to the NE. (after Böhme et al., 2011)

Terrestrial laser scanning

The unstable rock slope Tussen was scanned in 2008 and 2009 by TLS (Figure 81). The first acquisition was made on 6 September 2008 with four scans from four viewpoints, two of them along the back-scarp (A & B) and two from the slope (C & D). Viewpoints A, B and C were reused for the follow-up acquisition on 19 August 2009 (Figure 81). The assembled 2008 and 2009 TLS point clouds are composed of 13.5 and 10.4 million points, respectively, with mean resolutions of 4.0 and 5.5 cm (an average distance of approx. 200 m), respectively. The TLS datasets were treated and analysed by the University of Lausanne, Switzerland (Carrea et al., 2010; see Appendix 2, p. 23-28).

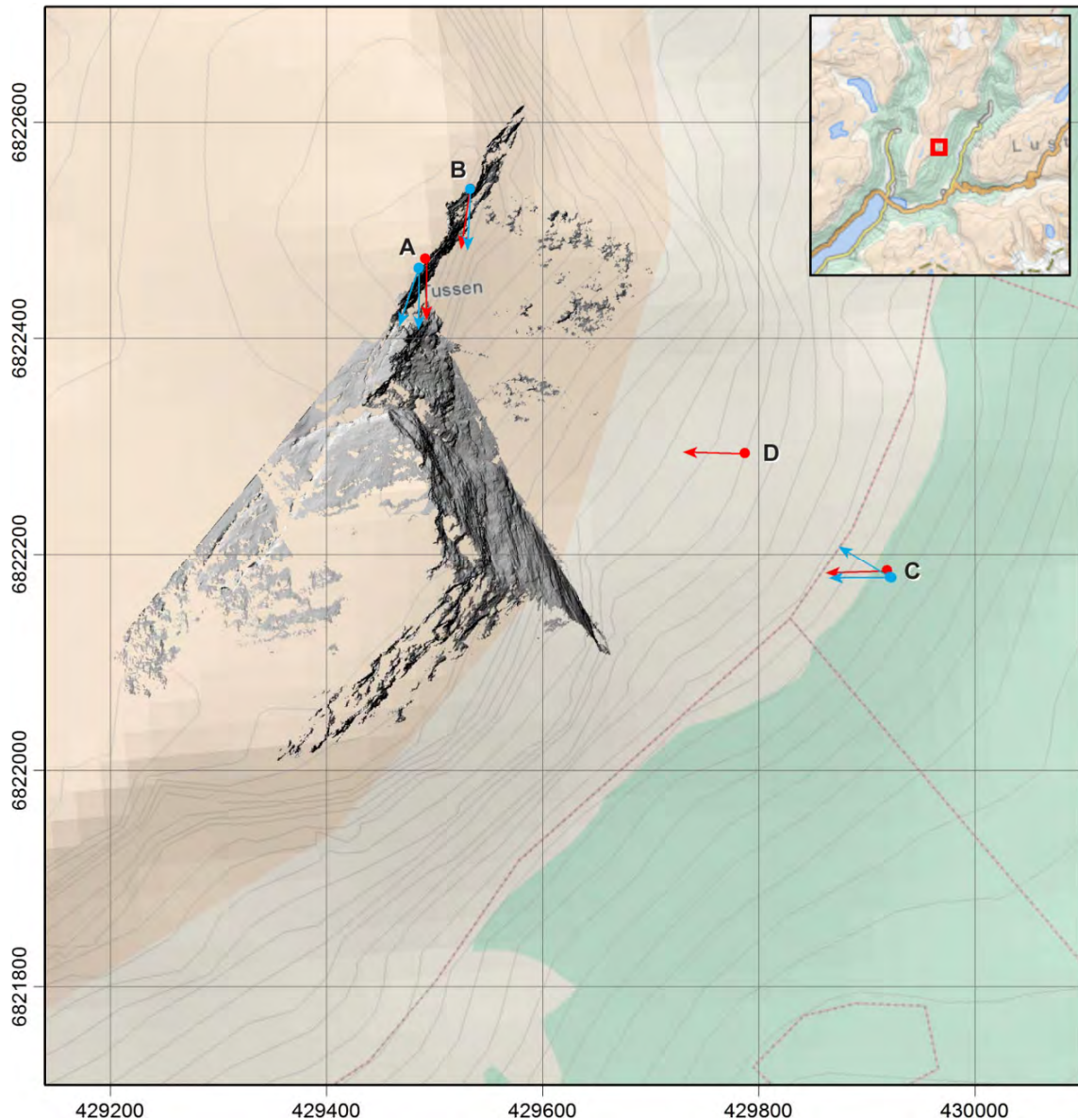


Figure 81. Map of the Tussen unstable rock slope showing the area scanned by TLS from different viewpoints in 2008 (red arrows) and 2009 (blue arrows).

The structural analysis of the 2009 TLS point cloud in Coltop3D revealed five major discontinuity sets that shape the rock mass at Tussen (Figure 82). The SSW-NNE-trending back-scarp of the instability and the back-bounding graben structure are formed by discontinuity sets J4 ($129^{\circ}/63^{\circ}$) and J5 ($298^{\circ}/78^{\circ}$). The front of the cliff is mainly formed by J4. The subvertical discontinuity sets J2 ($248^{\circ}/85^{\circ}$) and J3 ($028^{\circ}/90^{\circ}$) shape the NW-facing cliff. The main foliation S1 is shallow NW-dipping ($317^{\circ}/12^{\circ}$) and forms the top of the instability and outcrops also on the NW-facing cliff.

The comparison of both structural data measured in the field and on the high resolution DEM indicates that they have in part identical results (J2, J4, J5) or in parts similar (S1) shallow dipping foliation (whole sentence needs reconsideration). Only J3 detected in the DEM was not measured in the field. This is a steeply dipping plane that forms the northern wall of the slide block and cannot be reached in the field due to the steepness of the slope. The slight

variance of dip direction between field data and data extracted from the DEM is attributed to the selected observation points for terrestrial laser scanning that was taken from top north towards south only and is restricted to the northern part of the block only.

The kinematic feasibility tests (Figure 82) using a slope orientation of $140^{\circ}/60^{\circ}$ show a possibility for planar sliding on some surfaces of the steeply dipping discontinuity set J4. However, this joint set dips mostly steeper than the slope and structures are therefore not daylighting. A more gently SE-dipping structure is likely necessary to delimit a rockslide compartment that can slide. Toppling failure can occur along J5 discontinuities (Figure 82).

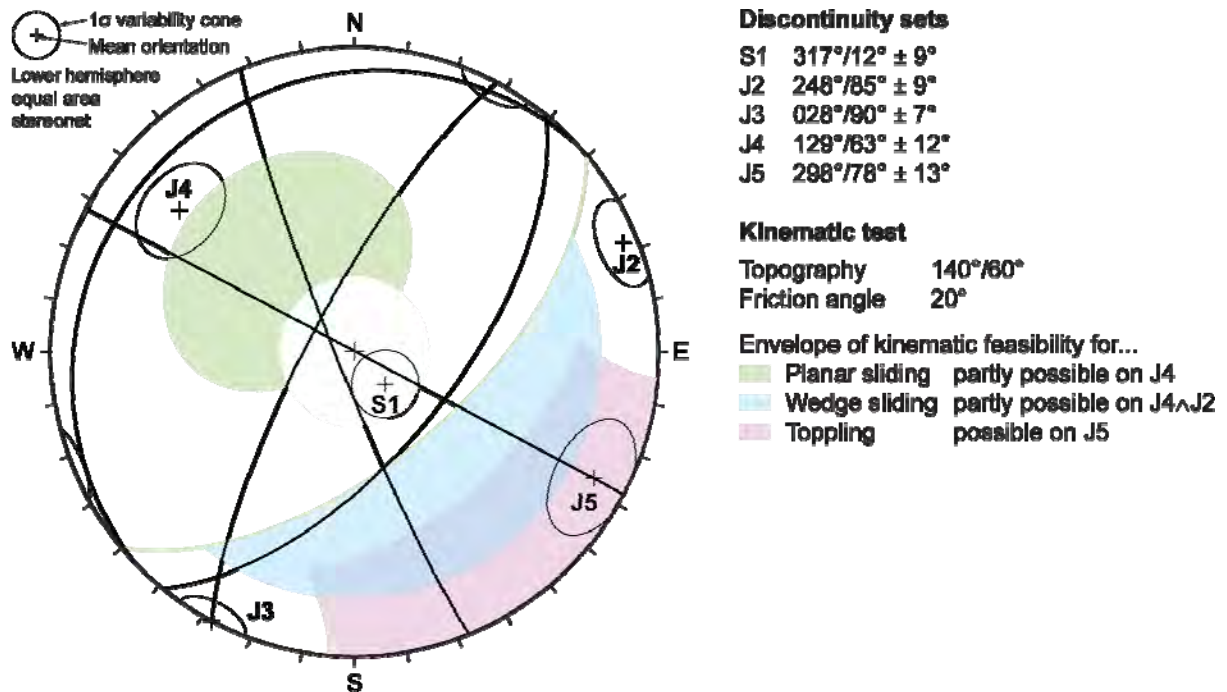


Figure 82. Stereonet of the main discontinuity sets at the Tussen instability (modified from Carrea et al., 2010). The kinematic feasibility tests use a slope orientation of $140^{\circ}/60^{\circ}$ and reveal possible planar sliding on J4, wedge sliding on J4 \wedge J2 and toppling on J5.

The shortest distance comparison is used to see differences in the DEM between two measurements and allows therefore to detect areas where rockfalls occurred in the time span between both measurements. The comparison between the 2008 and 2009 TLS datasets does not show significant slope movement or rockfall activity (Figure 83a) (see Oppikofer et al., 2009 for a methodological description). The scans made along the back-scarp (viewpoints A and B) include only a small stable area, which impedes a correct comparison of the TLS point clouds. The scans from viewpoints C and D would include a sufficiently large, stable area for a good comparison, but some scans were affected by atmospheric disturbances (scans: *tussen4* from 2008 and *tu3a* from 2009; Figure 83b). Consequently, they cannot be used for the displacement analysis.

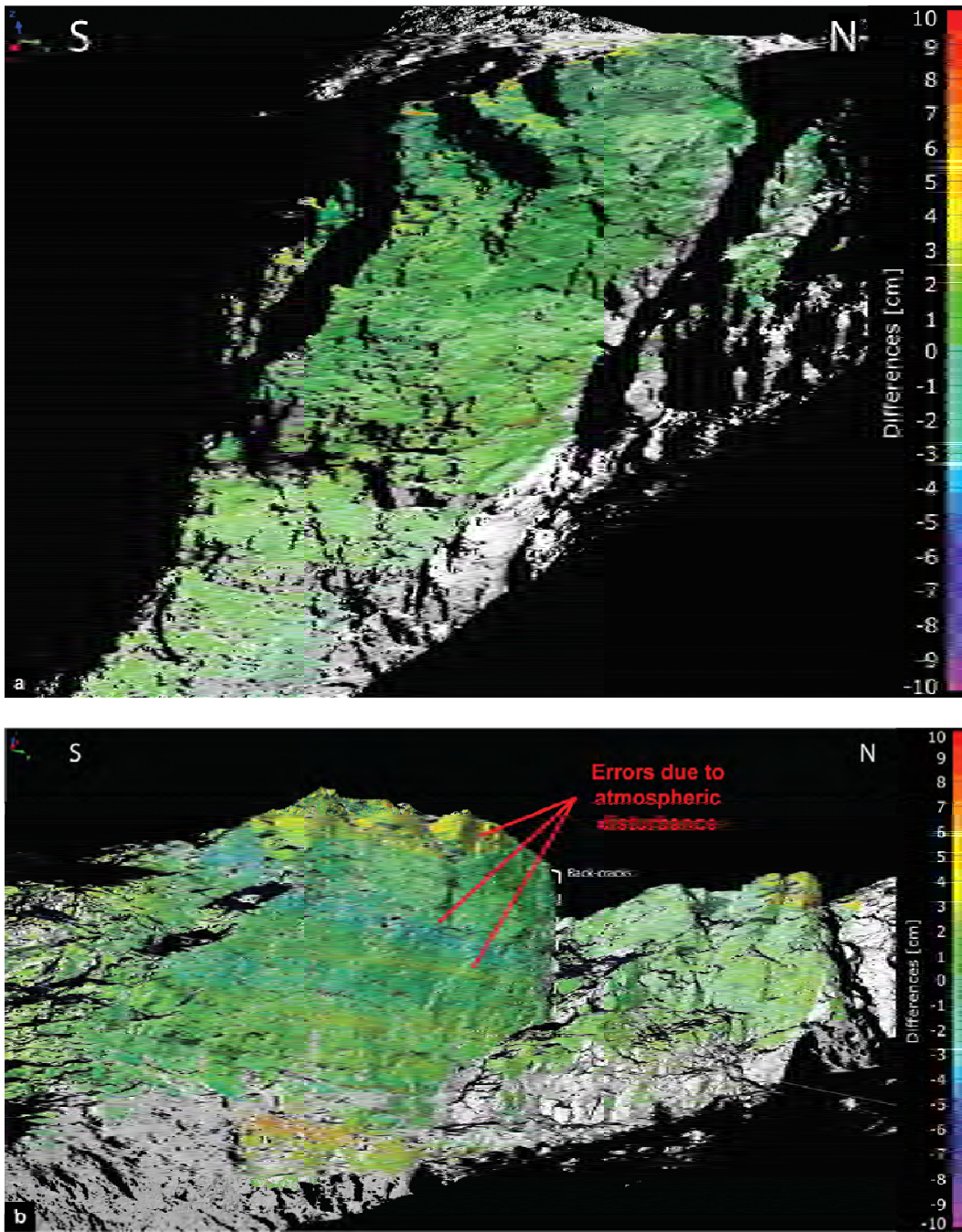


Figure 83. Shortest distance comparisons between the 2008 and 2009 TLS point clouds of the Tussen instability (from Carrea et al., 2010): a) comparison of scans from viewpoints A along the back-scarp; b) comparison of scans from viewpoints C & D that are affected by atmospheric disturbances.

dGPS

Three rover points and 1 fixed point were established in 2007. In 2008 a further fixed point was installed behind the graben structure at the top of the plateau. All points were measured in 2008 and 2009. Although there has been significant displacement of some of the rover points from one to the other years, these displacements have with only a few mm/yr been small and

not consistent over the entire observation interval and can therefore not be interpreted as certainly related to gravitational movement (Appendix 1). To come up with more consistent data, a longer measurement interval seems to be necessary.

Recommendations

No further TLS investigations are planned at the Tusser rock slope instability, but could be done in a few years depending on movement indications by dGPS. New TLS acquisitions should include a sufficiently large stable area (at least 25% of the scanned area) as has been done in 2009 from viewpoint C. We recommend a monitoring interval of 2 – 3 for the next years, which might be extended once the velocity of gravitational movement can be established with certainty, and in case the movement is as low as suggested by data obtained so far.

3.3.13 Årdal municipality

3.3.13.1 Locality Steiggjeberget (tunnel)

In June 1948, a small rockslide with an estimated volume of 20 000 – 60 000 m³ took place along the southern shore of Årdalsvannet. The rockslide caused a collapse of the southeastern part of the Steiggje-tunnel along the road between Årdalstangen and Øvre Årdal.

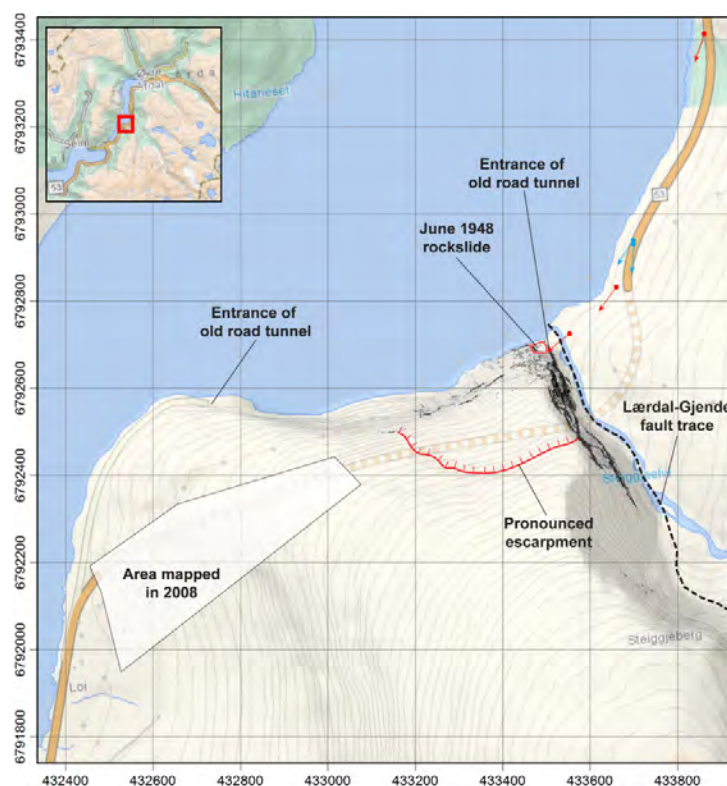


Figure 84. Situation map of Steiggjeberget in Årdal municipality. The extent of the June 1948 rockslide and the possible back-crack of a large instability are shown. The north-eastern part of Steiggjeberget was scanned by TLS in 2009 (red arrows) and 2010 (blue arrows). Stippled line marks the trace of the Tyin-Gjende-Lærdal detachment. The polygon indicates the area mapped in 2008. In addition, the old tunnel has been inspected and old measuring points located.

Steiggjæberget is situated on the eastern side of the lake Årdalsvatn by the RV53 road between Årdalstangen and Øvre Årdal (Figure 84). The rocks belong to the middle allochthonous unit of the Caledonian thrust-sheets, and are mangeritic to gabbroic with veins and lenticular masses of quartz-diorites. A major low-angle normal fault, the Lærdal-Gjende detachment, crops out close to the site (Figure 84, 85).

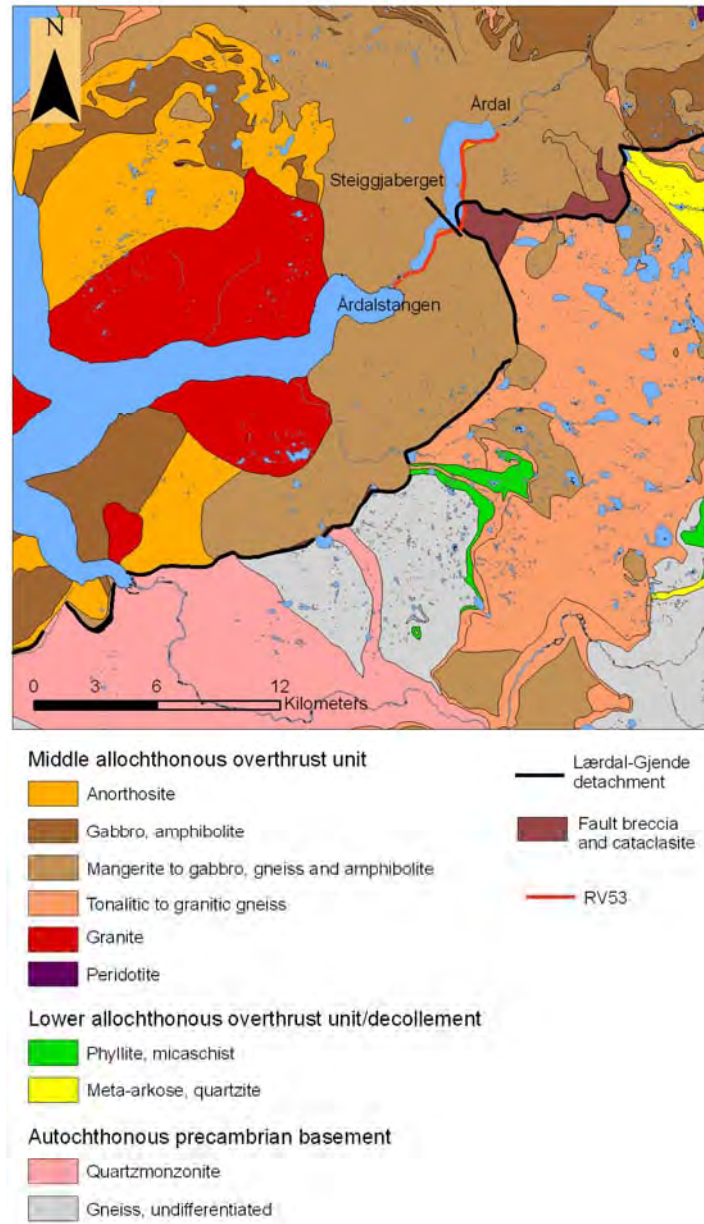


Figure 85. Geological map of the area around Årdalsfjorden. Extract from digital bedrock map 1:250 000 Årdal (Lutro and Tveten 1996)

According to eyewitnesses, the rockmass started to move slowly from the foot of the rockslope close to or below the water surface of Årdalsvatnet. The rockslide moved on a northerly dipping sliding plane. The collapse of the rock mass (Figure 86) created a wavecrest of 30-35 m height on the opposite side of the lake. In Øvre Årdal, the wave-height was estimated to 1.5 – 2m, and a barge was thrown 30-40 metres on land from the shore. The scar

from 1948 is visible from the main road. A vertical back-fracture, from which the rockmass apparently was detached, is still visible in the undestroyed part of the tunnel and also crops out above the tunnel along the mountain side.

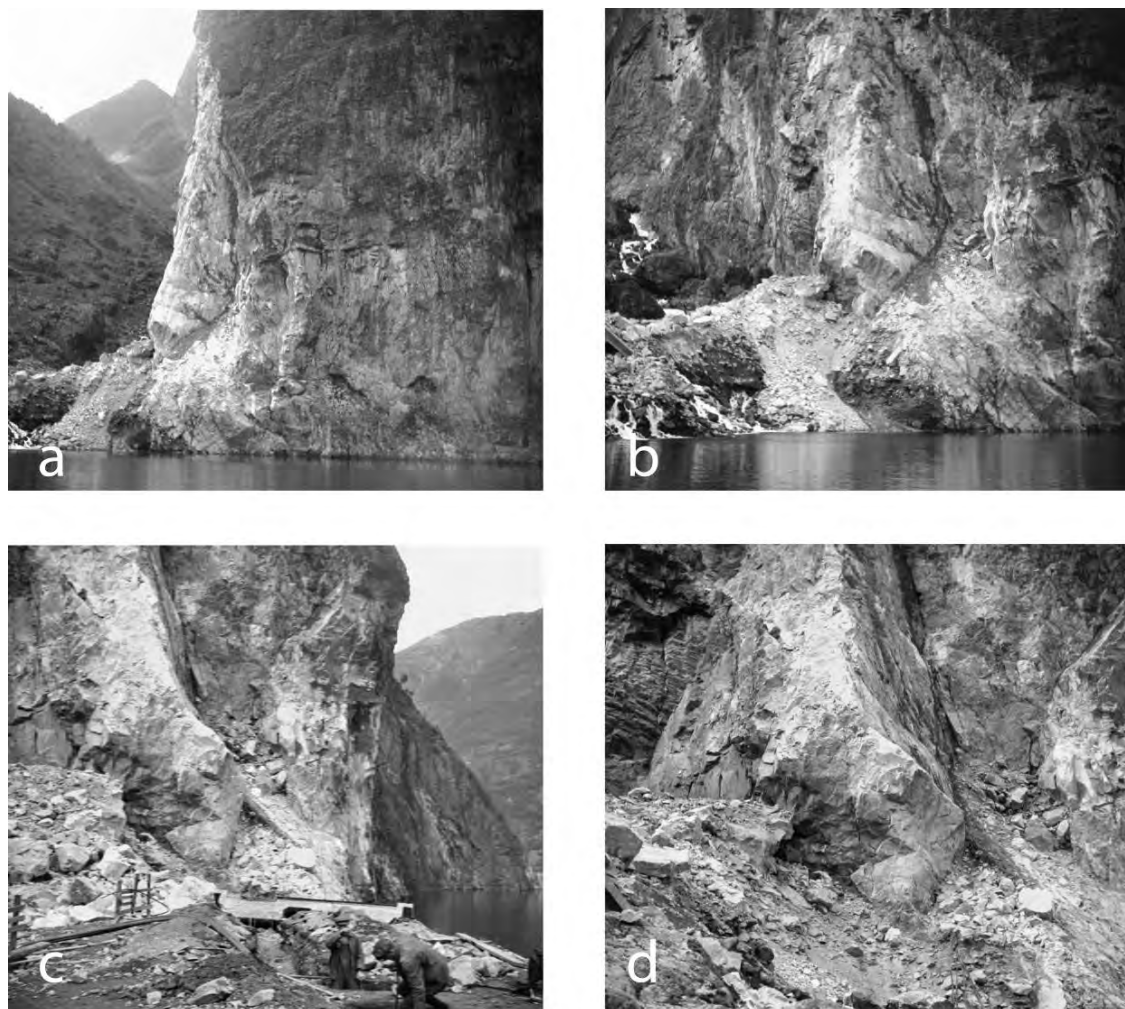


Figure 86. Photographs taken the day after the rockslide in 1948. a) is an overview taken from the lake, and b) is a close up of a. c) is taken from the road east of the tunnel outlet, showing a northerly steeply dipping fracture along which parts of the rock mass moved. d) is a close-up of c. Photos by Aase Udberg. Source: Fylkesarkivet Sogn og Fjordane Fylkeskommune.

The community has been concerned about the consequences of future rockslides along Årdalsvannet. Hence, the Ministry of Agriculture, in 1968, appointed a committee to evaluate the possibilities of future rockslides along the lake Årdalsvatn. The main focus was on the Steggjaberget site, and a number of reports based on detailed structural and engineering geological mapping, underwater-inspections and diamond drilling were published in the period 1968-1973. A total of six survey stations for manual measurements of displacements on fractures were established, and a simulation/model of water waves generated by a potential rock slide was also produced (Eie et al., 1971).

The conclusions from all the engineering geological reports (Norges geologiske undersøkelse, 1948; Årdal og Sunndal Verk, 1970; Vegdirektoratet Geologisk Seksjon, 1970; Jøsang, 1972; Statens Vegvesen Veglaboratoriet, 1972; Selmer-Olsen, 1972, Statens Vegvesen

Veglaboratoriet, 1973) were that the risk for a future rockslide was small. The conclusions were based on:

- The two mapped potential slide planes die out westward
- The two potential slide planes are neither connected nor overlap
- The friction on the potential slide planes is high (epidote sealed)
- Pore pressure/water pressure in the fractures is low
- The measurements from 1968-1972 indicate no ongoing ground deformation

(The survey stations from 1968 are now either destroyed and/or measurements have not been conducted as recommended).

The wave model, based on an anticipated volume of 120 000 m³ of rock, gave a maximum wave height of about 1.0 m at Årdalstangen and 3.2 m at Øvre Årdal (Eie et al., 1971).

The mountain side behind and above the new tunnel (Figure 84) was investigated in 2008. No “significant” fractures were found in that area. The area more to the north, in the vicinity of the old tunnel where the back-fracture should crop out, could not be visited because of very difficult accessibility.

3.3.13.2 Interpretation of lake-bathymetry

In 2008 Årdal municipality provided bathymetric data on Årdalsvatnet to NGU with the request to interpret those data with respect of prehistoric rock slope failures that deposited within the lake (Figure 87). These data are incomplete for the entire lake as the lake margin is missing in the data set. The deposit of the 1948 event could not be mapped, as this most likely deposited near the shore. In total we could at least detect three rockslide deposits (Figure 87, red, green, blue). One occurs in the same area as Steiggjeberg and is the deposit of a prehistoric event. Also 2.5-3 km to the north the deposits of at least two different generations of rockslides exist. However, the bathymetry does not allow a unique interpretation. Both deposits can also be interpreted as each being the deposits of two different events that sourced from similar areas and closely spaced in time.

Terrestrial laser scanning

Two TLS acquisitions were made at Steiggjeberg (Figure 84). The initial survey on 9 July 2009 included three scans from three positions and led to a unified point cloud with 6.2 million points (mean point spacing: 7.4 cm at an average distance of 510 m). A follow-up acquisition was made on 26 June 2010 with four scans from a single view point along the road.

The structural analysis of the 2009 TLS point cloud was made in Coltop3D by the University of Lausanne, Switzerland (Carrea et al., 2010, see Appendix 2, pp. 18-22). This point cloud was georeferenced initially using a 25 m DEM. For this report, the georeferencing has been improved using the new 10 m DEM. This re-georeferencing led to a reorientation of the TLS datasets by a clock-wise rotation of approx. 14°. As a consequence the measured discontinuity orientations had to be corrected, but the interpretation by Carrea et al. (2010) remains valid.

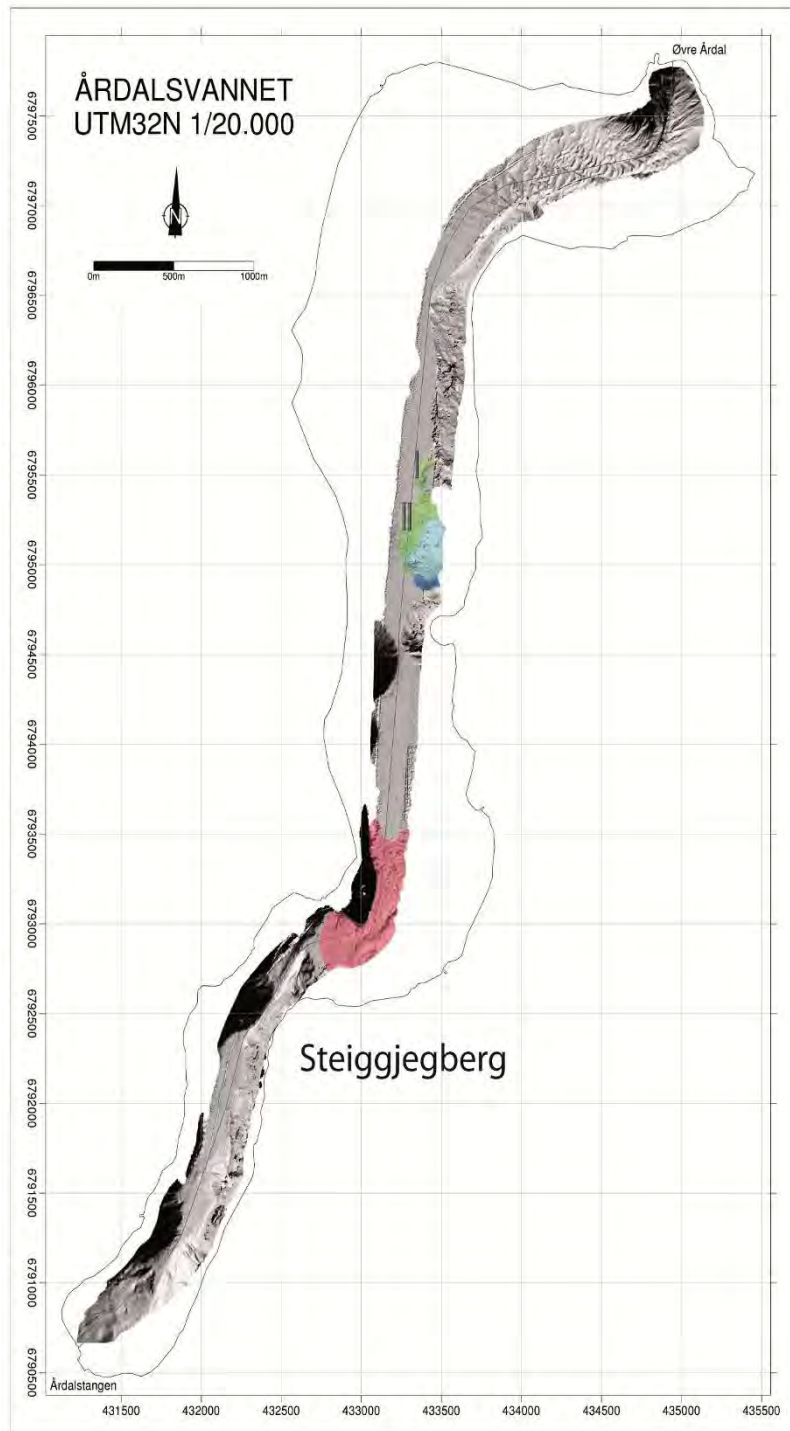


Figure 87. Bathymetric data of Årdalsvatnet with interpretation of deposits of rockslide deposits in colour. The deposit marked in red below Steiggjeborg is much larger than the event from June 1948 with an estimated volume of 20 000 – 60 000 m³. Therefore the deposit mapped in red represents a deposit of an early, likely prehistoric, event. In this area of the lake the bathymetry is incomplete and all data near the shore below Steiggjeborg are missing. No deposits from the 1948 event could be mapped suggesting that they deposited in near shore area. 2.5 – 3 km north of Steiggjeborg other rock slide deposits could be mapped. These belong to at least two (green, blue), and maybe four generation of events (I, II, light blue, dark blue).

The corrected discontinuity orientations are shown in Figure 88. The ENE-facing cliff above the tunnel entrance is mainly formed by discontinuities J2 ($072^{\circ}/84^{\circ}$) and J3 ($003^{\circ}/74^{\circ}$), while the lake-facing cliff is shaped by discontinuity sets J3 and J1 ($295^{\circ}/74^{\circ}$). No gently to moderately dipping structures can be found on the TLS point cloud, which is surprising given the proximity of the gently NW-dipping fault (estimated orientation: $295^{\circ}/23^{\circ}$). Kinematic feasibility tests were made for these two principal slope orientations. In the ENE-facing cliff planar sliding is partly possible on J2 and toppling is possible on the overhangs formed by J1 (Figure 88a). In the NNW-dipping cliff facing Årdalsvatnet, planar sliding on J3 and wedge sliding involving discontinuity sets J1, J2 and J3 are possible failure mechanism (Figure 88b). Toppling on J4 is also feasible. A preliminary analysis shows that the 1948 rockslide was a wedge failure formed by J3 as basal sliding surface and J2 as auxiliary sliding surface.

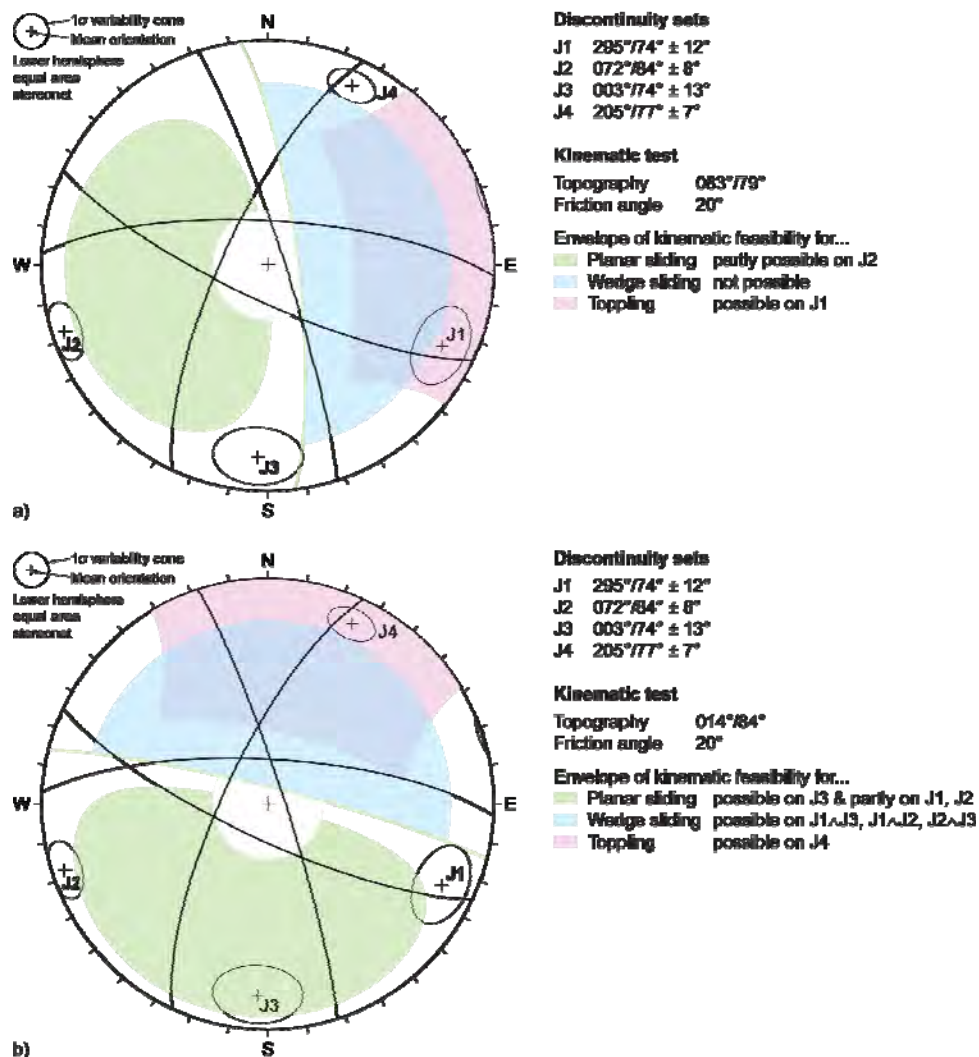


Figure 88. Stereographic projection of the main discontinuity sets at Steiggjeberg. The stereonet and the table show the corrected discontinuity orientations after re-georeferencing on the 10 m DEM. Kinematic feasibility tests for planar sliding, wedge sliding and toppling are shown for two slope orientations: a) the ENE face of the tunnel entrance ($083^{\circ}/79^{\circ}$); b) the NNW face towards Årdalsvatnet ($014^{\circ}/84^{\circ}$).

The comparison between the 2009 and 2010 TLS datasets reveal neither significant displacements nor small rockfall activity (Figure 89). However, the shortest distance comparison has a relatively large error margin (approx. 3 cm), which limits the detection of small, centimetric displacements.

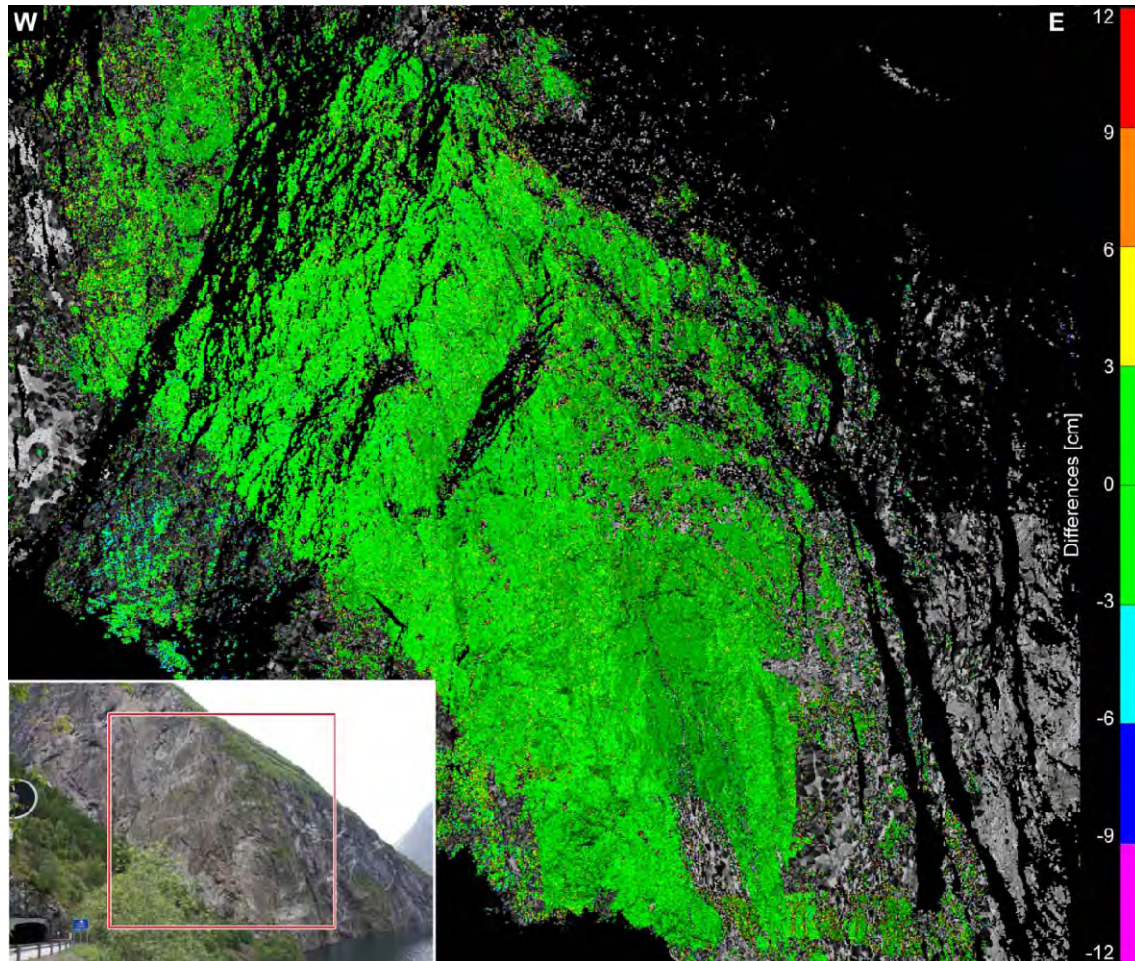


Figure 89. Shortest distance comparison between the 2009 and 2010 TLS point clouds at Steiggjeberg. The colour scheme shows the differences between the datasets. No significant movement or rockfall activity can be detected.

Recommendations

Further investigations at Steiggjeberg include the back-analysis of the 1948 rockslide (structures, mechanism, volume, slope stability) and the delimitation of potentially unstable volumes in 3D. This work will be done in 2011 using the available TLS datasets. A periodic monitoring by TLS (every 3 to 5 years) should be made to detect rockfall activity and pre-failure displacements that could indicate a future larger rockslide.

Based on that additional work, the installation of a crack-meter to monitor the supposed back-fracture in the old tunnel and in the rock-slope above the tunnel is suggested.

3.3.13.3 Locality Årdalstangen

The town of Årdalstangen in Årdal municipality lies between Årdalsfjorden and the Årdalsvatnet and is surrounded on both valley sides by steep cliffs that are prone to rockfalls. The lithologies in the study area are high-grade metamorphic rocks belonging to the Jotunheimen complex (pyroxene-bearing granulite and gneisses of gabbroic to quartz-mangeritic composition).

On 3 December 2009, a large rockfall occurred on the north-western valley side (Figure 90 a). Local authorities estimated a volume of 3000 m³. The rock mass fragmented into several blocks up to 2-3 m in diameter (Figure 90b). The blocks went around the existing rockfall protection dams and destroyed some arable land. One block even crossed the nearby residential road and destroyed the terrace of a house (Figure 90c, 91). Nobody was injured or killed.

Terrestrial laser scanning

An initial TLS point cloud of the SE-facing cliffs at Årdalstangen was acquired on 23 June 2010. Seven scans from two viewpoints on the rockfall protection dam were made (Figure 91) and unified to a single point cloud (9.5 million points; mean point spacing: 10.3 cm at a mean distance of 317 m). This dataset allowed creating a high-resolution DEM with a cell size of 25 cm (Figure 91).

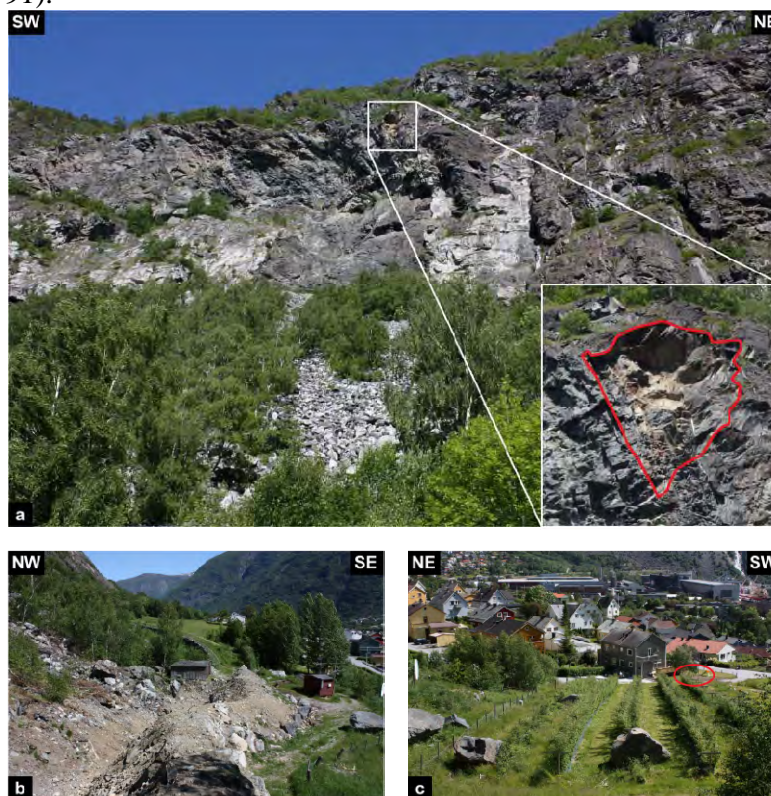


Figure 90. Pictures of the 3 December 2009 rockfall at Årdalstangen: a) view to the NW of the vertical cliff with a detail of the rockfall scar (inset); b) newly constructed temporary rockfall protection dam and debris of the 2009 rockfall; c) blocks in the arable land and remaining impact traces on a house (red ellipse).

A detailed structural analysis of the discontinuities at Årdalstangen will be made in 2011 based on the 2010 TLS point cloud in Coltop3D. This analysis will include kinematic

feasibility tests for planar and wedge sliding and toppling. The structures present in the scar of the 2009 rockfall will be in special focus.

The assumption of continuity between the present topography in the surroundings of the rockfall scar and the pre-event topography within the scar area allows the reconstruction of the topography in 3D. The differences between the pre- and post-event topography express the thickness of the rockfall (Figure 92). Due to the complex geometry of the scar and in order to avoid overhanging parts, an oblique TLS-DEM had to be created and used for the comparison (Figure 92a). Thus the computed thickness is measured in horizontal direction with an average thickness of 2.61 m (maximum: 6.47 m). Multiplying the average thickness by the scar area (269 m²) gives the total rockfall volume (704 m³).

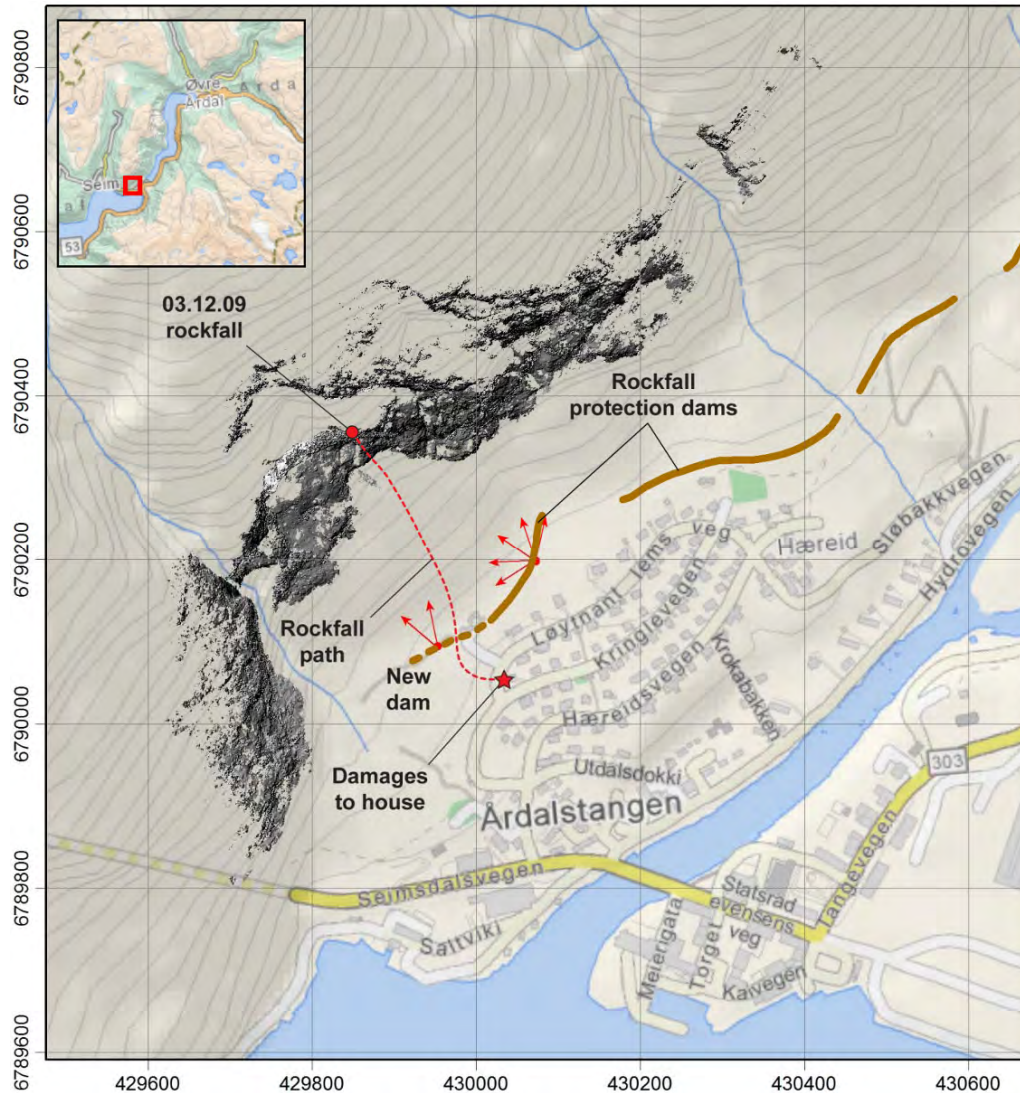


Figure 91. Map of the SE-facing cliffs at Årdalstangen (Årdal municipality). The hillshade of the TLS-DEM shows the extent scanned in 2010 from two viewpoints (red arrows). The release area of the 3 December 2009 rockfall and the approx. travel path of the block with longest run-out distance (red line and star) are indicated. Coordinates are in UTM32N.

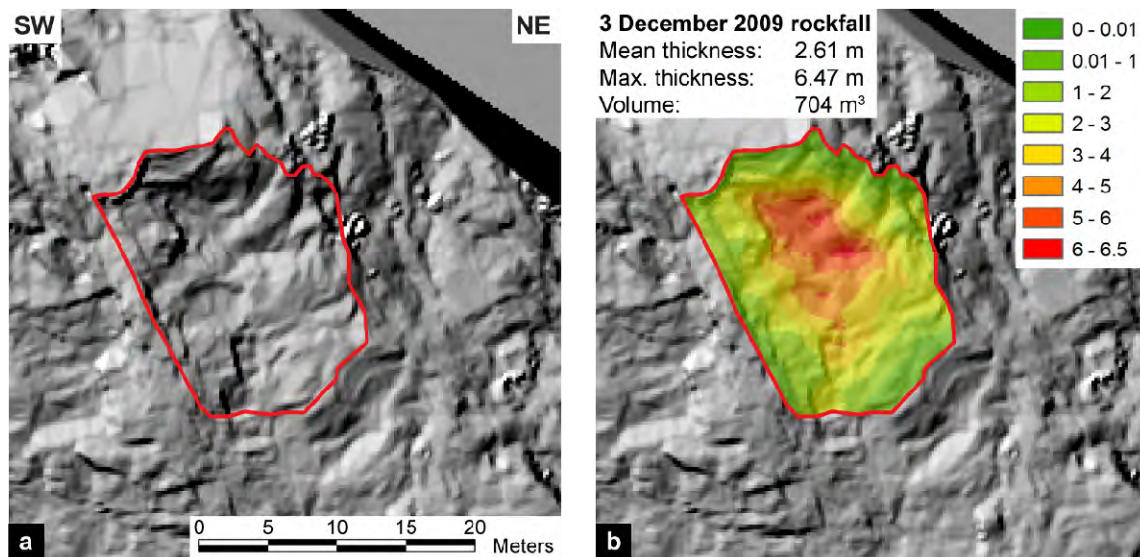


Figure 92. Frontal view of the December 2009 rockfall at Årdalstangen: a) Oblique TLS-DEM showing the extent of the rockfall release area; b) thickness (in metres) between the reconstructed pre-rockfall topography and the present topography.

Recommendations

Even though rockfall protection dams exist above the houses in Årdalstangen, we recommend performing detailed rockfall hazard mapping, including detailed structural analysis (based on TLS data and if possible field measurements), delimitation of unstable rock masses and run-out analyses. Periodic TLS monitoring every 1-2 years are helpful to locate areas with rockfall activity and/or small displacements that are indicators for future large rockfalls.

3.3.13.4 Locality Ramneberget (Øvre Årdal)

Ramneberget is a more than 600 m wide and 200 m high cliff facing the village of Øvre Årdal (Årdal municipality). The south facing cliff is prone to rockfalls and large scree slopes extend down to the settlement.

The lithology of the cliff is composed of high-grade metamorphic rocks belonging to the Jotunheimen complex (pyroxene-bearing granulite and gneisses of gabbroic to quartz-mangeritic composition).

Terrestrial laser scanning

A first TLS survey of Ramneberget was made on 8 July 2009 with seven scans from three viewpoints (Figure 93). The cleaned and unified point cloud is composed of 14 million points with an average spacing of 8.9 cm (at a mean distance of 369 m). A second TLS acquisition was performed on 23 June 2010 with 4 scans from 2 viewpoints (5.4 million points; mean point spacing: 11.6 cm at 459 m) (Figure 93).

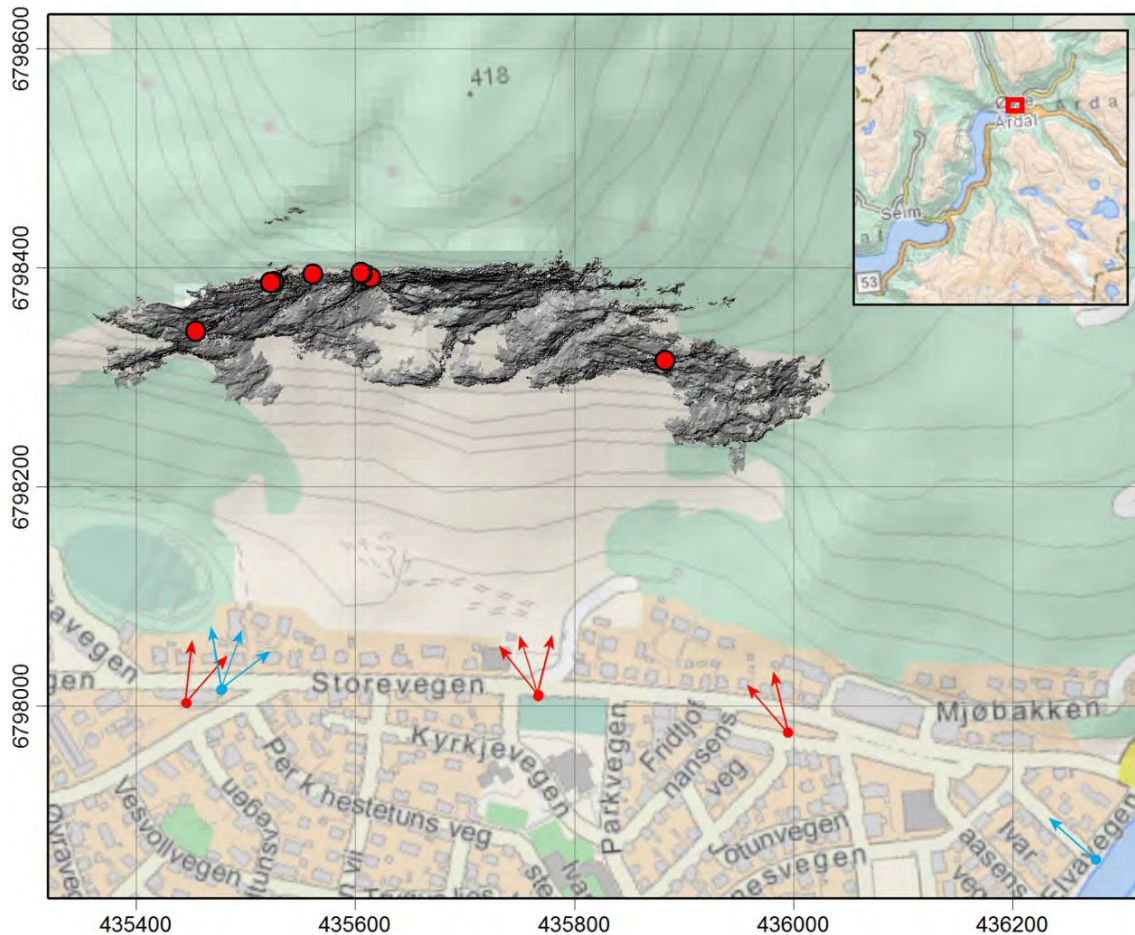


Figure 93. Map of the Ramneberget cliff above Øvre Årdal with the hillshade representation of the 2009 TLS-DEM. The locations of rockfalls that occurred between July 2009 and June 2010 (red dots), as well as the scan positions and view directions (2009: red arrows; 2010: blue arrows) are shown. Coordinates are in UTM32N.

The orientations of main discontinuities at Ramneberget were measured using the software Coltop3D. The structural analysis was made by the University of Lausanne, Switzerland (Carrea et al., 2010, see Appendix 2, pp. 9-13) using the 2009 TLS point cloud that was georeferenced using the 25 m DEM. Since then, a new 10 m DEM has become available and has been used to improve the georeferencing of the TLS datasets. The difference between the old and new georeferencing corresponds to a rotation of 6.8° . As a consequence the discontinuity orientations measured by Carrea et al. (2010) had to be corrected, but their discussion remains valid.

The corrected discontinuity orientations are shown in Figure 94. The major part of the cliff is formed by discontinuities J5 ($178^\circ/70^\circ$) and the overhanging set J4 ($010^\circ/66^\circ$). The kinematic feasibility tests show several possible failure modes using the orientation of discontinuity J5 as slope orientation (Figure 94). Planar sliding is possible on J5 and partly on J2. Wedge sliding is possible along the intersection line formed by J5 with J1, J2 and J3, respectively. The overhanging discontinuity set J4 satisfies the criteria for toppling failure.

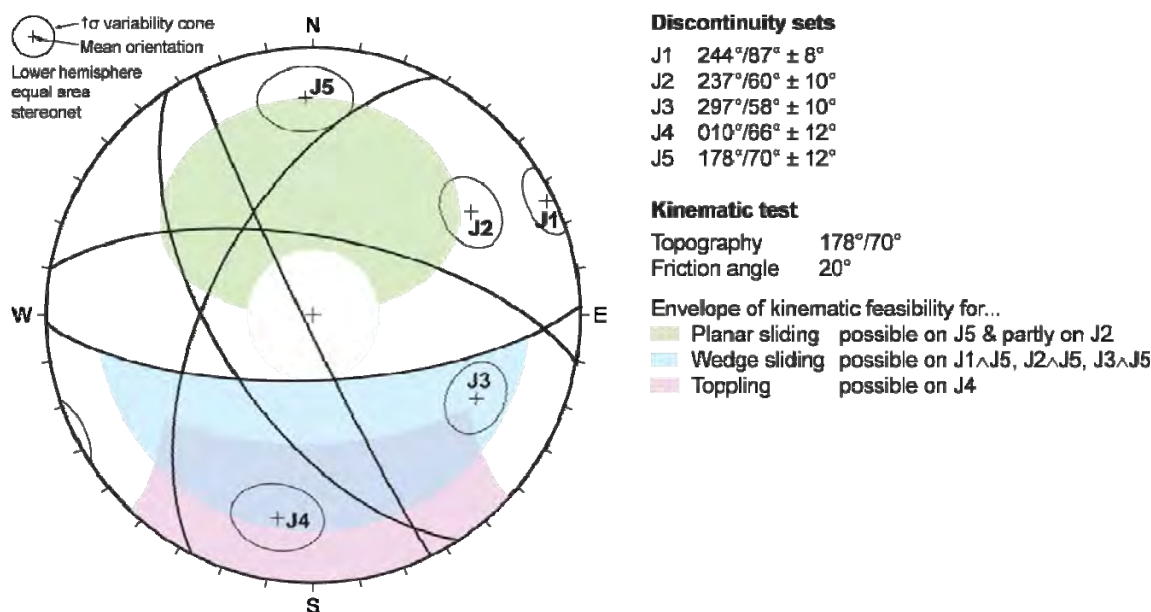


Figure 94. Stereographic projection of the main discontinuity sets at Ramneberget (Øvre Årdal). The stereonet and the table show the corrected discontinuity orientations after georeferencing on the new 10 m DEM. Kinematic feasibility tests for planar sliding, wedge sliding and toppling are shown assuming an average slope face of 178°/70° (J5).

The comparison of the 2009 and 2010 TLS point clouds does not reveal significant displacements of potentially unstable large blocks, but ten small rockfalls were detected (Figure 95a, b). These were visually identified on the shortest distance comparison between the 2009 and 2010 datasets, which necessitates several contiguous cells with coherent differences (Figure 95c, d). The volume of each rockfall was computed based on the differences between the multi-temporal point clouds. The measured volumes range from 0.014 to 0.636 m³ (Tab. 6). A volume of 0.014 m³ corresponds to the minimum detectable volume with the used approach and equals a cubic block with an edge length of 24 cm that weights less than 40 kg.

The rockfall release areas are mainly located in the lower parts of the cliff, except rockfalls #2 and #3 (Figure 95a, b). Eight out of ten rockfalls (#2 to #9) are detected in the central part of the cliff, which is much steeper than the western and eastern parts. Five rockfalls with volumes ranging from 0.034 to 0.115 m³ cluster in a relatively small area of about 10 m x 15 m (Figure 95a, b). This clustering of rockfalls could be related to higher internal stresses in the rock mass, which in turn could be an indication of instability of a larger compartment.

Recommendations

Given the proximity of houses to the scree slopes and the detected rockfall activity, we recommend to continue with TLS monitoring every 1-2 years. Ramneberget in Øvre Årdal should be followed up with detailed rockfall hazard mapping, including delimitation of unstable rock masses and run-out analyses.

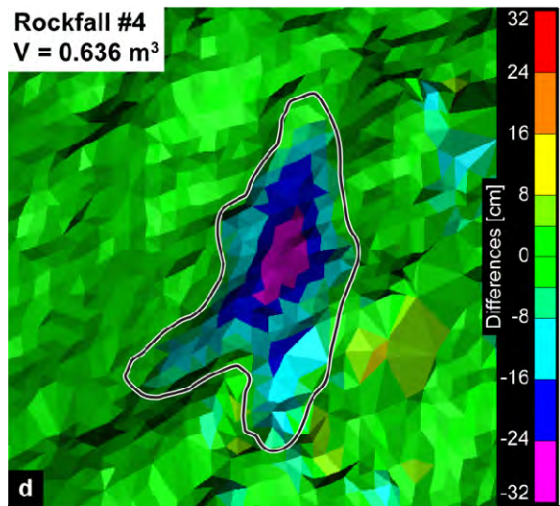
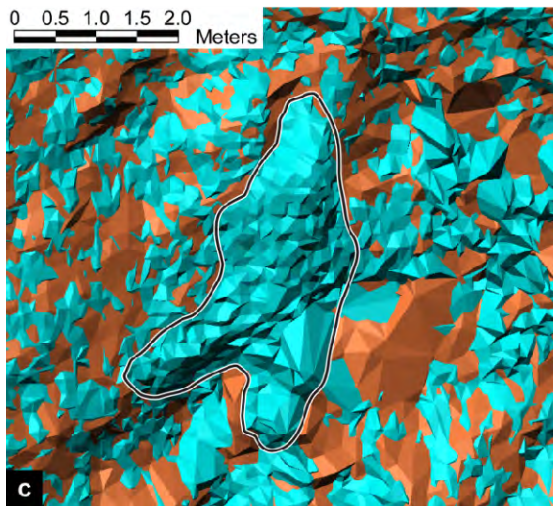
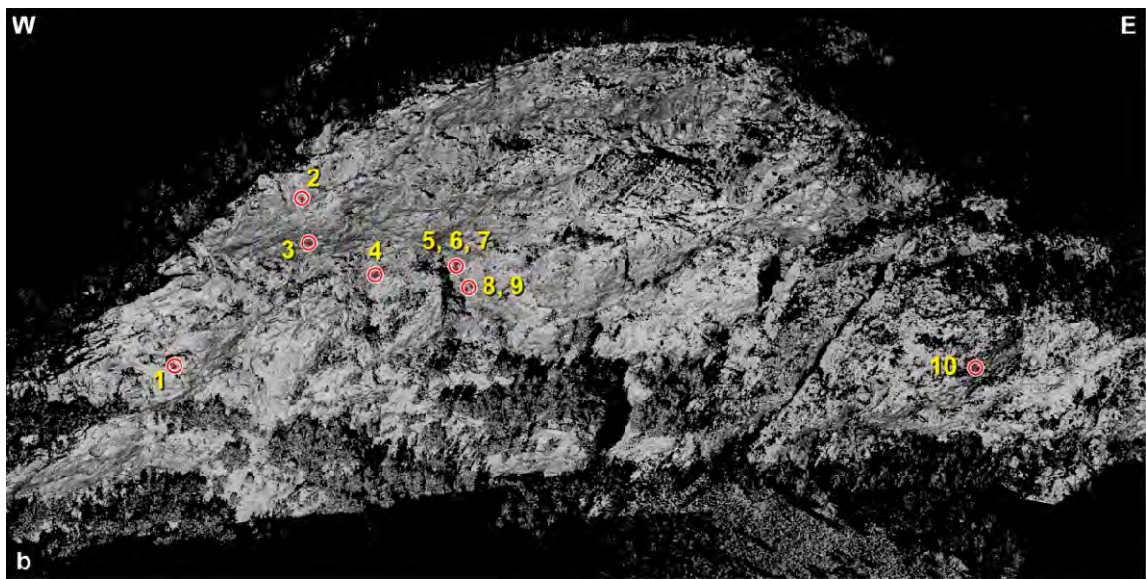
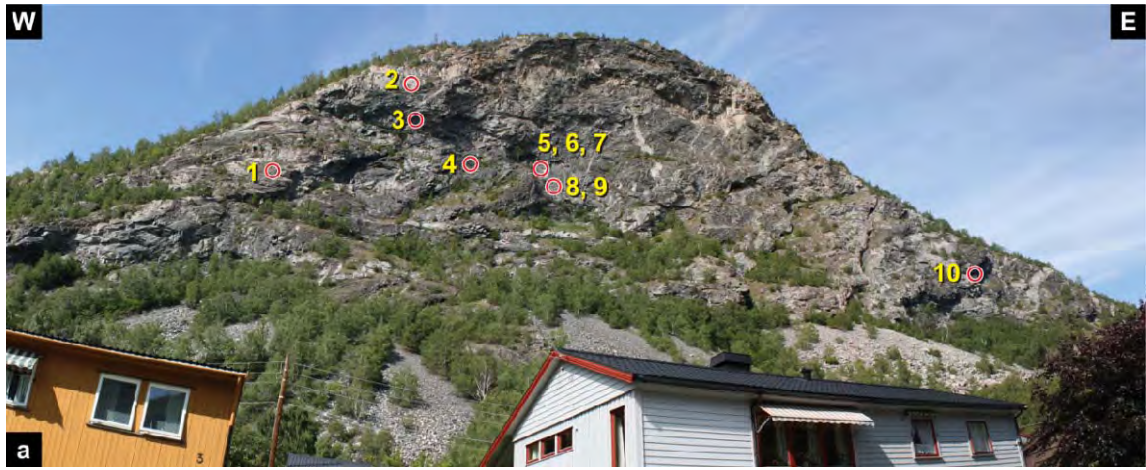


Figure 95. Location of the 2009-2010 rockfalls at Ramneberget (Øvre Årdal): a) panorama picture; b) 3D view of the 2010 TLS point cloud; c) detail of rockfall #4 with the meshed TLS point clouds (2009: light blue; 2010: orange); d) differences between the 2009 and 2010 TLS point clouds showing the missing volume due to rockfall #4.

Table 6. Location and volume of rockfalls at Ramneberget (Øvre Årdal) between July 2009 and June 2010. Rockfall # corresponds to numbering in Figure 95. Coordinates in UTM 32N.

Rockfall #	X [m]	Y [m]	Z [m]	Volume [m ³]
1	435454.2	6798342.1	180.8	0.015
2	435522.8	6798386.4	270.6	0.014
3	435526.0	6798387.3	247.0	0.067
4	435561.5	6798393.8	230.0	0.636
5	435604.9	6798395.3	234.7	0.034
6	435605.1	6798394.5	232.9	0.091
7	435605.4	6798394.6	236.1	0.115
8	435610.3	6798392.7	222.3	0.090
9	435613.4	6798390.7	224.2	0.059
10	435882.7	6798315.0	180.0	0.131

3.3.13.5 Locality Dalsuri (Øvre Årdal)

Dalsuri is a more than 1000 m long and up to 115 m high cliff facing the village of Øvre Årdal (Årdal municipality). The south-facing cliff is prone to rockfalls and scree slopes with large boulders extending down to the inhabited area.

The cliff is formed by high-grade metamorphic rocks belonging to the Jotunheimen complex (pyroxene-bearing granulite and gneisses of gabbroic to quartz-mangeritic composition).

Terrestrial laser scanning

TLS acquisition of the Dalsuri cliff were made on 9 July 2009 and 23 June 2010, each with four scans from two viewpoints (Figure 96). The cleaned and assembled point clouds comprise 8.5 and 4.8 million points for 2009 and 2010, respectively. The resulting mean point spacings are 9.3 cm and 11.9 cm, respectively (at a mean distance of ~500 m).

The structural analysis in Coltop3D was performed by the University of Lausanne, Switzerland (Carrea et al., 2010, see Appendix 3, pp. 14-17) using the 2009 TLS point cloud that was georeferenced with the 25 m DEM. The re-georeferencing on the new 10 m DEM modified the reported discontinuity orientations by a clock-wise rotation of 2°. The corrected orientations are shown in Figure 97. Discontinuity set J1 (329°/16°) is interpreted to be the main foliation. The main part of the cliff is shaped by the overhanging J3 discontinuities (007°/77°). Two other subvertical sets, J2 (073°/89°) and J4 (311°/74°), are also observed in the cliff at Dalsuri. The kinematic feasibility tests show that planar and wedge sliding is not possible on the measured discontinuities with the given slope orientation (188°/78°). The overhanging J3 discontinuities enable a toppling failure. Possible rockfalls can be detached from the back by J3, from the top by J1 (foliation) and laterally by J2 or J4.

The shortest distance comparison between the 2009 and 2010 TLS point clouds does not reveal any significant displacements of distinct compartments of large volume. However, this comparison reveals 22 small rockfalls (Figure 98). Rockfalls are found in most parts of the cliff, but a cluster with six rockfalls is detected in the lower, central part of the cliff (Fig. 98).

Using the approach described for the Ramneberg locality (see above), the volume of these rockfalls can be measured. The largest detected rockfall has a volume of 1.7 m³. The detailed volume analysis of the other rockfalls at Dalsuri needs to be made in 2011.

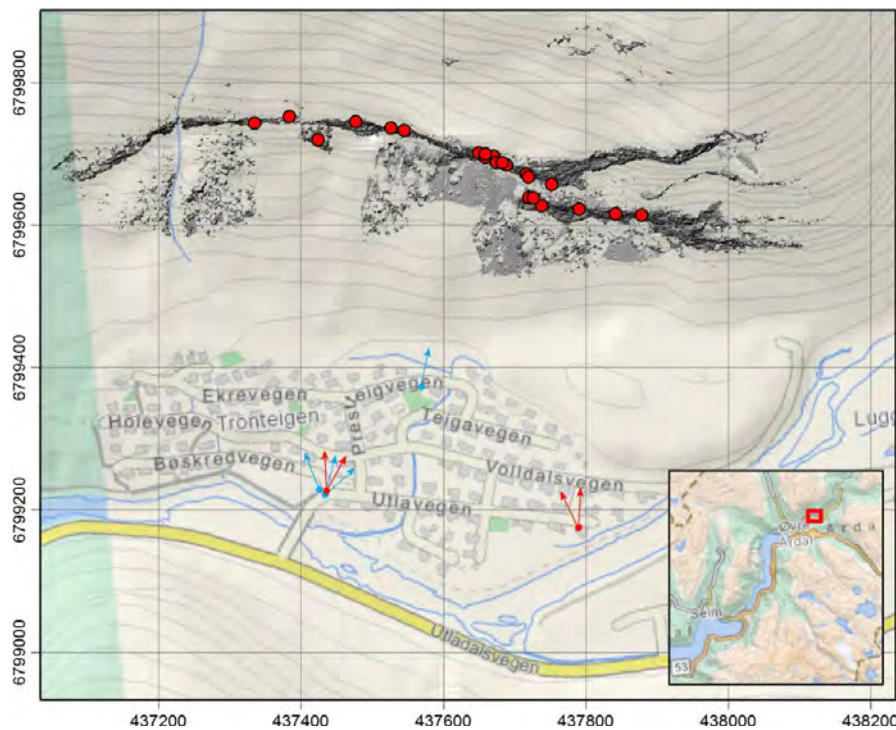


Figure 96. Location map of the Dalsuri cliff in Øvre Årdal. The locations of rockfalls that occurred between July 2009 and June 2010 (red dots), as well as the scan positions and view directions (2009: red arrows; 2010: blue arrows) are shown. Coordinates are in UTM32N.

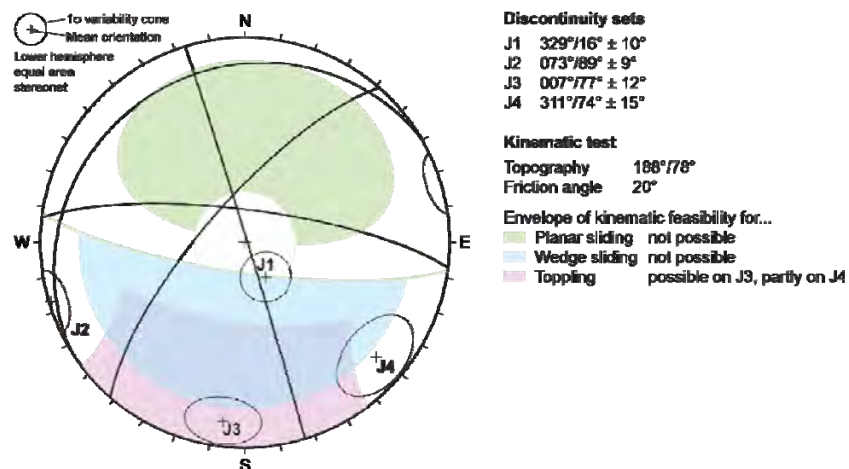


Figure 97. Stereonet of the main discontinuity sets at Dalsuri (Øvre Årdal). The discontinuity orientations reported by Carrea et al. (2010) were corrected after georeferencing on the new 10 m DEM. Kinematic feasibility tests for planar sliding, wedge sliding and toppling are shown assuming an average slope face of 188°/78°.

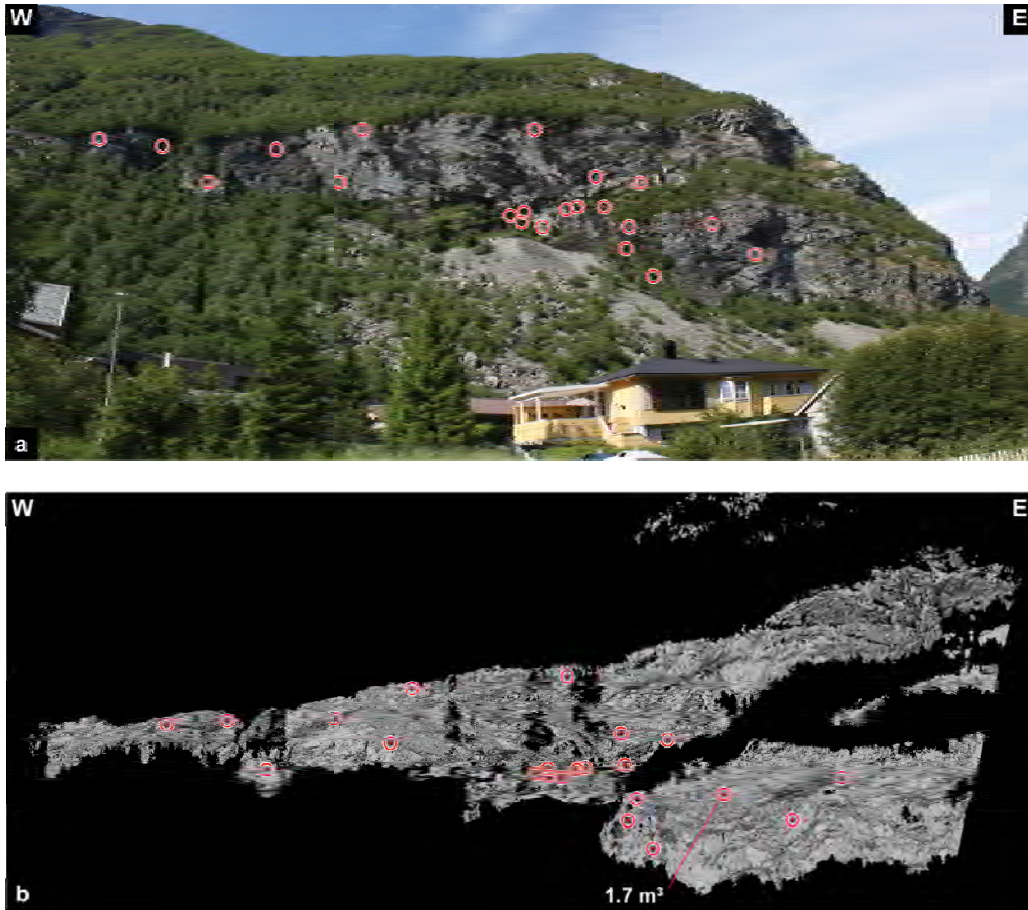


Figure 98. Location of rockfall activity at Dalsuri between 2009 and 2010: a) Panorama photograph taken from a TLS scan location; b) 3D view of the 2009 TLS point cloud showing the location of small rockfalls.

Recommendations

Given the proximity of houses to the scree slopes and the detected rockfall activity, we recommend to continue with TLS monitoring every 1-2 years. Dalsuri in Øvre Årdal should be followed up with detailed rockfall hazard mapping, including delimitation of unstable rock masses, quantification of rockfall activity and run-out analyses.

4. Suggestion for future work

4.1 Further work on known sites

The work on the mapping of unstable and potentially unstable slopes in Sogn og Fjordane county is already in an advanced stage, but has still to be continued to conclude the investigations at all sites. More field data acquisition has to be performed for the sites Skrednipa and several locations in the Vik municipality (Vik, Framfjord, Arnafjord). Further data evaluation has to be performed for the sites Vidme, Skrednipa, Vik and Osmundneset. Repeated TLS measurements will be performed at the sites in Årdal municipality. The dGPS measurements have to be continued, and for the sites Lifjellet and Gråberget, other monitoring methods such as extensometers have to be considered.

A final risk assessment has to be performed for all investigated sites. This will give advice on the localities where work can be considered as completed and those sites that need periodic or permanent monitoring. This risk assessment will be performed based on a method that is currently developed for Norway.

4.2 Systematic mapping for unknown sites and rock avalanche deposits

To be able to complete the mapping of unstable and potentially unstable slopes in Sogn og Fjordane county, we must make a area-wide detection of unstable slopes. Therefore, a systematic aerial image analysis is planned for the detection of all deposits of old rock avalanches and the detection of unknown unstable slopes. The work will be based on remote sensing analyses (on digital aerial images) and include GIS analyses. This systematic mapping work will be conducted in summer 2011 and include detailed mapping of all visually detected rock avalanche deposits and possible unstable slopes showing open cracks or signs of slope deformation. The data of this survey will be added to the current database of unstable slopes in the Sogn og Fjordane county. If more possible unstable slopes are detected, it has to be decided to whether more detailed analyses have to be performed on these sites in future.

4.3 Continuation of dGPS periodic monitoring

The dGPS monitoring has to be continued at all sites with installed points. The measurement interval has to be defined for each site based on the measured displacement rates and the geometrical setup of the instability. Most of the sites have to be measured on an annual basis for the next two years, and a decrease in measurement repetition has to be discussed again in a few years. New dGPS points have to be installed at Skjeringahaugane and Vik to better understand the extent and/or kinematics of rock deformation. Currently, no new sites have to be equipped with a dGPS monitoring system. However, this decision may have to be reconsidered after the area-wide remote sensing mapping for unknown sites, depending on whether more relevant sites have been detected.

4.4 Future TLS work

TLS data for structural analyses have been acquired today at all sites where it seemed necessary. With the exception of Viddalen the obtained data are of good quality and capture the interesting parts of the instability. At Viddalen a further scan should be made focussing more on the frontal part of the instability.

The need for TLS for monitoring will be evaluated based upon future dGPS results. Those will indicate when enough deformation has occurred so that it can be mapped out by TLS. However, velocities on most sites in Sogn og Fjordane are relatively low and several years are needed that a repetition will bring any results.

An exception is the rock slopes monitored in Årdal municipality. All of those slopes are prone to rockfalls rather than large rock slope instabilities. Hence, it has to be considered to continue the recommended future work within another project focusing on rockfall hazard mapping and rockfall monitoring.

4.5 Future InSAR work

Since 2010, NGU has been acquiring Radarsat-2 fine-mode satellite data over most of Sogn og Fjordane. By the fall of 2012, we will have enough data to reprocess this area. The

Radarsat-2 data have a pixel size of 5 by 9 metres, while the ERS data are 4 by 20 metres. This gives a moderate improvement in spatial resolution of the velocity measurements. More important is the fact that we should have six to seven images each year, leading to a more regular temporal sampling of the movement.

5. Conclusions

In the past three years NGU has worked on 25 unstable and potentially unstable rock slopes in Sogn og Fjordane. Most of those slopes do not deform consistently over the entire unstable area and at most sites a lot of structures exist that allow the instabilities to break in smaller blocks prior to a catastrophic failure. This suggests that it is more likely to experience a restricted rock slope failure in the future that does not have the high mobility of a rock avalanche. However, in settled areas and above water bodies, larger rockfalls can also cause severe consequences. This is in line with a historical analysis of this county, showing that a much larger number of large rock falls has occurred than rock avalanches (Henderson et al., 2008).

We also mapped Fjørlandfjord, Hyenfjord and Årdalsvatnet systematically for deposits of prehistoric and historic rock slope failures onshore and with help of a bathymetry and multiple prehistoric events were documented in Fjørlandfjord and Årdalsvatnet. It is likely that several hundreds of deposits exist on land and on the fjord bottom in Sogn og Fjordane. It is strongly recommended to map those deposits systematically to better estimate future failure scenarios.

Mapping on land included structural mapping of ten sites by on-site field mapping and nine sites by remote structural mapping using terrestrial laser scanning (TLS) technology in areas not easily accessible. The combination of both methods allow for a complete understanding of anisotropies within the rock mass which permits the establishment of the kinematics of slope deformation. These structural analyses are an essential part of any mapping of unstable rock slopes and should always been given high priority.

Kinematic analyses were performed for all of these sites and are resented in this report. These will be used when we evaluate hazard levels for each site as a next step.

Field work also included periodic monitoring of 14 sites using differential Global Positioning Systems (dGPS) and TLS at 4 sites. Most sites monitored by dGPS were visited on a yearly basis. These are the most robust deformation data we have today. However, at most sites deformation velocities are low with only a few mm per year and less. This requires collecting data over a larger period until slip rates can be trustfully established.

Synthetic aperture radar was applied for the entire county and slide velocities could be mapped out at at Osmundneset (Gloppen municipality). In the near future new RADAR data with higher temporal and spatial resolution will become available. These new data are promising to better map out deformations using this technology. In addition, a ground based RADAR was installed at Flåm in April 2011. Within one or two years we expect to get robust data to better map deformation in this area.

A large amount of work was carried out on the slope east of Flåm in Aurland valley and results have been reported in a separate report (NGU 2011.025).

In the last three years, three large instabilities have been discovered or taken into the monitoring program. These are Osmundneset in Gloppen municipality, Skrednipa in Sogndal

municipality, and Ovrís valley in Vik municipality. All sites are of considerable volumes, and catastrophic failures would result in disasters. The sites therefore have to be followed up. The site in the Ovrís valley is the fastest moving known rockslide in Sogn og Fjordane today. The site at Osmundneset deforms with measurable velocities, however it seems that the site is developing differently in different sectors. Velocities measured today at that site are not outstanding and similar to tens of other slowly deforming rock slopes in Norway. However, further investigation and periodic monitoring is needed. The Skrednipa site is known for the shortest time and we still work on better understanding the kinematics of deformation at this site. We also could not reliably determine the deformation velocities today. Some more effort will be spent on the site in summer 2011.

The largest velocities with 1.5 cm horizontal and 1.5 cm vertical movement were measured on the instability with a volume of approx. 1 Mm³ in the Ovrís valley. Opening of cracks has been measured at that site also in the 60's, 70's and 80's. Our data suggest a slight acceleration of movement of this instability. An acceleration of movement velocities was also documented for an instability called Lifjellet, although the velocity of that site with an calculated volume of 100.000 m³ is less than half of the velocity of the block in the Ovrís valley. However, at Lifjellet a collapse of a rockslope with a volume of 40.000 m³ occurred only 19 years ago. Installation of continuous monitoring and early warning systems should be discussed for those sites. A similar solution might be considered for relatively small instabilities that might fail without a long acceleration phase and that are positioned above houses (Gråberget in Høyanger municipality). However, velocities are smaller than at Lifjellet. Similarly, all other monitored instabilities in Sogn og Fjordane are in the order of mm/yr and not considered as critical on a short term. Nonetheless, periodic monitoring has to be continued.

Cosmogenic nuclide dating (CN) that has been applied to determine ages of rockslide deposits in Fjærlandsfjord and at the slope east of Flåm resulted in Late Pleistocene and Holocene ages. CN dating has also applied to the sliding planes at Skjeringahaugane (Luster municipality). Results indicate that the instability started moving at the beginning of the Holocene, and is progressive and accelerating while stepping forward. Long-term slip rates are in the same order as the slip rates measured by dGPS. We recommend the use of this technique also in future to date rock avalanche deposits and to determine long time slip rates over longer time periods. This is especially important in order to detect acceleration of slip rates.

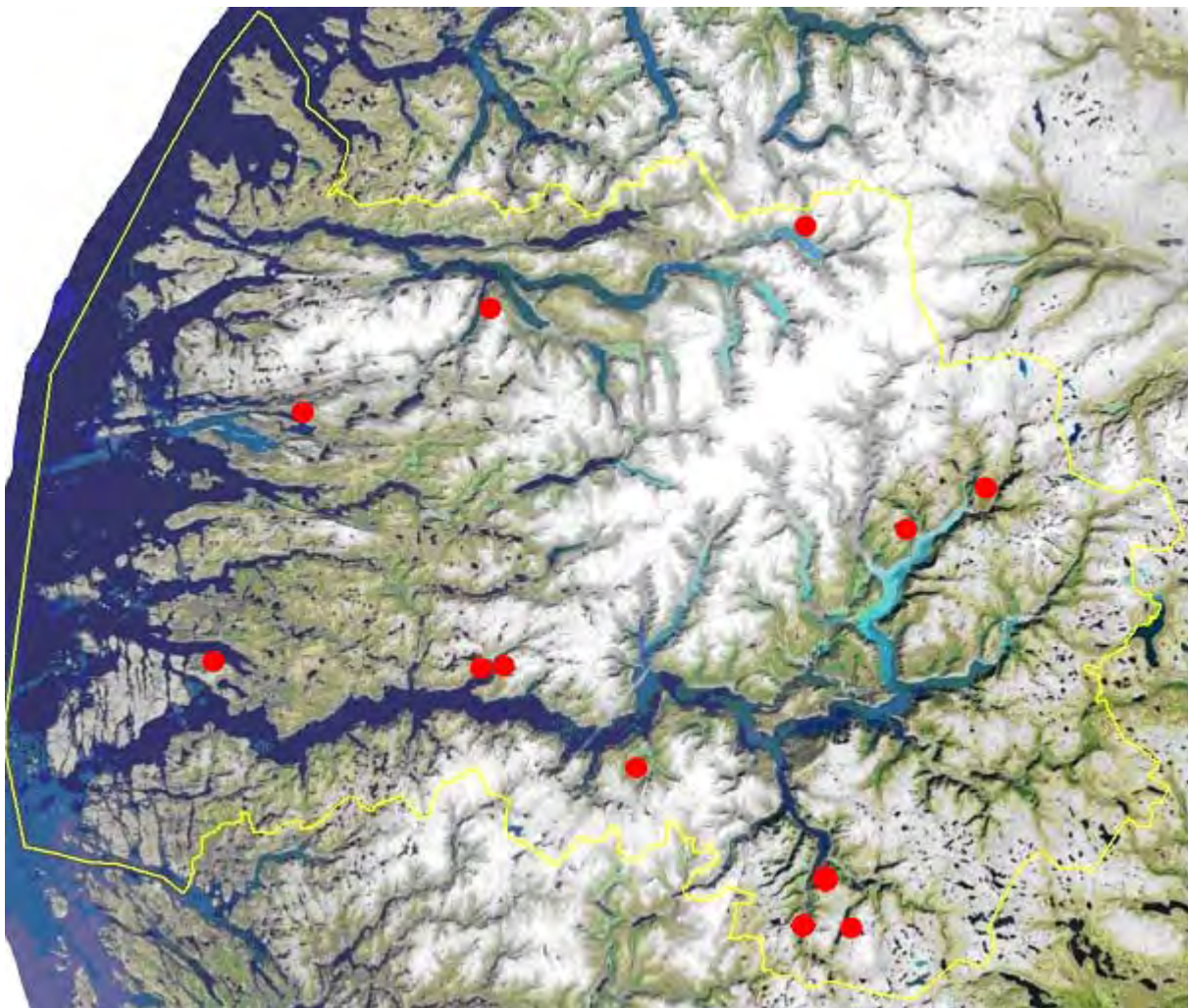
6. References

- Ballantyne, C.K.**, Stone, J.O., Fifield, L.K., 1998. Cosmogenic Cl-36 dating of postglacial landsliding at The Storr, Isle of Skye, Scotland. *Holocene* 8 (3), 347–351.
- Berardino, P.**, G. Fornaro, R. Lanari, and Sansosti, E. (2002), A new algorithm for surface deformation monitoring based on small baseline differential SAR interferograms, *IEEE Transactions on Geoscience and Remote Sensing*, 40(11), 2375-2383.
- Bigot-Cormier, F.**, Braucher, R., Bourlès, D., Guglielmi, Y., Dubar, M., and Stéphan, J.-F., 2005, Chronological constraints on processes leading to large active landslides, *Earth and Planetary science Letters*, v. 235, 141-150.
- Blikra, L.H.**, Longva, O., Braathen, A., Anda, E., Dehls, J.F., Stalsberg K., 2006. Rock slope failures in Norwegian fjord areas: Examples, spatial distribution and temporal pattern. In: Evans, S.G., Scaraascia Mugnozza, G., Strom A., Hermanns R.L., (eds.) *Landslides from massive rock slope failures*. Dodrecht, Springer, pp. 475- 496.
- Böhme, M.**, Saintot, A., Henderson, I. H. C., Henriksen, H. & Hermanns, R. L. 2011. Rock slope instabilities in Sogn and Fjordane County, Norway: a detailed structural and

- geomorphological analysis. In: Jaboyedoff, M. (ed.) *Slope Tectonics*. Geological Society, London, Special Publications, 351, 97 - 111.
- Bøe, R.**, Lepland, A., Blikra, L.H., Longva, O. and Sønstegeard, E. (2002): Postglacial mass movements in western Norway with special emphasis on the 2000-2200 and 2800-3200 BP periods – final report. Geological Survey of Norway report 2002.020, 115p.
- Carrea, D.**, Lévy, S., Derron, M.-H., Longchamp, C., Loye, A., Oppikofer, T. & Jaboyedoff, M., 2010: Analysis of groundbased Lidar data from Sogn og Fjordane County (Norway). Institute of Geomatics and Analysis of Risk, University of Lausanne, Lausanne, Switzerland.
- Chen, C. W.**, and Zebker, H. A. (2001), Two-dimensional phase unwrapping with use of statistical models for cost functions in nonlinear optimization, *J Opt Soc Am A*, 18(2), 338-351.
- Domaas, U.**, Rosenvold, B.S., Blikra, L.H., Johansen, H., Grimstad, E., Sørli, J.E., Gunleiksrud, O., Engen, A., Lægneid, O., 2002: Studie av fjellskred og dalsidestabilitet i fyllittområder. NFR rapport 20001132-2, 146p.
- Eie J.**, Solberg G., Tvinnereim K., Tørum A. 1971: Waves generated by landslides. In *Port and ocean Engineering under Arctic conditions*, Report Norwegian Technical University p. 489-513.
- Fenton, C R.**, Hermanns, R L, Blikra, L H, Kubik, P W, Bryant, C, Niedermann, S, Meixner, A, Groethals, M M. (2011). Regional ^{10}Be production rate calibration for the past 12 ka deduced from the radiocarbon-dated Grøtlandsura and Russenes rock avalanches at 69° N, Norway, *Quaternary Geochronology*. In press.
- Ferretti, A.**, C. Prati, and Rocca, F. (2001), Permanent scatterers in SAR interferometry, *IEEE Transactions on Geoscience and Remote Sensing*, 39(1), 8-20. Gosse, J.C., Phillips, F.M., 2001. Terrestrial in situ cosmogenic nuclides: theory and application. *Quaternary Science Reviews* 20 (14), 1475–1560.
- Harbitz, C. B.**, Domaas, U. & Varlid, E. 2001. Rock slide generated tsunamis - probability and hazard zoning in Åfjorden, Western Norway. *Fjellsprenningsteknikk - bergmekanikk - geoteknikk*. Oslo 2001, 27.1 - 27.13.
- Henderson, I.H.C.**, Saintot, A., Böhme, M., and Henriksen, H. 2008. Kartlegging av mulig ustabile fjellpartier, Sogn og Fjordane. Norges geologiske undersøkelse, NGU Report 2008.026, 114pp.
- Hendron, A. J. Jr.** & Patton, F. D. 1987. The Vaiont slide – a geotechnical analysis based on new geologic observations of the failure surface. In: Leonards, G. A. (ed.) *Dam Failures*. *Engineering Geology*, 24, 475–491.
- Hermanns, R.L.**, Niedermann, S., Villanueva-Garcia, A., Sosa-Gomez, J., Strecker, M.R., 2001. Neotectonics and catastrophic failure of mountain fronts in the southern intra-Andean Puna Plateau, Argentina. *Geology* 29 (7), 619–623.
- Hermanns, R.L.**, Niedermann, S., Ivy-Ochs, S., Kubik, P.W., 2004. Rock avalanching into a landslide-dammed lake causing multiple dam failure in Las Conchas valley (NW Argentina) — evidence from surface exposure dating and stratigraphic analyses. *Landslides* 1 (2), 113–122.
- Hermanns, R.L.**, Blikra, L.H., Naumann, M., Nilsen, B., Panthi, K.K., Stromeyer, D., Longva O., 2006. Examples of multiple rock-slope collapses from Köfels (Ötz valley, Austria) and western Norway. *Engineering Geology*, 83: 94-108.
- Hermanns, R L.**, Bunkholt, H, Böhme M, Fischer, L, Oppikfer, T, Rønning, J S, Eiken, T. (2011). Foreløpig fare- og risikovurdering av ustabile fjellparti ved Joasete-Furenkamben-Ramnanosi, Aurland kommune. NGU rapport 2011.025, (ISSN 0800-3416). 47 p.
- Hormes, A.**, Ivy-Ochs, S., Kubik, P., Ferrel, L., Michetti, A.M., 2008, ^{10}Be exposure ages of a rock avalanche and a late glacial moraine in Alta Valtellina, Italian Alps, *Quaternary International*, v. 190, 136-145.

- Høst, J.**, 2006. Store fjellskred i Norge, NGU, 87pp.
- Ivy-Ochs, S.**, Poschinger, A., Synal, H.-A., Maisch, M., 2009, Surface exposure dating of the Flims landslide, Graubünden, Switzerland. *Geomorphology*, 103: 104-112.
- Jaboyedoff, M.**, Metzger, R., Oppikofer, T., Couture, R., Derron, M., Locat, J. & Turmel, D., 2007: New insight techniques to analyze rock-slope relief using DEM and 3D-imaging cloud points: COLTOP-3D software. In: *Rock mechanics: Meeting Society's challenges and demands. Proceedings of the 1st Canada - U.S. Rock Mechanics Symposium, Vancouver, Canada, 27-31 May 2007*, eds. E. Eberhardt, D. Stead & T. Morrison, Taylor & Francis, London, pp. 61-68.
- Jøsang O.** 1972: Notat vedr. professor R. Selmer-Olsens brev av 16. mai til Arbeidsutvalget vedrørende rasfare i Årdal om "Steggjaberget riksveg 53 Årdal – Oppdragsrapport 46-S30, Veglaboratoriet, Jøsang 1972". Notat Ottar Jøsang, Veglaboratoriet 16.06.1972, 3 s.
- Lauknes, T. R.**, H. A. Zebker, and Y. Larsen (2011), InSAR Deformation Time Series Using an L1Norm Small-Baseline Approach, *IEEE Transactions on Geoscience and Remote Sensing*, 49(1), 536-546.
- Longva, O.**, Blikra, L.H. and Dehls, J.F. (2009): Rock avalanches – distribution and frequencies in the inner part of Storfjorden, Møre og Romsdal County, Norway. Geological Survey of Norway report 2009.002, 23p.
- NGI, rapport 76459-1, 1966, Investigation on rock slide area in Ovrís valley, West Norway, 14p.
- Norges Geologiske undersøkelse 1948: Ang. ras i tunnelen ved veien langs Årdalsvatnet. Notat 13.07.1948.
- NVE rapport 14.2011, Plan for skredfarekartlegging, 85p.
- Oppikofer, T.**, Jaboyedoff, M., Blikra, L.H. & Derron, M., 2009: Characterization and monitoring of the Åknes rockslide using terrestrial laser scanning. *Natural Hazards and Earth System Sciences*, vol. 9, no. 3, pp. 1003-1019.
- Sanchez, G.**, Rolland, Y., Corsini, M., Braucher, R., Bourlès, D., Arnold, M., and Aumaître, G. 2010. Relationships between tectonics, slope instability and climate change: Cosmic ray exposure dating of active faults, landslides and glacial surfaces in the SW Alps, *Geomorphology*, 117: 1-13.
- Scheidegger, A.E.**, 1973, On the prediction of the reach and velocity of catastrophic landslides. *Rock Mechanics*, vol. 5, 231-236.
- Selmer-Olsen R.** 1972: Steggjaberget riksveg 53 Årdal – Oppdragsrapport 46-S30, Veglaboratoriet, Jøsang 1972. Notat Geologisk Institutt NTH, 16.05.1972, 3 s.
- Statens Naturskadefond, repport 76459-1, 1984, Stabilitetsvurdering av skredområde og forslag til nærmere kontroll av stabilitetsutvikling, 7p.
- Statens Vegvesen, Veglaboratoriet 1973: Oppsetting av sinkbånd for kontroll av mulig utvidelse av sprekkene bak det tidligere antatt rasfarlige fjellpartiet ved østenden av den gamle Steggjatunnelen ved Årdalsvannet. Utførelse av kontrollmålinger., Rapport 5 s. + vedlegg.
- Statens Vegvesen Veglaboratoriet 1972: Avsluttende undersøkelse av det antatt rasfarlige fjellpartiet ved østenden av den gamle Steggjatunnelen ved Årdalsvannet. Rapport 46 – S30, Rapport 31 s. + vedlegg.
- Vegdirektoratet Geologisk Seksjon 1970: Registrering av mulige bevegelser langs sprekker i fjellet på forskjellige steder i Steggjatunnelen ved Årdalsvannet. Rapport, 3 s.
- Welkner, D.**, Eberhardt, E., and Hermanns, R.L. 2010. Hazard investigation of the Portillo rock avalanche site, central Andes, Chile, using an integrated field mapping and numerical modelling approach, *Engineering Geology*, 114: 278-297.
- Wyllie, D.C.**, and Mah, C.W., 2004, *Rock slope engineering*, Spon Press, New York, 430p.
- Årdal og Sunndal Verk 1970: Ras Steggjaberget 1948. Notat, 11.02.1970, 2s.

Rapport
om
Deformasjonsmålinger i potensielle fjellskred
Sogn og Fjordane
2005-10



Trond Eiken
Institutt for geofag
Universitetet i Oslo

Innhald

Samandrag	s. 1
Bakgrunn	s. 2
Metode	s. 2
Koordinatsystem	s. 3
Endringar	s. 4
Resultat	s. 5
Flåm/Aurland	s. 6
Aurland, Viddalen	s. 17
Hyllestad	s. 21
Høyanger, Gråberget	s. 24
Luster, Røssasete	s. 27
Vik, Daurmålshaugen	s. 30
Hyen, Osmundneset	s. 32
Fjærland, Skrednipa	s. 35
Eikefjord, Strandanipa	s. 37
Vidme, Flåm	s. 39

Område som ikkje er målt om i 2010, Stopelen, Høyanger, Oppigardshyrna, Stryn, og Tussen, Luster, er ikkje teke med i rapporten.

Samandrag

Dei fyrste målingane med GPS for å kartlegge deformasjonar i moglege fjellskredområde i Sogn og Fjordane vart utført i Flåm/Aurland og Høyanger (Stopelen) i 2005. Seinare er det etablert nett på i alt elleve stader i fylket, tre av desse nye i 2008. I 2009 er nokre av dei etablerte punktnetta ikkje målt om, dette gjeld Stryn, Eikefjord og Stopelen i Høyanger. Det er i 2009 sett ut nye punkt på Skrednipa i Fjærland og i 2010 eitt punkt på Skrednipa i Fjærland og nye punkt på Vidme i Flåm.

I 2010 er dei fleste av områda med påvist rørsle målt om, medan område som ikkje har synt signifikante teikn til endringar i tidlegare målingar ikkje er målt om i år. Mange av områda syner små endringar som gir signifikante utslag i statistisk test, men overestimert presisjon i målemetoden tilseier at ein bør vere konservativ i tolking av resultat. Det er difor usikre konklusjonar når berre to - tre målingar ligg til grunn for endringar på nokre få millimeter, eller at ein ikkje har klare trendar i resultatet når fleire år vart lagt til grunn.

Målingane så langt syner:

- Det er truleg litt rørsle i dei fleste punkta i Flåm/Aurland, storleik på endring varierer i ulike punkt, men to punkt, AU-14 og AU-12 peikar seg ut med endring ca. 1 cm/år.
- Det er relativt stor rørsle i eitt av punkta på Daurmålshaugen i Vik, meir enn 1 cm i både plan og høgd.
- Det er rørsle i dei to punkta i det austre området i Hyllestad, men relativt låg, ca 3mm pr. år.
- Det er teikn til rørsle i punkta ved Viddalsdammen.
- Det er usikre indikasjonar på rørsle i eitt av punkta på Gråberget ved Høyanger.

For dei andre område må målingane repeterast minst ein gong før ein kan seie noko om endringar.

Bakgrunn

Etter initiativ frå NGU ved Lars Harald Blikra vart det i august 2005 sett ut og målt inn 20 punkt i Flåm – Aurland for å kunne måle eventuell deformasjon i eit fjellområde med tydelege visuelle sprekker.. Arbeidet vart utført av Harald Elvebakk og Anja Midtun, NGU, og Trond Eiken UiO. I oktober 2005 vart det sett ut og målt inn sju punkt ved Stopelen i Høyanger, arbeidet her vart utført av Trond Eiken, UiO, med hjelp frå kommunen og Helge Henriksen frå Høgskulen i Sogn og Fjordane. Punkta i Flåm/Aurland vart målt om i september 2006 av Trond Eiken og Bernt Larsen frå UiO. I oktober 2006 vart det og etablert fire punkt på Oppigardshyrne i Stryn av Aline Saintot og Jomar Gellein NGU.

I 2007 vart alle gamle punkt målt om, og i tillegg vart det sett ut nye punkt i fem område: Strandanipa i Eikefjord, Tussen i Luster, Viddalsdammen i Aurland, Høgeheia i Hyllestad og Gråberget i Høyanger. I 2008 vart det gjort ommåling og nye målingar i tre område, Hyen, Luster og Vik.

I 2009 vart områda målt om med unntak av Stryn (Oppigardshyrna), Eikefjord (Strandanipa) og Stopelen (Høyanger). Og nye punkt sett ut på Skrednipa i Fjærland.

I 2010 er områda med unntak av Stryn, Stopelen og Tussen målt om, og det er etablert nye punkt på Vidme i Flåm og eitt ekstra punkt på Skrednipa i Fjærland.

Denne rapporten dokumenterer målingane frå 2005 til 2010 og gir resultat og statistiske testar på funne rørsler i form av endringar i koordinatane til punkt.

Metode



Alle målepunkta for GPS er markert med gjenga skruvar (5/8 UNC gjengar) som er limt fast i fjell. Gjengetypen gjer at GPS-antenner ved måling kan skruvast direkte på punktet med minimale feil i sentrering. Normalt vert antenna sett på ein ”trefot” (*Fig. 1*) som kan stillast horisontal, slik at antenna vert stilt sentrisk loddrett over sentrum av skruven. Høgd på antenna vert målt ved å måle avstandar på trefoten. I nokre punkt er bolten sett så skeiv at det er uråd å stille trefoten horisontal. Desse punkta er kommentert spesielt sidan dette utgjer ei feilkjelde.

Fig. 1 Trefot med antenne

Måleutstyret som er nytta er Javad/Topcon tofrekvente GPS- mottakarar, dels og med måling av GLONASS satellittar (GLONASS er eit russisk GNSS system som liknar GPS).

Målemetoden er statisk relativ fasemåling, med måling av eit nettverk av vektorar mellom punkt. Måleintervall (epokeintervall) er fem sekund, og måletid minst 30 minutt pr. vektor, men vanlegvis 60 minutt eller meir. Lengre måletider gir vinst i presisjon utan serleg auke i totaltida ein nyttar for målingane. Eit optimalt nettet vert bygt opp slik at alle punkt skal ha samband til minst tre andre punkt, men for fleire av områda her som har berre tre punkt vert ikkje dette kravet oppfylt.

GPS-vektorar er rekna i programmet ”TPS-Pinnacle” rekna som statiske vektorar med heiltals-løysing. I tillegg til vektorar estimerer og programmet standardavvik (σ) for vektorkomponentane. Estimert presisjon (standardavvik) på vektor komponentar er oftast betre enn 1 mm i X og Y, og 2 mm i Z (jordsentrisk XYZ-system), men i ein del tilfelle er standardavvika høgare enn dette. Det er geometriske eigenskapar ved satellitt systema kombinert med at måleområda er relativt langt mot nord som gjer at Z-komponenten i

vektorane normalt har 2-3 gongar høgre standardavvik. Z-komponenten i vektoren har mest å seie for høgdeskilnaden mellom punkt. Satellittane flytter seg på himmelen og måle geometrien vil dermed variere, noko som serleg gir utslag på resultat i høgde. Svak satellittgeometri kan gi meir upresise resultat for høgdeskilnader, utan at dette kjem fullt ut til uttrykk i standardavvika til resultatet. Standardavvika gir ikkje mål for uvisse i høve til "sanne" storleikar, men i høve til resultatata ein har fått (intern presisjon). Sidan dei fleste målingane vert gjort innanfor eit relativt kort tidsrom vil fleire vektorar ha om lag den same geometriske konfigurasjon for satellittar, og dermed ha ei systematisk påverking frå denne. Ommåling nokre timar seinare kan gi litt andre resultat, og den systematiske skilnaden som kan oppstå i dette tilfellet vert lite reflektert av standardavvika til resultatata som kjem fram.

Meteorologiske tilhøve vil og påverke resultatata, serleg for høgder. Ved prosessering av GPS-vektorar vert det nytta ein standardatmosfære som grunnlag. Store avvik får denne i temperatur, trykk eller luftråme vil gi systematiske feil i resultatata, med størst påverking på høgderesultat. Dette kan gi vesentlege utslag dersom målingane i ulike år vert gjort ved svært ulike vértilhøve. Bruk av aktuelle lokale meteorologiske data er eit alternativ, men er forkasta i praksis sidan ei eller fleire bakkenære målingar kan vere lite representative for lufta i større høgde og såleis introdusere andre systematiske feil.

Netta av GPS-vektorar er jamna ut ved nettutjamning etter minste kvadraters metode for å finne dei mest sannsynlege verda for koordinatane til punkta. Tilhøyrande standardavvik for koordinatar vert estimert gjennom utjamninga. Koordinatar for punkt vert rekna relativt til det lokale fastpunktet som er halde fast, dvs. har same koordinat frå år til år. Det er berre eitt fastpunkt i kvart av områda i Sogn, med unntak av området i Flåm/Aurland der det er tre fastpunkt.

Observasjonane vert gitt vekt etter estimert standardavvik for vektorane. Dersom dette estimatet er korrekt skal utjamninga av samla nett gi det same estimat for standardavvik som vektorane. For dei aktuelle netta ligg estimert presisjon faktorar på ca. 2 høgre. Dette indikerer at estimert presisjon for vektorane er optimistisk med ein slik faktor.

Konklusjonen ein må trekke av dette er at serleg for høgdekomponentane bør ein vere konservativ i tolking av endringar, sjølv om det er statistisk signifikant. Når det gjeld endringar i grunnriss er påverknad frå både geometri og meteorologi mindre, men det kan og her gi systematiske utslag.

Koordinatsystem

Alle koordinatar er referert til eit system gitt ved presis absolutt fastlegging av posisjonen til eitt eller fleire punkt i kvart område ut frå GPS-målingane og presise banedata. Dei fastlagde posisjonane er i ITRF2000/2005 referanseramme som ligg nær opptil EUREF89, men koordinatane kan avvike i høve EUREF89 med opptil ca. 1 m.

Koordinatar er gitt som UTM-koordinatar i sone 32 (sentralmeridian 9 grader aust).

Alle høgder er gitt som høgder over ellipsoiden, dvs. høgde over ein teoretisk referanseflate. For å korrigere til ortometriske høgder (over medelvtn) må høgder reduserast med ca. 46 m (Ref. geoidmodellen til Statens kartverk).

Endringar

Endringane over tid er dels framstilt i tabellar som syner koordinatar og endring av desse mellom målingar, med retning og avstand på endringa, eller som grafiske figurar (jfr. Fig. 2). Figurane for endringar syner grunnriss (N,E) og høgd kvar for seg. I tillegg til endring syner figurane og konfidensnivå, dvs. kor stor ei endring må vere for at den skal vere statistisk signifikant. Som signifikansnivå er valt 99%. Dette tilsvarar om lag 3x standardavviket for den funne endringa.

I grunnriss er endringa synt med ein svart pil og signifikansnivået synt med ein raud ellipse, eller ei fotpunktkurve (grøn) til ein ellipse som syner standardavviket til endringa i ulike retningar. Dersom ei endringspil går utanfor fotpunktkurva er endringa signifikant, om spissen ligg innanfor er endringa ikkje signifikant. (Fotpunktkurve og ellipse fell ofte saman slik at berre ellipsen er synleg).

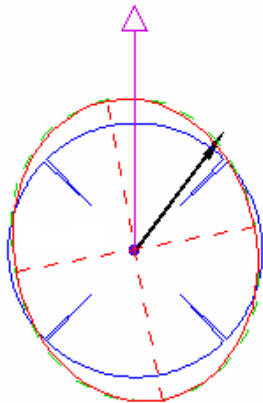


Fig. 2 Konfidensfigur

For høgde er endringane framstilt med sirkclar, blå sirkclar med "taggar" innover representerer senking (rørsle ned), raude sirkclar med "taggar" utover representerer heving (rørsle opp). Grensa for signifikant endring er gitt med ein vertikal pil. Dersom sirkelen ligg utanfor pilspissen er endringa signifikant, om pila endar innanfor sirkelen er den ikkje det. Dette er den viktigaste testen som vert utført for å undersøke om det er truleg at punkt har flytt på seg, eller om variasjonen i koordinatar truleg berre skuldast tilfeldige feil. Alle målingar har visse innslag av feil, og her vil feil på dei einskilde vektorane som vert målt forplante seg til feil i koordinatane som er resultatet. Verknaden av desse feila vert synt som standardavvik for koordinatane. Sjølv om det ikkje er noko som har flytta på seg kan ein ikkje forvente å få identiske resultat. Ein må difor teste om den funne endringa i koordinatar er så stor at den ikkje sannsynleg kan forklarast med feil i målingane. Teorien for dette kan kort forklarast til:

Ved fyrste gongs måling vert posisjonen til punktet fastlagt som UTM-koordinatar $(N,E,h)_1$ og estimert grannsemd (standardavvik) $(\sigma_N, \sigma_E, \sigma_h)_1$ (og korrelasjon mellom N og E koordinat). Ved ommåling vert det estimert tilsvarande posisjon $(N,E,h)_2$ og grannsemd. Ut frå dei to fastleggingane kan ein så teste om koordinatane til dei to tidspunkta er ulike. Svaret på denne testen er i utgangspunktet ja / nei og ikkje informativ ut over det.

Ved i staden å rekne kor mykje koordinatane har endra seg mellom dei to fastleggingane kan ein fastlegge ein "endringsvektor" i grunnriss og høgd. Vektorane er gitt ved:

$$\text{Vektor lengd: } dS = \sqrt{((N_2 - N_1)^2 + (E_2 - E_1)^2)}$$

$$\text{Vektor retning: } r = \text{atan}((E_2 - E_1) / (N_2 - N_1))$$

Denne vektoren vil ha grannsemd som er ein funksjon av grannsemda til koordinatane $(N,E)_1$ og $(N,E)_2$ - $(\sigma_N, \sigma_E)_1$ og $(\sigma_N, \sigma_E)_2$. Grannsemda til vektoren i ulike retningar kan framstillast som ein ellipse (eller strengt fotpunktkurva til ein ellipse). Eitt standardavvik har eit konfidensnivå på 67%, dvs det er 67% sannsyn for at ein tilfeldig observasjon ligg innanfor eitt standardavvik. For å auke sannsynet for at ein ikkje gjer feil slutning er det vanleg å nytte 95 eller 99% nivå for ein test, eller 5 eller 1% sannsyn for feil slutning. Varierende testnivå vil endre storleiken men ikkje forma på feilellipsen. Ein kan difor grafisk framstille endringsvektoren i høve til feilellipsen slik at om vektoren går utanfor feilellipsen så er det signifikant endring på det nivå feilellipsen er skalert til, og tilsvarande ikkje signifikant om vektoren endar inne i ellipsen.

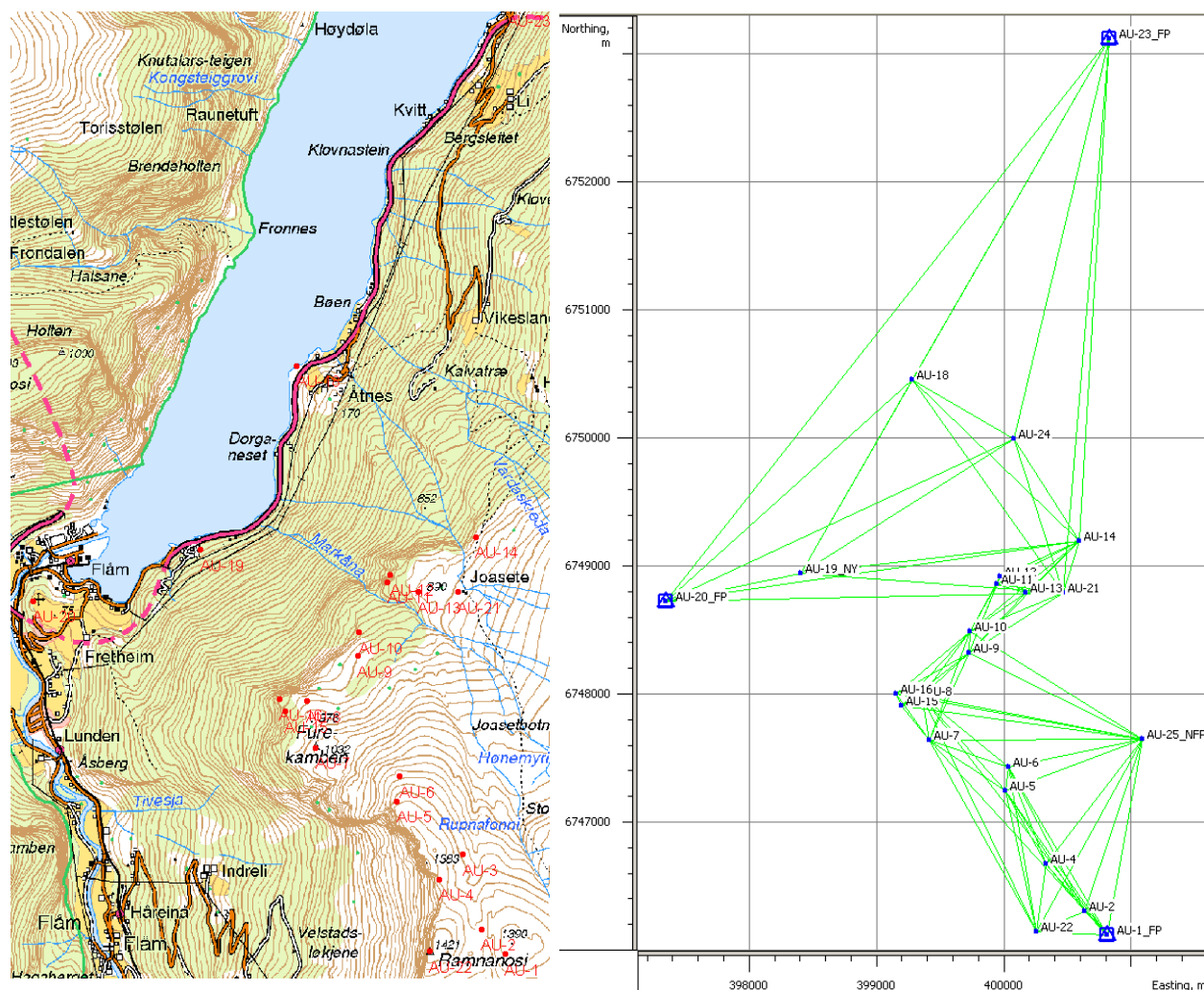
For vertikale endringar er det skilnaden mellom målingane og tilhøyrande standardavvik på differansen som vert estimert og testa tilsvarende. I den grafiske testen vert høgdeendring framstilt som ein sirkel, der radius i sirkelen svarar til endringa. For å skilje heving frå setning vert punkt med heving teikna med raude sirkclar med taggar "utover", og punkt med setning med blå sirkclar med "taggar" innover. Teststorleiken for signifikant endring vert framstilt som ein vertikal stolpe frå sirkelsentrum. Når radien i sirkelen er større enn lengda på stolpen, dvs går forbi enden på denne er endringa signifikant.

Dei grafiske figurane for endring kan såleis både syne kva for endring ein har i dei ulike punkta, og i tillegg syne om denne er signifikant eller ei. Ein kan og sjå korleis endringane er i høve til grensene for signifikans. Storleiken på signifikans ellipsane vil variere ut frå presisjonen til målingane som ligg til grunn og den geometriske utforminga av nettet. Til vanleg vil ein ha aukande storleik på feilellipsane di lengre ein kjem bort frå fastpunkt, og fleire godt fordelte fastpunkt er difor ein stor føremun. I nokre få tilfelle når standardavvik for ein koordinat vert estimert til å vere mindre enn 0,5 mm kan feilellipse mangle på figurane.

Resultat

Resultata er i det vidare presentert for kvart område i form av tabellar med koordinatresultat for kvar måling. Endring i koordinatar er synt i hovudtabell for ulike år i høve til fyrste måling, og i ein separat tabell er synt endringar mellom målingar (år). Grafiske figurar som visualiserer endringar med statistisk signifikanstest er synt for utvalde periodar. Kommenterar for til endringane er gitt for kvart område.

Flåm / Aurland



Figur 3: Kartet til venstre (Sk N50) syner plasseringa av punkta i Flåm/Aurland. Figuren til høgre syner vektornettet for 2005. Blå trekantar er fastpunkt. I 2006 er det i tillegg målt to ekstra punkt på Furekamben.

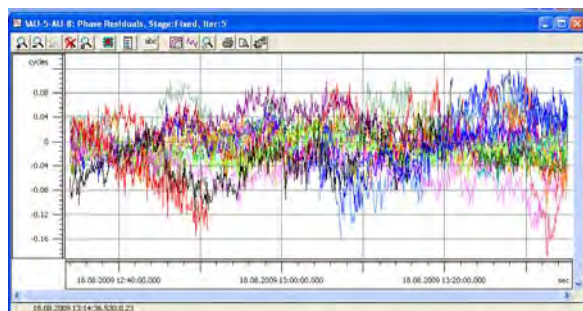
Om målingar og resultat

Det vart i slutten av august 2005 målt inn i alt 20 punkt i området mellom Flåm og Aurland. Området er snaufjell i øvre del, men til dels svært tett skog i lågare deler av området som til tider gjer GPS-målingane vanskelege, og er med på å gi mindre god presisjon på målingane for nokre av punkta.

Av dei 20 punkta som vart etablert i 2005 er tre punkt plassert i fast fjell og vert rekna som fastpunkt. I 2006 vart det etter ynskje frå Flåm Utvikling/NGI sett ut og målt to ekstra punkt på Furekamben i samband med mogeleg taubanestasjon. I 2009 vart punktet AU-19 borte. Ved dette punktet var det i 2008 gravearbeid og bolten var delvis øydelagd, i 2009 var blokka med bolten heilt fjerna slik at punktet er tapt. Det vart i staden etablert eitt nytt punkt i det same området (AU-19_NY). Det vart i tillegg i 2009 etablert eitt nytt punkt, AU-24, eit stykke ovanfor Vikesland. Det vart og etablert eit nytt fastpunkt (AU-25_NFP) ved elva sør for Joasete.

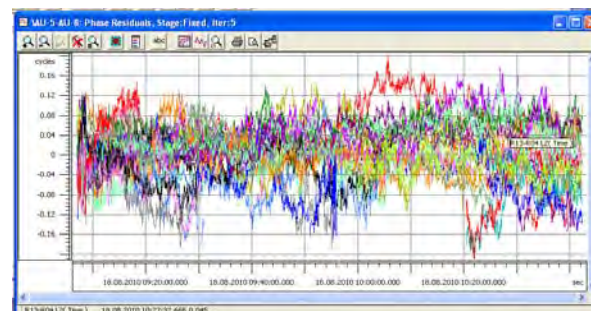
I 2010 er alle punkta målt om. Resultata for 2010 skil seg ut frå ein del tidlegare med mindre høgdeskilnader mellom ein del vitale punkt. Sidan dei fleste punkta i den øvre delen er sterkast knytt til fastpunkta AU-1_FP og AU-25_FP fører dette til eit resultat med større

høgdeverde på mange punkt, og i tidsserier for punkt ser det ut til at punkta i 2010 går opp, dvs. hevar seg. Dette er ikkje eit sannsynleg resultat, men det er ingen enkle årsaksforklaringar på dette. Satellittdekning (geometri for satellittar) er om lag den same i 2010 som i 2009. Presisjon for vektorar er litt dålegare i 2010, noko om skuldast meir atmosfærisk støy (jfr. Fig. 4). Meteorologiske tilhøve vil alltid variere, og for eksempelvektoren som er synt i figur 4 vil t.d. 10°C skilnad i referansetemperatur (frå 20 til 10 °C) endre høgdeskilnad med 7 mm. Sidan temperatur, trykk og fukt ikkje er målt vil dette vere variasjonar ein kan få i eit slikt observasjonsmateriale. I Flåm/Aurland med store høgdeskilnader til fastpunkt utgjør det større variasjonar enn i dei fleste andre områda. Ein tilsvarende situasjon med avvikande meteorologiske tilhøve er tidlegare peika på for 2007. Effekten av slike avvik er noko mindre etter at fastpunktet AU-25_FP er etablert, men stor nok til at ein kan få systematiske utslag i storleik cm på ein del punkt



2009:

Vector: AU-5 – AU-8
 {-718.5501, -777.2641, 24.3606}
 Rms=0.0019 Length=1058.7951
 (fixed:20/100)
 $\Delta h = 373,2154$



2010

Vector: AU-5 --> AU-8 (20°C)
 {-718.5412, -777.2615, 24.3747}
 Rms=0.0023 Length=1058.7875
 (fixed:34/100,float:1/0.012%)
 $\Delta h = 373.1986$

Vector: AU-5 --> AU-8 (10°C)
 {-718.5378, -777.2612, 24.3806}
 Rms=0.0024 Len=1058.7851
 (fixed:34/100,float:1/0.012%)
 $\Delta h = 373.1917$ m

Figur 4: Eksempel på vektorresultat 2009 og 2010. For 2010 er det rekna med 20 og 10 °C som temperatur ved havnivå. Normaltrykk og 50% luftråme i båe høve. Legg og merke til auka skala på residuala i figuren for 2010 – som indikerer meir atmosfærisk støy.

Koordinatar med endringar i høve til fyrste måling er synt for alle punkta i Tabell 1. I Tabell 2 er det synt endring mellom målingar (endring for kvart år), og tabellen syner at endringane i perioden 2006-07 er vesentleg større for så godt som alle punkt i høve til andre år, og tilsvarende mindre og dels i avvikande retning for 2007-08. Dette skuldast truleg ei systematisk påverking av vektorane mellom dei høge og dei låge punkta i 2007.

Resultata er synt som figurar for tre delområde, punkta ved sjøen (Figur 5), Joasete til Furekamben (Figur 6) og frå Furekamben til Ramnanosi (Figur 7). Ulike år er presentert for å gi best mogeleg dekning av alle punkt for dei åra det er målingar.

Kommentar til endringar Flåm/Aurland

Figur 5 syner punkt AU-18 og dei to nye punkta AU-19_NY og AU-24. For punktet AU-18 er det ikkje klare teikn til rørsle over perioden på fem år, variasjonane i koordinatar kan vere tilfeldige målefeil. Truleg er punktet AU-18 i fast fjell og kan nyttast som fastpunkt. For dei to nye punkta er det ut frå eitt års målingar vanskeleg å trekke endeleg konklusjon sidan endringane er relativt små og retning for endring avvikande frå tidlegare observasjonar i området.

Figur 6 syner endringar for punkta frå Furekamben til Joasete. Det er signifikant endring i grunnriss for alle punkta i området når ein legg periodane 2006-09 eller 2006-10 til grunn, med unntak av punktet AU-11 som syner om lag same endring men som på grunn av høge standardavvik ikkje har signifikant endring. I høgd er det berre AU-14 som har signifikant endring i resultatet for 2006-10, medan tidlegare resultat syner indikasjonar på setning i fleire av punkta.

Figur 7 syner punkta i den øvre delen frå Ramnanosi mot Furekamben. Endringane i desse punkta er gjennomgåande små og for eitt år ikkje signifikante. Endringar over fire-fem år er signifikante i både grunnriss og høgd for dei fleste punkta, og er ein klar indikasjon på at det er små rørsler og i dette området.

Konklusjon

Resultata frå 2010 avvik serleg for høgder ein del frå trenden over fleire år. Dette er mest truleg eit resultat av ytre meteorologiske faktorar under målinga. Resultata for 2010 syner og generelt mindre endringar enn i ein del tidlegare år.

I området frå Joasete til Furekamben er det klare teikn på at det er rørsle. Dei største endringane er i punkta AU-14 nord for Joasete og AU-12 på stupkanten vest for Joasete med endring ca. 1 cm pr. år.

Det er og klare teikn til endringar i andre punkt i området, men endringane er i storleik vesentleg mindre slik at berre endring observert over fleire år gir statistisk signifikant rørsle.

For dei to nye punkta etablert 2009 (AU-19_NY og AU-24) kan det ikkje trekkast sikre slutningar etter berre eitt års måling.

PUNKT	År	N	E	H	σ_N	σ_E	σ_H	dN	dE	Avst.	Retn.	dH
AU-1_FP	2010	6746120.0710	400810.1600	1430.7750				0.0000	0.0000	0.0000		
AU-20_FP	2010	6748724.8380	397342.0100	112.6950				0.0000	0.0000	0.0000		
AU-23_FP	2010	6753117.9200	400831.2450	69.8760				0.0000	0.0000	0.0000		
AU-25_FP	2010	6747647.8930	401088.5860	1160.5960				-0.0005	0.0004	0.0000		
AU-2	2005	6746302.8903	400635.2038	1395.2854	0.0007	0.0005	0.0017					
AU-2	2006	6746302.8900	400635.2046	1395.2812	0.0008	0.0005	0.0018	0.000	0.001	0.001	122.84	-0.004
AU-2	2007	6746302.8895	400635.2019	1395.2833	0.0013	0.0008	0.0021	-0.001	-0.002	0.002	274.63	-0.002
AU-2	2008	6746302.8886	400635.2010	1395.2827	0.0006	0.0004	0.0015	-0.002	-0.003	0.003	265.26	-0.003
AU-2	2009	6746302.8905	400635.2004	1395.2751	0.0005	0.0004	0.0010	0.000	-0.003	0.003	303.74	-0.010
AU-2	2010	6746302.8895	400635.2006	1395.2746	0.0006	0.0005	0.0011	-0.001	-0.003	0.003	284.40	-0.011
AU-3	2005	6746854.9430	400502.4577	1336.8511	0.0010	0.0006	0.0020					
AU-3	2006	6746854.9430	400502.4583	1336.8471	0.0007	0.0005	0.0018	0.000	0.001	0.001	100.00	-0.004
AU-3	2007	6746854.9442	400502.4553	1336.8462	0.0015	0.0010	0.0029	0.001	-0.002	0.003	329.52	-0.005
AU-3	2008	6746854.9418	400502.4557	1336.8486	0.0007	0.0005	0.0016	-0.001	-0.002	0.002	265.60	-0.003
AU-4	2005	6746671.3879	400327.8084	1402.1787	0.0009	0.0006	0.0018					
AU-4	2006	6746671.3876	400327.8073	1402.1732	0.0007	0.0005	0.0018	0.000	-0.001	0.001	283.05	-0.005
AU-4	2007	6746671.3915	400327.8041	1402.1788	0.0015	0.0009	0.0025	0.004	-0.004	0.006	344.37	0.000
AU-4	2008	6746671.3864	400327.8036	1402.1744	0.0006	0.0004	0.0015	-0.002	-0.005	0.005	280.72	-0.004
AU-4	2009	6746671.3899	400327.8028	1402.1655	0.0005	0.0003	0.0010	0.002	-0.006	0.006	321.84	-0.013
AU-4	2010	6746671.3910	400327.8035	1402.1643	0.0005	0.0005	0.0011	0.003	-0.005	0.006	335.91	-0.014
AU-5	2005	6747245.8905	400014.1372	1359.2934	0.0016	0.0009	0.0026					
AU-5	2006	6747245.8912	400014.1352	1359.2877	0.0007	0.0005	0.0019	0.001	-0.002	0.002	321.43	-0.006
AU-5	2007	6747245.8902	400014.1294	1359.2871	0.0013	0.0008	0.0023	0.000	-0.008	0.008	297.55	-0.006
AU-5	2008	6747245.8891	400014.1293	1359.2820	0.0006	0.0004	0.0015	-0.001	-0.008	0.008	288.83	-0.011
AU-5	2009	6747245.8938	400014.1301	1359.2846	0.0004	0.0003	0.0009	0.003	-0.007	0.008	327.70	-0.009
AU-5	2010	6747245.8932	400014.1302	1359.2795	0.0006	0.0004	0.0011	0.003	-0.007	0.008	323.44	-0.014
AU-6	2005	6747430.4219	400035.4699	1298.8257	0.0016	0.0009	0.0028					
AU-6	2006	6747430.4225	400035.4674	1298.8217	0.0007	0.0005	0.0018	0.001	-0.003	0.003	315.00	-0.004
AU-6	2007	6747430.4245	400035.4638	1298.8275	0.0014	0.0008	0.0023	0.003	-0.006	0.007	325.65	0.002
AU-6	2008	6747430.4211	400035.4620	1298.8154	0.0006	0.0004	0.0015	-0.001	-0.008	0.008	293.58	-0.010
AU-6	2009	6747430.4268	400035.4622	1298.8170	0.0004	0.0003	0.0009	0.005	-0.008	0.009	336.08	-0.009
AU-6	2010	6747430.4265	400035.4636	1298.8191	0.0005	0.0004	0.0011	0.005	-0.006	0.008	340.15	-0.007
AU-7	2005	6747642.2173	399417.6382	1079.2150	0.0016	0.0010	0.0029					
AU-7	2006	6747642.2173	399417.6359	1079.2228	0.0009	0.0006	0.0021	0.000	-0.002	0.002	300.00	0.008
AU-7	2007	6747642.2220	399417.6289	1079.2231	0.0016	0.0010	0.0031	0.005	-0.009	0.010	329.79	0.008
AU-7	2008	6747642.2169	399417.6287	1079.2113	0.0007	0.0006	0.0017	0.000	-0.009	0.010	297.32	-0.004
AU-7	2009	6747642.2222	399417.6280	1079.2111	0.0004	0.0003	0.0009	0.005	-0.010	0.011	328.51	-0.004
AU-7	2010	6747642.2201	399417.6304	1079.2181	0.0007	0.0005	0.0014	0.003	-0.008	0.008	321.94	0.003
AU-8	2005	6747983.5113	399353.2160	986.1405	0.0016	0.0010	0.0029					
AU-8	2006	6747983.5122	399353.2141	986.1556	0.0009	0.0006	0.0022	0.001	-0.002	0.002	328.16	0.015
AU-8	2007	6747983.5183	399353.2060	986.1499	0.0016	0.0011	0.0032	0.007	-0.010	0.012	338.88	0.009
AU-8	2008	6747983.5141	399353.2072	986.1444	0.0008	0.0006	0.0018	0.003	-0.009	0.009	319.61	0.004
AU-8	2009	6747983.5197	399353.2076	986.1381	0.0004	0.0003	0.0009	0.008	-0.008	0.012	350.00	-0.002
AU-8	2010	6747983.5192	399353.2108	986.1517	0.0007	0.0005	0.0014	0.008	-0.005	0.009	362.94	0.011

PUNKT	År	N	E	H	σ_N	σ_E	σ_H	dN	dE	Avst.	Retn.	dH
AU-9	2005	6748316.3132	399728.8202	948.5071	0.0017	0.0011	0.0032					
AU-9	2006	6748316.3123	399728.8221	948.5093	0.0011	0.0008	0.0025	-0.001	0.002	0.002	128.16	0.002
AU-9	2007	6748316.3197	399728.8122	948.5136	0.0016	0.0011	0.0030	0.007	-0.008	0.010	343.44	0.006
AU-9	2008	6748316.3156	399728.8138	948.5060	0.0008	0.0006	0.0018	0.002	-0.006	0.007	322.84	-0.001
AU-9	2009	6748316.3200	399728.8145	948.4964	0.0005	0.0004	0.0010	0.007	-0.006	0.009	355.59	-0.011
AU-9	2010	6748316.3201	399728.8168	948.5131	0.0007	0.0006	0.0015	0.007	-0.003	0.008	370.85	0.006
AU-10	AU-05	6748491.2691	399738.1889	885.8302	0.0018	0.0011	0.0032					
AU-10	AU-06	6748491.2710	399738.1871	885.8343	0.0012	0.0008	0.0028	0.002	-0.002	0.003	351.72	0.004
AU-10	AU-07	6748491.2790	399738.1761	885.8336	0.0018	0.0012	0.0033	0.010	-0.013	0.016	341.91	0.003
AU-10	2008	6748491.2732	399738.1776	885.8279	0.0008	0.0006	0.0018	0.004	-0.011	0.012	322.16	-0.002
AU-10	2009	6748491.2807	399738.1751	885.8167	0.0005	0.0004	0.0010	0.012	-0.014	0.018	344.50	-0.014
AU-10	2010	6748491.2815	399738.1761	885.8332	0.0007	0.0006	0.0015	0.012	-0.013	0.018	348.99	0.003
AU-11	2005	6748861.2224	399946.4906	870.5067	0.0037	0.0041	0.0076					
AU-11	2006	6748861.2228	399946.4994	870.5040	0.0032	0.0030	0.0052	0.000	0.009	0.009	97.11	-0.003
AU-11	2007	6748861.2208	399946.4837	870.5112	0.0036	0.0025	0.0072	-0.002	-0.007	0.007	285.49	0.005
AU-11	2008	6748861.2261	399946.4815	870.4893	0.0023	0.0020	0.0052	0.004	-0.009	0.010	324.58	-0.017
AU-11	2009	6748861.2274	399946.4851	870.4682	0.0016	0.0019	0.0036	0.005	-0.006	0.007	346.97	-0.038
AU-11	2010	6748861.2289	399946.4904	870.4916	0.0024	0.0027	0.0057	0.007	0.000	0.007	398.04	-0.015
PUNKT	År	N	E	H	σ_N	σ_E	σ_H	dN	dE	Avst.	Retn.	dH
AU-12	2005	6748917.2546	399966.0499	863.2413	0.0034	0.0025	0.0057					
AU-12	2006	6748917.2736	399966.0360	863.2456	0.0043	0.0035	0.0086	0.019	-0.014	0.024	359.79	0.004
AU-12	2007	6748917.2732	399966.0170	863.2612	0.0032	0.0019	0.0061	0.019	-0.033	0.038	332.76	0.020
AU-12	2008	6748917.2711	399966.0187	863.2352	0.0016	0.0013	0.0035	0.016	-0.031	0.035	330.97	-0.006
AU-12	2009	6748917.2852	399966.0177	863.2164	0.0009	0.0011	0.0020	0.031	-0.032	0.044	348.38	-0.025
AU-12	2010	6748917.2881	399966.0091	863.2317	0.0017	0.0019	0.0045	0.033	-0.041	0.053	343.77	-0.010
AU-13	2005	6748787.9195	400171.0192	936.5379	0.0017	0.0011	0.0031					
AU-13	2006	6748787.9213	400171.0188	936.5383	0.0011	0.0008	0.0025	0.002	0.000	0.002	386.08	0.000
AU-13	2007	6748787.9228	400171.0072	936.5513	0.0017	0.0011	0.0031	0.003	-0.012	0.012	317.08	0.013
AU-13	2008	6748787.9250	400171.0110	936.5334	0.0008	0.0006	0.0017	0.005	-0.008	0.010	337.61	-0.005
AU-13	2009	6748787.9282	400171.0133	936.5246	0.0006	0.0005	0.0012	0.009	-0.006	0.011	362.06	-0.013
AU-13	2010	6748787.9264	400171.0149	936.5440	0.0008	0.0006	0.0017	0.007	-0.004	0.008	364.52	0.006
AU-14	2005	6749194.4602	400596.5167	907.3582	0.0019	0.0013	0.0038					
AU-14	2006	6749194.4707	400596.5105	907.3464	0.0012	0.0009	0.0027	0.011	-0.006	0.012	366.04	-0.012
AU-14	2007	6749194.4782	400596.4948	907.3520	0.0022	0.0014	0.0041	0.018	-0.022	0.028	343.80	-0.006
AU-14	2008	6749194.4882	400596.4948	907.3198	0.0009	0.0007	0.0021	0.028	-0.022	0.036	357.74	-0.038
AU-14	2009	6749194.4984	400596.4910	907.3091	0.0006	0.0005	0.0012	0.038	-0.026	0.046	362.30	-0.049
AU-14	2010	6749194.5046	400596.4876	907.3170	0.0008	0.0007	0.0019	0.044	-0.029	0.053	363.07	-0.041
AU-15	2006	6747908.4275	399194.5582	964.6979	0.0011	0.0007	0.0026					
AU-15	2007	6747908.4366	399194.5503	964.6932	0.0018	0.0013	0.0042	0.009	-0.008	0.012	354.49	-0.005
AU-15	2008	6747908.4282	399194.5489	964.6842	0.0009	0.0007	0.0020	0.001	-0.009	0.009	304.78	-0.014
AU-15	2009	6747908.4337	399194.5508	964.6770	0.0005	0.0004	0.0011	0.006	-0.007	0.010	344.40	-0.021
AU-15	2010	6747908.4338	399194.5556	964.6908	0.0007	0.0005	0.0014	0.006	-0.003	0.007	375.08	-0.007
AU-16	2006	6748001.8248	399154.0024	928.2131	0.0014	0.0009	0.0031					
AU-16	2007	6748001.8341	399153.9936	928.2026	0.0020	0.0014	0.0046	0.009	-0.009	0.013	351.76	-0.011
AU-16	2008	6748001.8263	399153.9942	928.1965	0.0010	0.0010	0.0022	0.002	-0.008	0.008	311.52	-0.017
AU-16	2009	6748001.8346	399153.9951	928.1921	0.0005	0.0004	0.0011	0.010	-0.007	0.012	359.24	-0.021
AU-16	2010	6748001.8325	399153.9995	928.2074	0.0007	0.0006	0.0015	0.008	-0.003	0.008	377.07	-0.006

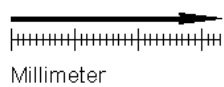
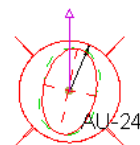
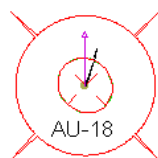
PUNKT	År	N	E	H	σN	σE	σH	dN	dE	Avst.	Retn.	dH
AU-18	2005	6750457.9108	399281.1999	58.2533	0.0022	0.0015	0.0048					
AU-18	2006	6750457.9132	399281.2019	58.2726	0.0015	0.0011	0.0034	0.002	0.002	0.003	44.23	0.019
AU-18	2007	6750457.9146	399281.1949	58.2422	0.0022	0.0014	0.0042	0.004	-0.005	0.006	341.37	-0.011
AU-18	2008	6750457.9163	399281.1945	58.2621	0.0011	0.0009	0.0027	0.005	-0.005	0.008	350.58	0.009
AU-18	2009	6750457.9156	399281.1959	58.2495	0.0007	0.0007	0.0016	0.005	-0.004	0.006	355.77	-0.004
AU-18	2010	6750457.9218	399281.1984	58.2601	0.0012	0.0009	0.0024	0.011	-0.002	0.011	391.37	0.007
AU-19	2005	6749100.0854	398572.8712	82.1033	0.0029	0.0020	0.0066					
AU-19	2006	6749100.0919	398572.8664	82.1305	0.0016	0.0011	0.0034	0.007	-0.005	0.008	359.51	0.027
AU-19	2007	6749100.1105	398572.8532	82.1068	0.0024	0.0014	0.0044	0.025	-0.018	0.031	360.39	0.004
AU-19	2008	6749100.1116	398572.8385	82.1260	0.0021	0.0015	0.0047	0.026	-0.033	0.042	343.00	0.023
AU-19_NY	2009	6748941.3576	398404.5841	105.9056	0.0007	0.0006	0.0016		Nytt-09	Tidl pkt borte!		
AY-19NY	2010	6748941.3647	398404.5885	105.9071	0.0012	0.0008	0.0025	0.007	0.004	0.008	35.32	0.001
AU-21	2005	6748789.7628	400464.0931	959.6934	0.0017	0.0011	0.0031					
AU-21	2006	6748789.7647	400464.0927	959.6975	0.0010	0.0007	0.0023	0.002	0.000	0.002	386.79	0.004
AU-21	2007	6748789.7642	400464.0829	959.7104	0.0017	0.0011	0.0032	0.001	-0.010	0.010	308.68	0.017
AU-21	2008	6748789.7670	400464.0848	959.6903	0.0008	0.0006	0.0017	0.004	-0.008	0.009	329.82	-0.003
AU-21	2009	6748789.7687	400464.0868	959.6860	0.0005	0.0004	0.0011	0.006	-0.006	0.009	347.91	-0.007
AU-21	2010	6748789.7663	400464.0897	959.6976	0.0009	0.0007	0.0020	0.004	-0.003	0.005	350.92	0.004
AU-22	2005	6746140.2527	400254.6871	1469.0051	0.0007	0.0005	0.0017					
AU-22	2006	6746140.2529	400254.6889	1468.9998	0.0007	0.0005	0.0017	0.000	0.002	0.002	92.96	-0.005
AU-22	2007	6746140.2516	400254.6836	1469.0030	0.0013	0.0007	0.0020	-0.001	-0.003	0.004	280.61	-0.002
AU-22	2008	6746140.2534	400254.6844	1469.0002	0.0006	0.0004	0.0014	0.001	-0.003	0.003	316.15	-0.005
AU-22	2009	6746140.2558	400254.6826	1468.9984	0.0004	0.0003	0.0009	0.003	-0.004	0.005	338.40	-0.007
AU-22	2010	6746140.2561	400254.6827	1468.9932	0.0005	0.0004	0.0011	0.003	-0.004	0.006	341.88	-0.012
AU-24	2009	6749988.3852	400082.4232	510.8752	0.0012	0.0014	0.0027		Nytt-09			
AU-24	2010	6749988.3922	400082.4266	510.8827	0.0016	0.0014	0.0034	0.007	0.003	0.008	28.79	0.007

Tabell 1: Resultatkoordinatar (N,E og H) med standardavvik (σN , σE og σH) og endring for koordinatar i høve til fyrste måling, gitt som endring i Nord, Aust (dN,dE), Avstand, Retning (gon - 400^g) og høgdeskilnad (dH).

PUNKT	År	Endringer mellom målinger			Retn. (°)	dH[m]
		dN[m]	dE[m]	Avstand [m]		
AU-2	2005-06	0.000	0.001	0.001	122.84	-0.004
AU-2	2006-07	-0.001	-0.003	0.003	288.34	0.002
AU-2	2007-08	-0.001	-0.001	0.001	250.00	-0.001
AU-2	2008-09	0.002	-0.001	0.002	380.53	-0.008
AU-2	2009-10	-0.001	0.000	0.001	187.43	-0.001
AU-3	2005-06	0.000	0.001	0.001	100.00	-0.004
AU-3	2006-07	0.001	-0.003	0.003	324.22	-0.001
AU-3	2007-08	-0.002	0.000	0.002	189.49	0.002
AU-4	2005-06	0.000	-0.001	0.001	283.05	-0.005
AU-4	2006-07	0.004	-0.003	0.005	356.26	0.006
AU-4	2007-08	-0.005	-0.001	0.005	206.22	-0.004
AU-4	2008-09	0.003	-0.001	0.004	385.69	-0.009
AU-4	2009-10	0.001	0.001	0.001	36.08	-0.001
AU-5	2005-06	0.001	-0.002	0.002	321.43	-0.006
AU-5	2006-07	-0.001	-0.006	0.006	289.13	-0.001
AU-5	2007-08	-0.001	0.000	0.001	205.77	-0.005
AU-5	2008-09	0.005	0.001	0.005	10.73	0.003
AU-5	2009-10	-0.001	0.000	0.001	189.49	-0.005
AU-6	2005-06	0.001	-0.003	0.003	315.00	-0.004
AU-6	2006-07	0.002	-0.004	0.004	332.28	0.006
AU-6	2007-08	-0.003	-0.002	0.004	231.00	-0.012
AU-6	2008-09	0.006	0.000	0.006	2.23	0.002
AU-6	2009-10	0.000	0.001	0.001	113.44	0.002
AU-7	2005-06	0.000	-0.002	0.002	300.00	0.008
AU-7	2006-07	0.005	-0.007	0.008	337.64	0.000
AU-7	2007-08	-0.005	0.000	0.005	202.50	-0.012
AU-7	2008-09	0.005	-0.001	0.005	391.64	0.000
AU-7	2009-10	-0.002	0.002	0.003	145.76	0.007
AU-8	2006-07	0.006	-0.008	0.010	341.09	-0.006
AU-8	2007-08	-0.004	0.001	0.004	182.28	-0.005
AU-8	2008-09	0.006	0.000	0.006	4.54	-0.006
AU-8	2009-10	-0.001	0.003	0.003	109.87	0.014
AU-9	2005-06	-0.001	0.002	0.002	128.16	0.002
AU-9	2006-07	0.007	-0.010	0.012	340.86	0.004
AU-9	2007-08	-0.004	0.002	0.004	176.31	-0.008
AU-9	2008-09	0.004	0.001	0.004	10.04	-0.010
AU-9	2009-10	0.000	0.002	0.002	97.23	0.017
AU-10	2005-06	0.002	-0.002	0.003	351.72	0.004
AU-10	2006-07	0.008	-0.011	0.014	340.03	-0.001
AU-10	2007-08	-0.006	0.002	0.006	183.89	-0.006
AU-10	2008-09	0.008	-0.003	0.008	379.52	-0.011
AU-10	2009-10	0.001	0.001	0.001	57.04	0.017
AU-11	2005-06	0.000	0.009	0.009	97.11	-0.003
AU-11	2006-07	-0.002	-0.016	0.016	291.93	0.007
AU-11	2007-08	0.005	-0.002	0.006	374.95	-0.022
AU-11	2008-09	0.001	0.004	0.004	77.94	-0.021
AU-11	2009-10	0.002	0.005	0.006	82.44	0.023

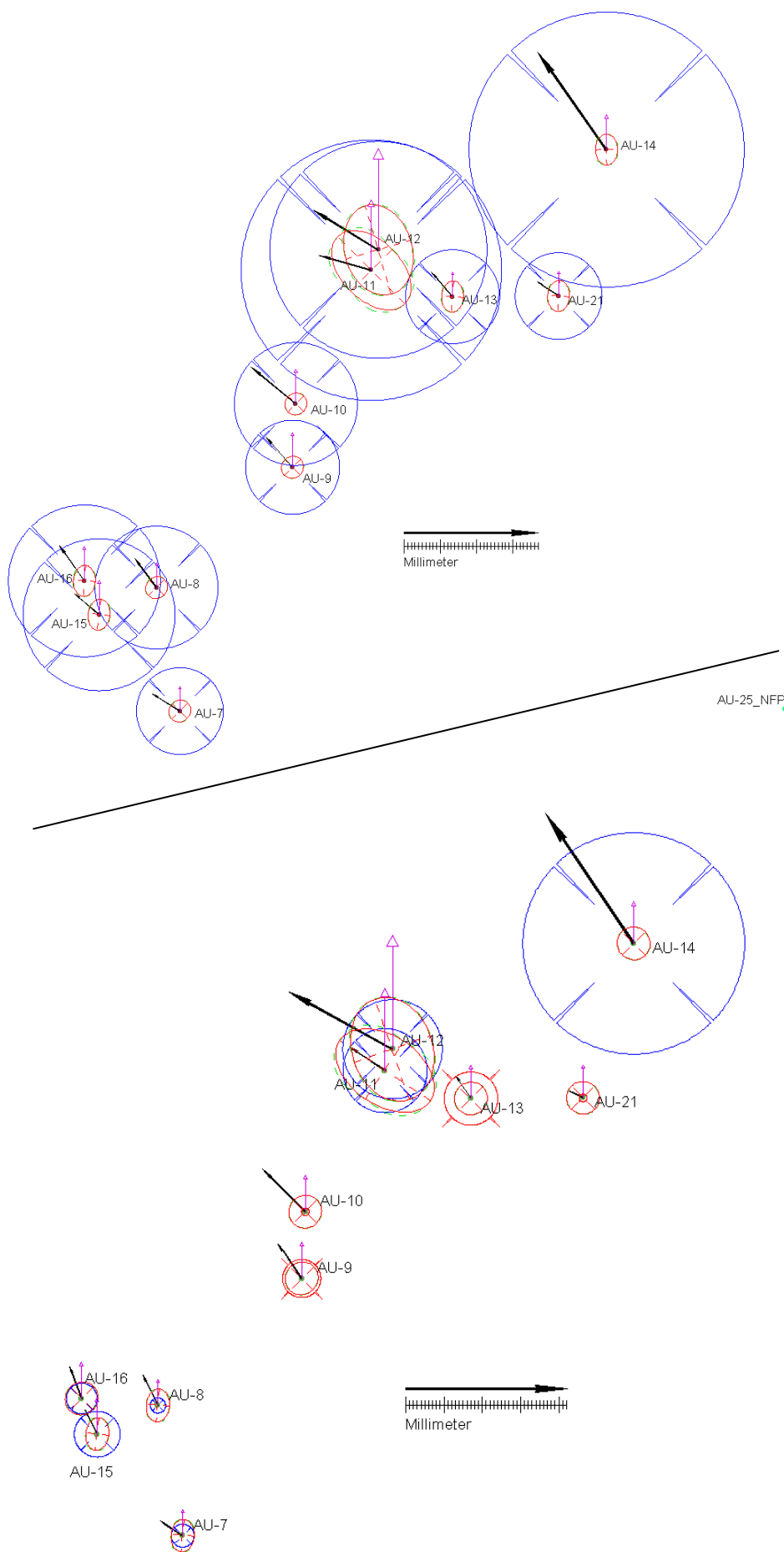
PUNKT	År	dN[m]	dE[m]	Avstand [m]	Retn. (°)	dH[m]
AU-12	2005-06	0.019	-0.014	0.024	359.79	0.004
AU-12	2006-07	0.000	-0.019	0.019	298.66	0.016
AU-12	2007-08	-0.002	0.002	0.003	156.68	-0.026
AU-12	2008-09	0.014	-0.001	0.014	395.49	-0.019
AU-12	2009-10	0.003	-0.009	0.009	320.71	0.015
AU-13	2005-06	0.002	0.000	0.002	386.08	0.000
AU-13	2006-07	0.002	-0.012	0.012	308.19	0.013
AU-13	2007-08	0.002	0.004	0.004	66.59	-0.018
AU-13	2008-09	0.003	0.002	0.004	39.67	-0.009
AU-13	2009-10	-0.002	0.002	0.002	153.74	0.019
AU-14	2005-06	0.011	-0.006	0.012	366.04	-0.012
AU-14	2006-07	0.007	-0.016	0.017	328.37	0.006
AU-14	2007-08	0.010	0.000	0.010	0.00	-0.032
AU-14	2008-09	0.010	-0.004	0.011	377.30	-0.011
AU-14	2009-10	0.006	-0.003	0.007	368.07	0.008
AU-15	2006-07	0.009	-0.008	0.012	354.49	-0.005
AU-15	2007-08	-0.008	-0.001	0.009	210.51	-0.009
AU-15	2008-09	0.005	0.002	0.006	21.18	-0.007
AU-15	2009-10	0.000	0.005	0.005	98.67	0.014
AU-16	2006-07	0.009	-0.009	0.013	351.76	-0.011
AU-16	2007-08	-0.008	0.001	0.008	195.11	-0.006
AU-16	2008-09	0.008	0.001	0.008	6.88	-0.004
AU-16	2009-10	-0.002	0.004	0.005	128.35	0.015
AU-18	2005-06	0.002	0.002	0.003	44.23	0.019
AU-18	2006-07	0.001	-0.007	0.007	312.57	-0.030
AU-18	2007-08	0.002	0.000	0.002	385.29	0.020
AU-18	2008-09	-0.001	0.001	0.002	129.52	-0.013
AU-18	2009-10	0.006	0.003	0.007	24.40	0.011
AU-19	2005-06	0.007	-0.005	0.008	359.51	0.027
AU-19	2006-07	0.019	-0.013	0.023	360.71	-0.024
AU-19	2007-08	0.001	-0.015	0.015	304.75	0.019
AY-19NY	2009-10	0.007	0.004	0.008	35.32	0.001
AU-21	2005-06	0.002	0.000	0.002	386.79	0.004
AU-21	2006-07	-0.001	-0.010	0.010	296.75	0.013
AU-21	2007-08	0.003	0.002	0.003	37.96	-0.020
AU-21	2008-09	0.002	0.002	0.003	55.15	-0.004
AU-21	2009-10	-0.002	0.003	0.004	144.01	0.012
AU-22	2005-06	0.000	0.002	0.002	92.96	-0.005
AU-22	2006-07	-0.001	-0.005	0.005	284.69	0.003
AU-22	2007-08	0.002	0.001	0.002	26.62	-0.003
AU-22	2008-09	0.002	-0.002	0.003	359.03	-0.002
AU-22	2009-10	0.000	0.000	0.000	20.48	-0.005
AU-24	2009-10	0.007	0.003	0.008	28.79	0.007

Tabell 2: Endringar mellom målingar for punkt. Tabellen syner endring for punkt mellom målingane i 2005-06, 06-07, 07-08, 08-09 og 09-10. Tabellen syner endring i Nord, Aust (dN,dE) og tilsvarande avstand og retning (gon - 400^g) og endring i høgd (dH)

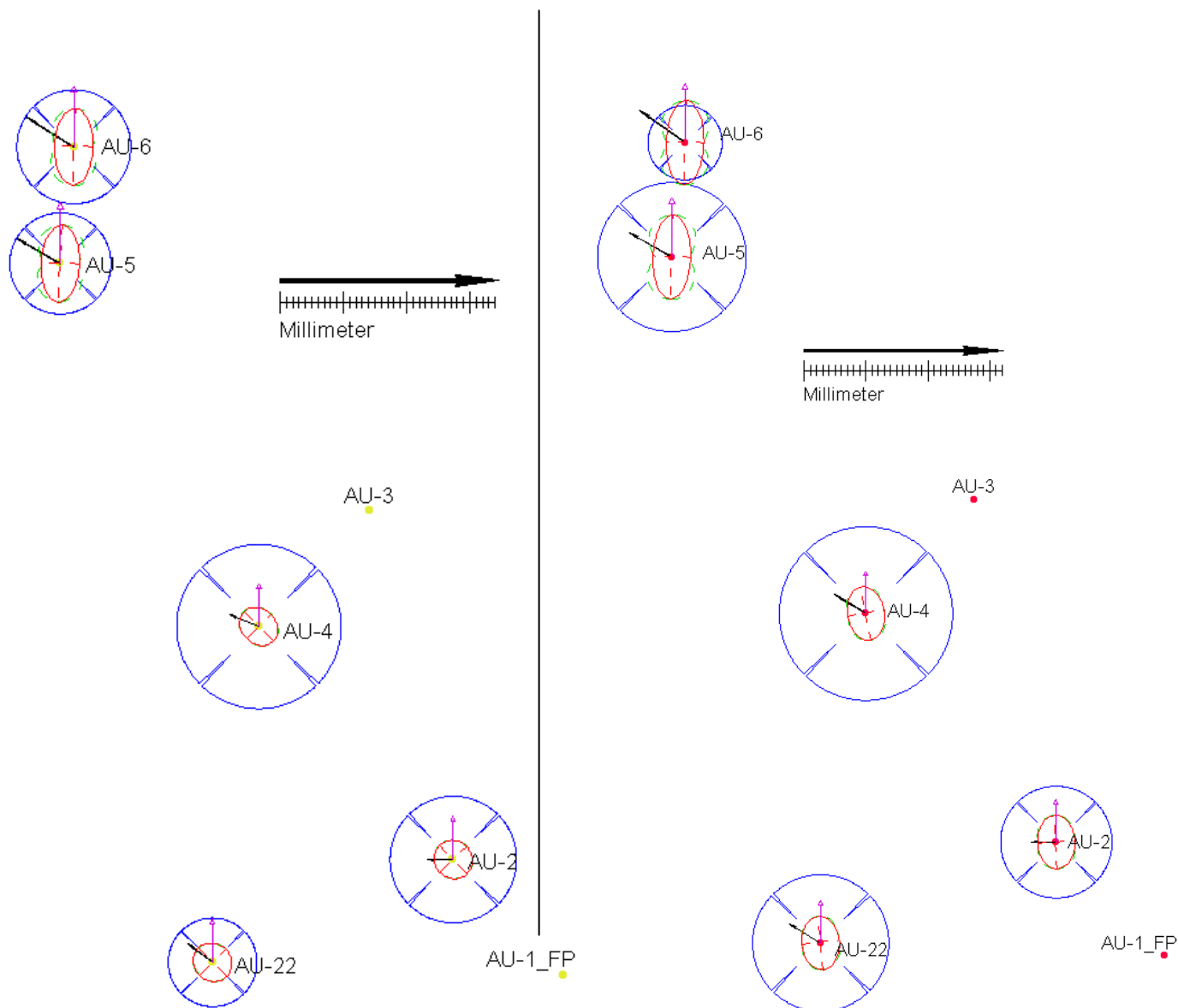


AU-19_NY

Figur 5: Plott av endringar i dei to nye punkta mot sjøen for 2009-10, saman med det eldre AU-18. Det er så vidt på eller over grensa til signifikant endring i planet.

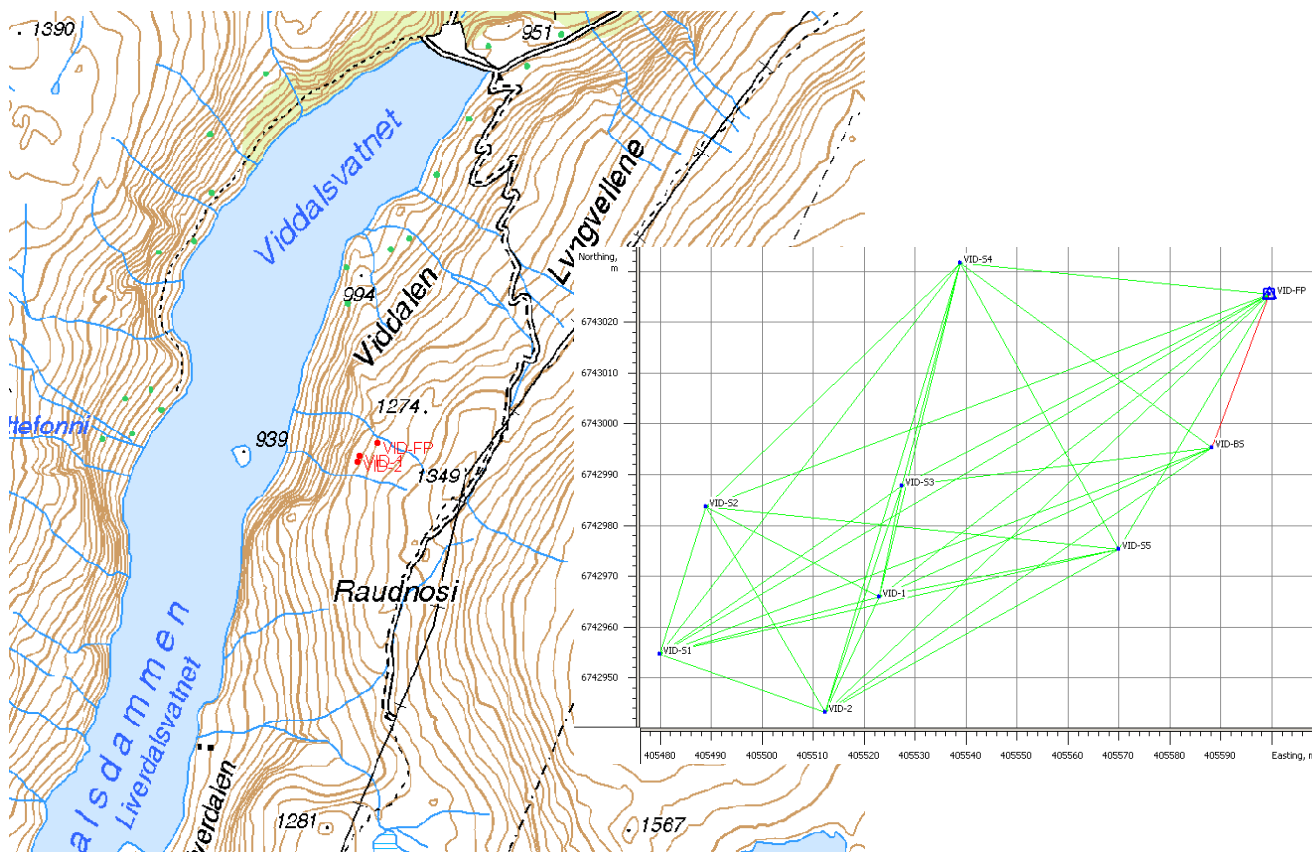


Figur 6: Plott av endringer i punkta fra Furekamben til Joasete. 2006-09 øvst, 2006-10 nedst.



Figur 7: Plott av endringer i punkta i øvre del mellom Ramnanosi og Furekamben. 2005-09 til venstre, 2005-10 til høyre.

Aurland -Viddalen



Figur 8: Kart (Sk N50) og riss over punkta i Viddalen.

Målinger - resultat

Det vart i 2007 etablert tre nye punkt ved Viddalsdammen i Aurland. Eitt fastpunkt og to punkt i mogeleg ustabil fjell. I 2008 etablerte "E-CO Vannkraft AS" fleire nye punkt kring dei gamle i form av støypte søyler, ca, 1,5 meter høge. Både gamle og nye punkt er målt inn i 2008, -09 og -10. I 2010 er det berre målt i kort tid i fastpunktet VID-FP pga. batterisvikt, og nettet er difor i stor grad knytt til søyla VID-S5. Dette punktet har vore stabilt innanfor ca 1 mm og fører difor berre til ein mindre auke i uvisse for resultatata.

Resultat for koordinatar er gitt i tabell 3 - 4 og figur 9 - 10.

To punkt, VID-BS og VID-S1 syner over fleire år relativt store endringar, men dette skuldast mest truleg usikker fundamentering av søylene og ikkje reelle rørsler..

For 2010 er det svært små endringa for det siste året, 2-3 mm i plan for alle punkta, men ingen signifikante endringar over eit år. I høgd er det jamt over setningar i alle punkt i storleik nokre millimeter.

Det er signifikante endringar i plan i NGU-punkta i høve til resultatata for 2007, men knapt signifikante endringar i høve til 2008 resultatata, over eitt års tidsspenn er det ingen signifikante endringar. Standardavvika for koordinatane er svært små slik at signifikansgrenser vert låge og tilfeldige feil kan stå fram som signifikante endringar i punkta.

Akkumulert over fleire år er endringane i Viddal signifikante, slik at det er teikne til små rørsler i området. Resultata for 2010 indikerer og litt setning i alle punkt som samsvarar med trenden over tida det er målt i Viddal.

Konklusjon

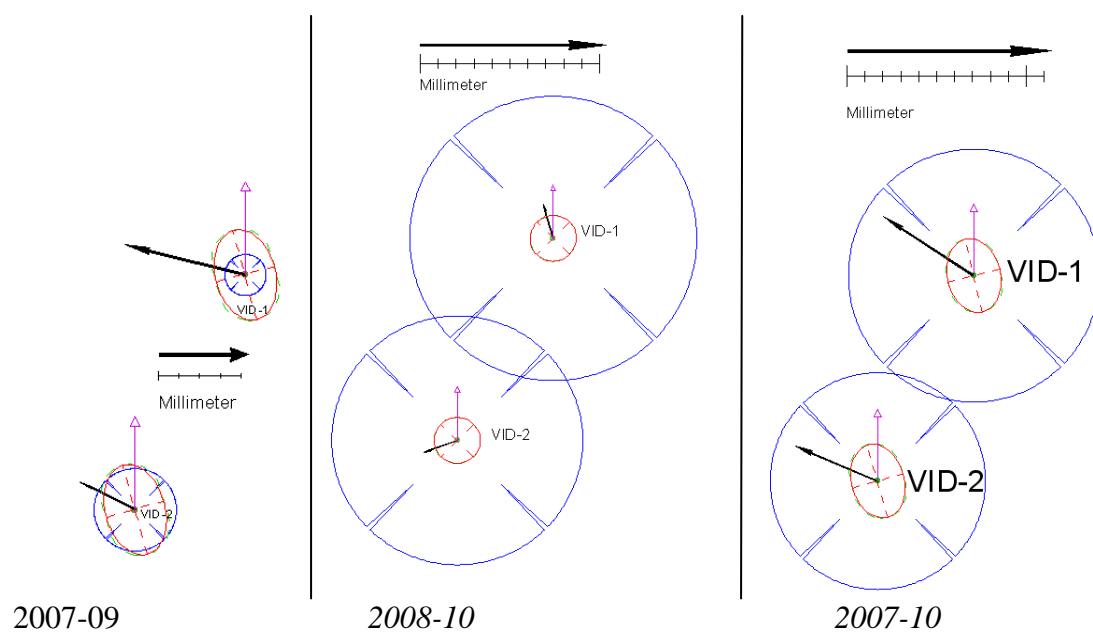
Det er signifikante endring i punkt ved måling over fleire år som kan indikere rørsle, men endringane er små og heilt på grensa til det som kan klassifiserast som observert rørsle.

PUNKT	År	N (UTM)	E (UTM)	H (ell.)	σ_N [m]	σ_E [m]	σ_H [m]	dN [m]	dE [m]	Avst. [m]	Retning [^o gon]	dH [m]
VID-FP	2009	6743025.4880	405599.5580	1289.9330								
VID-BS	2008	6742995.2723	405588.2516	1291.8073	0.0006	0.0006	0.0016					
VID-BS	2009	6742995.2693	405588.2414	1291.8063	0.0005	0.0004	0.0012					
VID-BS	2010	6742995.2719	405588.2380	1291.8034	0.0004	0.0003	0.0008	0.000	-0.014	0.014	298.13	-0.004
VID-1	2007	6742965.9807	405522.9921	1264.3921	0.0006	0.0004	0.0011					
VID-1	2008	6742965.9823	405522.9872	1264.3960	0.0005	0.0005	0.0013	0.002	-0.005	0.005	320.09	0.004
VID-1	2009	6742965.9822	405522.9861	1264.3908	0.0004	0.0003	0.0010	0.002	-0.006	0.006	315.60	-0.001
VID-1	2010	6742965.9838	405522.9873	1264.3850	0.0003	0.0003	0.0007	0.003	-0.005	0.006	336.51	-0.007
VID-2	2007	6742943.2368	405512.2838	1264.2349	0.0006	0.0004	0.0011					
VID-2	2008	6742943.2397	405512.2801	1264.2399	0.0005	0.0005	0.0012	0.003	-0.004	0.005	342.32	0.005
VID-2	2009	6742943.2380	405512.2814	1264.2329	0.0004	0.0003	0.0010	0.001	-0.002	0.003	329.52	-0.002
VID-2	2010	6742943.2389	405512.2788	1264.2289	0.0003	0.0003	0.0007	0.002	-0.005	0.005	325.31	-0.006
VID-S1	2008	6742954.6895	405479.8394	1257.2678	0.0006	0.0006	0.0016					
VID-S1	2009	6742954.7023	405479.8293	1257.2638	0.0004	0.0003	0.0011	0.013	-0.010	0.016	357.47	-0.004
VID-S1	2010	6742954.7054	405479.8286	1257.2603	0.0004	0.0003	0.0008	0.016	-0.011	0.019	362.02	-0.008
VID-S2	2008	6742983.6555	405488.9501	1257.4251	0.0006	0.0006	0.0014					
VID-S2	2009	6742983.6540	405488.9511	1257.4175	0.0004	0.0003	0.0010	-0.002	0.001	0.002	162.57	-0.008
VID-S2	2010	6742983.6535	405488.9492	1257.4193	0.0004	0.0003	0.0008	-0.002	-0.001	0.002	226.92	-0.006
VID-S3	2008	6742987.7236	405527.3270	1264.8015	0.0006	0.0006	0.0016					
VID-S3	2009	6742987.7248	405527.3276	1264.7962	0.0006	0.0005	0.0014	0.001	0.001	0.001	29.52	-0.005
VID-S3	2010	6742987.7228	405527.3286	1264.7927	0.0003	0.0003	0.0007	-0.001	0.002	0.002	129.52	-0.009
VID-S4	2008	6743031.6261	405538.8996	1263.5744	0.0006	0.0006	0.0014					
VID-S4	2009	6743031.6254	405538.9032	1263.5734	0.0004	0.0003	0.0010	-0.001	0.004	0.004	112.23	-0.001
VID-S4	2010	6743031.6237	405538.9024	1263.5722	0.0004	0.0003	0.0008	-0.002	0.003	0.004	145.11	-0.002
VID-S5	2008	6742975.3869	405569.8508	1289.0628	0.0006	0.0006	0.0013					
VID-S5	2009	6742975.3845	405569.8526	1289.0603	0.0004	0.0004	0.0010	-0.002	0.002	0.003	159.03	-0.002
VID-S5	2010	6742975.3856	405569.8516	1289.0617	Fastpunkt							

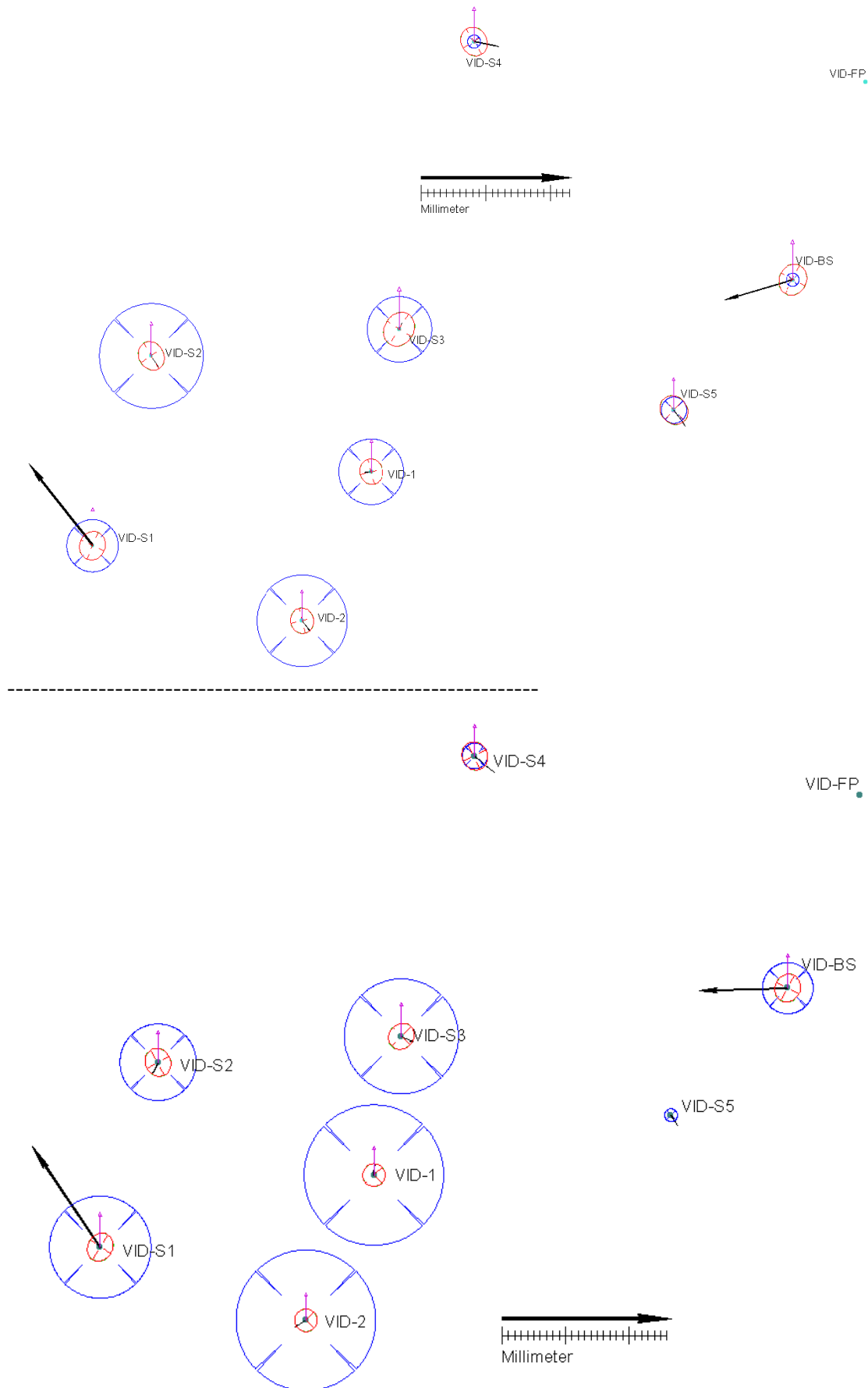
Tabell 3: Resultat for Viddalen 2007-10. Tabellen syner koordinatar (N,E og H) med standardavvik (σ_N , σ_E og σ_H) og endring for koordinatar i høve til fyrste måling, gitt som endring i Nord, Aust (dN,dE), Avstand, Retning (gon - 400^o) og høgdeskilnad (dH).

PUNKT	År	Endring mellom målinger			Retn. (°)	dH[m]
		dN[m]	dE[m]	Avstand [m]		
VID-1	2007-08	0.002	-0.005	0.005	320.09	0.004
VID-1	2008-09	0.000	-0.001	0.001	294.23	-0.005
VID-1	2009-10	0.002	0.001	0.002	40.97	-0.006
VID-2	2007-08	0.003	-0.004	0.005	342.32	0.005
VID-2	2008-09	-0.002	0.001	0.002	158.44	-0.007
VID-2	2009-10	0.001	-0.003	0.003	321.21	-0.004
VID-S1	2008-09	0.013	-0.010	0.016	357.47	-0.004
VID-S1	2009-10	0.003	-0.001	0.003	385.86	-0.004
VID-S2	2008-09	-0.002	0.001	0.002	162.57	-0.008
VID-S2	2009-10	-0.001	-0.002	0.002	283.62	0.002
VID-S3	2008-09	0.001	0.001	0.001	29.52	-0.005
VID-S3	2009-10	-0.002	0.001	0.002	170.48	-0.004
VID-S4	2008-09	-0.001	0.004	0.004	112.23	-0.001
VID-S4	2009-10	-0.002	-0.001	0.002	228.00	-0.001

Tabell 4: Endring mellom målinger for Viddalen 2007-10. Tabellen syner endring i Nord, Aust (dN,dE) og tilsvarande avstand og retning (gon - 400^g) og endring i høgde (dH)

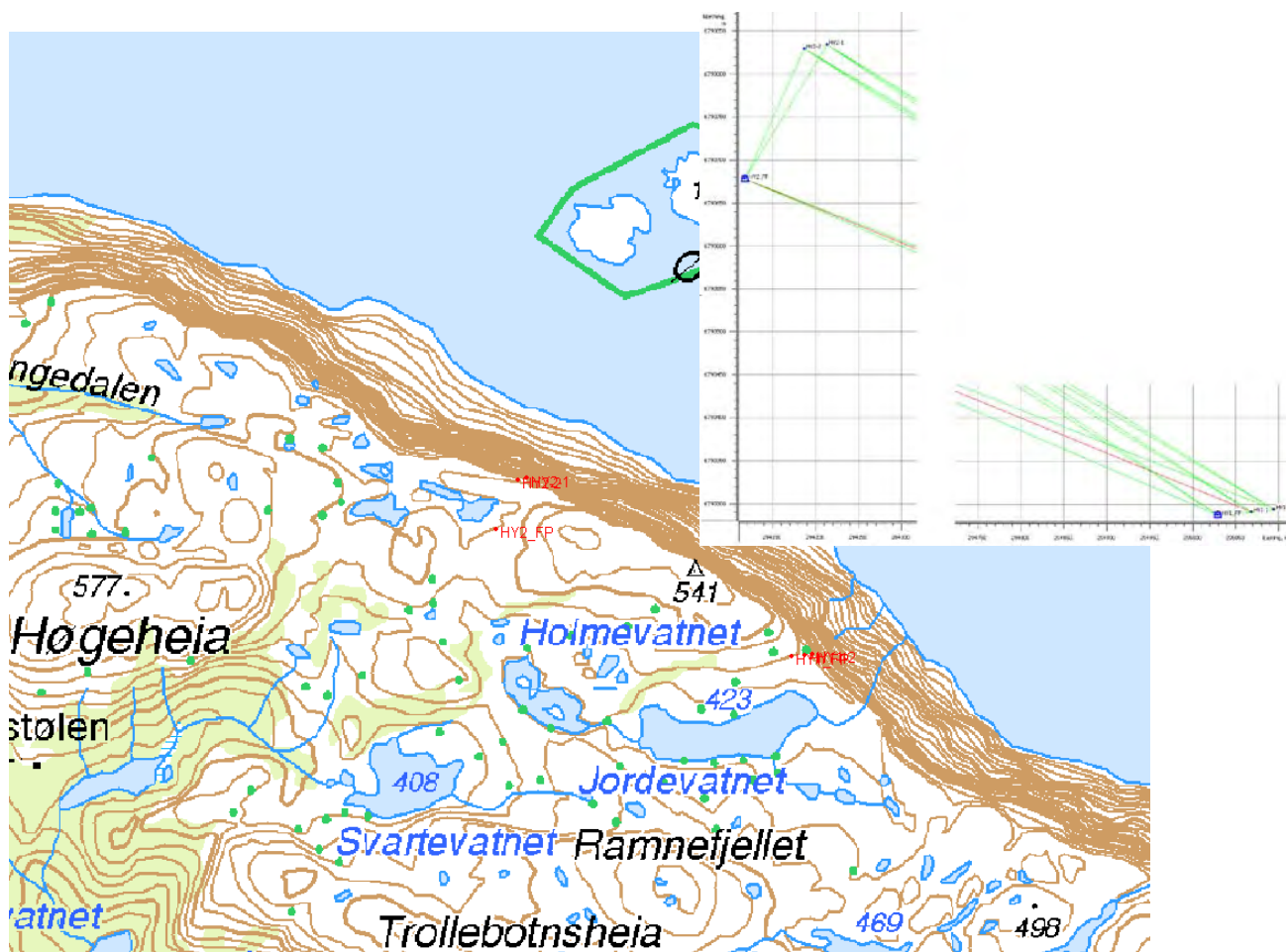


Figur 9: Endring av NGU-punkt i Viddalen 2007-09 (til venstre), 2008-10 i midten og 2007-10 (til høgre).



Figur 10: Endring av alle punkt i Viddalen 2008-09 (øverst) og Viddal 2008-10 (nedst)

Hyllestad



Figur 11: Kart (Sk N50) og riss over punkta i Hyllestad.

Målingar - resultat

Det vart i 2007 etablert seks nye punkt nordaust for Høgeheia i Hyllestad. Punkta er plassert med tre i eit austleg område (HY1-) og tre i eit vestleg (HY2-). Eit fastpunkt og to punkt i mogeleg ustabil fjell i kvart av områda. Punkta er målt om i 2008, 09 og 10, og resultat for koordinatar er gitt i tabell 5 og 6 og grafisk i figur 12.

Båe punkta i område HYL-1- syner signifikante endring i grunnriss over perioden 2007-10. Storleiken på dei årlege endringane varierer litt, men trenden i rørsle er relativt lik for åra det er målt over.

I det vestre området (HYL-2-) er det ingen observerte signifikante endringar.

Konklusjon

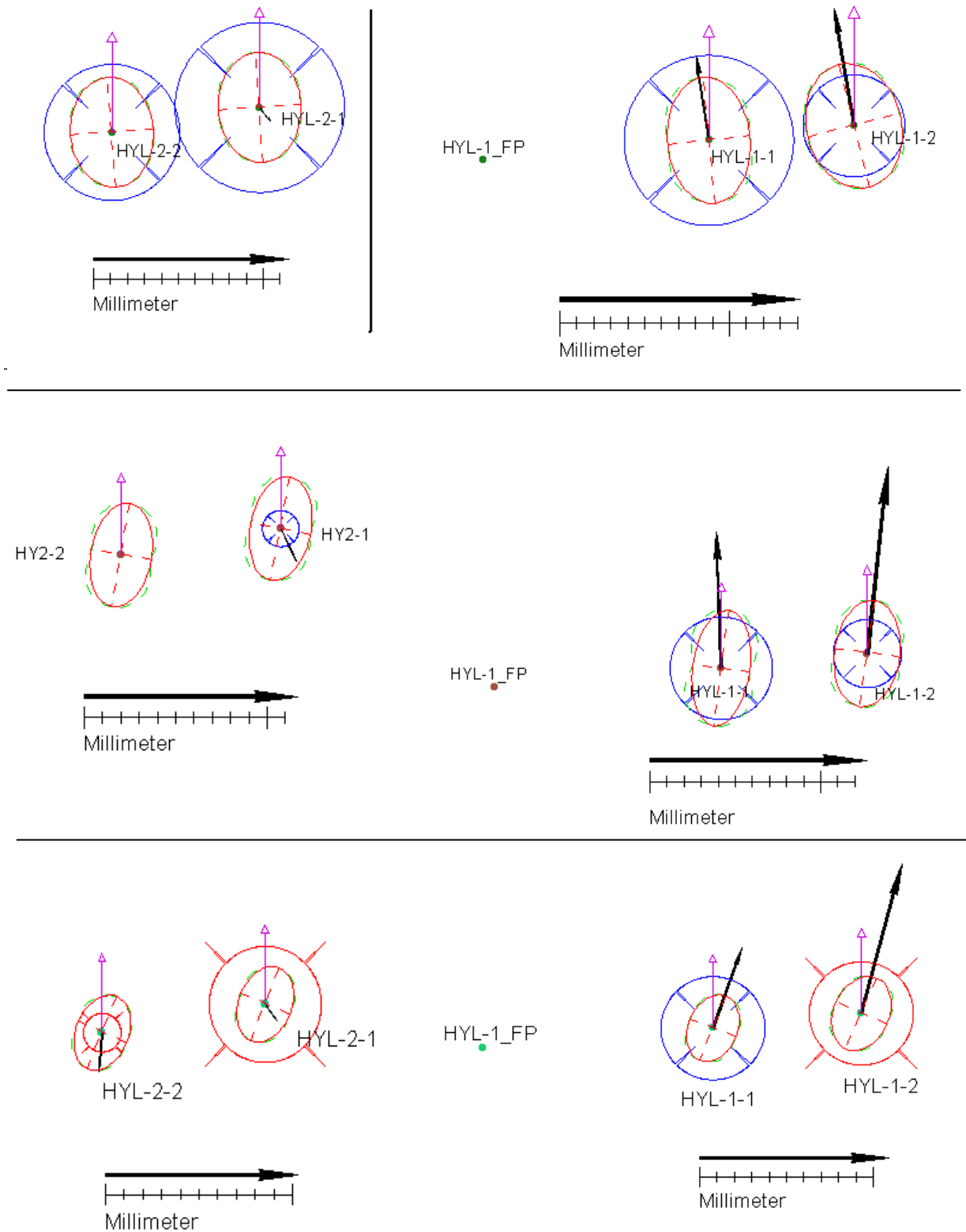
Ut frå resultatata er det rimeleg å konkludere med at det er rørsle i punkta HYL-1-1 og HYL-1-2 med horisontal endring i storleik 2-4 mm pr år.

PUNKT	År	N (UTM)	E (UTM)	H (ell.)	σ_N [m]	σ_E [m]	σ_H [m]	dN [m]	dE [m]	Avst. [m]	Retning [° gon]	dH [m]
HYL1_FP	FP	6790287.0217	295029.1018	506.1030								
HYL2_FP	FP	6790678.0630	294117.7750	526.8480								
HYL-1-1	2007	6790290.4202	295068.9903	505.9616	0.0010	0.0004	0.0013					
HYL-1-1	2008	6790290.4232	295068.9883	505.9623	0.0004	0.0003	0.0010	0.003	-0.002	0.004	362.57	0.001
HYL-1-1	2009	6790290.4255	295068.9895	505.9562	0.0007	0.0007	0.0018	0.005	-0.001	0.005	390.46	-0.005
HYL-1-1	2010	6790290.4277	295068.9899	505.9593	0.0005	0.0004	0.0010	0.008	0.000	0.008	396.61	-0.002
HYL-1-2	2007	6790292.9960	295094.6498	503.8097	0.0009	0.0005	0.0013					
HYL-1-2	2008	6790292.9981	295094.6486	503.8051	0.0005	0.0004	0.0012	0.002	-0.001	0.002	366.95	-0.005
HYL-1-2	2009	6790293.0030	295094.6486	503.8065	0.0008	0.0008	0.0019	0.007	-0.001	0.007	389.19	-0.003
HYL-1-2	2010	6790293.0067	295094.6513	503.8083	0.0005	0.0004	0.0011	0.011	0.002	0.011	8.87	-0.001
HYL-2-1	2007	6790833.9329	294213.2701	546.3371	0.0008	0.0004	0.0011					
HYL-2-1	2008	6790833.9321	294213.2702	546.3330	0.0004	0.0003	0.0009	-0.001	0.000	0.001	192.08	-0.004
HYL-2-1	2009	6790833.9319	294213.2709	546.3320	0.0007	0.0007	0.0016	-0.001	0.001	0.001	157.04	-0.005
HYL-2-1	2010	6790833.9311	294213.2708	546.3359	0.0005	0.0004	0.0010	-0.002	0.001	0.002	176.39	-0.001
HYL-2-2	2007	6790829.5332	294187.1084	544.4011	0.0008	0.0004	0.0011					
HYL-2-2	2008	6790829.5352	294187.1082	544.4002	0.0004	0.0003	0.0009	0.002	0.000	0.002	393.65	-0.001
HYL-2-2	2009	6790829.5337	294187.1091	544.3975	0.0007	0.0007	0.0016	0.000	0.001	0.001	60.51	-0.004
HYL-2-2	2010	6790829.5333	294187.1082	544.4013	0.0005	0.0004	0.0010	0.000	0.000	0.000	329.52	0.000

Tabell 5: Resultat for Hyllestad 2007-10. Tabellen syner koordinatar (N,E og H) med standardavvik (σ_N , σ_E og σ_H) og endring for koordinatar i høve til fyrste måling, gitt som endring i Nord, Aust (dN,dE), Avstand, Retning (gon - 400^g) og høgdeskilnad (dH).

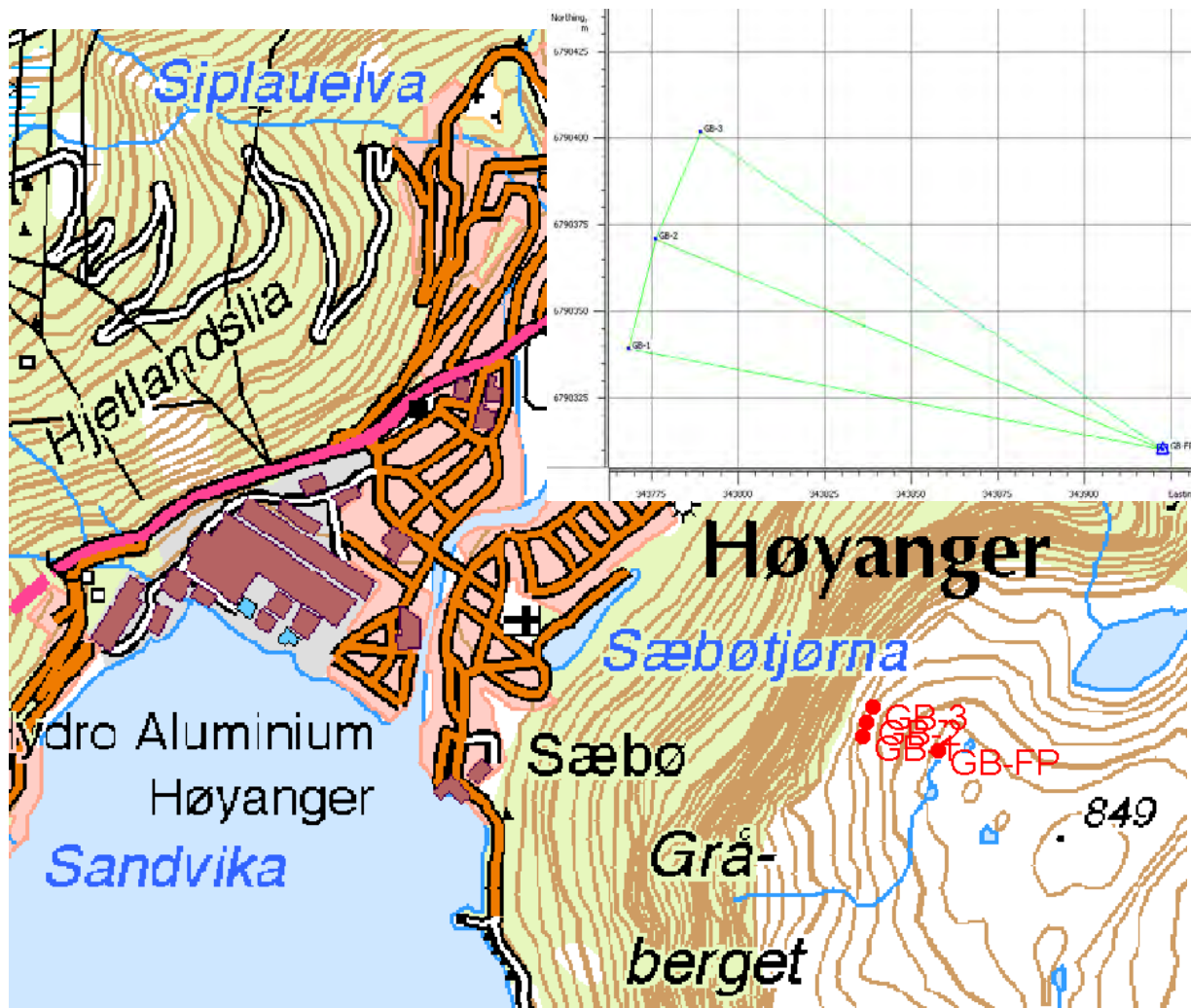
PUNKT	År	Endring mellom målingar			Retn. (°)	dH[m]
		dN[m]	dE[m]	Avstand [m]		
HYL-1-1	2007-08	0.003	-0.002	0.004	362.57	0.001
HYL-1-1	2008-09	0.002	0.001	0.003	30.61	-0.006
HYL-1-1	2009-10	0.002	0.000	0.002	11.45	0.003
HYL-1-2	2007-08	0.002	-0.001	0.002	366.95	-0.005
HYL-1-2	2008-09	0.005	0.000	0.005	400.00	0.001
HYL-1-2	2009-10	0.004	0.003	0.005	40.13	0.002
HYL-2-1	2007-08	-0.001	0.000	0.001	192.08	-0.004
HYL-2-1	2008-09	0.000	0.001	0.001	117.72	-0.001
HYL-2-1	2009-10	-0.001	0.000	0.001	207.92	0.004
HYL-2-2	2007-08	0.002	0.000	0.002	393.65	-0.001
HYL-2-2	2008-09	-0.002	0.001	0.002	165.60	-0.003
HYL-2-2	2009-10	0.000	-0.001	0.001	273.38	0.004

Tabell 6: Endring mellom målingar for Hyllestad 2007-10. Tabellen syner endring i Nord, Aust (dN,dE) og tilsvarende avstand og retning (gon - 400^g) og endring i høgde (dH)



Figur 12: Punktplott for Hyllestad, vestre område til venstre, austre område til høyre. 2007-09 øvst., 2007-10 i midten og 2008-10 nedst.

Høyanger - Gråberget



Figur 13: Kart (Sk N50) og måleriss over punkta på Gråberget

Målingar - resultat

Det vart i 2007 etablert fire nye punkt på Gråberget i Høyanger. Eitt fastpunkt og tre punkt i mogeleg ustabil fjell. Punkta er målt om i -08, -09 og 10.

Resultata i tabell 7 og 8 og figur 14 syner at det er indikert nokre så vidt signifikante endringar mellom år, men ingen klare trend i endring for dei ulike målingane, med unntak av for GB-3 horisontalt, der det er ein tilnærma lik trend i retning over dei to siste åra.

Endringane er små og det er usikkert om det er reell rørsle, sjølv om det så vidt er signifikant statistisk sett.

Konklusjon

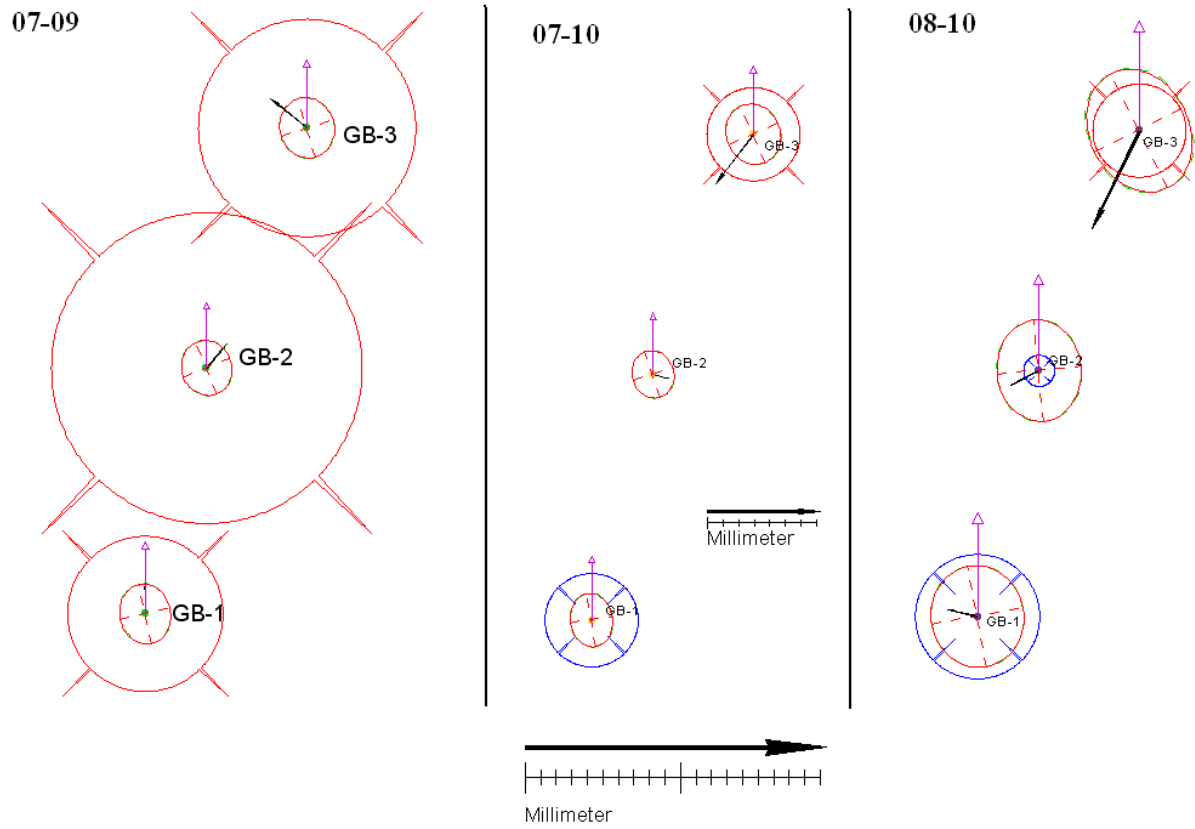
Ut frå resultata kan det ikkje konkluderast sikkert med at det er rørsle i området, men for punktet GB-3 er det indikasjon på små endringar i materialet.

PUNKT	År	N (UTM)	E (UTM)	H (ell.)	σ_N [m]	σ_E [m]	σ_H [m]	dN [m]	dE [m]	Avst. [m]	Retning [° gon]	dH [m]
GB-FP	2008	6790310.1340	343922.4420	873.8030								
GB-1	2007	6790339.2180	343768.3982	814.0891	0.0004	0.0002	0.0008					
GB-1	2008	6790339.2175	343768.4001	814.0904	0.0010	0.0009	0.0019	-0.001	0.002	0.002	116.38	0.001
GB-1	2009	6790339.2198	343768.3982	814.0937	0.0005	0.0005	0.0013	0.002	0.000	0.002	0.00	0.005
GB-1	2010	6790339.2176	343768.3980	814.0855	0.0004	0.0004	0.0011	0.000	0.000	0.000	229.52	-0.004
GB-2	2007	6790370.8503	343776.3249	820.6618	0.0003	0.0002	0.0007					
GB-2	2008	6790370.8509	343776.3278	820.6627	0.0010	0.0008	0.0017	0.001	0.003	0.003	87.01	0.001
GB-2	2009	6790370.8519	343776.3262	820.6714	0.0005	0.0005	0.0012	0.002	0.001	0.002	43.44	0.010
GB-2	2010	6790370.8496	343776.3257	820.6621	0.0004	0.0004	0.0011	-0.001	0.001	0.001	145.76	0.000
GB-3	2007	6790401.7633	343789.2325	816.3957	0.0004	0.0003	0.0008					
GB-3	2008	6790401.7666	343789.2332	816.3964	0.0012	0.0010	0.0020	0.003	0.001	0.003	13.31	0.001
GB-3	2009	6790401.7649	343789.2305	816.4024	0.0005	0.0005	0.0012	0.002	-0.002	0.003	342.96	0.007
GB-3	2010	6790401.7598	343789.2303	816.3991	0.0005	0.0005	0.0012	-0.003	-0.002	0.004	235.72	0.003

Tabell 7: Resultat for Gråberget, Høyanger 2007-10. Tabellen syner koordinatar (N,E og H) med standardavvik (σ_N , σ_E og σ_H) og endring for koordinatar i høve til fyrste måling, gitt som endring i Nord, Aust (dN,dE), Avstand, Retning (gon - 400^g) og høgdeskilnad (dH).

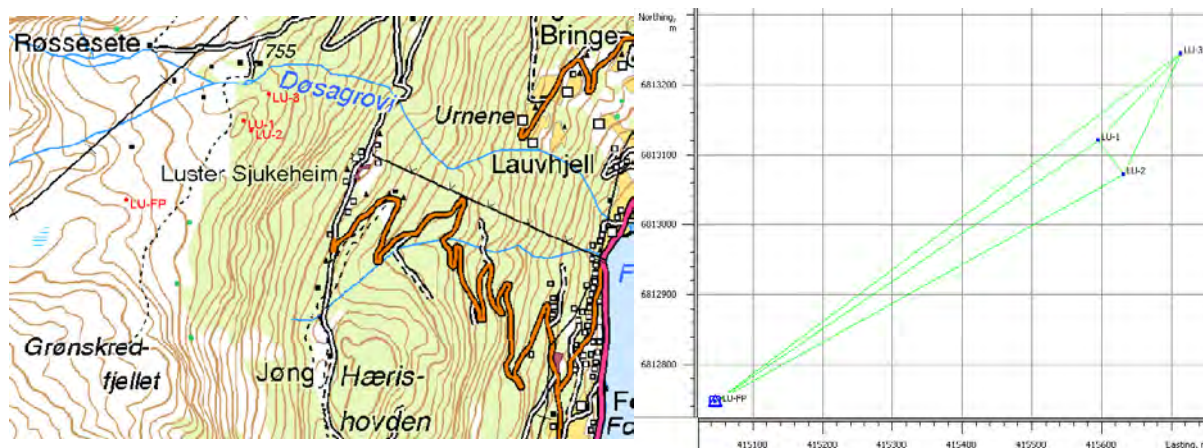
PUNKT	År	Endring mellom målingar				
		dN[m]	dE[m]	Avstand [m]	Retn. (°)	dH[m]
GB-1	2007-08	-0.001	0.002	0.002	116.38	0.001
GB-1	2008-09	0.002	-0.002	0.003	356.04	0.003
GB-1	2009-10	-0.002	0.000	0.002	205.77	-0.008
GB-2	2007-08	0.001	0.003	0.003	87.01	0.001
GB-2	2008-09	0.001	-0.002	0.002	335.56	0.009
GB-2	2009-10	-0.002	-0.001	0.002	213.63	-0.009
GB-3	2007-08	0.003	0.001	0.003	13.31	0.001
GB-3	2008-09	-0.002	-0.003	0.003	264.23	0.006
GB-3	2009-10	-0.005	0.000	0.005	202.50	-0.003

Tabell 8: Endring mellom målingar for Gråberget, Høyanger 2007-10. Tabellen syner endring i Nord, Aust (dN,dE) og tilsvarende avstand og retning (gon - 400^g) og endring i høgde (dH)



Figur 14: Endringer i punkta på Gråberget, 2007-09 (venstre). 2007-10 (midten) og 2008-10 (til høyre)

Røssasete - Luster



Figur 15: Kart (Sk N50) og måleriss over punkta på Røssasete i Luster.

Målingar - resultat

Det er i 2008 etablert og målt inn eitt fastpunkt og tre punkt i sprekkområdet ovanfor Luster sjukeheim. I 2009 er det sett ned ein ny bolt rett ved sida av LU-3 som ikkje var fast. Eit problem med ein mottakar i 2009 gjorde at måletida i LU-1 vart svært kort (10 minutt), og presisjonen i dette punktet er difor vesentleg lågare enn for dei andre.

Punkta er målt om i 2010 men den tidlegare bolten i LU-3 (frå 2008) kunne ikkje målast, og det er difor eit brot i måleserien for dette punktet. Dette punktet var det som i 2009 synte størst vertikal og horisontal endring (i den "dårlege" bolten frå 2008 som var både laus og skeiv), og det er difor noko usikkert om det var bolten som var skuld i den store endringa vertikalt i dette punktet.

Resultata i tabell 9-10 og figur 16 syner at endringane for 2009 -10 er små, vesentleg mindre enn i fjor, og i LU-3 er det ingen vertikal endring, men ein liten signifikant horisontal. Dei to andre punkta syner ikkje signifikante endringar det siste året.

Sidan resultata er noko sprikande og det har vore endringar i boltar i eitt av punkta og det i tillegg er lang avstand til fastpunkt er det vanskeleg å trekke sikre konklusjonar om endringar.

Konklusjon

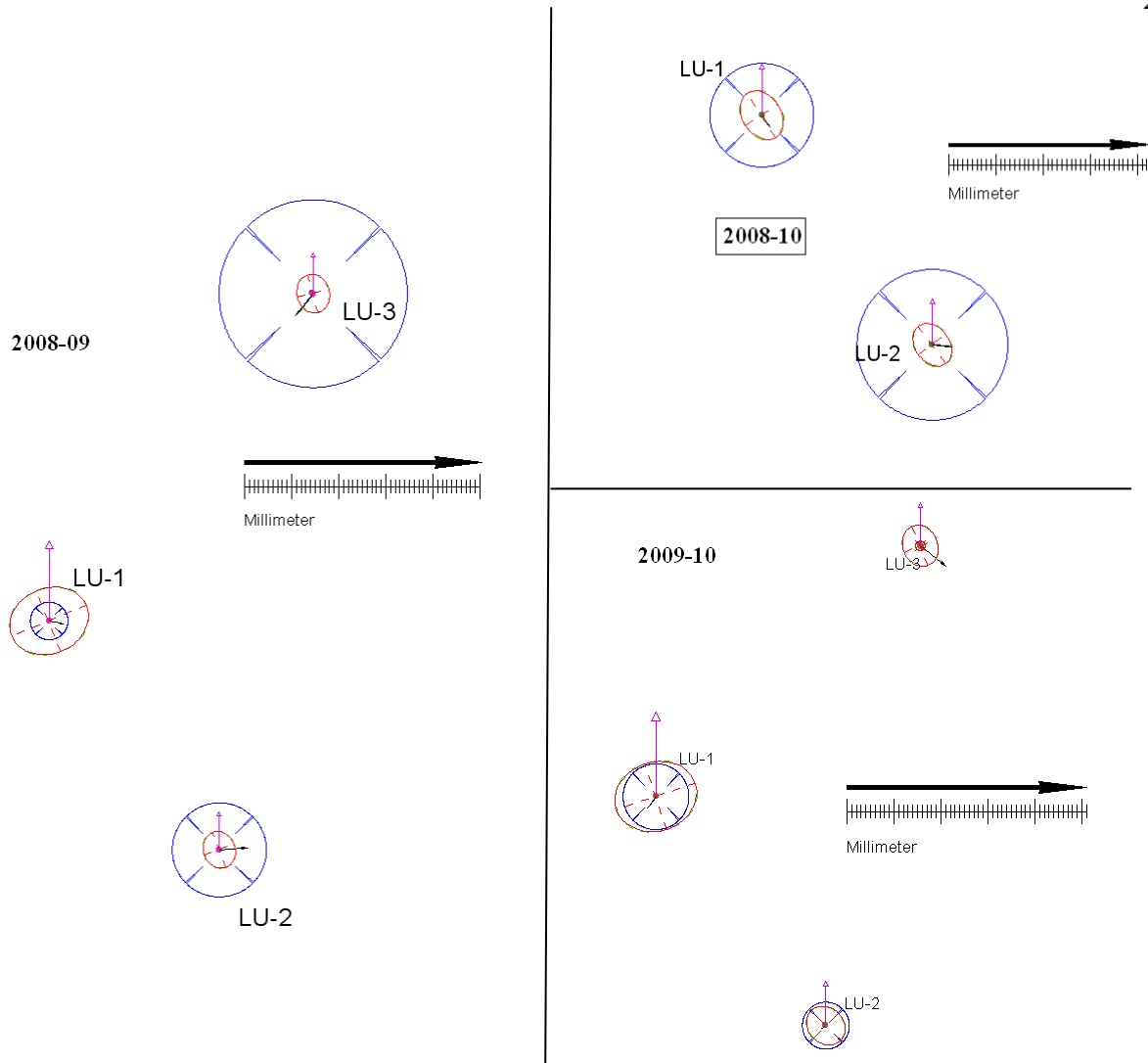
Ut frå resultata etter tre målingar er konklusjonane noko usikre, men det er signifikant vertikal rørsle i to av punkta og horisontal endring i eitt punkt, dette kan representere reelle endringar i punkta.

PUNKT	År	N (UTM)	E (UTM)	H (ell.)	σN [m]	σE [m]	σH [m]	dN [m]	dE [m]	Avst. [m]	Retning [° gon]	dH [m]
LU-FP	2009	6812746.8140	415045.5380	896.7000								
LU-1	2008	6813120.0878	415595.1861	829.4297	0.0011	0.0009	0.0022					
LU-1	2009	6813120.0871	415595.1895	829.4258	0.0021	0.0026	0.0052	-0.001	0.003	0.003	112.93	-0.004
LU-1	2010	6813120.0851	415595.1884	829.4187	0.0013	0.0012	0.0028	-0.003	0.002	0.004	155.08	-0.011
LU-2	2008	6813071.3534	415631.3496	812.9446	0.0010	0.0008	0.0020					
LU-2	2009	6813071.3538	415631.3551	812.9344	0.0008	0.0008	0.0018	0.000	0.005	0.006	95.38	-0.010
LU-2	2010	6813071.3531	415631.3543	812.9291	0.0011	0.0011	0.0025	0.000	0.005	0.005	104.06	-0.016
LU-3	2008	6813244.3245	415713.3767	788.9288	0.0011	0.0009	0.0024					
LU-3	2009	6813244.3194	415713.3727	788.9090	0.0008	0.0007	0.0016	-0.005	-0.004	0.006	242.34	-0.020
LU-3		Bolt Borte										
LU-3_NY	2009	6813244.5182	415713.1487	788.9022	0.0008	0.0006	0.0017					
LU-3_NY	2010	6813244.5145	415713.1537	788.9030	0.0012	0.0011	0.0025	-0.004	0.005	0.006	140.56	0.001

Tabell 9. Resultat for punkt ved Røssasete i 2008-10. Resultata for LU-1 i 2009 er noko usikre på grunn av kort måletid. Gamal bolt i LU-3 er borte i 2010. Tabellen syner koordinatar (N,E og H) med standardavvik (σN , σE og σH) og endring for koordinatar i høve til fyrste måling, gitt som endring i Nord, Aust (dN,dE), Avstand, Retning (gon - 400^g) og høgdeskilnad (dH).

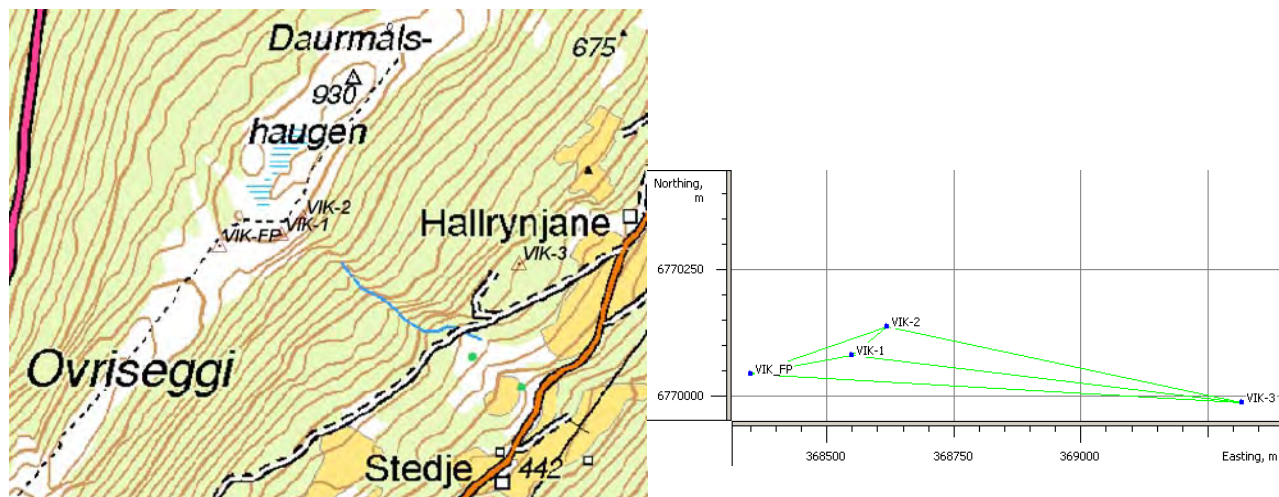
PUNKT	År	Endring mellom målingar			Retn. (°)	dH[m]
		dN[m]	dE[m]	Avstand [m]		
LU-1	2008-09	-0.001	0.003	0.003	112.93	-0.004
LU-1	2009-10	-0.002	-0.001	0.002	232.01	-0.007
LU-2	2008-09	0.000	0.005	0.006	95.38	-0.010
LU-2	2009-10	-0.001	-0.001	0.001	254.24	-0.005
LU-3	2008-09	-0.005	-0.004	0.006	242.34	-0.020
LU-3_NY	2009-10	-0.004	0.005	0.006	140.56	0.001

Tabell 10. Endringar mellom år for punkt ved Røssasete i 2008-10.



Figur 16: Endringar i punkta på Røssasete i Luster, 2008-09

Daurmålshaugen - Vik



Figur 17: Kart (Sk N50) og måleriss over punkta på Daurmålshaugen i Vik.

Målingar

Det er i 2008 etablert og målt inn eitt fastpunkt og to punkt i sprekkområdet på Daurmålshaugen i Vik. Punkta er målt om i 2009, og det er samstundes etablert eitt nytt punkt ved foten av skråninga ned mot gardane Hallrynjane.

I Vik syner punktet VIK-1 framleis klar signifikant endring frå år til år. For 2009-10 er endringa litt større enn for 2008-09 både i plan og høgd. I VIK-2 er det ingen signifikante endringar observert. I VIK-3 er det ei lita endring i mellom målingane som kan vere rørsle, men med berre to målingar er det for usikkert til å konkludere med at det er rørsle i punktet. Resultata er synt i tabell 11 og 12 og figur 18.

Konklusjon

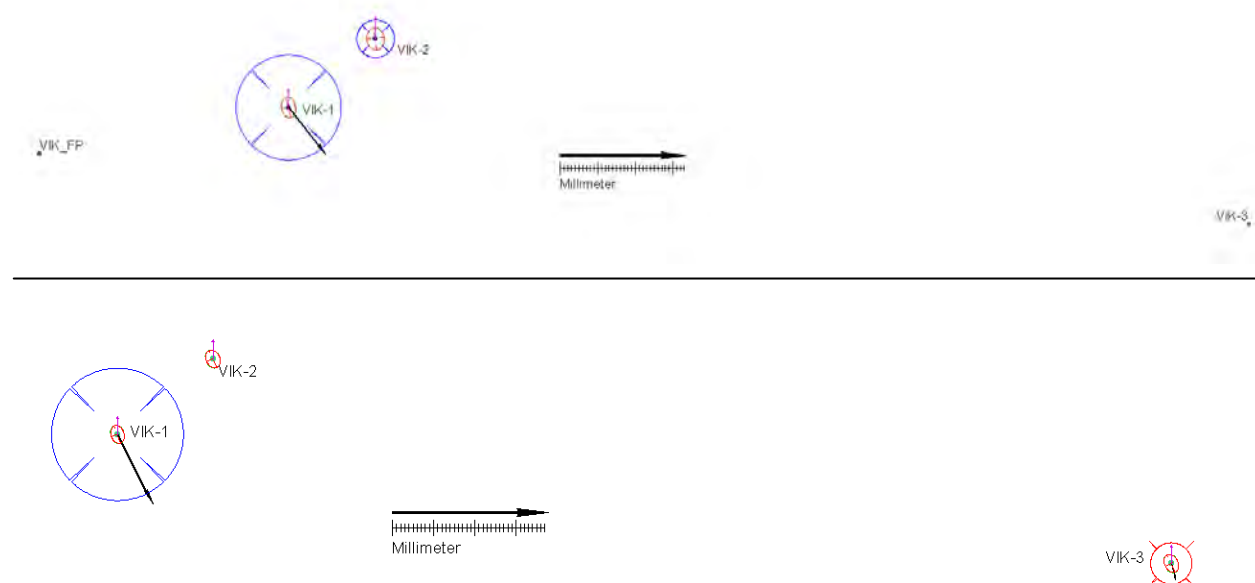
Resultata syner at det er relativt stor rørsle i punktet VIK-1, både i plan og høgd. I dei andre punkta kan det ikkje påvisast sikre endringar.

PUNKT	År	N (UTM)	E (UTM)	H (ell.)	σ_N [m]	σ_E [m]	σ_H [m]	dN [m]	dE [m]	Avst. [m]	Retning [° gon]	dH [m]
VIK_FP	FP	6770043.8890	368351.5830	942.1710								
VIK-1	2008	6770081.1319	368550.3822	946.5458	0.0008	0.0006	0.0015					
VIK-1	2009	6770081.1191	368550.3924	946.5314	0.0004	0.0002	0.0006	-0.013	0.010	0.016	157.17	-0.014
VIK-1	2010	6770081.1025	368550.4009	946.5157	0.0006	0.0005	0.0013	-0.029	0.019	0.035	163.93	-0.030
VIK-2	2008	6770135.8776	368619.8193	941.7359	0.0009	0.0007	0.0018					
VIK-2	2009	6770135.8782	368619.8200	941.7304	0.0004	0.0003	0.0007	0.001	0.001	0.001	54.89	-0.005
VIK-2	2010	6770135.8777	368619.8199	941.7307	0.0006	0.0005	0.0014	0.000	0.001	0.001	89.49	-0.005
VIK-3	2009	6769987.5230	369317.0034	628.9373	0.0004	0.0003	0.0007					
VIK-3	2010	6769987.5191	369317.0045	628.9421	0.0006	0.0005	0.0013	-0.004	0.001	0.004	182.50	0.005

Tabell 11: Resultat for endringer for punkta på Daurmålshaugen i Vik, 2008-09. Tabellen syner koordinatar (N,E og H) med standardavvik (σ_N , σ_E og σ_H) og endring for koordinatar i høve til fyrste måling, gitt som endring i Nord, Aust (dN,dE), Avstand, Retning (gon - 400^g) og høgdeskilnad (dH).

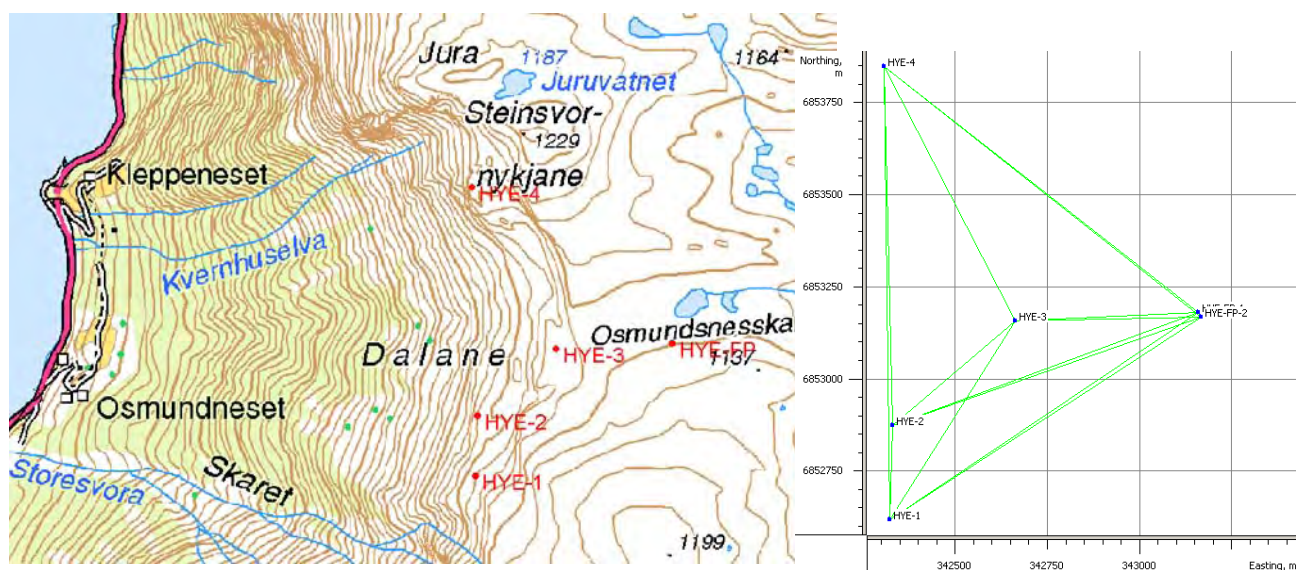
PUNKT	År	Endring mellom målingar			Retn. (°)	dH[m]
		dN[m]	dE[m]	Avstand [m]		
VIK-1	2008-09	-0.013	0.010	0.016	157.17	-0.014
VIK-1	2009-10	-0.017	0.008	0.019	169.87	-0.016
VIK-2	2008-09	0.001	0.001	0.001	54.89	-0.005
VIK-2	2009-10	-0.001	0.000	0.001	212.57	0.000
VIK-3	2009-10	-0.004	0.001	0.004	182.50	0.005

Tabell 12: Endringer mellom år for punkta på Daurmålshaugen i Vik, 2008-10.



Figur 18: Endringer i punkta på Daurmålshaugen i Vik, 2008-09 (øvt) og 2009-10 (nedst).

Osmundneset - Hyen



Figur 19: Kart (Sk N50) og måleriss over punkta over Osmundneset i Hyen.

Målinger

Det er i 2008 etablert og målt inn eitt fastpunkt og fire punkt i sprekkområdet ovanfor Osmundneset i Hyen. I 2009 er punkta målt om og det er i tillegg etablert eit nytt fastpunkt som kan erstatte det tidlegare som hadde skeiv bolt og var ugunstig plassert. I 2010 er alle punkta målt om, og ei ny samla utjamning av målingane frå i fjor og i år for å sikre at koordinat på det nye fastpunktet stemmer med det gamle. Koordinatane for 2009 er difor litt endra i høve til tidlegare rapport.

Det er svært små rørsler i alle punkt det siste året, men over to år er endringane i HY-4 signifikante og begge åra går i same retning, slik at det kan ikkje utelukkast at det er litt rørsle i dette punktet. For dei andre punkta er observerte endringar små og det er ikkje klare indikasjonar på rørsle. I høgd er det ingen vesentlege endringar for 2009-10. Resultata er synt i tabell 13 og 14 og figur 20.

Konklusjon

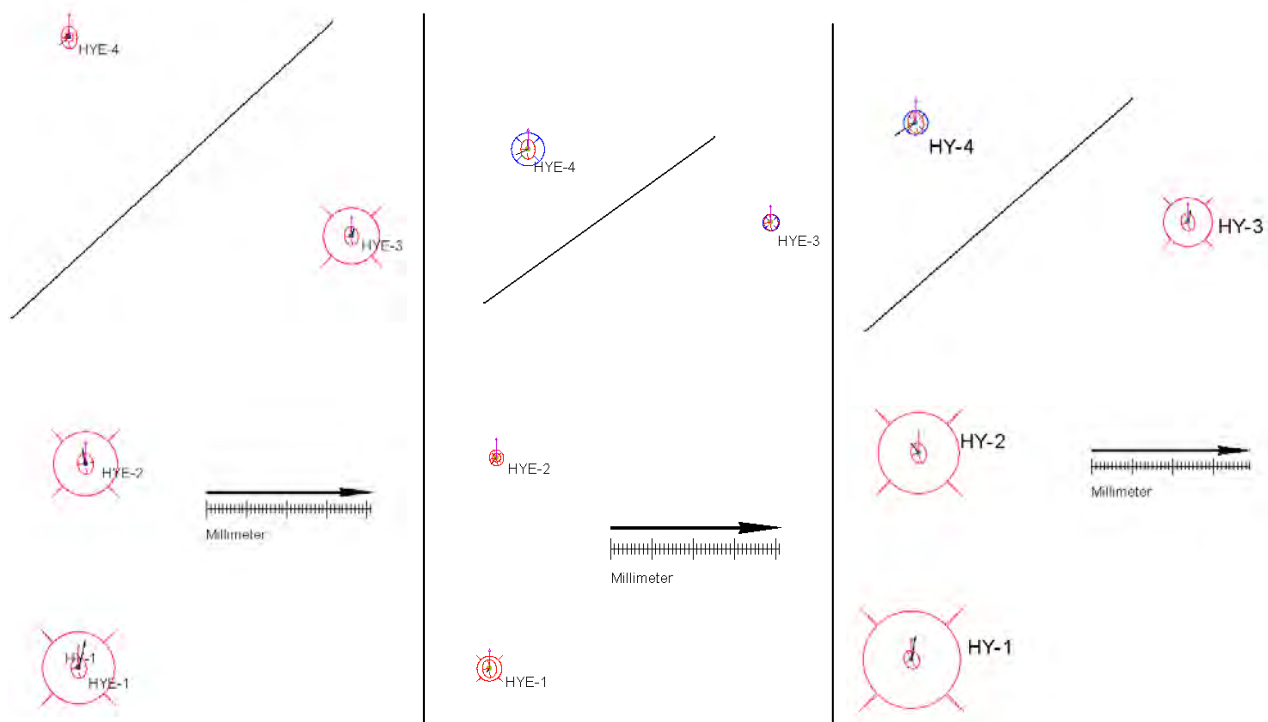
Resultata etter to ommålingar indikerer at det kan vere rørsle i punktet HY-4, men konklusjonen er noko usikker.

PUNKT	År	N (UTM)	E (UTM)	H (ell.)	σN [m]	σE [m]	σH [m]	dN [m]	dE [m]	Avst. [m]	Retning [^g gon]	dH [m]
HYE-FP-1	2009	6853182.2280	343157.3310	1145.8970								
HYE-FP-2	2009	6853168.7918	343166.5133	1150.8690	0.0005	0.0004	0.0013					
HYE-1	2008	6852618.7633	342321.2341	1067.7332	0.0006	0.0005	0.0014					
HYE-1	2009	6852618.7699	342321.2357	1067.7420	0.0006	0.0004	0.0012	0.007	0.002	0.007	15.14	0.009
HYE-1	2010	6852618.7685	342321.2346	1067.7452	0.0005	0.0004	0.0010	0.005	0.001	0.005	6.10	0.012
HYE-2	2008	6852874.2637	342329.7858	1032.1803	0.0007	0.0005	0.0014					
HYE-2	2009	6852874.2672	342329.7851	1032.1888	0.0005	0.0004	0.0012	0.003	-0.001	0.004	387.43	0.008
HYE-2	2010	6852874.2659	342329.7844	1032.1897	0.0005	0.0004	0.0010	0.002	-0.001	0.003	363.92	0.009
HYE-3	2008	6853159.3655	342662.4024	1112.6543	0.0006	0.0004	0.0013					
HYE-3	2009	6853159.3674	342662.4031	1112.6617	0.0005	0.0004	0.0011	0.002	0.001	0.002	22.47	0.007
HYE-3	2010	6853159.3679	342662.4033	1112.6602	0.0005	0.0004	0.0010	0.002	0.001	0.003	22.84	0.006
HYE-4	2008	6853848.9590	342305.4169	1158.8790	0.0007	0.0005	0.0016					
HYE-4	2009	6853848.9571	342305.4145	1158.8801	0.0006	0.0004	0.0012	-0.002	-0.002	0.003	257.37	0.001
HYE-4	2010	6853848.9561	342305.4122	1158.8765	0.0005	0.0005	0.0011	-0.003	-0.005	0.006	264.81	-0.002

Tabell 13: Resultat for endringer for punkta på Osmundneset i Hyen 2008-10. Tabellen syner koordinatar (N,E og H) med standardavvik (σN , σE og σH) og endring for koordinatar i høve til fyrste måling, gitt som endring i Nord, Aust (dN,dE), Avstand, Retning (gon - 400^s) og høgdeskilnad (dH).

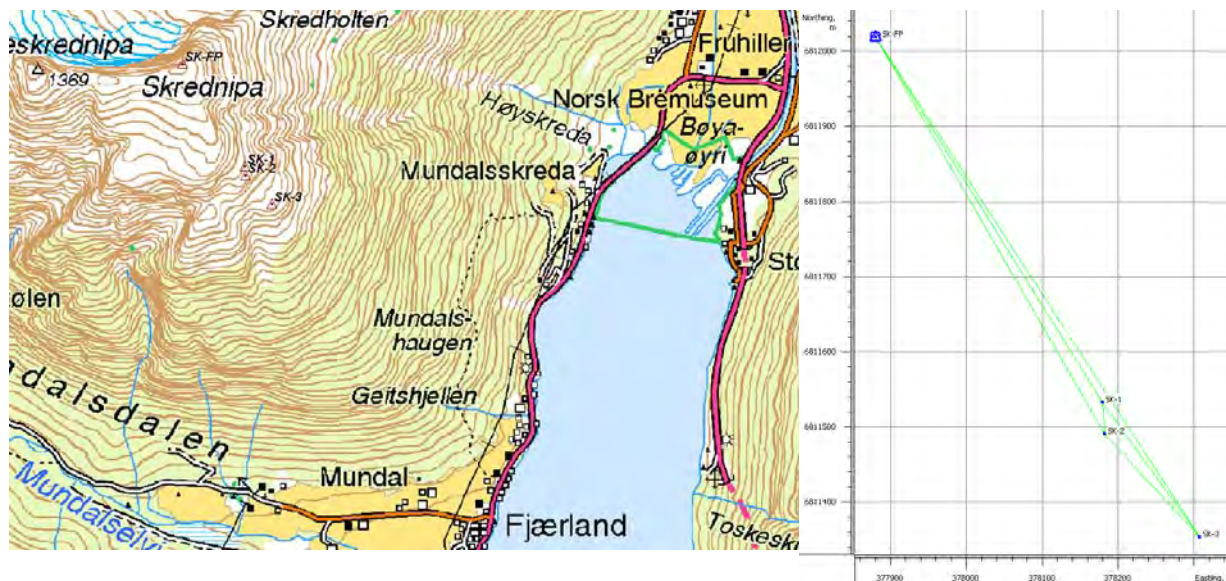
PUNKT	År	Endring mellom målingar			Retn. (^g)	dH[m]
		dN[m]	dE[m]	Avstand [m]		
HY-1	2008-09	0.007	0.001	0.007	10.51	0.010
HY-1	2009-10	-0.001	-0.001	0.002	225.78	0.002
HY-2	2008-09	0.003	-0.001	0.004	378.40	0.010
HY-2	2009-10	-0.001	0.000	0.001	210.51	0.000
HY-3	2008-09	0.002	0.000	0.002	7.46	0.008
HY-3	2009-10	0.001	0.001	0.001	50.00	-0.002
HY-4	2008-09	-0.002	-0.003	0.004	261.56	0.002
HY-4	2009-10	-0.001	-0.002	0.002	270.48	-0.005

Tabell 14: Endringar mellom år for punkta i Hyen, 2008-10.



Figur 20: Endringar i punkta over Osmundneset i Hyen, 2008-09, 2009-10 og 2008-10 (venstre, midtre og høgre delfigur)

Skrednipa - Fjærland



Figur 21: Kart (Sk N50) og måleriss over punkta på Skrednipa i Fjærland.

Målingar og resultat

Det er i 2009 etablert og målt inn eitt fastpunkt og tre punkt på ryggen frå toppen av Skrednipa og ned mot Fjærland. Eitt fjerde punkt som ikkje kunne settast ut i 2009 pga. øydelagt bor er etablert i 2010 i samband med ommåling av punkta. Punkta er synt på kart i Figur 22 og i Tabell 15.

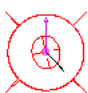
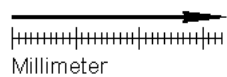
Resultata over berre eitt år og som syner små, så vidt signifikante endringar i to av punkta er difor usikre. At endringane i høgd tilseier heving er og ein indikasjon på at resultatet er usikkert. Det trengs minst ei måling til før ein kan trekke konklusjonar om eventuelle endringar.

Konklusjon

Det kan ikkje etter ei ommåling påvisast klare endringar i punkta.

PUNKT	År	N (UTM)	E (UTM)	H (ell.)	σ_N [m]	σ_E [m]	σ_H [m]	dN [m]	dE [m]	Avst. [m]	Retning [° gon]	dH [m]
SK-FP	FP	6812018.7730	377880.6760	1327.1940								
SK-1	2009	6811532.2153	378179.3200	1120.2831	0.0007	0.0007	0.0015					
SK-1	2010	6811532.2150	378179.3202	1120.2828	0.0003	0.0002	0.0006	0.000	0.000	0.000	162.57	0.000
SK-2	2009	6811490.1723	378182.3567	1113.2161	0.0007	0.0006	0.0015					
SK-2	2010	6811490.1689	378182.3577	1113.2191	0.0003	0.0002	0.0006	-0.003	0.001	0.004	181.79	0.003
SK-3	2009	6811353.4429	378307.9429	1007.6855	0.0008	0.0007	0.0017					
SK-3	2010	6811353.4396	378307.9455	1007.6921	0.0003	0.0002	0.0006	-0.003	0.003	0.004	157.52	0.007
SK-4	2010	6811248.8317	378405.8278	927.0070	0.0004	0.0003	0.0007					

Tabell 15: Resultat for koordinatar og endringar for punkt på Skrednipa i Fjærland 2009-10. Tabellen syner koordinatar (N,E og H) med standardavvik (σ_N , σ_E og σ_H) og endring for koordinatar i høve til fyrste måling, gitt som endring i Nord, Aust (dN,dE), Avstand, Retning (gon - 400°) og høgdeskilnad (dH).

 SK-1 SK-2 SK-3 SK-4

Figur 22: Endringar i punkta på Skrednipa 2009-10

Eikefjord - Strandanipa



Figur 23: Kart over (Sk N50), og måleriss under syner plasseringa av punkta på Strandanipa.

Målingar - resultat

Det vart i 2007 etablert tre nye punkt på Strandanipa i Eikefjord. Eitt fastpunkt og to punkt i mogeleg ustabil fjell.

Punkta er målt om i 2008 og 2010. Resultata er presentert i tabell 16-17 og figur 24. Resultata tyder på at det ikkje er endringar i punkta. Mellom dei tre målingane som er gjort er to horisontale og ei vertikal endring signifikante, men ligg like over grense for signifikans, og er i tillegg svært små. Målingane varierer i retning på endringsvektor mellom år, og er i same storleik som reell målepresisjon.

Konklusjon

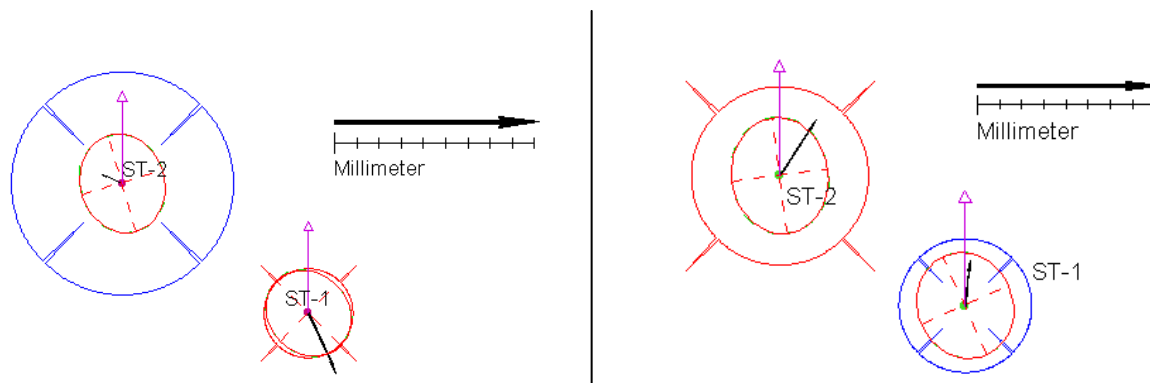
Det er ikkje påvist klart signifikante endringar i punkta på Strandanipa, men det kan ikkje utelukkast at det er små rørsler i punkta.

PUNKT	År	N (UTM)	E (UTM)	H (ell.)	σ_N [m]	σ_E [m]	σ_H [m]	dN [m]	dE [m]	Avst. [m]	Retning [° gon]	dH [m]
ST-FP	FP	6836273.8000	309542.9750	719.5210								
ST-1	2007	6836168.0906	309486.6487	707.6257	0.0002	0.0002	0.0004					
ST-1	2008	6836168.0882	309486.6498	707.6278	0.0006	0.0006	0.0013	-0.002	0.001	0.003	172.64	0.002
ST-1	2010	6836168.0902	309486.6500	707.6250	0.0005	0.0004	0.0011	0.000	0.001	0.001	119.00	-0.001
ST-2	2007	6836179.7416	309469.9052	705.1839	0.0002	0.0002	0.0004					
ST-2	2008	6836179.7421	309469.9041	705.1784	0.0007	0.0006	0.0013	0.001	-0.001	0.001	327.16	-0.005
ST-2	2010	6836179.7452	309469.9059	705.1818	0.0005	0.0004	0.0011	0.004	0.001	0.004	12.23	-0.002

Tabell 16: Resultat for Strandanipa, Eikefjord 2007-08. Tabellen syner koordinatar (N,E og H) med standardavvik (σ_N , σ_E og σ_H) og endring for koordinatar i høve til fyrste måling, gitt som endring i Nord, Aust (dN,dE), Avstand, Retning (gon - 400°) og høgdeskilnad (dH).

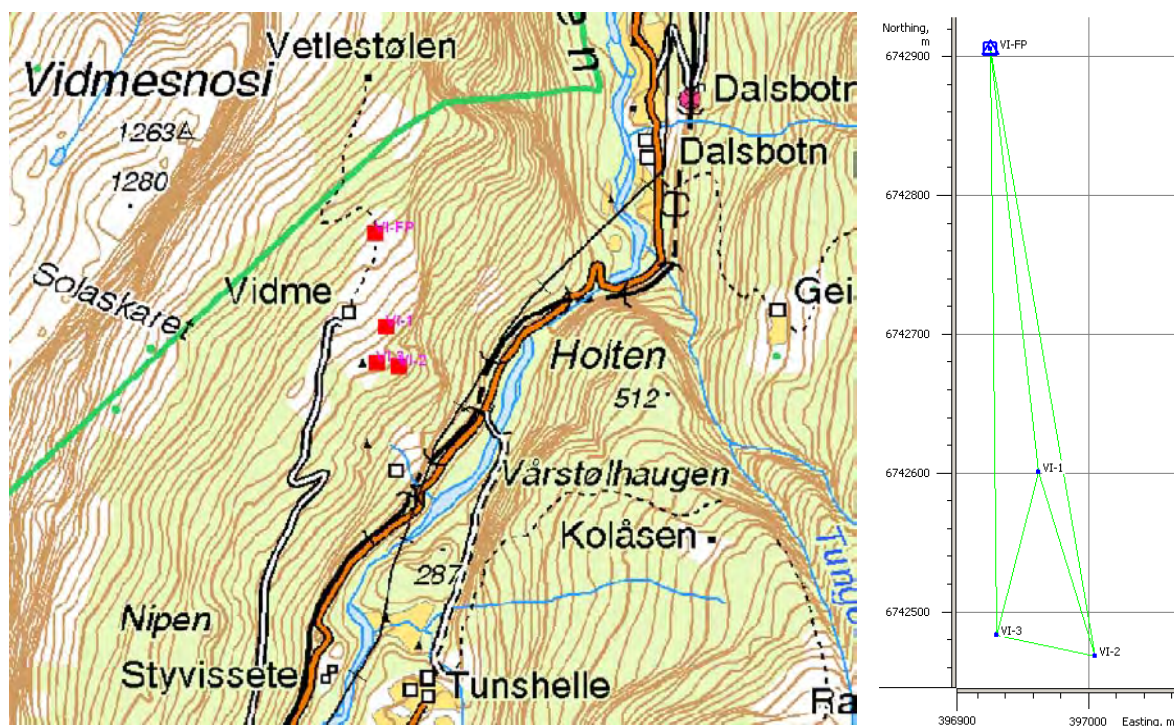
PUNKT	År	Endring mellom målingar			Retn. (°)	dH[m]
		dN[m]	dE[m]	Avstand [m]		
ST-1	2007-08	-0.002	0.001	0.003	172.64	0.002
ST-1	2008-10	0.002	0.000	0.002	6.35	-0.003
ST-2	2007-08	0.001	-0.001	0.001	327.16	-0.005
ST-2	2008-10	0.003	0.002	0.004	33.49	0.003

Tabell 17: Endringar mellom målingar for punkta på Strandanipa, 2007-10. NB det er eitt og to år mellom målingane.



Figur 24: Endringar Strandanipa 2007-08 (venstre) og 2008-10 (høgre).

Vidme - Flåm



Figur 25: Kart (Sk N50), og måleriss som viser plasseringa av punkta på Vidme.

Målinger - resultat

Det vart i 2010 etablert og målt inn eit fastpunkt og tre nye punkt på moglege blokker i rørslø ved Vidme i Flåm.

Området ligg relativt vanskeleg til med omsyn til satellittmålingar, med maskering av sikt mot vest og nordvest. Resultata ut frå vel to timars måling ser likevel ut til å vere gode med standardavvik om lag på same nivå som for andre område. Området ligg slik til at det berre bør målast i det tidsrommet på dagen det er mest tilgjengelege satellittar.

Koordinatresultat er gitt i tabell 18.

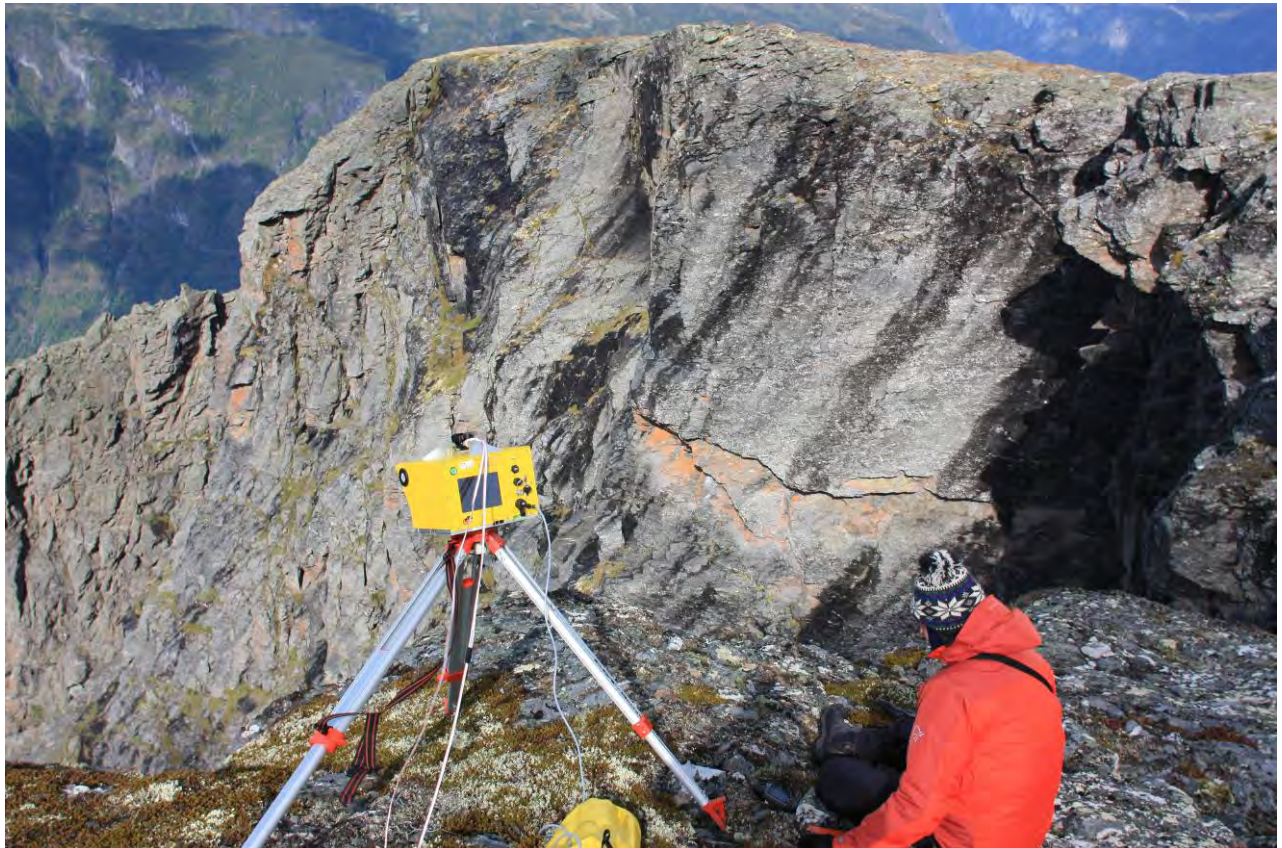
PUNKT	År	N (UTM)	E (UTM)	H (ell.)	σN [m]	σE [m]	σH [m]	dN [m]	dE [m]	Avst. [m]	Retning [$^{\circ}$ gon]	dH [m]
VI-FP	2010	6742905.0730	396928.9520	664.7970								
VI-1	2010	6742600.5858	396964.1901	575.1213	0.0007	0.0006	0.0014					
VI-2	2010	6742468.4307	397004.9603	541.1650	0.0007	0.0007	0.0016					
VI-3	2010	6742483.5437	396933.8641	556.1314	0.0010	0.0008	0.0020					

Tabell 18: Førebels koordinatar for punkta på Vidme. Tabellen viser koordinatar (N,E og H) med standardavvik (σN , σE og σH).



UNIL | University of Lausanne
Faculty of Geosciences and Environment
Institute of Geomatics and Risk Analysis
Amphipôle
CH-1015 Lausanne

Analysis of groundbased LiDAR data from Sogn og Fjordane County (Norway)



D. Carrea, S. Lévy, M.-H. Derron, C. Longchamp, A. Loye, T. Oppikofer, M. Jaboyedoff

IGAR - August 2010

Faculty of Geosciences and Environment
Institute of Geomatics and Risk Analysis

|||||
Phone +41 21 692 35 32 | Fax +41 21 692 35 35 | michel.jaboyedoff@unil.ch

Executive Summary

We summarize here the main outcomes of the LiDAR datasets analysis for 7 sites. In addition, we make some recommendations to optimize the future LiDAR acquisition campaigns. If a full cover of the site has been done once, it is usually not necessary to scan the entire site again, but some specific well-chosen scans are sufficient to monitor changes and displacements.

The goal of this work is to present and discuss the information extracted from the TLS scans in a way that this information can be used for future geological interpretations. As only observations from the LiDAR datasets are discussed here, this report does not intend to provide a complete analysis of the sites.

<p>Årdal (Ramneberg)</p>	<p>Years of scanning: 2009.</p> <p>Area scanned: entire cliff.</p> <p>Discontinuity sets: J1: 248/81, J2: 242/54, J3: 304/57, J4: 015/72, J5 - TOPO: 179/65.</p> <p>Kinematics tests: potential planar sliding with J2 and toppling with J4.</p> <p>Displacements: not done (only one year of data).</p> <p>Remarks: large site, but easy to access. Main issue: rockfalls on houses. Elements at risk at the foot of the cliff.</p> <p>Recommendations: scan again the entire cliff for rockfall activity.</p>
<p>Volldal (Dalsuri)</p>	<p>Years of scanning: 2009.</p> <p>Area scanned: entire cliff.</p> <p>Discontinuity sets: J1: 327/15, J2: 071/89, J3: 005/76, J4: 309/73.</p> <p>Kinematics test: potential toppling with J3 and J4.</p> <p>Displacements: not done (only one year of data).</p> <p>Remarks: large site, but easy to access. Main issue: rockfalls on houses. Elements at risk at the foot of the cliff.</p> <p>Recommendations: scan again the entire cliff for rockfall activity.</p>
<p>Old tunnel</p>	<p>Years of scanning: 2009.</p> <p>Area scanned: top of the cliff.</p> <p>Discontinuity sets: J1: 280/71, J2: 058/84, J3: 350/70, J4: 190/80.</p> <p>Kinematics test: Fjord face: wedge sliding with J3 & J1, J2 & J1, J3 & J1, potential sliding plane with J3 and toppling with J4. Tunnel face: planar sliding J2 and toppling with J1.</p> <p>Displacements: not done (only one year of data).</p> <p>Remarks: only the top of the cliff was scanned. Main issue: rockfalls on the</p>

	<p>road but rockslide not excluded on the fjord side.</p> <p>Recommendations: scan again the upper part for future comparison.</p>
Tussen	<p>Years of scanning: 2008, 2009.</p> <p>Area scanned: top of the moving part, main scarp, sliding block and first back-cracks.</p> <p>Discontinuity sets: S1: 317/12, J2: 248/85, J3: 028/90, J4: 129/63, J5: 298/78.</p> <p>Kinematics test: possible planar sliding on J4 and toppling with J5.</p> <p>Displacements: no displacement was detected.</p> <p>Remarks: more points of reference are needed to be accurate.</p> <p>Recommendations: scan again the back-cracks and the plateau behind to have a better reference for future comparisons.</p>
Vidalen	<p>Years of scanning: 2009.</p> <p>Area scanned: top of the suspected unstable block, back and front south cliff.</p> <p>Discontinuity sets: S1: 310/43, J1: 167/72, J2: 274/75, J3: 108/40, J4: 015/65, J5: 226/82.</p> <p>Kinematics test: The tests indicate also a slight potential of planar sliding on S1 and a potential wedge sliding with S1 and J1 depending on friction angle.</p> <p>Displacements: not done (only one year of data)</p> <p>Remarks: only the very top part (top scarp) of the instability was surveyed.</p> <p>Recommendations: to scan again the backscarp and, if possible, from another point of view to complete the overview.</p>
Vik	<p>Years of scanning: 2009.</p> <p>Area scanned: top of the suspected unstable cliff area.</p> <p>Discontinuity sets: J1: 028/25, J2: 288/70, J3: 015/88, J4: 025/25.</p> <p>Kinematics test: potential planar sliding on J4 and toppling on J3.</p> <p>Displacements: not done (only one year of data)</p> <p>Remarks: only the very top part of the instability was surveyed.</p> <p>Recommendations: Keep the same point of view for future scans and combine with field measurement of discontinuity sets.</p>

Flâm	<p>Years of scanning: 2008, 2009.</p> <p>Area scanned: Upper site – the cliff, Lower site – main unstable block.</p> <p>Discontinuity sets: Upper site – S1: 243/35, J2: 205/72, J3: 243/89 Lower site: S2: 304/35, J5: 008/55, J6: 075/75, J7: 128/33, J8: 178/58</p> <p>Kinematics test: Upper site – possible planar sliding on S1, Lower site – unable to determine clear mechanism</p> <p>Displacements: General trend westward in the lower site (~2cm).</p> <p>Remarks: Lower site – increase the scanning of the supposed stable part.</p> <p>Recommendations: Upper site – scan the same area to see if there is any change. Lower site –one scan of the block including a stable part should be enough to detect if there is any movement.</p>
------	--------------------------------------------------------------------------------------------------------------------------------------------------------------------------------------------------------------------------------------------------------------------------------------------------------------------------------------------------------------------------------------------------------------------------------------------------------------------------------------------------------------------------------------------------------------------------------------------------------------------------------------------------------------------------------------------------------------------------------------------------------------

Table of content

I	INTRODUCTION	7
II	SITES LOCATIONS	7
III	DATA AND PROCESSING	8
III.1	Data acquisition	8
III.2	Processing method	8
III.3	Geological and structural interpretation.....	8
IV	SOGN OG FJORDANE STUDY AREAS	9
IV.1	Årdal (Ramneberg)	9
IV.1.1	Discontinuity analysis.....	10
IV.1.2	Movement analysis	12
IV.1.3	Discussion.....	13
IV.2	Volldal (Dalsuri)	14
IV.2.1	Discontinuity analysis.....	15
IV.2.2	Movement analysis	17
IV.2.3	Discussion.....	17
IV.3	Old Tunnel	18
IV.3.1	Movement analysis	22
IV.3.2	Discussion.....	22
IV.4	Tussen.....	23
IV.4.1	Discontinuity analysis.....	24
IV.4.2	Movement analysis	27
IV.4.3	Discussion.....	28
IV.5	Vidalen.....	29
IV.5.1	Discontinuity analysis.....	29
IV.5.2	Movement analysis	32
IV.5.3	Discussion.....	32
IV.6	Vik.....	33
IV.6.1	Discontinuity analysis.....	33
IV.6.2	Movement analysis	35
IV.6.3	Discussion.....	35
IV.7	Flåm.....	36
IV.7.1	Discontinuity analysis.....	37
Upper site	37
Lower site	39
IV.7.2	Movement analysis	41
IV.7.3	Integration with airborne data.....	42
IV.7.4	Punctual dip measurements on the DEM.....	42
IV.7.5	Planar traces.....	43
IV.7.6	Discussion.....	44
V	GENERAL CONCLUSIONS.....	44

I Introduction

This report is made in the frame of the collaboration between the Geological Survey of Norway (NGU) and the Institute of Geomatics and Risk Analysis of the University of Lausanne (IGAR). NGU asked IGAR to monitor some of the Sogn og Fjordane County major instabilities by Terrestrial Laser Scanning (TLS).

All the data of 2008 and 2009 were cleaned, aligned georeferenced and finally delivered to NGU in December 2009. That was the first part of this work. The goal of this second part is to present and discuss the information extracted from the TLS scans, so that this information can be used for future geological interpretations. Only the observations from the LiDAR datasets are discussed here. Because no field survey was performed, this report does not intend to provide a complete analysis of the sites.

II Sites Locations

All the sites discussed in this report are located in the Sogn og Fjordane County (Western Norway). These sites are mapped in Figure 1.



Figure 1: Location map of the sites of instabilities of Sogn og Fjordane County presented in this report (<http://kart.statkart.no>).

III Data and processing

III.1 Data acquisition

The data were acquired in summer 2008 with the NGU's ILRIS-3D^{ER} by M.-H. Derron and NGU. In 2009, data were acquired by A. Loye and M.-H. Derron with the NGU's ILRIS-3D^{ER}. All the scans were done in « Enhanced Range », last pulse mode.

III.2 Processing method

The scans were processed at IGAR during the winter 2009-2010. The main processing steps are:

- Parsing with the Optech parser. The parser converts LiDAR raw data in a point cloud in a XYZ coordinate system.
- Cleaning: deleting outsiders and vegetation where it masks the rock, with Pifedit (InnovMETRIC).
- Alignment with PolyWorks[®] (InnovMETRIC) v10.1 ImAlign™.
- Georeferencing: with PolyWorks[®] v10.1 ImAlign and ImInspect™ using the references mentioned hereafter. The coordinates/projection/geoid system is UTM Zone 32N – WGS84, in meter. To georeference the terrestrial laser scans of Årdal, Volldal, Old tunnel, Tussen, Vik and Vidalen are made using a DEM 25 m and Flåm with using a DEM 1 m, both provided by NGU.

III.3 Geological and structural interpretation

The main steps of the interpretation are:

The point clouds from the terrestrial scans are interpreted using a beta-version of Coltop3D (developed at IGAR): discontinuities identification, dips measurements and colour coding of rock faces. The measurements of discontinuities are, if possible, made on stable parts in order to avoid variations induced by slope movement.

The stereoplot (lower hemisphere, equal area) are produced with Dips 5.1 (Rocscience). All the measurements are given as dip direction and dip angle.

The displacements are measured using PolyWorks[®] v10.1 ImInspect™. A full point cloud grouping all the scans of one year includes some internal alignment errors in between the scans (usually around 3 cm). That makes then difficult to use this overall point cloud to detect small displacements. So, according to Oppikofer and Jaboyedoff (2009), when it was possible a piece-wise comparison was used, i. e. the comparison was done between single scans of two different years instead of using the full point cloud. This requires that these single scans include a stable part that can be used as reference in addition of the part which is supposed to move.

IV Sogn og Fjordane study areas

IV.1 Årdal (Ramneberg)

The Ramneberg cliff (Figure 2) is a high sub-vertical wall, facing the village of Øvre Årdal. The cliff is around 600 m large and faces south. A large scree slope lies at the foot of the cliff, showing the rockfall activity of the cliff. A total of 7 scans were processed to have the full cliff. This site was scanned for structural analysis and to estimate the volume of rockfall between each year comparing the scree deposit.



Figure 2: Panorama of the Ramneberg cliff from the eastern scanning point. Some houses are located at the foot of the cliff.

As the precise location of the scanning points was not recorded, Figure 3 is an estimation of the 2009 campaign of scans. Some field pictures taken by A. Lo ye were used to determine the location and direction of the scanning points as accurately as possible.



Figure 3: Scanning points of 2009 TLS data (in blue). The location of the points was estimated from field photographs, as for the overall directions (arrows) of scanning. Orthophoto from Statens Kartverk (<http://kart.statkart.no>). Pink lines indicate subvertical J5 discontinuity set.

IV.1.1 Discontinuity analysis

The discontinuity analysis was made on the 2009 TLS point cloud and based on field observations. The representation with the color coding of Coltop3D (Figure 4) shows clearly the predominance of facets dipping towards S to W (from green to blue). The pink facets are almost vertical.

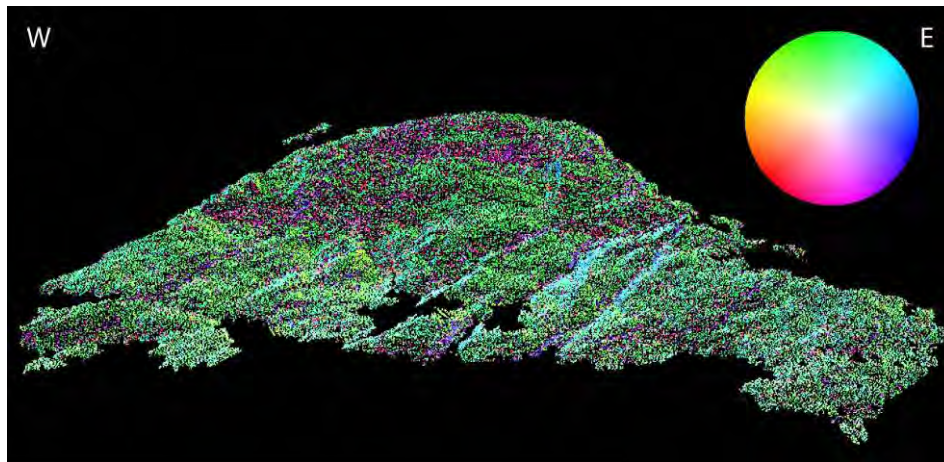


Figure 4: Example of a Coltop 3D view of the point cloud. The colour of each point of the scan is given by the orientation (using the pole) of the surface at this point in the color wheel. The view is from a point at the South of the cliff.

The interpretation of the cliff structure is not obvious, but five main sets of discontinuities were identified and measured on the terrestrial LiDAR data. The measurements were then imported into Dips to estimate the mean orientations and standard deviations. These measurements are presented in Figure 5.

Discontinuity set	Mean dips	Standard deviation
J1	248/81	8°
J2	242/54	10°
J3	304/57	10°
J4	015/72	12°
J5	179/65	12°

The discontinuity set J5 makes the main slope face of the unstable cliff. J2 seems to be a major penetrative joint affecting all the rock mass (Figure 4). It will be interesting to see in field if it is possible to see J2 on the other face of the mountain to estimate how far it propagates in the rock mass.

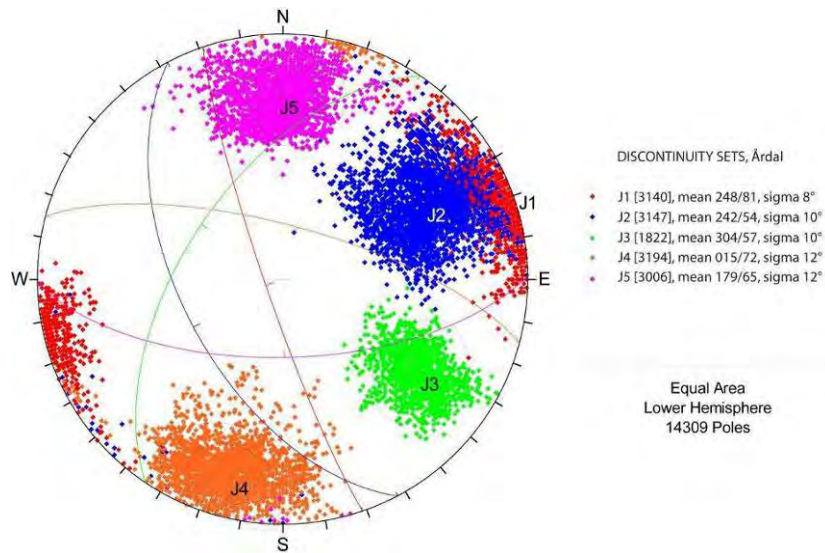


Figure 5: Stereoplot of the main surfaces of discontinuity for Årdal (Ramneberg). The contour lines represent the ± 1 -sigma and 2-sigma dispersion.

Some of these discontinuity surfaces are qualitatively displayed on Figure 6 and Figure 7.

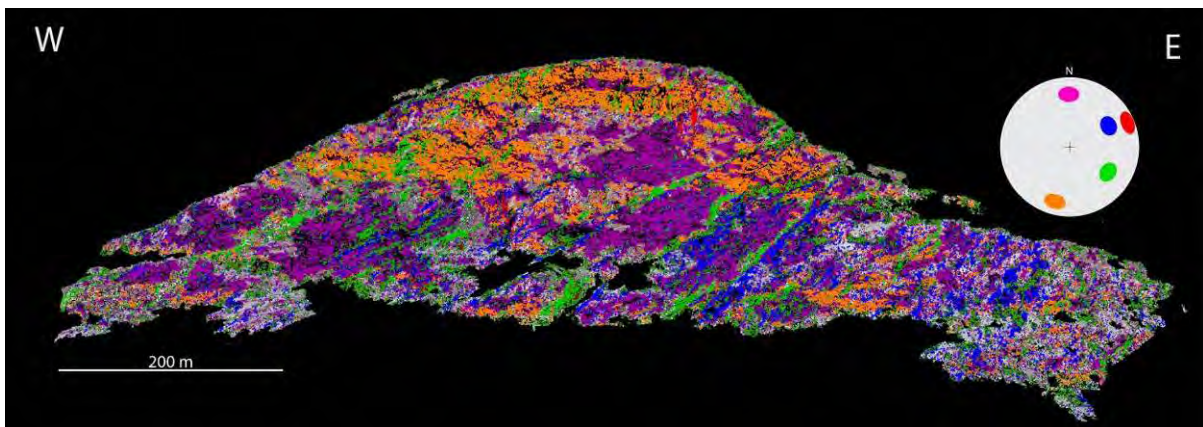


Figure 6: LiDAR point cloud classified according to the main discontinuities sets (red=J1, blue=J2, green=J3, orange=J4, pink=J5).



Figure 7: Panoramic view of the cliff with some examples of the main discontinuity sets (red=J1, blue=J2, green=J3, orange=J4, pink=J5).

The kinematic tests (Figure 8) provide a first hypothetical mechanism of slope movement. Using the value of J5 (179/65) as topographic surface of the slope, it is possible to identify a potential planar sliding on J2 and toppling with J4.

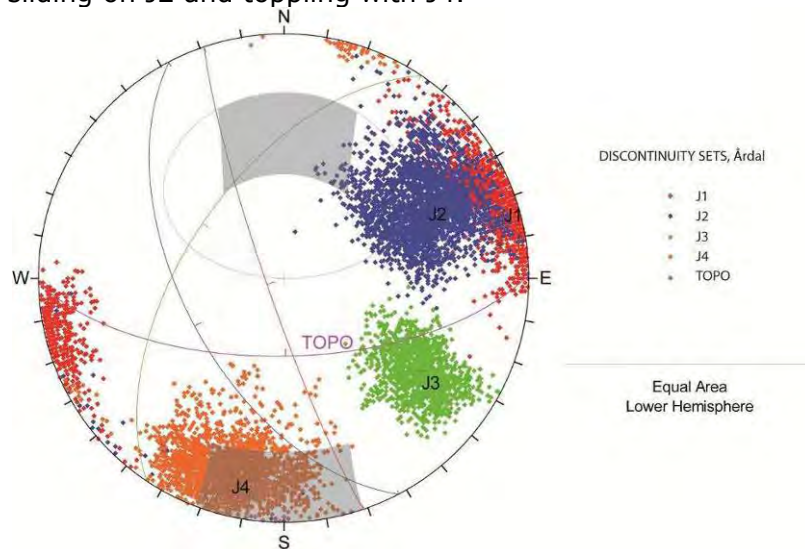


Figure 8: Kinematic test shows potential planar sliding with the J2 and toppling with J4 using TOPO (J5) as topographic surface of the cliff.

Where the topography becomes more steeper or vertical or even overhanging, it is possible to expect some wedge sliding with J1 & J5, J2 & J5 and J3 & J5. Some overhangs can be seen in the upper part of the cliff.

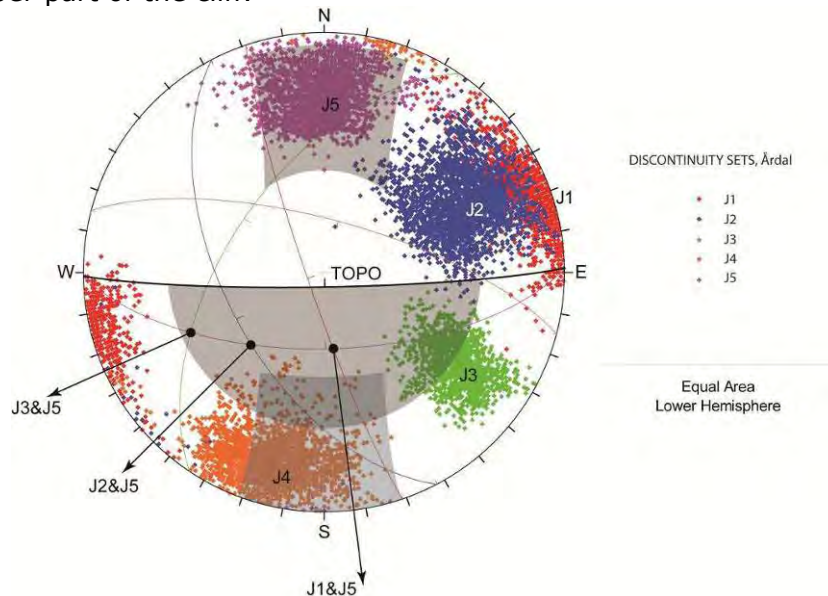


Figure 9: Using a steeper topographic surface of the cliff, new kinematic test shows potential planar sliding with the J5 and J2, toppling with J4 and some potential wedge sliding with J1, J2 and J3.

IV.1.2 Movement analysis

As this scan is the first that has been achieved in Øvre Årdal, it is not possible to perform any movement analysis. This campaign can be used in the future as reference for movement detection or to locate rockfall activities.

IV.1.3 Discussion

The cliff is structurally controlled by two sets of sub-vertical discontinuities (J4 and J5) controlling the general orientation of the cliff. Three faults are cutting the cliff, two of them (J2 and J3) dipping from North-East to South-West and a last one (J1) almost vertical from North to South. J4 discontinuity set, combined with J5 (TOPO), seems to be relevant for stability issues. It will be interesting to compare this point cloud with future scans to see the evolution of the cliff and the amount of rock material that has fallen in the lapse of time between the two campaigns of scans. As the site is relatively small and easy to access, future scanning of the entire cliff should not be a problem.

We must point out that houses are very close to the rock face. We can even see on *Norge / Bilder* that some of them were built in the foot of rockfall deposits! The dip angle from the top of the cliff to the nearest houses is over 40° (and 28° from the top of the scree), indicating that the houses are clearly in the propagation range of blocks. Then a great attention must be paid to any rockfall activities in the face.

IV.2 Volldal (Dalsuri)

The Volldal site (Figure 10) is a 1 kilometer-long, 400 meter-high cliff located 2.5 kilometers northeast of Ramneberg cliff, near the small village of Tronteigen. It is almost vertical and is overall facing South (pink and red colours on the Coltop 3D point cloud, Figure 12). A few houses are located at the foot of the cliff near a large scree slope. Many overhangs are threatening the settlements. This site was scanned for structural analysis.



Figure 10: Panorama of the Dalsuri cliff from the Tronteigen village (South). A large scree slope is visible at the foot of the cliff.

As for Årdal, no record of the location of the scanning points was available. Therefore their location were estimated (Figure 11) from the photographs taken by the LiDAR device on the field. Four scans were performed for this site.



Figure 11: Scanning points of 2009 TLS data (in blue). Location (points) and direction (arrows) of scanning points are estimated from field photographs. Orthophoto from Statens Kartverk (<http://kart.statkart.no>).

IV.2.1 Discontinuity analysis

The discontinuity analysis was made on the 2009 TLS point cloud of the entire cliff.

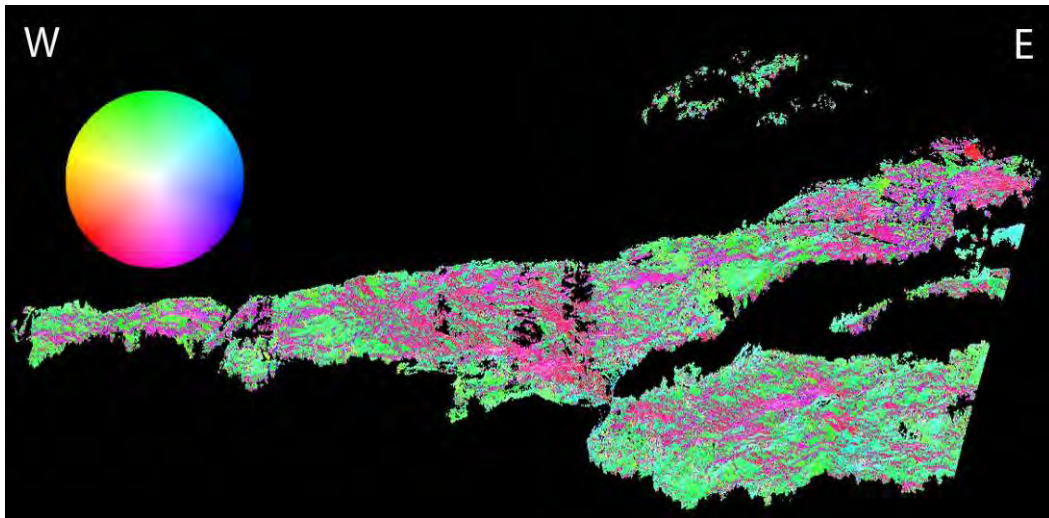


Figure 12: Example of a Coltop 3D view of the point cloud. The color of each point of the scan is given by the orientation (using the pole) of the surface at this point in the colour wheel. The view is from a point at the South of the cliff.

Four main sets of discontinuities were identified. They control the structure of the cliff. The stereoplot (Figure 13) shows the measurements and mean values of the sets:

Discontinuity set	Mean dips	Standard deviation
J1	327/15	10°
J2	071/89	9°
J3	005/76	12°
J4	309/73	15°

The J1 set could be the main foliation of the cliff, but this has to be confirmed by field analysis. Some of these discontinuity sets are displayed in Figure 14 and Figure 15. The red lines in Figure 15 are shallow dipping structures formed by the intersection of discontinuities J1 with the relief.

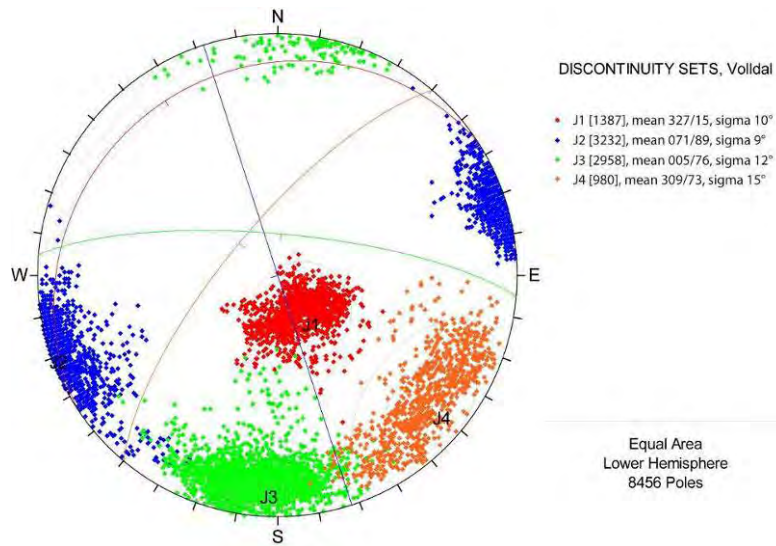


Figure 13: Stereoplots of the main surfaces of discontinuity for Volldal. The contour lines represent the ± 1 -sigma and ± 2 -sigma dispersion.

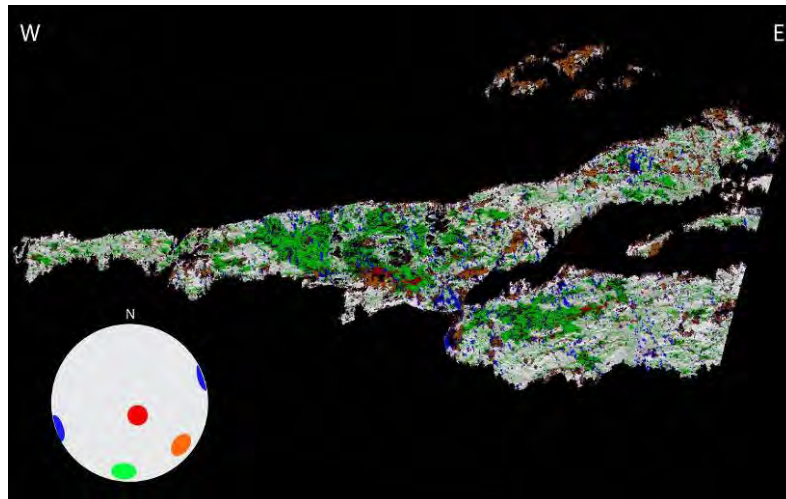


Figure 14: LiDAR point cloud classified according to the main discontinuity sets (red=J1, blue=J2, green=J3, orange=J4).



Figure 15: Panoramic view of the cliff with some examples of the main discontinuity sets (red=J1, blue=J2, green=J3, orange=J4).

The kinematic tests (Figure 16) provide a first hypothetical mechanism of failure in Dalsuri. According to the main topography of the cliff, it is possible to identify potential toppling with J3 and J4. On the whole cliff it is expected to have overhangs

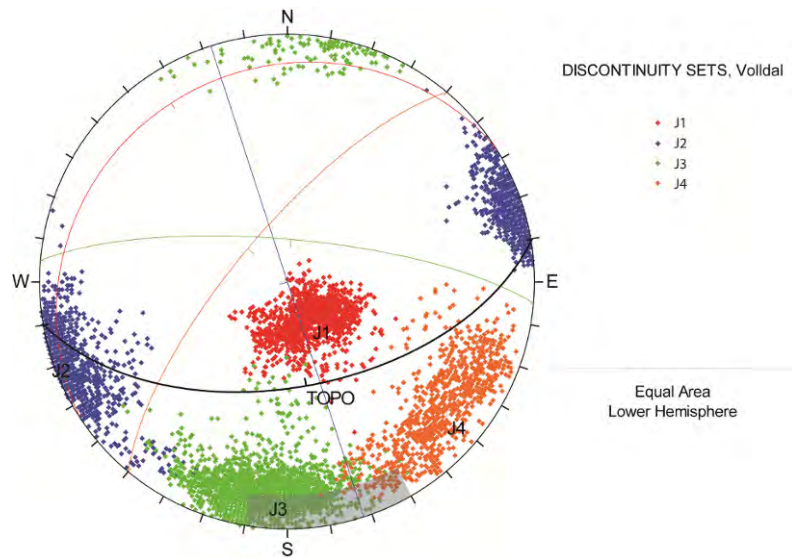


Figure 16: Kinematic test shows potential toppling with J3 and J4.

IV.2.2 Movement analysis

With only one year of scanning, it is not possible to perform any movement analysis. This dataset can be used as a reference for future analysis.

IV.2.3 Discussion

The main concern for this site is rock fall instability issues. Some houses are located at the foot of the cliff and close to the scree slope. Indications of past events are visible under the left side of the cliff (Figure 10). Toppling can strongly be expected by discontinuity sets J3 and J4. The J2 set is almost perpendicular to the general orientation of the cliff and can form blocks at some places with the J1 and J4 sets. As for Årdal, future scans of the entire cliff will not be difficult and can provide valuable information about the volume of rock falls threatening the settlements at the foot of the cliff. We must point out that houses are very close to the rock face, particularly on the western part. The dip angle from the top of the cliff to the nearest houses is 33° (and 27° from the top of the scree), indicating that the houses are clearly in the propagation range of blocks. Then a great attention must be paid to any rockfall activities in the face.

IV.3 Old Tunnel

This site is an escarpment located above the portal of an old tunnel of a road in Sogn of Fjordane. The panoramic view (Figure 17) is created from pictures taken from different points of view. This is the reason why the picture seems incorrect in its lower part. Nevertheless the interesting part, –the upper cliff–, is correctly represented and the major discontinuities are observable. This site was first scanned for structural analysis and for movement analysis in future. Figure 18 shows the estimated location and direction of the scanning point. Four scans were taken from locations close to each other.



Figure 17: Panorama of the cliff overhanging the old national road tunnel. Only the upper part of the cliff has been scanned.

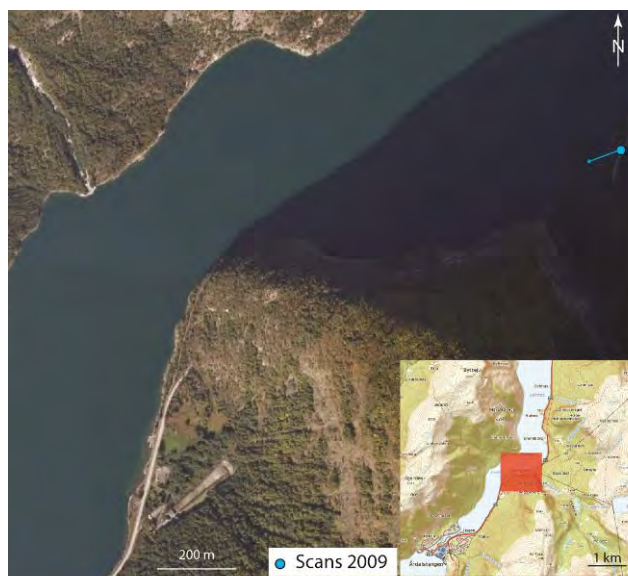


Figure 18: Scanning points of 2009 TLS data (in blue). Blue arrows indicate the direction of scanning. Orthophoto from Statens Kartverk (<http://kart.statkart.no>).

Discontinuity analysis

The discontinuity analysis was made on the 2009 TLS point cloud of the top of the cliff, which shows the most remarkable facets. As shown in Figure 19, most of the facets have orientations from NW to SE (colour violet to green). At many places the rock is fractured and many overhangs are visible, evidences of previous detachments.

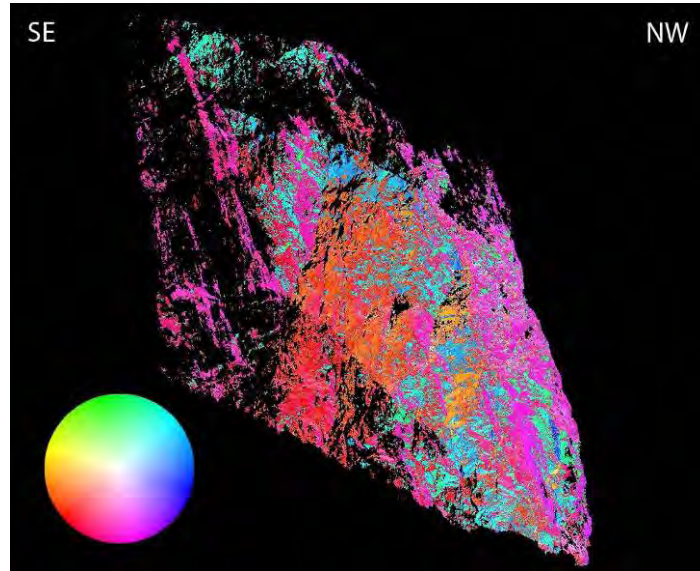


Figure 19: Example of a Coltop 3D view of the point cloud. The colour of each point of the scan is given by the orientation (using the pole) of the surface at this point in the colour wheel.

Four main orientations of discontinuities were identified on this cliff. Measurements of their orientations were obtained from the LiDAR points and plotted in a stereoplot (Figure 20):

Discontinuity set	Mean dips	Standard deviation
J1	280/71	12°
J2	058/84	8°
J3	350/70	13°
J4	190/80	7°

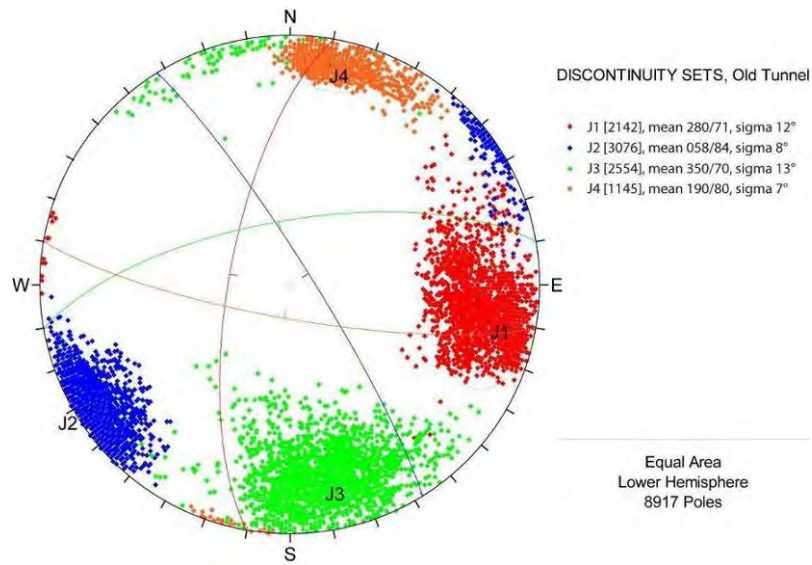


Figure 20: Stereonet of the main surfaces of discontinuity for the old tunnel cliff. The contour lines represent the ± 1 -sigma and ± 2 -sigma dispersion.

The main foliation could not be determined from scan for this site. Some of the discontinuity surfaces are displayed in Figure 21 and Figure 22.

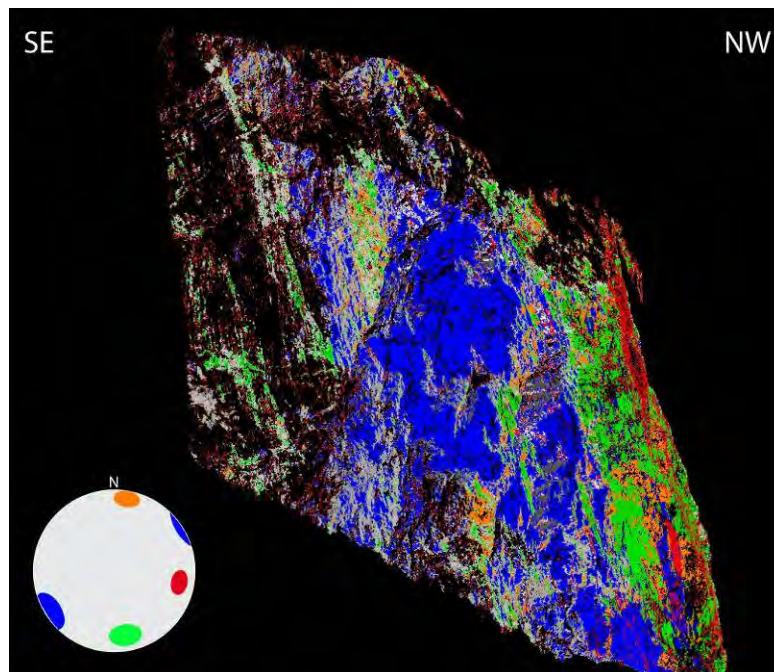


Figure 21: LiDAR point cloud classified according to the main discontinuity sets (red=J1, blue=J2, green=J3, orange=J4).

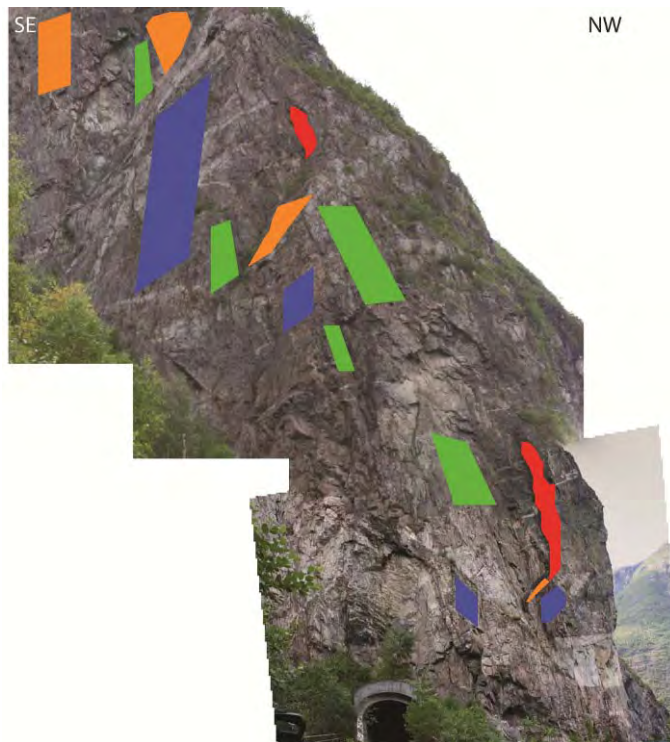


Figure 22: View of the old tunnel cliff with some examples of the 4 main discontinuity sets (red=J1, blue=J2, green=J3, orange=J4).

Kinematic tests are provided on the two different faces of the instability. The first kinematic test is for the face above the portal called "Tunnel face". It shows potential planar sliding on J2 and toppling on J1.

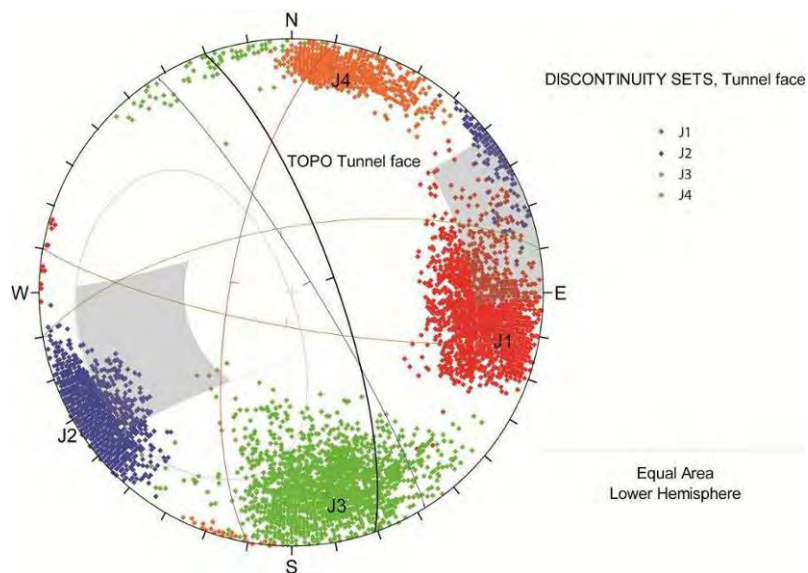


Figure 23: Kinematic test for the tunnel face orientation of topography. It shows potential planar sliding with J2 and also toppling mainly with J1.

The second kinematic test is for the face overhanging the fjord called "Fjord face". It shows some potential wedge sliding with $J1 \wedge J3$, $J1 \wedge J2$ and $J2 \wedge J3$, and also a potential planar sliding on J3 and toppling on J4.

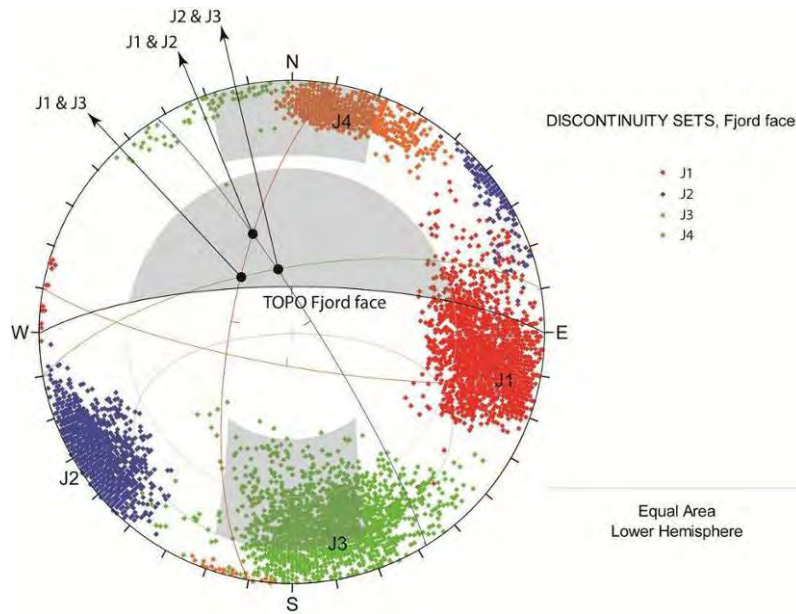


Figure 24: Kinematic test for the fjord face orientation of topography. It shows potential planar sliding with J3, toppling with J4 and wedge in J1 & J3, J1 & J2 and J2 & J3.

IV.3.1 Movement analysis

With only one year of scanning, it is not possible to perform any movement analysis. This dataset can be used as a reference for future analysis.

IV.3.2 Discussion

The orientation of the cliff is controlled by three sets of discontinuities (J2, J3 and J4). Most of the blocks are formed by these sets. J1 is an East-facing discontinuity set which can also form blocks with J2 and J3.

Due to the historical events of rock falls on this road, another campaign of scans can bring further information, about the rockfall hazard (intensity and frequency) for users of the road depending on the priority for this site. It will be interesting in the future to scan from a boat to have the face overhanging the fjord. Those scans could help to determine if there is some large rockslide hazard that could provoke tsunamis.

IV.4 Tussen

Tussen is located around 4 kilometers north of Fortun, at the end of Lustrafjorden. At the top of the slope a large plateau (300 m wide and 400 m long) is marked by numerous cracks, which can be large and deep. An example of these back-cracks can be seen at the rear of Figure 25. The scanned rock block is in fact in a higher position than the plateau. Figure 26 is a panorama from the base of the cliff, assembled from pictures taken by the LiDAR device.



Figure 25: Panorama of the Tussen site in 2009 (with the back-cracks) from the top of the cliff (points of scanning 1 and 2 on Figure 27).



Figure 26: Panorama of the Tussen site from the base of the cliff (point of scanning 3, on Figure 27)

Tussen area was scanned the 19th of August 2009 by M. Böhme of NGU (six scans). The first campaign of scans from 2008 (five scans) was scanned by NGU. The location of the two sets of data is mapped in Figure 27. This site was scanned for structural analysis and for movement analysis.

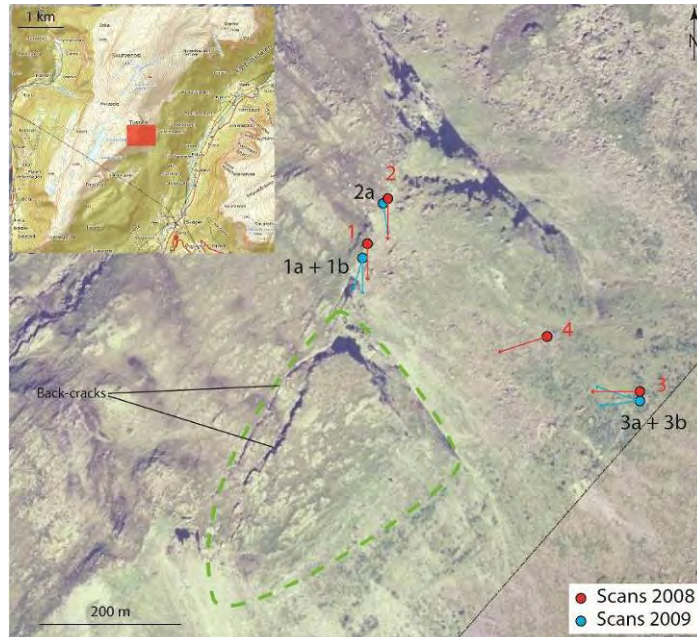


Figure 27: Scanning points of 2008 TLS data (red) and 2009 TLS data (blue). For each set of data, directions of scanning are indicated (arrows). The unstable part is indicated by the green dashed line. Orthophoto from Statens Kartverk (<http://kart.statkart.no>).

IV.4.1 Discontinuity analysis

The discontinuity analysis was made on the 2009 TLS point cloud (Figure 28) on the cliff and the back-cracks directly at the rear of the rock block.

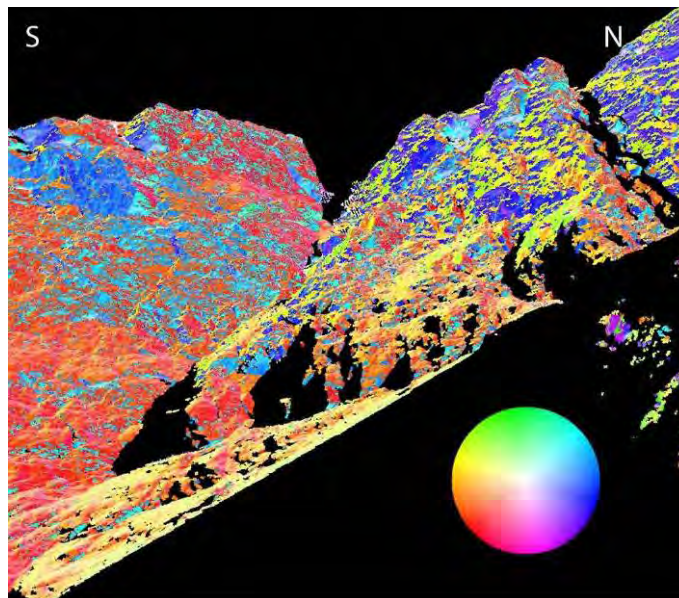


Figure 28: Example of a Coltop 3D view of the point cloud. The colour of each point of the scan is given by the orientation (using the pole) of the surface at this point in the colour wheel. This figure is a view corresponding to the panorama in Figure 26 from point of scanning 4.

Five main discontinuity sets were identified on the TLS data. The measurements were plotted in a stereoplot (Figure 29) using Dips[®]:

Discontinuity set	Mean dips	Standard deviation
S1	317/12	9°
J2	248/85	9°
J3	028/90	7°
J4	129/63	12°
J5	298/78	13°

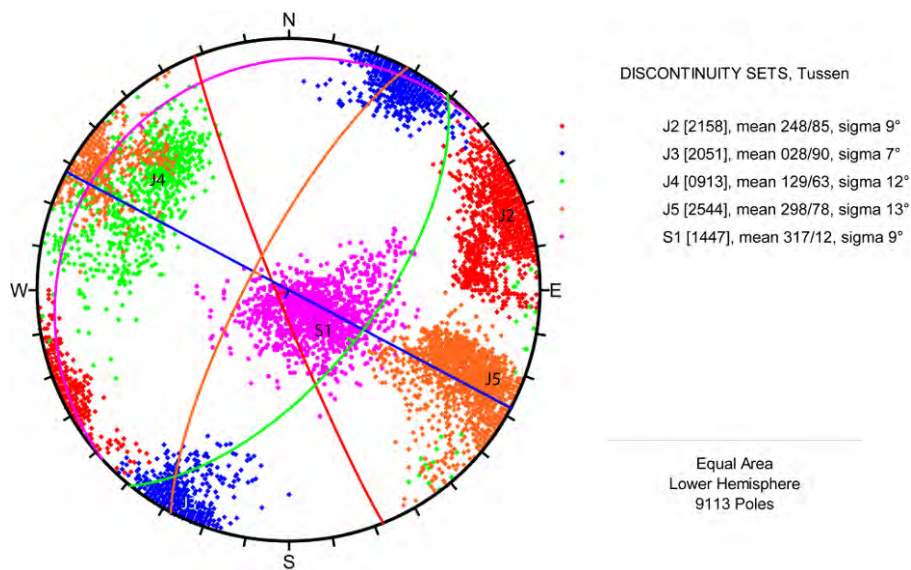


Figure 29: Stereoplot of the main surfaces of discontinuity for Tussen. The contour lines represent the ± 1 -sigma and 2-sigma dispersion.

The first discontinuity set is labelled S1 because it corresponds probably to the main foliation. These observations must be confirmed by field measurements. Some of these discontinuity surfaces are qualitatively displayed on the Figure 30 (point cloud) and Figure 31 and Figure 32 (pictures).

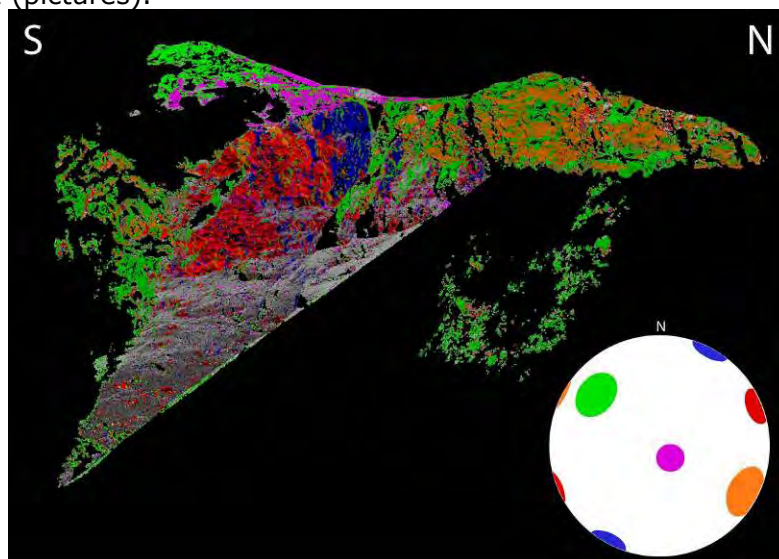


Figure 30: LiDAR point cloud classified according to the main discontinuity sets (pink=S1, red=J2, blue=J3, green=J4, orange=J5). This figure is a view corresponding to the panorama in Figure 26 from point of scanning 4.



Figure 31: View from the top of the cliff with main discontinuity sets (pink=S1, red=J2, blue=J3, green=J4). The slide plane in green corresponds to the discontinuity set J4.



Figure 32: View from the base of the cliff with some examples of the main discontinuity sets (pink=S1, red=J2, blue=J3, green=J4, orange=J5).

Kinematics tests (Figure 33) were done mainly as a test of J4 being a potential sliding plane. The kinematics tests show also that the possibility of a planar sliding on J4 can not be excluded. Finally, kinematic tests show a potential toppling on J5.

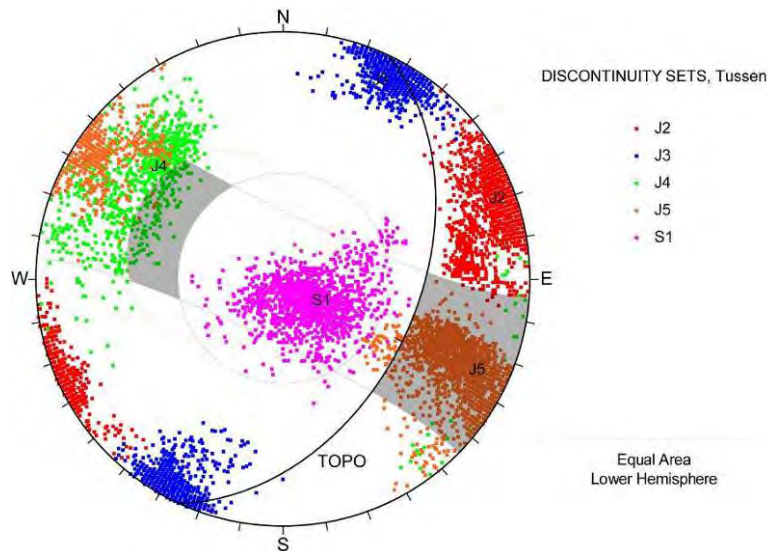


Figure 33: Kinematic tests on Tussen show potential toppling mechanism with J5 and a planar sliding on J4.

Measurements on the two main back-cracks, using Polyworks[®], show that the mean spacing of the first crack is 8 meters, and the second is 3-4 meters. The rock block in front of these cracks is also 8 meters higher than the lowered block. The Figure 34 schematizes these observations.

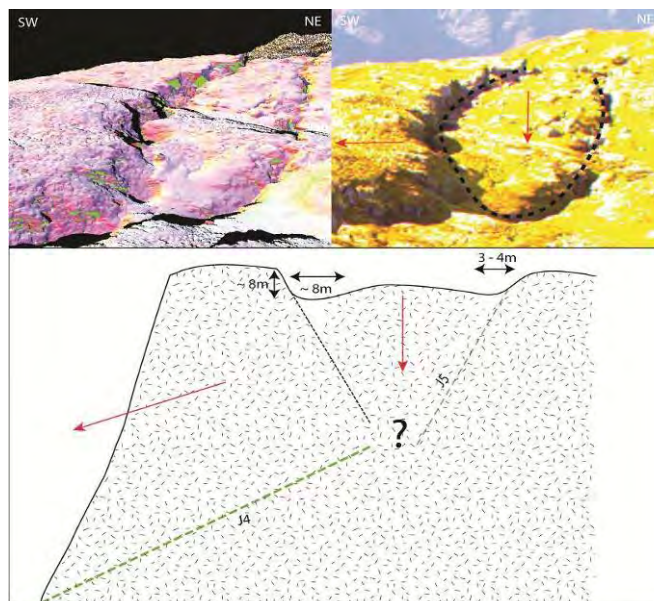


Figure 34: Schema of the back-cracks with measurements of the spacing between the sides of the cracks.

IV.4.2 Movement analysis

Point clouds from scanning campaigns 2008 and 2009 are used to detect potential movements. First all the scans of 2008 were merged in one set and then all the scans of 2009 in another set. But the internal alignment errors of these two sets are of the same order of magnitude than a potential displacement. Then when comparing the full 2008 with the full 2009 point clouds, alignment errors appears as constant displacement (Figure 35) parallel to the direction of scanning (axis X). Another possible cause to explain these

horizontal stripes is that the air density changed during one of the scans because of temperature variation close to the cliff.

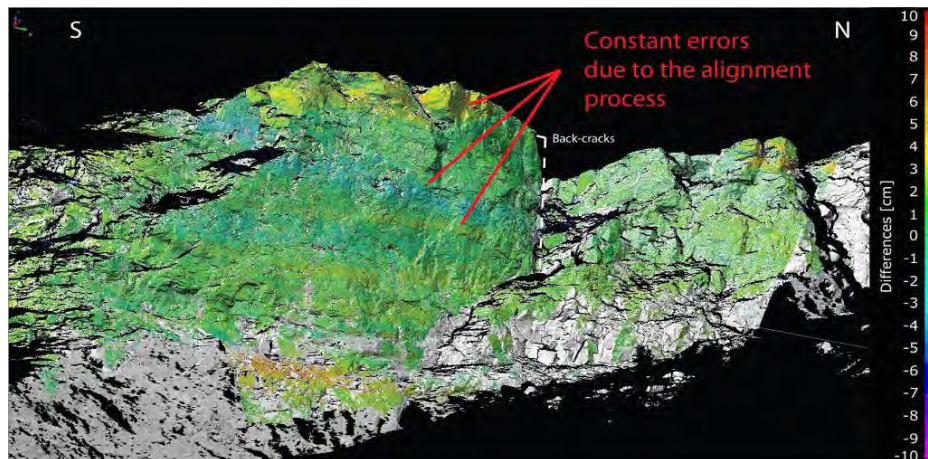


Figure 35: Example of the errors in the comparison between two point clouds each formed by many scans.

Then to highlight true displacements a comparison between one scan of 2008 and the corresponding scan of 2009 was done. As shown in Figure 36, no significant displacement was detected in the Tussen cliff between 2008 and 2009. The method of shortest distance from reference (2008) to new data (2009) was used. Nevertheless a closer attention is needed to this area in the future.



Figure 36: Piece-wise comparison between scans tussen1 (2008) and tu1a, tu1a2, tu1b (2009). No significant movement appears.

IV.4.3 Discussion

The results of movement analysis can be explained two ways. First, no effective displacement occurred between 2008 and 2009. This hypothesis is reasonable as no big visible change can be seen between the two sets of photographs taken by the LIDAR device. The second possible explanation is that there is lack of stable part in the scans used. We cannot exclude that the entire block is slightly moving. This hypothesis has to be verified by scanning again the cliff but this time, if possible, with a larger fixed area that could be used as reference.

IV.5 Vidalen

This site (Figure 37) is located in the eastern shore of the lake Viddallsvatnet. It is a large rockslide (around 700 m wide) with vertical cliffs and a loose block in the center. This site was scanned mainly for structural analysis.



Figure 37: Panorama of the Vidalen site from the scanning point.



Figure 38: Scanning point of 2008 TLS data (yellow). Directions of scanning are indicated by the arrows. Green dashed line shows the limit of the instability. Orthophoto from Statens Kartverk (<http://kart.statkart.no>).

IV.5.1 Discontinuity analysis

As the central part of the site is made of loose blocks the discontinuity analysis was achieved on the backscarps. The 2008 point cloud (Figure 39) was used for this step.

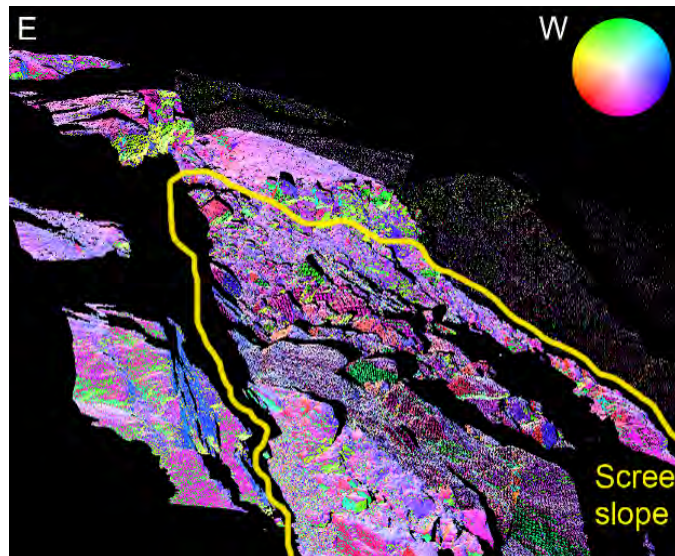


Figure 39: Example of a Coltop 3D view of the point cloud. The colour of each point of the scan is given by the orientation (using the pole) of the surface at this point in the colour wheel.

Six main discontinuity sets were identified on the TLS data. The measurements were plotted in a stereoplot (Figure 39), using Dips[®]:

Discontinuity set	Mean dips	Standard deviation
S1	310/43	7°
J1	167/72	7°
J2	274/75	9°
J3	108/40	9°
J4	015/65	11°
J5	226/82	7°

The yellow discontinuity seems to be the main foliation. It can be seen on the blocks at the rear of the site and on the rock at the front of the view in Figure 41 and Figure 42. In the central part of the slope, similar orientations are visible but they are not to be considered as the blocks are certainly tilted.

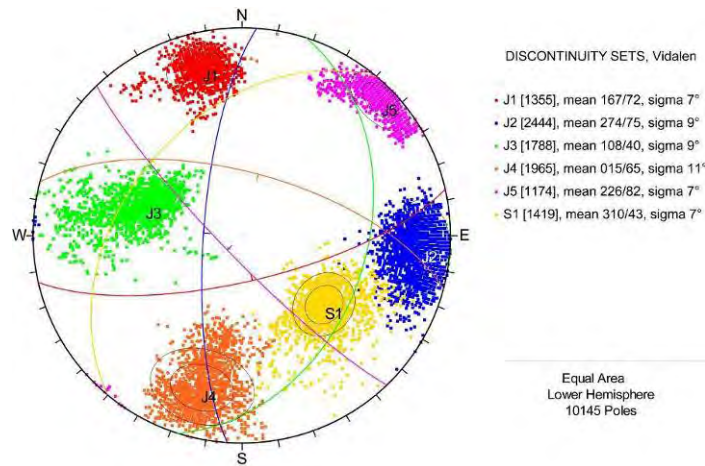


Figure 40: Stereonet of the main surfaces of discontinuity for Vidalen. The contour lines represent the ± 1 -sigma and 2-sigma dispersion.

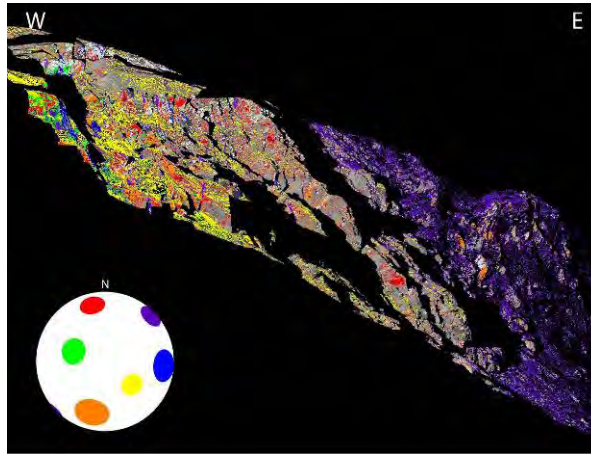


Figure 41: LIDAR point cloud classified according to the main discontinuity sets (yellow=S1, red=J1, blue=J2, green=J3, orange=J4, pink=J5).



Figure 42: View from the scanning point with the main discontinuity sets (yellow=S1, red=J1, blue=J2, green=J3, orange=J4, pink=J5).

Kinematics tests were done with the measurements on the 2008 TLS point cloud. Results show a potential planar sliding on S1 or toppling with J3.

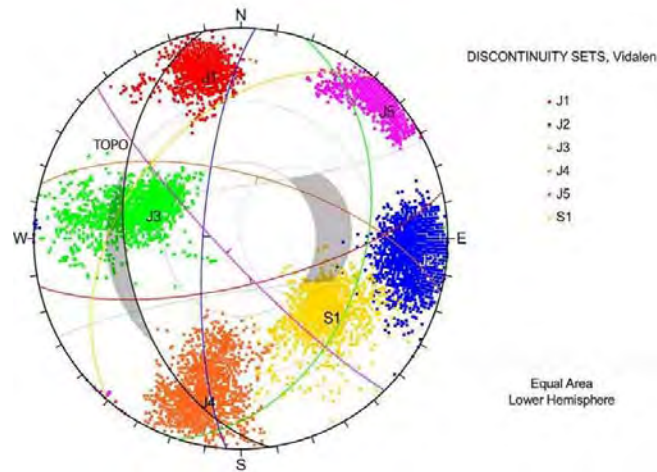


Figure 43: Kinematic tests on Vidalen show no real potential mechanism of slope movement, except a slight potential planar sliding with S1 and a potential wedge with J1 & S1.

IV.5.2 Movement analysis

With only one year of scanning, it is not possible to make any movement analysis. The 2008 TLS dataset may be used as a reference for the next campaigns.

IV.5.3 Discussion

To have an exhaustive analysis of this site, we recommend to scan again the backscarp and, if possible, from another point of view. This could allow a better identification of the processes active in Vidalen. The loose blocks visible in Figure 37 do not represent a significant threatening as there is no infrastructure right below, but if the entire rockslide falls into the lake, huge waves may be generated in the reservoir. The results obtained for the discontinuities orientations should be used with other topographical and field observations to better constrain the volume of the block that could slide or topple.

IV.6 Vik

Vik instability is located above Ovredal. At the top of the slope of the South face of the mountain (Figure 44 and Figure 45). This site was scanned mainly for structural analysis.



Figure 44: Panorama of Vik instability area from the south.

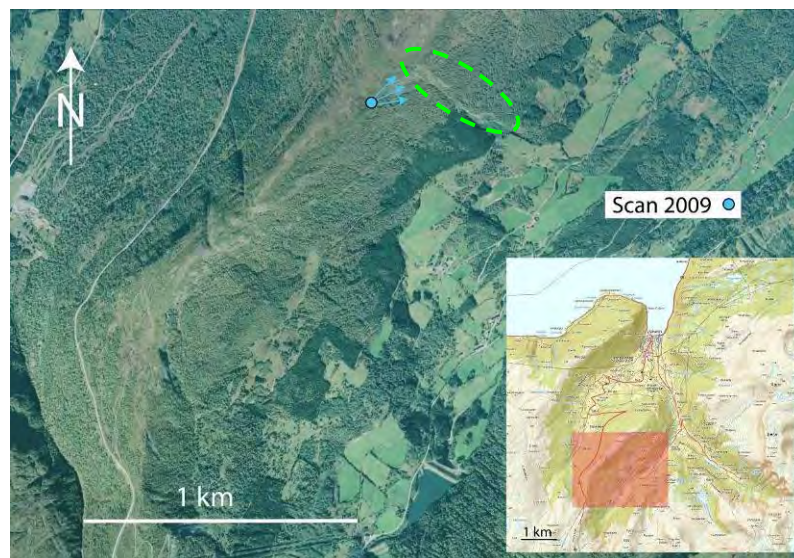


Figure 45: Scanning points of 2009 TLS data (blue). For each set of data, directions of scanning are indicated (arrows). Dashed green line indicates the instability Orthophoto from Statens Kartverk (<http://kart.statkart.no>).

IV.6.1 Discontinuity analysis

Scans were acquired in 2009 from a long distance, in an area with a high vegetation density. Then only measurements on a part of the cliff were possible. Nevertheless some discontinuity sets were identified.

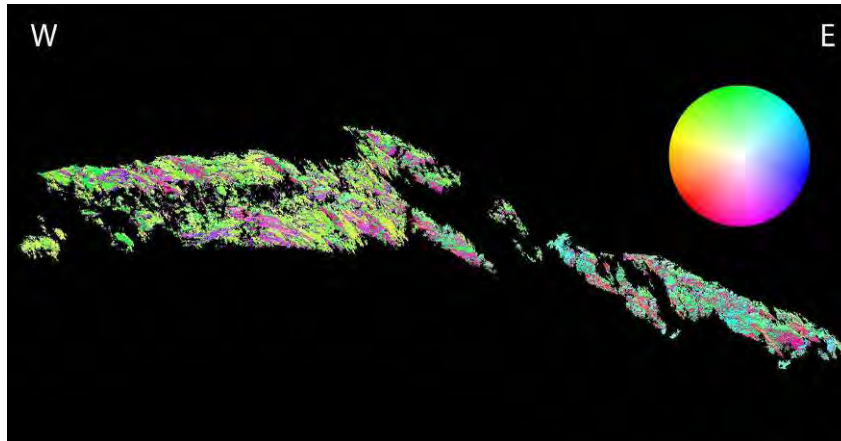


Figure 46: Example of a Coltop 3D view of the point cloud. The colour of each point of the scan is given by the orientation (using the pole) of the surface at this point in the colour wheel.

Four main discontinuity sets were identified on the TLS data. The measurements were plotted in a stereoplot (Figure 47), using Dips:

Discontinuity set	Mean dips	Standard deviation
J1	028/25	12°
J2	288/70	7°
J3	015/88	9°
J4	130/60	10°

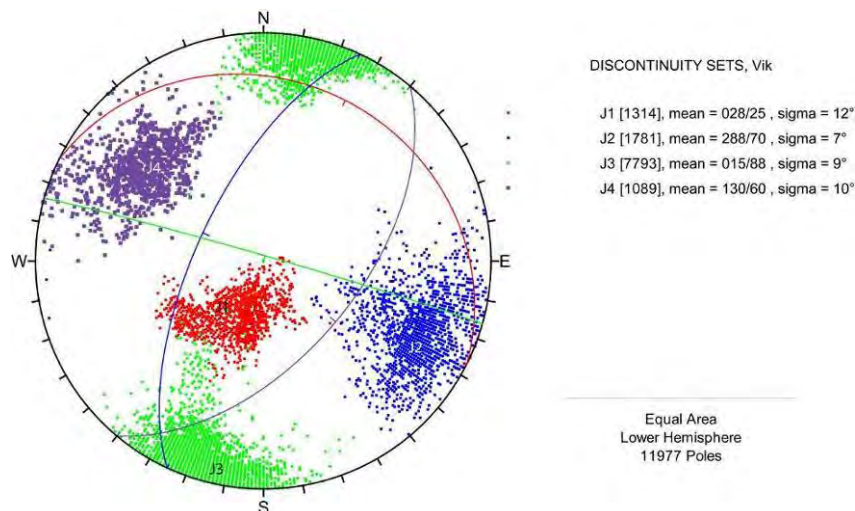


Figure 47: Stereoplot of the main surfaces of discontinuity for Vik. The contour lines represent the ± 1 -sigma and ± 2 -sigma dispersion.

J3 seems to be a potential toppling surface. These observations must be confirmed by field surveys.

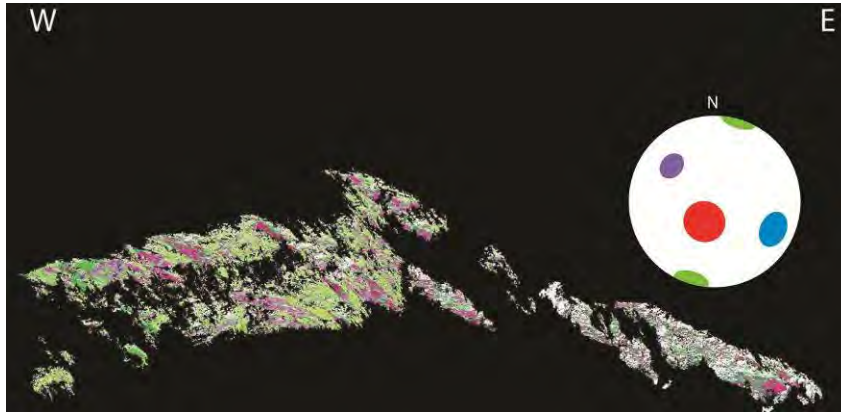


Figure 48: LIDAR point cloud classified according to the main discontinuity sets (green=J1, pink=J2, blue=J3, red=J4).

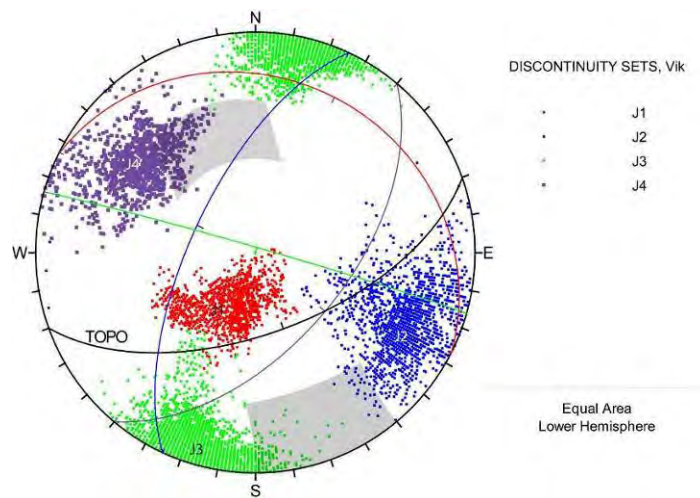


Figure 49: Kinematic tests on Vik instability shows slight potential planar sliding on J4 and a potential toppling on J3.

Kinematic tests are provided for the upper part of Vik. It shows some potential planar sliding on J4 and slight potential toppling on J3 with some local variation of the topography.

IV.6.2 Movement analysis

With only one year of scanning, it is not possible to perform any movement analysis. This dataset can be used as a reference for future analysis.

IV.6.3 Discussion

For future scans will be interesting if possible to scan more of the lower cliff to complete kinematic test. Presently only the top scarp was analyzed and that should be extended to the lower part (by laser scanning or fieldwork). At this stage the main mechanism of instability seems to be a planar sliding on J4.

IV.7 Flåm

This part was already delivered beginning of 2010, as a master student at NGU was working on this site. The goal was to provide to the student discontinuities measurements in order to proceed to kinematics tests and stability analysis.

Two sites at Flåm were scanned with the terrestrial LiDAR, so-called hereafter "upper site" and "lower site". Scanner positions and parameters are recorded in M. Böhme's fieldbook (NGU).

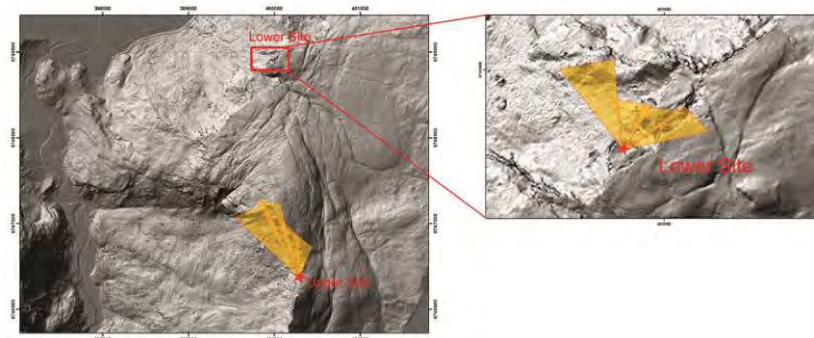


Figure 50: Upper and lower scanned sites and LiDAR positions (stars) at Flåm.



Figure 51: Panoramic view of the upper site from the scanning point.



Figure 52: Panoramic view of the lower site from the scanning point.

IV.7.1 Discontinuity analysis

Upper site

The upper cliff at Flåm is a 250 metres high sub-vertical wall, oriented NW-SE (=dipping ~SW). The representation with the colour coding of Coltop3D (Figure 53) shows clearly the predominance of facets dipping towards S to W (from blue to purple).

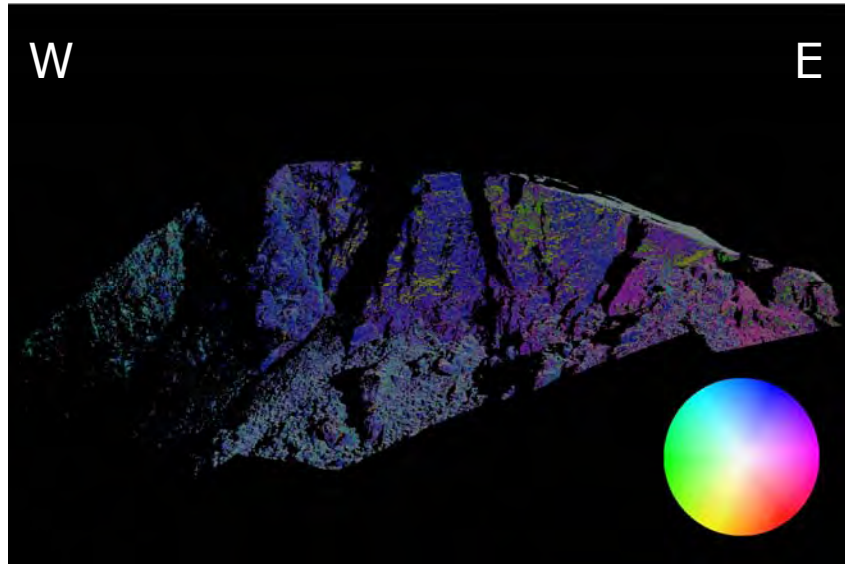


Figure 53: Example of a Coltop3D view of the cloud of points. The colour of each point of the scan is given by the orientation (using the pole) of the surface at this point in the colour wheel.

Three main sets of discontinuities were identified and measured on the terrestrial LiDAR data. The measurements were then imported into Dips to estimate the mean orientations and standard deviations. These measurements are presented in Figure 53.

Discontinuity set	Mean dips	Standard deviation
J1	243/35	11°
J2	205/72	10°
J3	243/89	9°

The first set of discontinuities is indicated as S1 because it corresponds probably to the main foliation. Nevertheless, this statement should be confirmed by field observations, at the base of the cliff if possible.

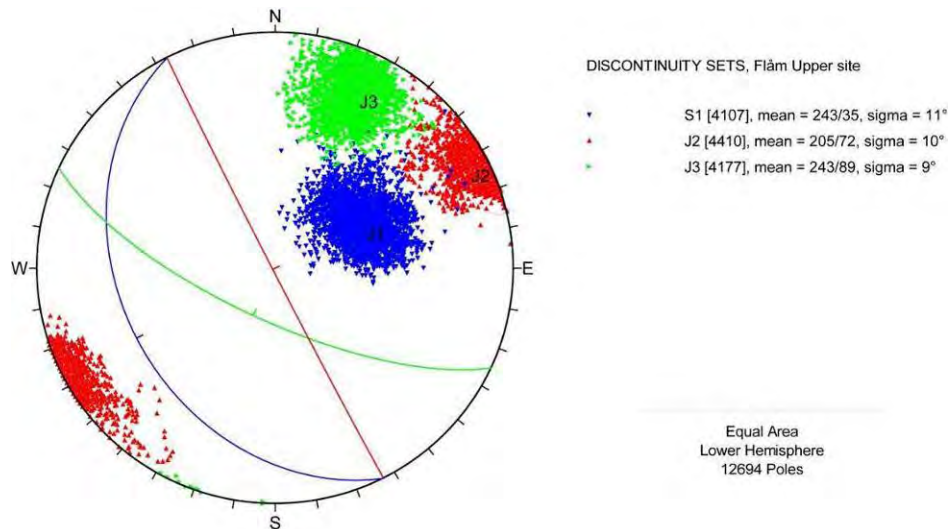


Figure 54: Stereoplot of the main surfaces of discontinuity for the upper site of Flâm. The circles represent the ± 1 -sigma and ± 2 -sigma dispersion.

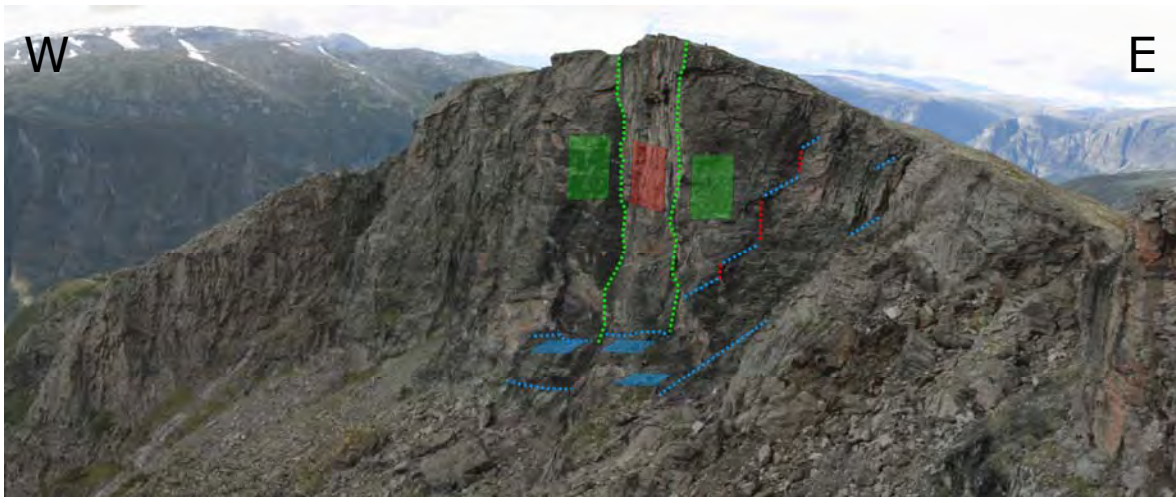


Figure 55: view of the upper site with some examples of the 3 main discontinuity sets (blue=S1, red=J2, green=J3).

Some of these discontinuity surfaces are qualitatively displayed on the picture of Figure 54. When we classified all the points of the scan according to the 3 sets of discontinuities (using mean ± 2 sigma), it appears that the rock face is almost entirely composed of facets belonging to one of this discontinuity set (Figure 55).

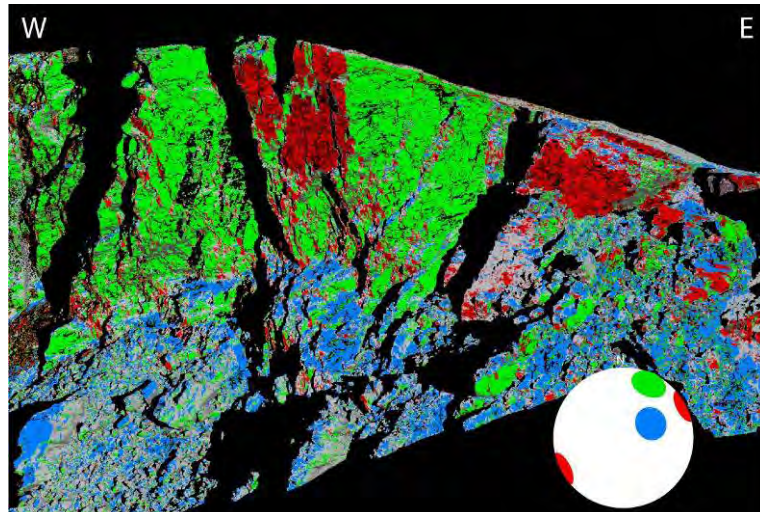


Figure 56: LiDAR points cloud classified according to the main sets of discontinuities (blue=S1, red=J2, green=J3, gray=other).

In conclusion, the cliff is structurally controlled by three sets of discontinuities, two sub-vertical (J2 and J3) controlling the general orientation of the cliff and one with a shallower dip angle (S1). S1, dipping W to NW, is possibly the foliation. It has to be noticed that large and persistent surfaces of S1 type are present at the base of the cliff and that its mean dip angle is 35° , which is steep enough to act as a sliding plane. S1 appears to play a key role for the stability at the foot of the wall, J2 and J3 forming the other sides of the blocks.

Lower site

The structural analysis of the lower site of Flåm is much less obvious than for the upper site. Here the rock is strongly deformed and crashe d, some fold hinges are visible and surfaces are undulating. The hummocky aspect of the surface is visible in the Figure 56. In addition, the point of view on the moving block is limited to its upper part and a small part of the back scarp.

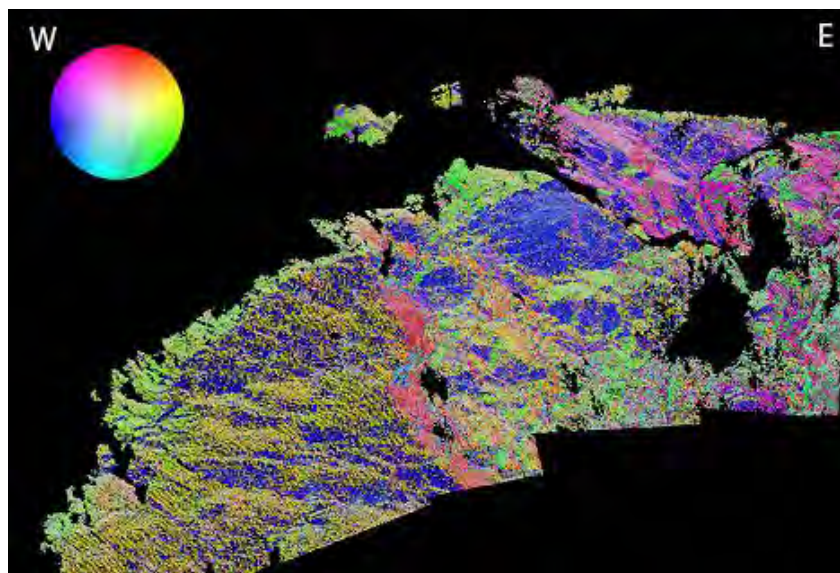


Figure 57: Example of a Coltop3D view of the cloud of points for the lower site.

Nevertheless, 5 main orientations of discontinuities can be recognized on this outcrop. Measurements of their orientations were made from the LiDAR points and plotted in a stereoplot (Figure 57):

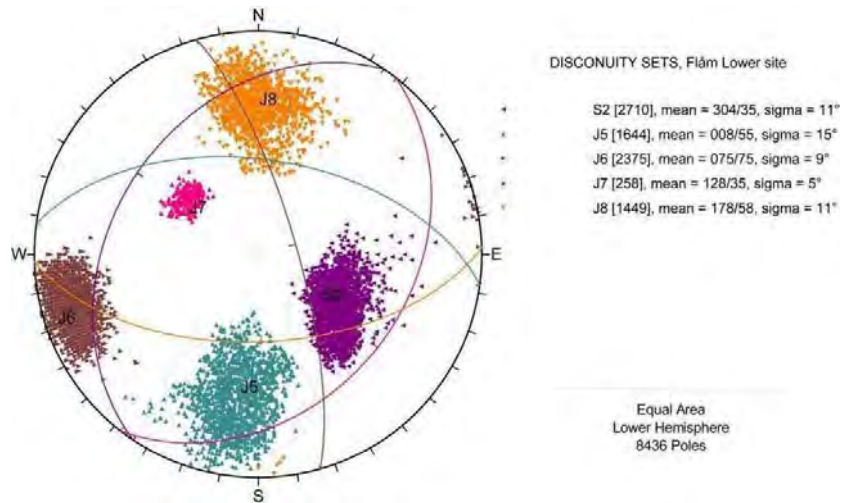


Figure 58: Stereoplot of the main surfaces of discontinuity for the lower site of Flâm. The circles represent the ± 1 -sigma and ± 2 -sigma dispersion.

Five main discontinuity sets were identified on the TLS data:

Discontinuity set	Mean dips	Standard deviation
S2	304/35	11°
J5	008/55	15°
J6	075/75	9°
J7	128/33	5°
J8	178/58	11°

The discontinuity S2, gently dipping NW may represent the main orientation of the foliation. But we cannot exclude that folds affect the foliation and that its orientation is locally very different. As shown on Figures 58 and 59, the SW facing part of the block is mostly controlled by a combination of S2 and J6 discontinuities. The rear of the block and the back scarp seems to be cut according the orientations of J7 and J8.

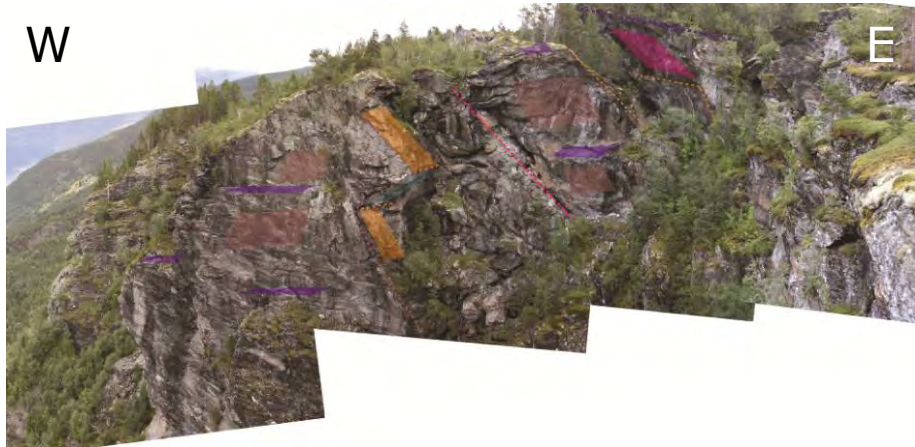


Figure 59: View of the lower site with some examples of the 5 main discontinuity sets (violet=S2, green=J5, brown=J6, pink=J7, orange=J8).

The LiDAR analysis of the lower site provides measurements of discontinuities on a small area only. It is difficult to assess how these measurements are representative of larger structures and is not only local features perhaps made during the block displacement and crushing. We try in the next chapter to match these measurements with bigger features observed on the airborne DEM.

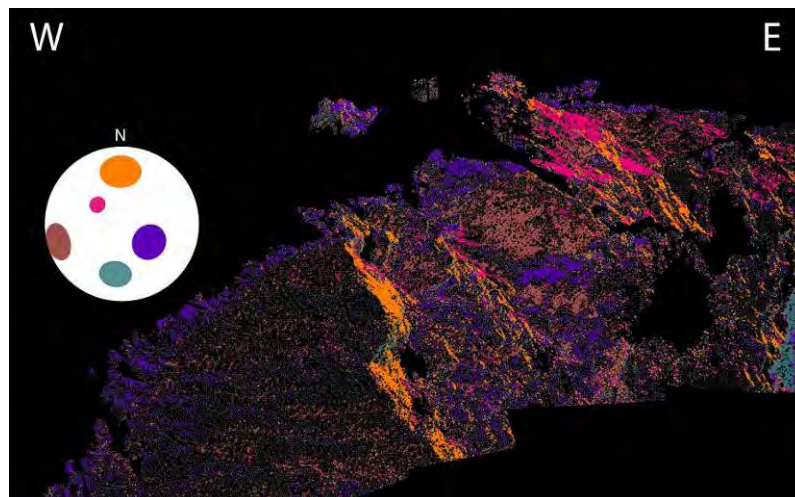


Figure 60: top) LiDAR points cloud classified according to the main sets of discontinuities; bottom) simplified representation of the main sets of discontinuities on a panoramic picture (deformed).

It is important to point that the information collected here are only about the top of the moving block and of the back scarp. Information about the base of the block and the presence of a potential basal surface are missing. It is then difficult to propose any mechanism of instability with only these data.

IV.7.2 Movement analysis

Movement analyses are made only on the lower site because in the upper site the scans do not overlap. A rotational movement of the large block or local area of this block can be expected. But it is difficult to find real movement because of the small stable part of alignment. Nevertheless some small rockfalls were observed.

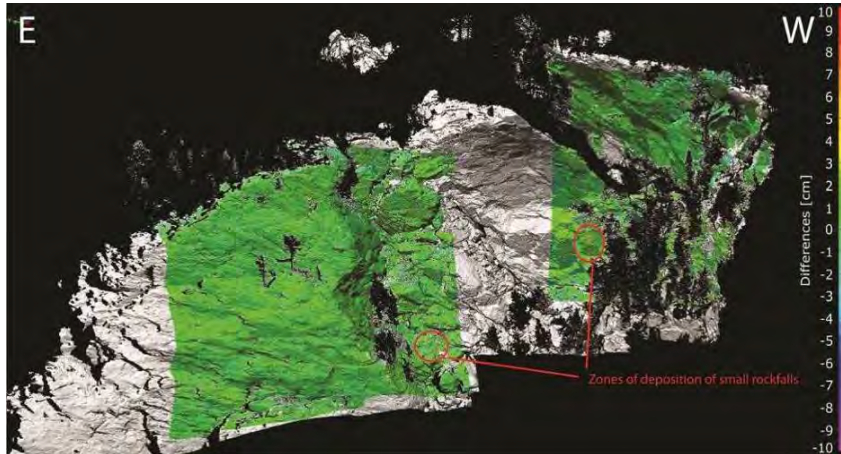


Figure 61: Movement comparison between 2008 and 2009 on the block of the lower site. Because of small stable part for alignment, it is difficult to define clear movement. The only differences between the two scans are created by small rockfalls.

IV.7.3 Integration with airborne data

A rapid inspection of the airborne DEM was done in order to pick up some cliffs orientations and draw some planar traces. This is not a geological interpretation (which will be done by the master student), but only some extra data. In particular, we have focused the measurements on locations impossible to reach.

IV.7.4 Punctual dip measurements on the DEM

Where terrestrial LiDAR scans are available, the sets of discontinuities defined previously are used (S1, J2 and J3). In other locations, the point measurements were collected under the generic name "cliff". At each point, the coordinates xyz, dip direction and dip angle are provided. All the points are saved in shapefiles.

It is relatively easy to link the features on the terrestrial scans to those observed on the airborne DEM for the upper site. Small structures are related to big ones. But for the lower site, a lot of the features observed in the terrestrial scans seem to have only local extensions.

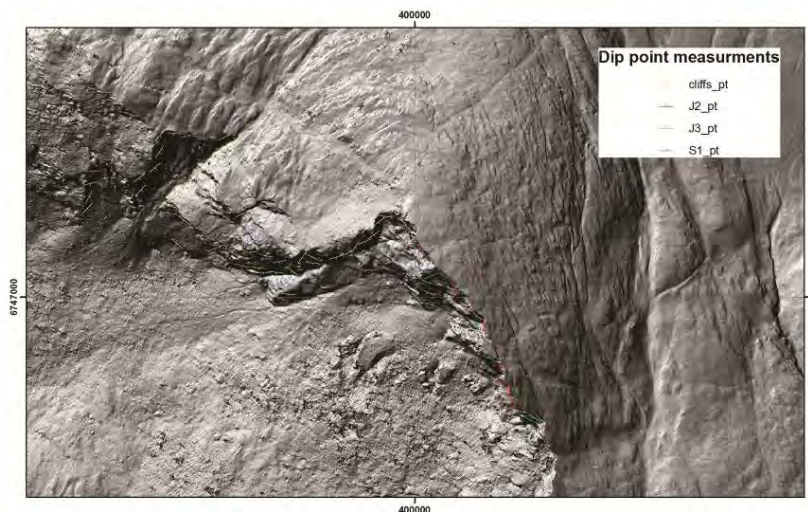


Figure 62: Examples of punctual dip orientation/angle measurements made directly on the 1 m airborne DEM.

IV.7.5 Planar traces

The planar traces are the intersections of geometrical planes with the topography. We have fit as well as possible planes to lineaments of the airborne DEM. Of course these planar traces do not follow exactly the lineaments which are frequently not along planar surfaces or composed of several sets of discontinuities. Nevertheless these planar traces can help to link the geometry of the main cracks and lineaments to field observations or terrestrial scans. The traces are provided in a shapefile3D, with the dip direction and angle of the best fit plane as arguments. The traces have not been interpreted geologically and some of them may not be related to the instability but other surface features.

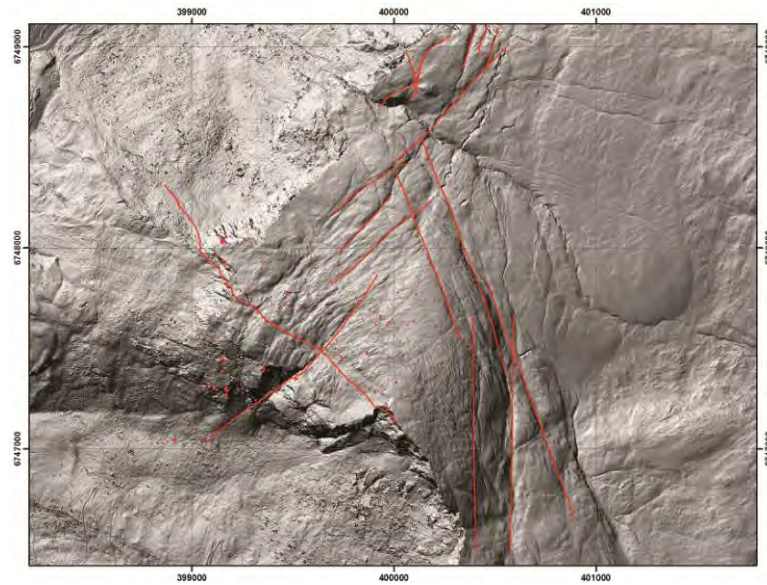


Figure 63: Planar traces along lineaments observed on the airborne DEM. **Erreur ! Source du renvoi introuvable.** In order to illustrate the intersection of a plane with the topography, the shows the intersection pattern of a plane of orientation 300/35 (~S1) passing by the crack on the top.

The red area is the part of the relief above the plane and the blue area the part under the intersection plane. This shows simply that in this area S1 can geometrically daylight at the base of the cliff.

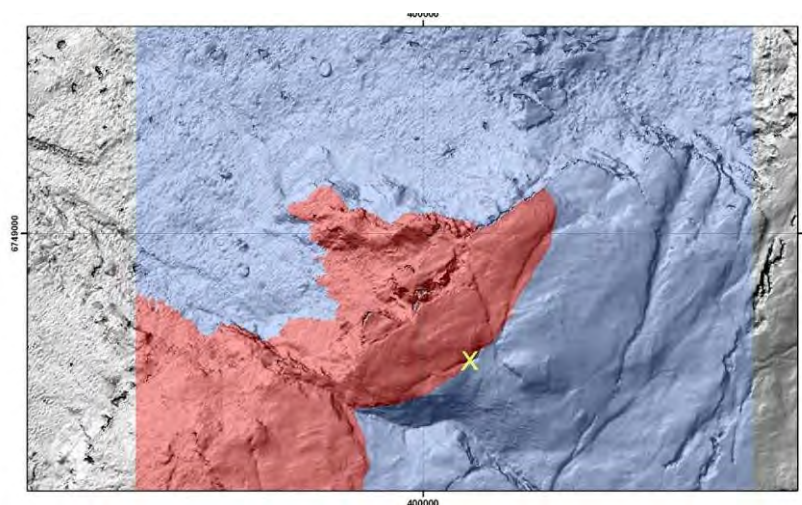


Figure 64: Intersection of plane (orientation 300/35 and passing by the yellow cross) with the topography in the area of the lower site.

IV.7.6 Discussion

As said previously this work has been done to extract and to provide the main structural information from the terrestrial laser scanning to a NGU's master student. These data can be used for kinematics tests in order to assess the mechanisms of instability. If the mechanism of planar sliding in the upper part is quite obvious, the lower part is much more chaotic and will require further investigations.

V General conclusions

The results of the analysis with terrestrial laser scanning of the seven large sites were described in this report. For two of them the main issue is clearly rockfalls on infrastructures (Årdal and Volldal). Considering the proximity of houses, the situation is even very risky for Årdal and Volldal and a great attention should be paid to any activity at these places. Local inhabitants and authorities should be informed about how to behave in case of activities in the cliffs. In the Old tunnel site, an old road is exposed to rockfall, but from the data we have a larger rock slide cannot be excluded on the fjord side. For the four other sites (Tussen, Vidalen, Vik and Flåm), the main issue is rockslide of large blocks. In all the cases it was possible to extract the orientations of the major sets of discontinuities and some kinematics tests have provided possible failure mechanisms for most of them. Nevertheless, we must be aware that almost all the scans used here cover only a part of the instabilities and that they may not be representative of the entire instability.

As scanning a large site can be time consuming (acquisition and processing) we have tried as far as possible to propose some advices for future LiDAR campaigns. This is particularly important for displacement detection. A general advice is to try to have on one single scan a moving part and stable one, in order to avoid internal alignment errors. But this is not always possible in the field when scanning such large areas. Two of the seven sites, Flåm and Tussen, have presently datasets which can be used for displacement assessment (several year of scanning). Nevertheless on these two sites, no clear movements were detected by LiDAR scanning. Some small rock fall activities could be detected, but no displacement of a large block. A small displacement rate (mm/y) is possible, but then the time frame of scanning of 1 year is too short to detect such a movement. Nevertheless, it worth for the future to proceed to some specific scans in order to check if any evolution occurs.